УНИВЕРЗИТЕТ У БЕОГРАДУ

ФАКУЛТЕТ ЗА ФИЗИЧКУ ХЕМИЈУ

Бранислав Ж. Миловановић

КВАНТНОХЕМИЈСКО ПРОУЧАВАЊЕ СУПРАМОЛЕКУЛСКИХ СТРУКТУРА ГУАНИНА

докторска дисертација

Београд, 2021

UNIVERSITY OF BELGRADE

FACULTY OF PHYSICAL CHEMISTRY

Branislav Ž. Milovanović

QUANTUM CHEMICAL STUDY OF GUANINE SUPRAMOLECULAR STRUCTURES

Doctoral Dissertation

Belgrade, 2021

Ментори:

др Михајло Етински, ванредни професор, Универзитет у Београду, Факултет за физичку хемију

др Игор Попов, виши научни сарадник, Универзитет у Београду, Институт за мултидисциплинарна истраживања и Универзитет у Београду, Институт за физику

Чланови комисије:

1) др Милена Петковић, редовни професор, Универзитет у Београду, Факултет за физичку хемију
2) др Мирослав Ристић, доцент, Универзитет у Београду, Факултет за физичку хемију
3) др Ивана Станковић, виши научни сарадник, Универзитет у Београду, Институт за хемију, технологију и металургију

Датум одбране: _____

Ова докторска дисертација је у целости израђена на Факултету за физичку хемију Универзитета у Београду. Средства за израду докторске дисертације су обезбеђена са пројекта ОИ172040, финансираног од стране Министарства за образовање, науку и технолошки развој Републике Србије а чији је руководилац др Михајло Етински, ванредни професор Факултета за физичку хемију Универзитета у Београду.

Велику захвалност дугујем својим менторима, Михајлу који ме је увео у свет квантне хемије и молекулске динамике, и Игору који ми је помогао да боље разумем периодичне системе. Читаво школовање би било незамисливо без подршке моје породице и пријатеља и због тога сам им бескрајно захвалан.

Квантнохемијско проучавање супрамолекулских структура гуанина

Сажетак

Гуанини и деривати гуанина испољавају способност да се самоорганизују у разнолике супрамолекулске структуре у биолошким али и небиолошким срединама. Присуство моновалентног или двовалентног катјона у оваквим системима диктира самоорганизацију у гуанинске квадруплексе или гуанинске нанотраке, који представљају потенцијалне кандидате у виду супрамолекулских платформи за примене у оквиру молекуларне електронике. У живим организмима, гуанински квадруплекси су идентификовани као терапеутски региони у туморним ћелијама, чија стабилизација са различитим лигандима може зауставити абнормалну рекомбинацију. Модерне квантнохемијске методе попут (временски-зависне) теорије функционала густине и методе чврсте везе засноване на теорији функционала густине пружају битне детаље карактеристика гуанинских квадруплекса и молекулских нанотрака гуанина на атомском нивоу. У оквиру ове дисертације, испитано је неколико најбитнијих особина гуанинских квадруплекса и гуанинских нанотрака декорисаних риленским бојама. Најпре је истражен утицај катјона на инфрацрвени спектрални одзив гуанинског квадруплекса када интерагује са различитим комплексима металопорфирина, који имају потенцијал као лекови у третману тумора. Интеракција металопрофирина и гуанина проузрокује промене спектралних карактеристика истежуће вибрације карбонилне групе гуанина у оквиру квадруплекса, што се може употребити као маркер за испитивање сличних потенцијалних лекова у третману тумора. Истражен је и афинитет синтетисаних квадруплекса ка везивању двовалентних катјона координисаних између сваког суседног слоја у квадруплексу с обзиром да овај начин везивања двовалентних јона може довести до измене карактеристика ниско побуђених стања ових система. У воденој средини, супрамолекулски дизајн, који укључује квартет цитозина са молекулима воде између два гуанинска квартета, може да координише двовалентне катјоне између сваког суседног слоја чинећи ове структуре интересантним за оптоелектронске намене. С тим у вези, посебна пажња је посвећена утицају катјона на побуђена стања са раздвајањем наелектрисања у оквиру ових система. Утврђено је да катјони алкалних метала, који су у великој мери присутни у квадруплексима, при

биолошким условима нису способни да значајно утичу на побуђена стања испитиваних квадруплекса. Исто важи и за случај катјона земноалкалних метала, који су координисани између сваког другог слоја квадруплекса. С друге стране, положај максимума флуоресцентног спектра је могуће изменити са различитим катјонима алкалних метала. Када се двовалентни катјони поставе између сваког слоја квадруплекса, прелази са преносом наелектрисања су значајно стабилизовани што је важно са аспекта потенцијалне примене ових система у оптоелектроници. На самом крају рада, испитана је самоорганизација и оптичке особине гуанинских нанотрака формираних од гуанина који су супституисани риленским бојама на површини графена. Гуанинске нанотраке супституисане риленским бојама, као и водонично везане молекулске мреже испољавају тенденцију ка формирању танких молекулских филмова, који покривају велике површине и који међусобно имају сличне особине побуђених електронских стања. Ово указује на присуство дугоживећих стања са потпуним раздвајањем наелектрисања, што је значајно са аспекта примене у оптоелектроници.

Кључне речи: квадруплекс, гуанин, побуђена стања, раздвајање наелектрисања, самоорганизација, електроника, теорија функционала густине

Научна област: физичка хемија

Ужа научна област: физичка хемија – квантна хемија, физичка хемија – спектрохемија, физичка хемија – хемијска термодинамика, материјали

УДК број:

Quantum chemical study of guanin supramolecular structures

Abstract

Guanine and its derivates tend to self-assemble into various different supramolecular architectures in both biological and non-biological environments. Presence of the monovalent or divalent cations in the system dictates self-assembly into guanine quadruplexes or G-ribbons which represents promising supramolecular platforms for molecular electronics application. *In vivo*, guanine quadruplexes are identified as therapeutic regions in tumorous cells whose stabilization with different ligands can prevent abnormal recombination of the cell. Modern quantum chemical methods such as (time-dependent) density functional theory and density functional based tight binding can provide valuable atomistic insights into the characteristics of diverse guanine quadruplex and ribbon nanostructures. In this thesis, several key characteristics of the guanine-based quadruplexes are addressed as well as the rylene dye decorated guanine ribbons. Firstly, infrared spectral fingerprint of the potential anti-tumor drug metalloporphyrin complexes has been studied and results suggested that the presence of the different cations within the metalloporphyrin system can modulate spectral characteristics of the guanine quadruplex carbonyl stretching mode, which can serve as a marker for future studies of the similar promising anti-tumor drug candidates. Affinity of the synthesized quadruplex structures towards divalent cations imposed between every adjacent quadruplex layer has been examined since this binding mode of the divalent cations is able to modulate excited state properties of these systems. In aqueous solution, the supramolecular design associated with water-mediated cytosine quartet imposed between guanine quartets could be able to host divalent cations in the unusual binding mode which makes these quadruplexes interesting candidates for optoelectronic applications. Therefore, special attention is dedicated to understand interplay between the cation types and the charge separation states of these systems. It has been determined that biologically abundant alkali metal cations are not able to significantly modulate excited state properties of the studied quadruplexes. The same holds for the alkaline earth cations when imposed between every other layer within the quadruplex. On the other hand, maxima of the fluorescence spectra could be modulated using alkaline cations. When using divalent cations imposed between every quadruplex layer, charge transfer states are significantly modulated (stabilized), which is also important

from the aspects of optoelectronics. At the end of the thesis, self-assembly and the optical properties of the rylene dye decorated guanine supramolecular architectures on the graphene surface is studied. Both rylene decorated guanine ribbon and reference hydrogen bonded organic frameworks tend to form molecularly thin films that cover large surface area with similar electronic absorption properties. These findings suggest a presence of the prospective long-living charge-separated excited states, which can be significant for the optoelectronic applications.

Keywords: quadruplex, guanine, excited states, charge separation, self-assembly, electronics, density functional theory

Scientific field: Physical chemistry

Scientific discipline: Physical Chemistry – Quantum Chemistry, Physical Chemistry – Spectrochemistry, Physical Chemistry – Chemical Thermodynamics, Materials

UDC number:

Садржај:

Листа скраћеница

ДНК – дезоксирибонуклеинска киселина

G_4 – гуанински квартет (G-*quartet*, енгл.)

GQ – гуанински квадруплекс (G-*quadruplex*, енгл.)

PDB – *Protein Data Bank*, енгл.

G_8 – гуанински октет (G-*octet*, енгл.)

DFT – теорија функционала густине (*Density Functional Theory*, енгл.)

TDDFT – временски зависна теорија функционала густине (*Time Dependent Density Functional Theory*, енгл.)

EDA – анализа разлагања енергије (*Energy Decomposition Analysis*, енгл.)

DFTB – метода чврсте везе засноване на теорији функционала густине (*Density Functional Tight Binding*, енгл.)

BOMD – Борн-Опенхајмерова молекулска динамика (*Born–Oppenheimer Molecular Dynamics*, енгл.)

HOMO – највиша попуњена молекулска орбитала (*Highest Occupied Molecular Orbital*, енгл.)

LUMO – најнижа непопуњена молекулска орбитала (*Lowest Unoccupied Molecular Orbital*, енгл.)

NMR – нуклеарна магнетна резонанција (*Nuclear Magnetic Resonance*, енгл.)

CT – *Charge Transfer*, енгл.

UV – ултраљубичасто зрачење (*Ultra Violet*, енгл.)

1eTDM –матрица густине једноелектронског прелаза (*One-Electron Transition Density Matrix*, енгл.)

CS – Charge Separation, енгл.

DOT – густина побуђених стања (*Density Of Transition*, енгл.)

HOF – водонично везане органске мреже (*Hydrogen bonded Organic Frameworks*, енгл.)

HOPG - високо уређени пиролитички графит (*Highly Ordered Pyrolytic Graphite,* енгл.)

DOS – густина стања (*Density Of States*, енгл.)

1. Увод

Примарна улога нуклеотидних азотних база или нуклеобаза у (живом) свету какав познајемо је да су оне чиниоци основних градивних конституента нуклеинских киселина. Захваљујући јединственом молекулском препознавању, нуклеотидне азотне базе имају способност да се организују у изузетне биолошки релевантне структуре помоћу тзв. Вотсон-Крик (*Watson–Crick*, енгл.) спаривања водоничних веза.[1] Овакав начин самоорганизације нуклеобаза је изузетан с обзиром да пружа начин за складиштење генетских информација есенцијалних за развиће, функционисање и репродукцију свих познатих организама. Заједно са пентозним шећерима и фосфатним групама, нуклеобазе формирају нуклеотиде који представљају градивне блокове полимерних молекула познатијих као полинуклеотиди. Полинуклеотидни низ сам по себи представља примарну структуру нуклеинских киселина, док поменуто Вотсон-Крик спаривање нуклеобаза доводи до формирања карактеристичних (каноничних) секундарних структура нуклеинских киселина (нпр. дупли хеликс код дезоксирибонуклеинске киселине – ДНК, Слика 1.1.в). Поред поменутог Вотсон-Крик спаривања нуклеобаза, одређене нуклеобазе показују способност да се међусобно спарују и тзв. Хугстиновим (*Hoogsteen*, енгл.) типом водоничних веза (Слика 1.1.е)[2]. Овај тип спаривања нуклеобаза доводи до појаве разноликих (неканоничних) секундарних структура нуклеинских киселина (Слика 1.1.г-ђ). Са оваквим карактеристичним типом спаривања се посебно истиче гуанин. Познато је да у структурама на крајевима линеарних хромозома постоје области које су богате гуанинима и у којима се јављају неканоничне секундарне структуре са интересантним заштитним биолошким својствима попут локалне стабилизације хромозома и спречавања абнормалне рекомбинације[3]-[6]. У оквиру неканоничних секундарних структура, у чијем формирању учествује гуанин, могу се уочити еквивалентни супрамолекулски мотиви. Један од најчешћих и најједноставнији тип ових мотива је тзв. гуанински квартет (G-*quartet*, енгл. – G_4, Слика 1.2.)[5]. При *in vivo* условима, у теломерној ДНК (терми-

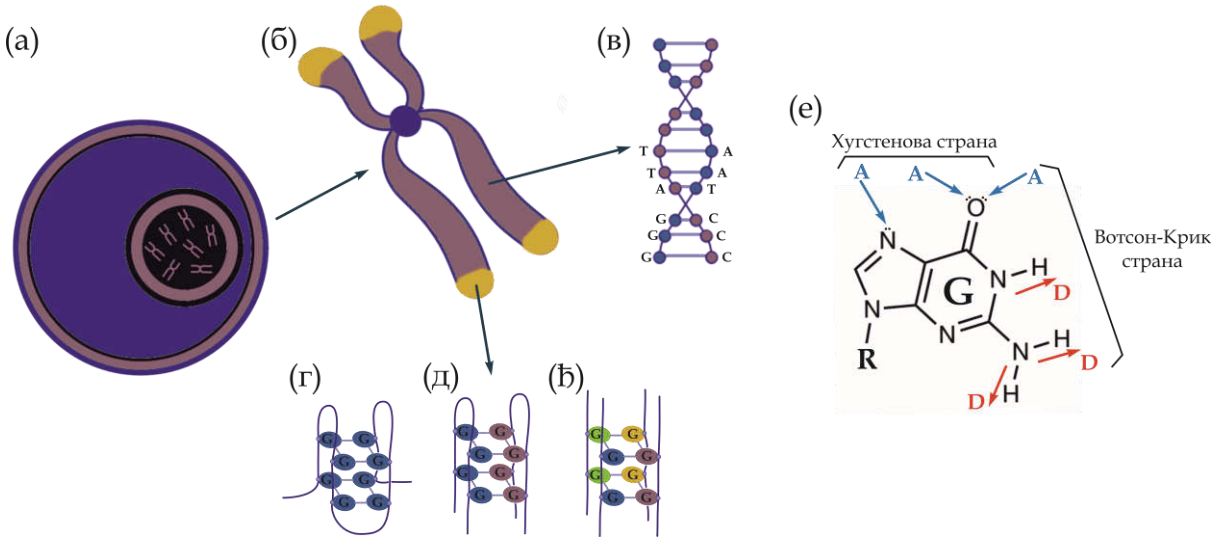

Слика 1.1. *Шематски приказ организације нуклеобаза унутар хромозома. Шематски приказ* (а) *ћелије код еукариота,* (б) *хромозома са жутом бојом назначеним теломерним регионима,* (в) *дуплог хеликса унутар ДНК са назначеним геномом као пример стандардне каноничне секундарне структуре,* (г) *унимолекуларних,* (д) *бимолекуларних и* (ђ) *тетрамолекуларних гуанинских квадруплекса као примери неканоничних структура у којима учествује гуанин. Нуклеобазе које припадају различитим полинуклеотидним ланцима су обојени различитом бојом. Са* **G**, **A**, **T** *и* **C** *су означене нуклеобазе гуанин, аденин, тимин и цитозин, редом.* (е) *Могућа места за успостављање водоничних веза код гуанина. Вотсон-Крик и Хугстин стране су такође назначене.* **A** *означава акцепторско место док* **D** *означава донорско место за водоничну везу. Са* **R** *је означено место везивања гуанина за пентозни шећер.*

налне секвенце линеарних хромозома), могуће је формирање и узастопно наслаганих G_4 структура које се међусобно додатно стабилишу нековалентним *stacking*[1] интеракцијама. Сукцесивно наслагане G_4 структуре формирају тзв. гуанински квадруплекс (G-*quadruplex*, енгл. – GQ, Слика 1.2.)[7]. Просторна организација гуанина унутар GQ у свом средишту оставља простор за везивање моновалентних јона који додатно стабилизују ове супрамолекулске структуре[8]. При *in vivo* условима, то су најчешће Na^+ и K^+ јони. За GQ се сматра се да код еукариотских хромозома служи као место везивања за рибонуклеопротеин теломеразу[9], који има значајну улогу у контролисању механизама који доприносе формирању тумора[10], [11]. Поред гуанина, квартете могу да формирају и друге нуклеобазе, попут аденина, урацила или цитозина[12], [13]. Појаве оваквих квартета не морају да утичу на формирање секундарне структу-

[1] У српском језику не постоји адекватна терминологија за појам „*stacking interactions*“ који је устаљен у литератури на енглеском језику. Глагол „*to stack*“ се може превести као „*наслагати*“, док за саму интеракцију између молекула до које долази услед слагања истих не постоји посебна реч. Стога ће се у наставку текста користити термини: *stacking* интеракција/е.

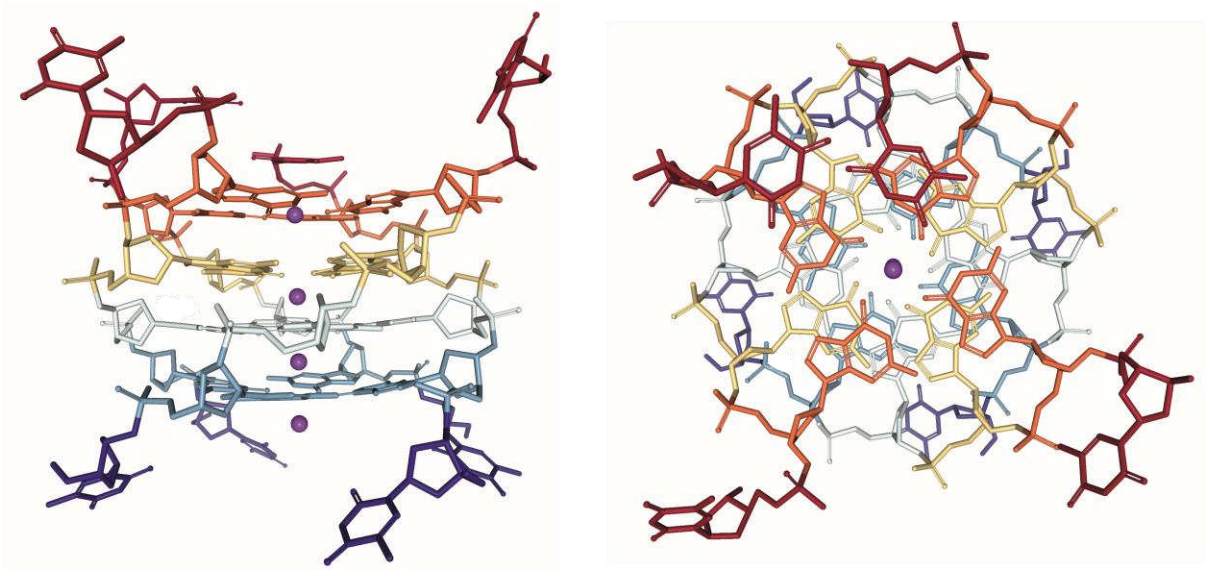

Слика 1.2. *Структура из „профила“* (*лево*) *и са погледом на централни јонски канал* (*десно*) *тетрамолекуларног* GQ *са* PDB (*Protein Data Bank, енгл.*) *ознаком* 2O4F[14]. G_4 *структуре у оквиру* GQ *су обојене различитим бојама. Љубичасте сфере представљају места везивања катјона. Структура је визуализована уз помоћ* NGL *софтвера*[15].

ре карактеристичне за GQ, већ могу и да се уграде у GQ и притом ступе у интеракцију са G_4 градивним слојевима квадруплекса стварајући мешовити квадруплекс. Том приликом, њихова интеракција са јонима није значајно нарушена.

Иако заступљени унутар нуклеинских киселина, GQ се на исти начин могу формирати и у растворима гуанина/гуанозина и/или њихових деривата уз присуство различитих јона[16]. У одсуству јона, гуанини/гуанозини и/или њихови деривати показују тенденцију ка формирању тракастих структура на површима и у растворима[17]. Две наслагане G_4 структуре се називају гуанинским октетима (G-*octet*, енгл. – G_8) и представљају минималан модел GQ (Слика 1.3.). Стабилност GQ је условљена са неколико фактора: 1) присуством јона у унутрашњем централном каналу као и његовим особинама (јонски радијус и наелектрисање); 2) кооперативност и јачина успостављених водоничних веза између суседних молекула гуанина; 3) солватациона енергија система[18]–[23].

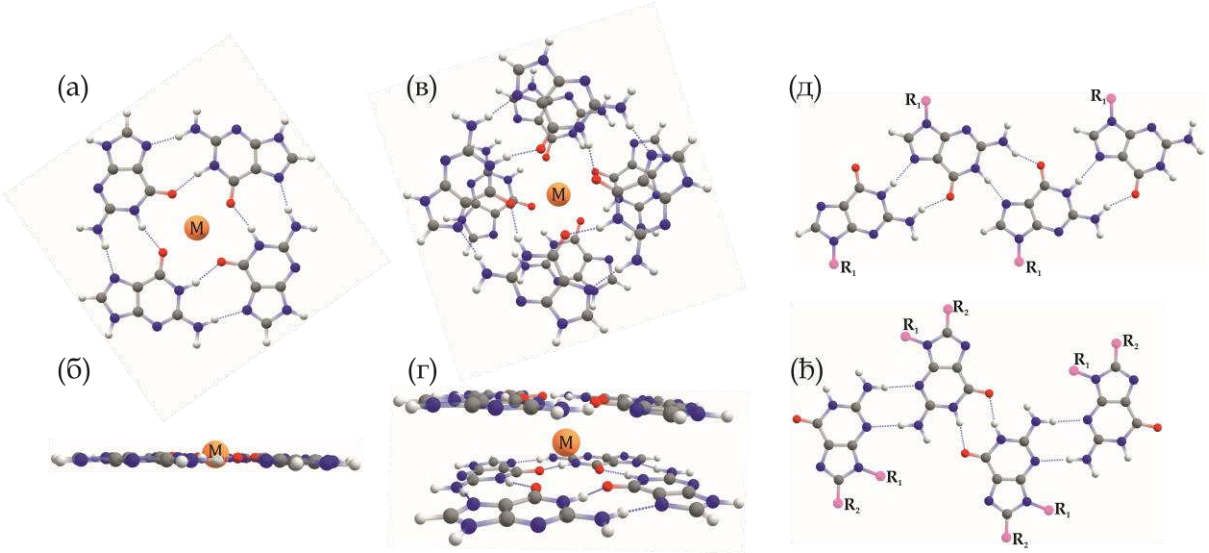

Слика 1.3. *Структуре* (а) *и* (б) G_4, (в) *и* (г) G_8, (д) *и* (ђ) *два типа гуанинских нанотрака. Водоничне везе су означене испрекиданим линијама. Метални катјон у средиштима структура* G_4 *и* G_8 *је означен са* **M**. *Са* $\mathbf{R_1}$ *и* $\mathbf{R_2}$ *су означена места на којима гуанини који формирају нанотраке могу бити супституисани различитим функционалним групама/молекулима.*

Овакав прилагодљив али уједно и селективан начин спаривања нуклеобаза отвара могућност за манипулисање овим структурама у циљу примене у нанотехнологији и хемијској биологији. За GQ, који се налазе у оквиру теломерних структура, а на основу њихових физичкохемијских својстава, је предочено да имају потенцијал као мете у терапијама против тумора[24]. С друге стране, овакве супрамолекулске структуре су такође интересантне са аспекта нанотехнологије с обзиром на њихову способност самоорганизације и могућности ковалентног декорисања одговарајућим молекулима са повољним својствима (нпр. електричне или оптички активне функционалне групе/молекули)[17], [25]–[31]. Такође, могућност везивање различитих катјона код GQ отвара могућност за конструкцију супрамолекулских система који би испољавали селективни афинитет само према одређеним јонима (нпр. токсичним Pb^{2+} или Hg^{2+}), те би овакви системи представљали тзв. јонофоре[5], [30]–[33].

Своју способност самоорганизације, супрамолекулске структуре гуанина попут GQ и гуанинских нанотрака, дугују јединственом начину спаривања њиховим основним градивним јединицама – гуанинима. Истовремено, интеракција GQ са јонима, Хугстинов начин везивања гуанина помоћу водоничних веза, интеракција између суседних слојева G_4 и интеракција са

околином, оставља велики маневарски простор за фино подешавање њихових особина. Ови системи се могу произвести у кристалној форми, воденим или органским растворима и притом су осетљиви и на факторе попут температуре, електричног поља, pH, јонске јачине, апсорпције електромагнетног зрачења, итд. С друге стране, веома важна биолошка улога GQ у генетским процесима је такође вредна истраживања. Нпр. код еукариотских организама, стабилизација теломерних GQ код туморних ћелија може зауставити нежељену репликацију. Овај феномен осликава потенцијал GQ за примене у терапијама тумора. Стога је испитивање фундаменталних особина ових система важно и са аспекта примене у нанотехнологији и хемијској биологији. Тренутни фокус физичкохемијских истраживања везаних за ове системе је: испитивање интеракција које су заслужне за стабилности ових структура, интеракција GQ са разним молекулима (лигандима) и катјонима, самоорганизација и особине ковалентно декорисаних гуанинских супрамолекулских структура (наножице, метал-органске мреже, итд.), испитивање особина побуђених стања биолошких и синтетисаних гуанинских супрамолекулских структура. Да би се темељно разумели фундаментални процеси који доводе до тога да гуанинске супрамолекулске структуре имају изванредне особине и поред примене најсавременијих експерименталних техника неопходан је *in silico* приступ. Квантнохемијске методе и методе молекулске механике у том смислу представљају веома погодан алат за подробније испитивање ових система на атомском нивоу и тумачење експериментално запажених резултата.

1.1. Предмет и циљеви истраживања

Предмет истраживања у оквиру ове докторске дисертације су неке од фундаменталних особина основног и побуђених стања супрамолекулских структура гуанина. Мотиви за ово истраживање су изложени у претходном поглављу и у складу са тим су постављени следећи циљеви истраживања:

- Испитивање природе и јачине интеракције катјона из централног јонског канала са G_4-металопорфиринским комплексима у сврхе дизајнирања

што ефикаснијих лиганада за примене у терапијама за сузбијање тумора. Посебан акценат је стављен на испитивање конформационе стабилности и спектралног вибрационог одзива ових система у зависности од присутног лиганда.

- Испитивање афинитета GQ, као и мешовитих квадруплекса према везивању двоструко наелектрисаних катјона у њиховом централном каналу.
- Анализа утицаја катјона из централног јонског канала као и солватационих ефеката на особине побуђених стања GQ (флуоресценција, прелази са преносом наелектрисања).
- Испитивање енергетике и побуђених стања самоорганизованих ковалентно декорисаних молекула гуанина са риленским бојама на графену у супрамолекулске структуре – нанотраке и водонично-везане молекулске мреже.

1.2. Теоријска методологија

Резултати овог истраживања су добијени уз помоћ неколико различитих метода заснованих на квантној хемији, као и уз помоћ молекулске динамике са пољем сила. Све коришћене методе су већ низ година устаљене на пољу рачунарске хемије. Велики део истраживања је заснован на теорији функционала густине (*Density Functional Theory*, енгл. – DFT) и временски зависној теорији функционала густине (*Time Dependent Density Functional Theory*, енгл. – TDDFT). За примену DFT методе, коришћени су стандардни функционали (CAM-B3LYP[36]-[38], M062X[39], PBE[40] и BLYP[36], [37]), као и различити базни скупови. За адекватно третирање дисперзионих интеракција је коришћена Гримова (*Grimme*, нем.) D3 корекција[41], [42]. Енергија интеракције фрагмената дефинисаних у системима је по потреби темељније испитана уз помоћ анализе разлагања енергије (*Energy Decomposition Analysis*, енгл. – EDA)[43]. Поред DFT метода, коришћена је и мање захтевна семиемпиријска метода чврсте везе на бази теорије функционала густине (*Density Functional Tight*

Binding, енгл. – DFTB). DFT и DFTB су коришћене и у оквиру Борн-Опенхајмерове молекулске динамике (*Born–Oppenheimer Molecular Dynamics*, енгл. – BOMD) за генерисање потенцијалне површи система. Осим електронских структурних метода, за потребе молекулске динамике су коришћени и класични потенцијали – поља сила. За имплицитне симулације водене средине је коришћен COSMO солватациони модел[44, 45].

За статичке DFT прорачуне и оптимизације су коришћени програмски пакети Gaussian09[46], Gaussian16[47] и Turbomole[48]. CP2K софтвер[49] је коришћен за молекулску динамику са пољем сила и са DFT потенцијалима, док је NAMD софтвер[50] коришћен само за молекулску динамику са пољем сила. Поља сила су припремљена уз помоћ AmberTools18 софтверског пакета[51]. Сви прорачуни који су укључивали коришћење DFTB методе су изведени уз помоћ DFTB+ софтвера[52]. Ради евалуације резултата добијених са DFTB методом, за периодичне прорачуне на бази DFT-ја коришћен је и SIESTA код[53]. Од помоћног софтвера за припремање и анализу геометријских параметара испитиваних система коришћени су VMD[54], TRAVIS[55, 56] и Chemcraft[57], док су за анализу побуђених стања коришћени Multiwfn[58] и TheoDORE[59]. Специфичности прорачуна и модела испитиваних система су дате у оквиру објављених научних радова који се налазе у прилогу.

1.3. Објављени научни радови

У току израде ове докторске дисертације објављено је шест научних радова (наведени по датуму објављивања):

Branislav Milovanović, Milena Petković, Mihajlo Etinski, Properties of the Excited Electronic States of Guanine Quartet Complexes with Alkali Metal Cations, *J. Serb. Chem. Soc.*, **2020**, 85 (8), pp 1021-1032.

https://doi.org/10.2298/JSC191025140M *IF(2020) 1,240*

Branislav Milovanović, Ivana M. Stanković, Milena Petković, Mihajlo Etinski, Modulating Excited Charge Transfer States of G-Quartet Self-Assemblies by Earth Alkaline Cations and Hydration, *J. Phys. Chem. A*, **2020**, 124 (40), pp 8101-8111.

https://doi.org/10.1021/acs.jpca.0c05022 *IF(2020) 2,781*

Branislav Milovanović, Milena Petković, Mihajlo Etinski, Igor Popov, Water-Mediated Interactions Enhance Alkaline Earth Cation Chelation in Neighboring Cavities of a Cytosine Quartet in the DNA Quadruplex, *J. Phys. Chem. B*, **2021**, 125 (43), pp 11996-12005.

https://doi.org/10.1021/acs.jpcb.1c05598 *IF(2020) 2,991*

Ana Stanojević, Branislav Milovanović, Ivana M. Stanković, Mihajlo Etinski, Milena Petković, The Significance of the Metal Cation in Guanine-Quartet – Metalloporphyrin Complexes, *Phys. Chem. Chem. Phys.*, **2021**, 23, pp 574-584.

https://doi.org/10.1039/D0CP05798C *IF(2020) 3,676*

Branislav Milovanović, Mihajlo Etinski, Igor Popov, Self-Assembly of Rylene-Decorated Guanine Ribbons on Graphene Surface for Optoelectronic Applications: A Theoretical Study, *Nanotechnology*, **2021**, 32 (43), pp 435405.

https://doi.org/10.1088/1361-6528/ac162c *IF(2020) 3,874*

Branislav Milovanović, Milena Petković, Mihajlo Etinski, Alkaline Earth Cations Binding Mode Tailors Excited-State Charge Transfer Properties of Guanine Quadruplex: A TDDFT Study, *Spectrochim. Acta A*, **2022**, 267 (Part 2), pp 120584.

https://doi.org/10.1016/j.saa.2021.120584 *IF(2020) 4,098*

На основу члана 23. став 3, Правилника о докторским студијама на Универзитету у Београду, Сената Универзитета у Београду, од 13. 04. 2016. године, односно на основу члана 18. став 3. Правилника о докторским студијама, изради, оцени и одбрани докторске дисертације Факултета за физичку хемију Универзитета у Београду, од 16. 09. 2016. године, ова докторска дисертација је конципирана као скуп објављених научних радова, који представљају тематску целину.

Дозвола за пренос ауторских права за сваког од издавача у чијем је часопису објављен научни рад је такође дата у прилогу пре самог научног рада.

2. Преглед резултата

2.1. Интеракција G_4 са металопорфиринским комплексима

Метални комплекси засновани на порфиринима представљају класу једињења од изузетног значаја за живи свет. Магнезијум порфирин комплекс је есенцијалан за живот на планети Земљи с обзиром на његову улогу у зеленим пигментима биљака и алги. Стога је ово једињење темељно истражено и са експерименталног[60]-[68] и са теоријског аспекта[69]-[71]. Поред тога, испитиване су и синтетичке варијанте овог једињења[72, 73], као и оне варијанте порфирина у којима уместо магнезијума фигурише калцијум[74]-[76]. Сам порфирин и деривати порфирина су (приближно) планарни молекули, који притом имају и димензије упоредиве са G_4, те стога представљају погодне кандидате за лиганде за GQ. Поред геометријских аспеката, различити супституенти у виду функционалних група или катјона у централној шупљини порфирина могу довести до оптималније интеракције са GQ[77]-[82]. Геометрија самог комплекса зависи од тога да ли се у централној шупљини порфирина налазе два протона или катјони магнезијума и калцијума (Mg^{2+} и Ca^{2+}). У случајевима када су у унутрашњој шупљини порфирина присутна два протона или Mg^{2+}, читав комплекс остаје планаран, док у случају Ca^{2+}, катјон бива измештен ван равни порфирина. Оваква разноликост у геометријама комплекса је условљена само јонским радијусом с обзиром да оба катјона, као и два протона који су њима замењени, имају исто формално наелектрисање. Ово оставља могућност за темељније испитивање утицаја јонског радијуса на интеракцију лиганда са G_4, као најједноставнијег модела за опис интеракције лиганда и GQ.

У оквиру једног од објављених научних радова, *The Significance of the Metal Cation in Guanine-Quartet – Metalloporphyrin Complexes* (*Phys. Chem. Chem. Phys.*, **2021**, 23, 574-584) датог у прилогу 1., применом молекулске динамике засноване на DFT методи испитани су конформациона стабилност и спектрални одзив истежуће карбонилне вибрације гуанина за три G_4-M-порфирин комплекса, где је $M=H_2$, Mg^{2+} и Ca^{2+}. Истежућа вибрација карбонилне групе гуанина у оквиру

GQ је осетљива према нековалентним интеракцијама и стога представља користан маркер за испитивање интеракција GQ са окружењем и лигандима[83]-[87]. Конкретно, код GQ овај вибрациони мод испољава црвени померај услед водоничног везивања између гуанина и интеракције карбонилног кисеоника са катјонима присутним у централном јонском каналу[88].

Резултати симулација молекулске динамике за сва три комплекса указују да не постоје значајне термалне флуктуације, те да је статички приступ у испитивању нековалентних интеракција оваквих система оправдан. Пратећи раздаљине центара маса порфирин-катјон и катјон-G_4, запажено је да су највеће флуктуације присутне код система са Ca^{2+}, као и да Ca^{2+} осцилује између порфирина и G_4. С друге стране, Mg^{2+} је стабилно везан у централној шупљини порфирина. Спектрални померај истежуће карбоксилне вибрације је испраћен уз помоћ спектра снаге (*power spectrum*, енгл.), који је израчунат као Фуријеова (*Fourier*, фра.) трансформација аутокорелационе функције брзине. Највећи утицај на спектар снаге има Ca^{2+} са померајем од 56 cm^{-1} у односу на систем са H_2 уместо катјона. Mg^{2+} испољава померај од свега 11 cm^{-1}. Највећи утицај Ca^{2+} на спектар снаге корелира са резултатима статичких прорачуна, односно да Ca^{2+} појачава нековалентне интеракције између гуанина. Ради поређења, испитани су и спектри снага G_8 система без катјона, као и са Mg^{2+} и Ca^{2+}. Резултати за ове системе су показали да је спектрални утицај Mg^{2+} и Ca^{2+} идентичан и да се ради о померају од 23 cm^{-1}. Ово је такође могуће објаснити чињеницом да су оба јона у случају G_8 система позиционирани у самом средишту структуре, док је у случају G_4-Ca^{2+}-порфиринског комплекса катјон доста ближи G_4 структури, те да је интеракција са атомима кисеоника карбоксилних група јача, а самим тим и црвени померај у спектру већи. Сумарно, резултати симулација молекулске динамике засноване на DFT методи су оснажиле исправност статичких прорачуна и дале увид у промене спектралних карактеристика услед модификације нековалентних интеракција код оваквих система.

2.2. Афинитет квадруплекса према катјонима

Значај катјона за стабилизацију квадруплекса је већ истакнут у уводу ове дисертације. Афинитет G_4 и GQ према алкалним и земноалкалним јонима је добро истражено са аспекта стабилизације ових структура[22], [86]–[97]. Алкални метали могу да заузимају позиције између сваког G_4 у оквиру GQ, док земноалкални метали то чине између сваког другог G_4 услед дестабилизујућег електростатичког одбијања двоструко наелектрисаних катјона.

Афинитет GQ према катјонима алкалних метала је био предмет истраживања неколико теоријских студија[96], [101]–[103] с обзиром на биолошки значај ових катјона. На G_8 моделу је показано да је природа интеракције алкалних катјона са гуанинима првенствено електростатичка, док је орбитална интеракција која потиче од преноса наелектрисања из највише попуњене молекулске орбитале (*Highest Occupied Molecular Orbital*, енгл. – HOMO), локализоване на кисеонику молекула гуанина, у најнижу непопуњену молекулску орбиталу (*Lowest Unoccupied Molecular Orbital*, енгл. – LUMO), која је локализована на катјонима, дупло слабија од електростатичке интеракције[96]. Додавањем G_4 слојева и катјона алкалних метала на овај модел је показано да енергија везивања сваког наредног јона у систему остаје приближно иста, што је приписано уравнотежењу између дестабилизујућих електростатичких интеракција и стабилизујућих солватационих ефеката, као и електронског екранирања у систему[103].

Афинитет GQ према двовалентним катјонима је још израженији у поређењу са катјонима алкалних метала[35], [91], [96], [100], [104]–[108]. Разматрани су катјони попут Be^{2+}[92], Mg^{2+}[92], [93], [100], [105]–[108], Ca^{2+}[91]–[93], [100], [105]–[107], Sr^{2+}[90], [91], [93], [96], [104]–[108], Ba^{2+}[91], [93], [104]–[109], Mn^{2+}[104], [106], Pb^{2+}[35], [93], [108], [110], Cu^{2+}[111], Zn^{2+}[93], Cd^{2+}[93], Hg^{2+}[93] и катјони лантаноида[112], а који могу послужити као алтернатива Na^+ и K^+, који се најчешће срећу у биолошким системима. Енергетика везивања двовалентних катјона за G_8 је у основи иста као и код катјона алкалних метала, с тим што се двовалентни катјони нешто јаче везују[93]. Многи од наведених катјона су генотоксични у смислу да приликом измене са Na^+ или K^+ *in vivo* потенцијално

могу проузроковати да теломерне секвенце изгубе своју функцију. У том смислу се посебно истичу Cd^{2+}, Pb^{2+} и Hg^{2+} катјони, који испољавају велики афинитет према GQ, те је могуће да се иреверзибилно измене са Na^+ или K^+ катјонима и том приликом уводећи велике структурне измене, које могу довести до деактивације примарне функције теломерног региона у оквиру ДНК[93]. Јонски радијус је такође битна карактеристика катјона која пре свега има утицаја на просторну организацију GQ. Последично, мањи катјони попут Li^+, Mg^{2+} и Mn^{2+} испољавају тежњу да се координишу у равни G_4 и тиме глобално дестабилизују GQ[104], [106]. Супротно, катјони са малим јонским радијусом попут Li^+ боље стабилизују каноничне водонично-везане ДНК парове[113].

Поред биолошког аспекта, разнолик афинитет према двовалентним катјонима и катјонима алкалних метала пружа могућност да се GQ употребе као градивни блокови за различите наноструктуре. Нпр. уз помоћ гел електрофорезе, у присуству Na^+, K^+ и Mg^{2+} катјона, је могуће направити GQ наножице, које могу послужити као системи за пренос наелектрисања[5], [114]. У литератури се налазе и примери молекулских разделника наелектрисања на бази GQ[115], као и система који опонашају фотосинтетички реакциони центар, односно антена комплекс[116], [117]. Ковалентно декорисани гуанини могу да послуже за конструисање водонично везаних молекулских мрежа[27], [29]–[31], [117]. Овакви системи се намећу као потенцијална основа за многе материјале који би имали интересантна оптичка, електронска, магнетна и каталитичка својства. Више речи о основним карактеристикама побуђених стања квадруплекса и начином манипулације истих ће бити у наредном поглављу.

У оквиру једног од објављених научних радова, *Water-Mediated Interactions Enhance Alkaline Earth Cation Chelation in Neighboring Cavities of a Cytosine Quartet in the DNA Quadruplex*, (*J. Phys. Chem. B*, **2021**, 125 (43), pp 11996-12005), датог у прилогу 2., испитан је афинитет различитих квадруплекса према катјонима земноалкалних метала. Различити квадруплекси су подразумевали разматрање четири експерименталне кристалне структуре, које унутар централног јонског канала координишу два катјона земноалкалних метала између сваког суседног G_4[12], [13], [118], односно сваког другог G_4[90]. Две од четири структуре у свом саставу

имају и квартете сачињене од пиримидинских нуклеобаза – квартете урацила[12] и цитозина[13] (слике 1. и 2. у прилогу 2.). Све четири разматране структуре су експериментално одређене дифракцијом X-зрака. Приликом одређивања структура квадруплекса са катјонима земноалкалних металима у растворима помоћу нуклеарне магнетне резонанције (*Nuclear Magnetic Resonance*, енгл. – NMR), наилази се на потешкоће с обзиром да спектрални сигнал потиче од атомских врста попут ^{43}Ca, ^{87}Sr и ^{137}Ba[91], [119]. Стога, у PDB бази изостају експериментално одређене структуре квадруплекса на овај начин. У овом истраживању, од катјона земноалкалних метала су разматрани Ca^{2+}, Sr^{2+} и Ba^{2+}. Кристалне структуре квадруплекса, одабране на овај начин, пружају могућност да се разматра афинитет истих према двовалентним катјонима земноалкалних метала, као и да се упореди интеракција ових катјона са различитим типовима квадруплексима. Пажљив одабир структура даје увид у геометријска и енергетска ограничења приликом везивања земноалкалних катјона између сукцесивних G_4 слојева. Применом EDA методологије као и прорачуна енергија интеракције у вакууму и воденој средини (уз помоћ имплицитног солватационог модела – COSMO) је разматрана горе наведена проблематика.

Резултати овог истраживања су показали да је енергија везивања двовалентног катјона унутар централног јонског канала GQ, у коме је већ присутан један двовалентни катјон, а у првој следећој доступној шупљини значајно мања у поређењу са енергијом везивања првог катјона. Такође, ова енергија је значајно мања у поређењу са моновалентним катјонима везаним у свакој суседној шупљини, као и у поређењу са двовалентним катјонима везаним у свакој другој доступној шупљини. Ово указује да је везивање катјона земноалкалних метала између сваког слоја G_4 у воденој средини није повољно, те да је неопходно да квадруплекс буде хидратисан у раствору са нпр. великом јонском јачином како би се јони координисали унутар сваке доступне шупљине. Такође је показано да је енергија измене Na^+ катјона са Ca^{2+} катјонима у воденој средини између сваког суседног G_4 слоја неповољна, односно да износи око 49 kcal/mol. Ситуација је слична у случају квадруплекса који у својој структури уместо једног G_4 слоја поседује квартет урацила. Овај квадруплекс, услед

структурних ограничења, омогућава да се двовалентни јони Ba^{2+} позиционирају даље један од другог унутар централног јонског канала, што доприноси смањењу неповољног електростатичког одбијања. Међутим, Ba^{2+} катјон ,који се налази у непосредној близини квартета урацила, испољава позитивну енергију везивања, што укупан ефекат везивања два Ba^{2+} катјона у суседним шупљинама квадруплекса чини енергетски неповољним у воденој средини. Други разматрани квадруплекс сачињен од једног квартета цитозина, уметнутог између два G_4 квартета, омогућава повољно везивање два Ba^{2+} катјона у суседним шупљинама. Овакав ефекат је приписан појачаној електростатичкој интеракцији између јона и атома кисеоника који припадају молекулима воде и који су саставни део квартета цитозина. Ови молекули воде, који водоничним везама омогућавају да се квартет цитозина формира, истовремено испољавају негативније парцијално наелектрисање на атомима кисеоника у поређењу са атомима кисеоника код гуанина. Овакав геометријски склад цитозина и молекула воде омогућава јачу електростатичку интеракцију Ba^{2+} катјона позиционираних у суседним шупљинама са атомима кисеоника молекула воде. Истовремено, умањено је и електронско екранирање, па је закључак да овај квадруплекс може да испољи позитиван афинитет према двовалентним јонима везаним у суседним шупљинама квадруплекса у воденој средини. Овакав закључак је значајан с обзиром да се овакав начин везивања катјона у централном јонском каналу може искористити за модулацију особина побуђених стања, о чему ће бити више речи у наредном поглављу. Такође, везивање двовалентних катјона на овај начин је значајно за разумевање начина припреме квадруплекса у воденим растворима, а који се касније могу користити ради интеграције у наноуређаје.

2.3. Утицај структуре и типа катјона на побуђена стања квадруплекса

Како би се процеси који се одвијају на атомском нивоу у оквиру наносистема у потпуности разумели, поред најмодернијих експерименталних техника, неопходан је и теоријски третман у виду примене разних квантнохемијских метода. Системе на бази GQ није заобишла заинтересованост за евентуалну примену на пољу молекулске електронике или оптоелектронике. С тим у вези, у литератури је посвећено доста пажње изучавању побуђених стања ових система[88], [119]–[139]. Истраживања показују да је фотофизика GQ условљена величином система, односно бројем G_4 јединица које учествују у формирању GQ. Поред тога, битна је и релативна оријентација нуклеобаза, односно структурни фактори у систему као и присуство јона. Експериментални подаци указују да у апсорпционом спектру GQ доминирају прелази који су окарактерисани као Френкелови (*Френкель*, рус.) ексцитони, као и прелази са преносом налекетрисања, тј. CT прелази (*Charge Transfer*, енгл.)[120], [121], [128], [130], [133]–[135], [138] Моновалентни катјони унутар централног јонског канала GQ утичу на интермолекулски пренос енергије у смислу да га чини ефикаснијим[123]. Још један од примера утицаја катјона на побуђена стања ових система је у различитом флуоресцентном одговору у зависности да ли су у систему присутни Na^+ или K^+ катјони[124]. У случају Na^+ катјона стања из којих се врши емисија су ексцитонског карактера, док су у случају K^+ катјона то CT стања. Овај ефекат је приписан мањој мобилности K^+ катјона унутар централног јонског канала услед већег јонског радијуса с обзиром да су NMR подаци указивали да не постоји значајна разлика у организацији гуанина унутар GQ услед измене катјона. Група претходних истраживања се односила и на проучавање јонизације гуанина након апсорпције ултраљубичастог (*Ultra Violet*, енгл. - UV) зрачења с обзиром да се тада производи гуанински радикал катјон, који учествује у низу оксидативних процеса унутар ДНК[131], [132], [135]–[137], [139], [140]. Оно што се у литератури до тренутка писања ове дисертације није могло пронаћи је утицај двовалентних јона на побуђена стања GQ. Поред утицаја катјона на

побуђена стања такође је корисно испитати и структурни утицај, тј. присуство других типова квартета унутар квадруплекса, а поготово оних који могу да дозволе да унутар централног јонског канала двовалентни јони буду везани у свакој доступној шупљини. Овакав начин везивања катјона би требало да доведе до значајне стабилизације CT стања окарактерисаних великим моментом прелаза услед присуства јаког електричног поља унутар централног јонског канала. Детаљније разумевање особина побуђених стања GQ је значајно са становишта потенцијалне употребе ових система у молекулској електроници и/или оптоелектроници.

У оквиру једног од објављених научних радова, *Properties of the Excited Electronic States of Guanine Quartet Complexes with Alkali Metal Cations*, (*J. Serb. Chem. Soc.*, **2020**, 85 (8), pp 1021-1032) датог у прилогу 3., је истражен утицај различитих катјона алкалних метала на геометријске параметре и првих осам побуђених стања G_4 система. Овим истраживањем је направљена теоријска подлога за лакше разумевање побуђених стања код сложенијих система овога типа, односно вишеслојних квадруплекса. Поред испитивања вертикалних ексцитација, испитани су и минимуми првог синглетног побуђеног стања, односно детаљна анализа њиховог CT садржаја. Сви прорачуни су изведени уз помоћ DFT методе, а касније анализа карактера побуђених стања је изведена уз помоћ дескриптора добијених анализом матрице густине једноелектронског прелаза (*One-Electron Transition Density Matrix*, енгл. 1eTDM).

Резултати овог истраживања су потврдили претходне резултате који се тичу структура G_4, а који су пронађени у литератури, односно да мањи јони попут Li^+ испољавају тенденцију да се нађу ближе средишту централне шупљине G_4, док се већи катјони попут Na^+ и K^+ позиционирају ван равни квартета. Поред слагања структурних карактеристика са литературом, уочена је и локализација ексцитација на више од једног гуанина, и то са CT карактеристикама које укључују суседне и дијагоналне гуанине G_4 структуре. Из стања са преносом наелектрисања, односно CT стања, није било могуће изоловати стања која се одликују свеукупним раздвајањем наелектрисања, односно CS стања (*Charge Separation*, енгл.). Начин на који је дефинисан коришћен дескриптор то није

дозвољавао. Ово је указало да је неопходно променити методологију карактеризације побуђених стања код ових система како би се разјаснило која од CT стања карактерише потпуно раздвајање наелектрисања на крају ексцитације. Најнижих осам побуђених синглетних стања код G_4 система без катјона су окарактерисана са високим CT садржајем. Присуство катјона алкалних метала не утиче значајно на CT садржај, али утиче на померање првог и другог светлог стања у систему ка мањим, односно већим енергијама, редом. Овај батохромни, односно хипсохромни померај је независан од типа катјона алкалног метала. Оптимизацијом минимума првог побуђеног синглетног стања ових система се долази до закључка да су у минимуму S_1 стања окарактерисана као локализована *ππ** стања на једном од гуанина. При геометријама минимума првог побуђеног стања се примећује разлика у односу на присуство различитих катјона. Ова разлика између адијабатских и вертикалних ексцитација се приписује сложеним геометријским променама, којима систем подлеже приликом оптимизације првог побуђеног стања. Ови резултати показују да присуство различитих катјона алкалних метала утиче на положај максимума флуоресцентног спектра G_4 система.

Након испитивања побуђених стања квартета, у оквиру једног од објављених научних радова, *G-Quartet Self-Assemblies by Earth Alkaline Cations and Hydration*, (*J. Phys. Chem. A*, **2020**, 124 (40), pp 8101-8111), датог у прилогу 4., испитан је утицај катјона и хидратације на побуђена стања G_8 система. G_8 систем представља минимални модел за описивање особина GQ. Овога пута је употребљена молекулска динамика базирана на DFT методи, како би се испитала конформациона флексибилност система и боље описале вертикалне ексцитације, односно електронски апсорпциони спектар система. Такође, други приступ у дефинисању дескриптора побуђених стања уз помоћ 1eTDM је омогућио да се CS стања изолују од CT стања. Од катјона су овога пута разматрани Li^+, Na^+, K^+, Mg^{2+} и Ca^{2+}. Солватациони ефекти за један од система (G_8-Na^+) су разматрани укључивањем експлицитних молекула воде у прорачун, а чији су положаји одређени помоћу молекулске динамике са пољем сила.

Резултати молекулске динамике октета са поменутим јонима у гасној фази у основном указују на већу флексибилност квартета, што је и очекивано с обзиром на то да због величине система у разматрање нису узети пентозни шећери са фосфатним групама. Сви октети координисани са катјонима алкалних метала испољавају сличне особине основног стања. Код катјона алкалних метала, катјон са најмањим јонским радијусом, Li^+, највише доприноси дисторзији појединачних квартета унутар G_8 система. Код система G_8-Na^+ је пронађено најкраће просечно растојање катјон-кисеоник што омогућава успостављање најјачих водоничних веза између гуанина. У случају катјона земноалкалних метала интеракција катјона и кисеоника је очекивано најјача с обзиром на формално веће наелектрисање. Такође је изражена и већа ригидност структура у односу на катјоне алкалних метала. У случају G_8-Mg^{2+} система је примећено да гуанини испољавају тенденцију ка преклапању са најближим суседима, притом нарушавајући структуре појединачних квартета и доводећи до слабљења водоничних веза што се манифестује највећим средњим растојањем донор (H)-акцептор (O).

Структурне девијације у основном стању се благо одражавају и на побуђена стања G_8-$M^{+/2+}$ система. Слично као у G_4-M^+ системима катјони алкалних метала не утичу значајно на побуђена стања октета. CT садржај у системима се повећава на око 31% у односу на октет без катјона код кога је тај проценат нешто мањи и износи 26,9%. Када су у питању катјони земноалкалних метала, ту долази до нешто приметније разлике у спектрима и њиховим карактеристикама. Уочено је веће раздвајање између првог и другог светлог стања, хипсохромно померање $n\pi^*$ стања, као и стабилизација CT стања, односно померање истих ка мањим енергијама у спектру. Ефекат је приписан појачаној стабилизацији n орбитала на атомима кисеоника, што повећава енергију потребну за ексцитацију електрона из ових орбитала у π^* орбитале. Ипак, садржај CS стања није значајно модификован и износи од 20,3 до 24,4%, са изузетком G_8-Li^+ система код кога је најмањи и износи 16,6%. Допринос CS стања на енергијама испод 5 eV је незнатан, око 1% осим код G_8-Mg^{2+} система где је око 4%. Ови подаци указују на комплексни утицај катјона на геометријску структуру основног стања као и

особине побуђених стања. Разумевање ових утицаја је кључно како би се GQ структуре ефикасно могле користити у нанотехнологији за уређаје са подесивим оптичким особинама. Солватација структуре G_4-Na^+ са експлицитно третираним молекулима воде доноси неколико закључака. Вода додатно повећава садржај и стабилизује CT стања у испитиваном енергетском оквиру те је приметно и повећање CT садржаја за око 10%. Поред тога, идентификована су и стања где побуђени електрон из π орбитала гуанина на крају ексцитације бива локализован на молекулима воде. Присуство експлицитних молекула воде у моделу је омогућило да се ова стања детектују, и то у широком опсегу енергија. Постојање оваквих стања указује на могућност да иста постоје и у GQ у биолошком окружењу, те да могу довести до оштећења ДНК након апсорпције UV зрачења из широке области енергија. Ипак, резултати добијени на моделу без пентозних шећера са фосфатним групама су само сугестивни, с обзиром да би се очекивало додатно заклањање гуанина од електричног поља молекула воде у случају да су пентозни шећери са негативно наелектрисаним фосфатним групама присутни.

Испитивање побуђених стања квадруплекса је настављено на системима за које је претходно разматран и афинитет према катјонима (видети поглавље 2.2.), односно експериментално одређеним структурама, које унутар централног јонског канала координишу два катјона земноалкалних метала између сваког суседног G_4[12], [13], [118], односно сваког другог G_4[90]. Две разматране структуре у свом саставу имају и квартете урацила[12] односно цитозина[13]. Резултати овог истраживања су објављени у научном раду *Alkaline Earth Cations Binding Mode Tailors Excited-State Charge Transfer Properties of Guanine Quadruplex: A TDDFT Study* (*Spectrochim. Acta A*, **2022**, 267 (Part 2), pp 120584) датом у прилогу 5. Из поменутих система је екстраховано шест компјутационих модела (погледати слике 1. и 2. у прилогу 5.). Пет од шест модела укључују двовалентне катјоне земноалкалних метала (Ca^{2+} и Ba^{2+}), који су координисани између сваког слоја и један модел са Sr^{2+} катјонима између сваког другог слоја ради поређења. Као и у научним радовима датим у прилозима 3. и 4., методологија истраживања је подразумевала израчунавање вертикалних ексцитација применом TDDFT

методе за експериментално одређене геометрије и темељну анализу прелаза уз помоћ 1eTDM. Солватациони ефекти за један од испитиваних система су такође симулирани узимањем експлицитних молекула воде у разматрање, а чија је конфигурација добијена молекулском динамиком са пољем сила. Пажљивим одабиром фрагмената у систему је омогућено да се спектрални профил рашчлани на доприносе који потичу од локалних ексцитација (ексцитони), ексцимерских (***exci****ted di****mer*** **–** *excimer*, енгл.) доприноса и чистих CT стања.

Резултати анализе спектара ових система указују да ексцитонски и ексцимерски доприноси доминирају апсорпционим профилом. За квадруплексе са високо-симетричним и равним квартетима ексцимерска стања надвладавају ексцитонска и јављају се у широким енергетским опсезима. Такође, иако је допринос CT стања у апсорпционом спектру мали, осцилаторна снага ових прелаза не може у потпуности да се занемари. Посебна пажња је посвећена CT стањима од којих су сва заправо идентификована као CS стања. С тим у вези уз разматрање апсорпционог профила разматрана је и густина побуђених стања, тј. DOT (*Density Of Transition*, енгл. – DOT). Испитивањем DOT профила примећује се повећање садржаја CS стања као и њихово померање ка мањим енергијама. Квадруплекси који у својој структури имају бар две суседне G_4 јединице испољавају велики удео CS стања у DOT. Нпр., за највећи испитивани систем сачињен од пет G_4 слоја и четири Ca^{2+} катјона од најнижих 80 побуђених синглетних стања 75% је идентификовано као CS стања. Поред тога, већина ових стања је стабилизована испод првог светлог стања у спектру. Још један тип интересантних CS стања је уочен код система са Ca^{2+} катјонима, као и код система са два Ba^{2+} катјона и једним квартетом урацила, односно код свих система где се налазе бар два суседна G_4 квартета и два двовалентна катјона у суседним шупљинама централног јонског канала. Овај тип CS стања је окарактерисан ексцитацијом електрона из π орбитала локализованим на гуанинима у виртуелне *d* орбитале Ca^{2+}, односно Ba^{2+} катјона. Примећени ефекти који катјони индукују у овим системима су приписани постојању јаког електричног поља унутар квадруплекса, које стабилизује прелазе са великим моментом прелаза као што су $\pi\pi^*$ и гуанин-катјон CS стања. Солватација система

са три G_4 слоја и два Ca^{2+} катјона са експлицитним молекулима воде доводи до истих ефеката као и у случају G_8-Ca^{2+} система.

Темељним разматрањем побуђених стања квадруплекса заснованим на анализи 1eTDM се може закључити да су ови системи вредни даљег испитивања, пре свега због велике присутности CS стања, као и могућности подешавања њихових енергија супрамолекулским дизајном, односно величином система, катјонима и присуством различитих квартета у самој структури.

2.4. Самоорганизација и оптичка својства ковалентно декорисаних гуанинских нанотрака

Самоорганизација молекулских система представља један од елегантних начина за припрему наноуређаја са пожељним особинама за примене у оквиру молекулске електронике и оптоелектронике. Нуклеобазе, а посебно гуанини, су репрезентативни примери микроскопских градивних блокова за функционалне наноструктуре с обзиром на њихову способност самоорганизације помоћу нековалентних интеракција. Међутим, материјали засновани на структурама сачињеним искључиво од нуклеобаза нису погодни за практичну примену с обзиром на њихову UV оптичку активност. Са овим у вези, у литератури се налази низ различитих органских једињења која у некој мери испољавају способност самоорганизације, али не и у мери у којој су то способне да учине нуклеобазе са својим карактеристичним молекулским препознавањем[141]-[147]. Комбиновањем самоорганизационих способности нуклеобаза и погодних оптичких особина једињења којима је могуће функционализовати нуклеобазе се добијају тзв. водонично-везане органске мреже (*Hydrogen bonded Organic Frameworks*, енгл. HOF)[28]-[31], [148]. Примера HOF система на бази гуанина има у литератури и заснивају се на ковалентном декорисању гуанина молекулима на бази риленских боја. Конкретно ради се о нафтален-1,4:5,8-би(дикарбоксимид) (NDI) и 2,5,8,11-тетрахексилперилен-3,4:9,10-би(дикарбоксимид) (PDI) молекулима[26], [27]. Предност HOF система је могућност лаке манипулације особинама истих коришћењем различитих

оптички активних јединица. Демонстрирана је способност синтетичког GQ да кроз своју стубасту структуру каналише фотогенерисане шупљине (*electron holes*, енгл.) када GQ чине гуанини који су супституисани риленским бојама[25]-[31]. У овом случају просторна организација игра кључну улогу с обзиром да након ексцитације у светла $\pi\pi^*$ стања локализована на риленским бојама у систему долази до раздвајања наелектрисања, односно до релаксације кроз дугоживеће CS стање у коме је шупљина локализована на гуанинима, а ексцитовани електрон (*excited electron*, енгл.) на риленским бојама. Конкретно, у случају гуанин-PDI (GPDI) система, време живота $G^{\bullet+}PDI^{\bullet-}$ CS стања је 1,2±0,2 ns[31]. Релативно дугачко време живота је приписано делокализацији ексцитованог електрона на суседним PDI хромофорама. Код система гуанин-TDI (GTDI) пронађен је још један интересантан тип дугоживећих CS стања у којима је наелектрисање раздвојено на суседним TDI јединицама, али овога пута без учешћа гуанина ($TDI^{\bullet+}TDI^{\bullet-}$). Сличне каратеристике побуђених стања се срећу и код HOF система организованих на површинама[26]-[28]. Овакве карактеристике побуђених стања у комбинацији са супрамолекулским дизајном чини ове структуре изузетно примамљивим за примене у оквиру оптоелектронике. Поред риленских боја као супституенти гуанина/гуанозина у литератури се налазе и олиготиофени[149]-[152], олиго(*p*-фе-нилен-винилен)[153], бор-дипирометен[154] и бутилфинеил[155]. Експериментални аспект припреме ових система је изузетно компликован и нпр. у случају GPDI захтева грубо око 116 часова припреме (за детаље синтезе погледати референцу [31]). Такође, карактеризација ових система захтева коришћење неколико различитих комплексних експерименталних техника. Материјали на бази супституисаних гуанина се могу сматрати и кандидатима за конструисање флексибилних фотоволтаика с обзиром да испољавају тенденцију ка формирању (атомски) танких филмова на површинама. У том случају неопходно је да танки молекулски филмови буду депоновани на транспарентним електродама, а у том смислу се посебно истиче графен. Кристални хетероспојеви полупроводника и графена, где су карактеристике полупроводника подешене за одређене намене, су темељно испитивани протеклих година[156]-[158]. Поред тога, експериментално

су реализоване самоорганизоване структуре разних риленских боја на високо уређеном пиролитичком графиту[159] (*Highly Ordered Pyrolytic Graphite,* енгл. - HOPG), као и гуанина/гуанозина супституисаних са олиготиофенима[149]–[152]. Ипак, разумевање процеса који се одвијају у овим системима на атомском нивоу није довољно проучено с обзиром на комплексност и величину система. Захтевност са компјутационог аспекта се огледа у томе да у литератури недостају подаци о структурним, енергетским и оптичким карактеристикама оваквих система.

На самом крају истраживања у оквиру ове докторске дисертације пажња је посвећена самоорганизацији и оптичким особинама гуанинских нанотрака. Резултати су сумирани у објављеном научном раду *Self-Assembly of Rylene-Decorated Guanine Ribbons on Graphene Surface for Optoelectronic Applications: A Theoretical Study* (*Nanotechnology*, **2021**, 32 (43), pp 435405), датог у прилогу 6. Теоријски приступ у оквиру овог рада је подразумевао коришћење DFT и DFTB метода како би се анализирала својства самоорганизованих GPDI молекула у водонично-везане гуанинске нанотраке на графену. Комбинација DFT и DFTB пружа балансиран третман прецизности и брзине прорачуна испитиваних система с обзиром да су модели система у овом случају сачињени од неколико стотина атома. Природа интеракције између адсорбованих GPDI молекула на графену је разматрана уз помоћ EDA методологије, док су оптичке особине испитане са TDDFT методом. Поред GPDI организованих у нанотраке, разматрани су и HOF системи сачињени од G_2PDI молекула (један PDI супституише два гуанина са обе стране) какви су претходно експериментално синтетисани[26], [27], у циљу компаративне анализе карактеристика. Најпре је испитан начин и енергетика организације и GPDI на графену уз помоћ DFTB методе, док је евалуација резултата урађена DFT методом. Показано је да се енергије везивања GPDI молекула не разликују значајно када се примењују ове две методе (око 0,2 meV/атому). До објављивања ових резултата HOF системи овог типа су се проучавали само са класичним потенцијалима тј. пољима сила[27], и то само у циљу тачнијег тумачења структура добијених рендгеноструктурном анализом. На почетку истраживања су испитане енергије адсорпције једног

молекула GPDI на графену како би се открили евентуалне преференције ка одређеном начину везивања. Мапирањем енергије адсорпције молекула GPDI у функцији растојања од графена и релативне оријентације у односу на графен је показано да нема јединствених праваца у којима би се ови молекули адсорбовали на графену. Такође, адсорпција GPDI са своје бочне стране није ни приближно енергетски повољна као паралелна адсорпција. Изоенергетске GPDI конформације дозвољавају различите почетне услове за стварање молекулских нанотрака или HOF структура. Уследило је испитивање два могућа типа молекулских нанотрака сачињених од GPDI као и HOF структура (слика 2. у прилогу 6). Анализирана су само два типа GPDI нанотрака с обзиром на стерна ограничења која се сусрећу услед присуства PDI функционалних група којима су супституисани гуанини. Најпре су оптимизацијом добијене једнодимензионе а потом, уз примену периодичних услова, и дводимензионалне GPDI нанотраке на графену. Оваква анализа је спроведена како би се идентификовали типови водоничних веза којима су GPDI јединице везане, тј. водоничних веза успостављених између молекула гуанина, али и између PDI функционалних група. EDA анализа контаката између суседних јединица које чине ова два типа GPDI нанотрака је показала да су за повољне интеракције у сличној мери одговорни електростатички, поларизациони и дисперзиони доприноси. За само формирање GPDI нанотрака су заслужне повољне интеракције између гуанина, али се доприноси контаката између PDI функционалних наногрупа не смеју занемарити. Након добијања мономолекулског слоја GPDI нанотрака на графену, оптимизовано је и више варијанти наслаганих GPDI нанотрака, односно две, три наслагане и бесконачно много (уз помоћ периодичних услова) наслаганих GPDI нанотрака. Затим су прорачунате енергије везивања за ове системе и на основу њихове анализе је закључено да би раст GPDI нанотрака у равни графена требао бити повољнији од формирања вертикалних наслаганих структура. Сличан закључак се намеће и за разматрани HOF систем. Ипак, овакви закључци у идеализованим условима примењеног модела су само сугестивни с обзиром на флексибилну природу ових молекула у растворима. Поред сличне енергетике и начину интеракције са графеном, GPDI нанотраке

и HOF систем се одликују и сличном електронском структуром што је утврђено израчунавањем профила густине стања (*Density Of States*, енгл. – DOS) у близини HOMO и LUMO орбитале. Након испитане организације и енергетике ових система, пажња је посвећена и својствима њихових побуђених стања. За модел сачињен од двослојних GPDI нанотрака, односно двослојне HOF структуре, са по укупно осам молекула/супрамолекулских градивних јединица, је израчунат електронски апсорпциони спектар/DOT који је разложен на доприносе локализованих, ексцимерских и CS стања на исти начин као што је то урађено са апсорпционим профилом GQ са двовалентним катјонима (видети поглавље 2.3.). Код свих система је утврђено да имају висок садржај CS стања у DOT међу којима је потврђено присуство $G^{\bullet+}PDI^{\bullet-}$ и $PDI^{\bullet+}PDI^{\bullet-}$ CS стања, а која управо чине ове системе занимљивим са аспекта оптоелектронике. Повећано присуство $PDI^{\bullet+}PDI^{\bullet-}$ CS стања код GPDI нанотрака у односу HOF структуре је приписано повољној просторној организацији градивних јединица. Такође, показано је да код једног типа GPDI нанотрака као и код HOF структуре $G^{\bullet+}PDI^{\bullet-}$ CS стања могу бити директно побуђена након апсорпције фотона. Постојање CS стања, која се одликују просторним раздвајањем шупљине и ексцитованог електрона између слојева у систему, кандидује ове системе као потенцијалне компоненте фотоволтаика с обзиром да се ради о атомски-танким графен-GPDI хетероструктурама.

3. Закључак

У оквиру ове дисертације су теоријским приступом разматране особине супрамолекулских структура гуанина у широком смислу. Акценат је стављен на неке од најважнијих карактеристика ових система у основном електронском стању, као што је интеракција G_4 са металопорфиринским лигандом, интеракција различитих катјона са централним јонским каналом квадруплекса и самоорганизација ковалентно декорисаних гуанина у нанотраке на графену. Такође, темељно су испитана и побуђена стања гуанинских квадруплекса и нанотрака, са посебним освртом на факторе који модулирају електронску апсорпцију као што су супрамолекулски дизајн, тип катјона у систему и присуство молекула растварача. У склопу ове дисертације су коришћене тренутно стандардне методе квантне хемије, а које су уједно и најчешће коришћене у литератури за третман овде разматраних система. Ради се о методама заснованим на теорији функционала густине, а поред њих је коришћена и молекулска динамика са класичним потенцијалима.

Подаци из литературе указују на огроман потенцијал супрамолекулских структура заснованих на молекулском препознавању нуклеобаза, а међу којима посебно место заузима гуанин. Донекле компликован начин припреме и карактеризације је успорио развој и умањио интересовање за овакве системе. Стога је темељна теоријска потпора и разумевање појединости на атомском нивоу у вези са супрамолекулским структурама гуанина изостала. Систематско теоријско истраживање супрамолекулских структура гуанина у оквиру ове дисертације је пружило следеће закључке:

- Спектрални одзив у инфрацрвеном делу спектра GQ у зависности од присуства различитих металопорфиринских комплекса је потенцијално могуће употребити за праћење начина везивања оваквих лиганда који могу бити од значаја у анти-туморној терапији. Применом молекулске динамике је уочено и да исправност статичких прорачуна за овакве системе није потребно додатно преиспитивати, те да су сами по себи

довољно поуздани и корисни за откривање потенцијалних молекула кандидата за GQ анти-тумор терапије.

- На примеру експериментално доступних синтетичких квадруплекса демонстриран је утицај супрамолекулског дизајна на стабилност структура. Утврђено је да би наизменично постављени квартети гуанина и цитозина (са молекулима воде) могли да координишу двовалентне катјоне воденој средини у свакој суседној шупљини квадруплекса.
- Из анализе утицаја катјона и растварача на побуђена стања квадруплекса је изведено је неколико закључака. Катјони алкалних метала, као ни катјони земноалкалних метала везани у свакој другој доступној шупљини квадруплекса не могу значајно да модификују апсорпционе карактеристике квадруплекса. Међутим, на примеру G_4 је показано да флуоресцентни одговор система на присуство различитих катјона алкалних метала није исти, те да се ово може искористити у аналитичке сврхе. С друге стране, катјони земноалкалних метала везани у свакој доступној шупљини квадруплекса доводе до значајних промена у апсорпционом спектру. Примећена је значајна стабилизација CS стања испод светлих стања у спектрима. Поред тога, детектовано је и постојање прелаза са молекула гуанина на катјоне земноалкалних метала. Утицај растварача (воде) се манифестовао кроз додатну стабилизацију свих типова CS стања.
- Испитивање супрамолекулске организације декорисаних молекула гуанина у молекулске нанотраке на графену је указало на афинитет ка формирању мономолекулских слојева овог типа уместо вертикално наслаганих структура. Карактеристике побуђених стања гуанинских нанотрака испољавају сличност са експериментално испитаним HOF системима кроз присуство два типа, са становишта молекулске електронике, интересантних CS стања.

Литература

[1] M. H. F. Wilkins, A. R. Stokes, and H. R. Wilson, "Molecular structure of nucleic acids," *Nature*, vol. 171, no. 4356, pp. 738–740, 1953.

[2] K. Hoogsteen, "The structure of crystals containing a hydrogen-bonded complex of 1-methylthymine and 9-methyladenine," *Acta Crystallogr.*, vol. 12, no. 10, pp. 822–823, 1959.

[3] W. I. Sundquist and A. Klug, "Telomeric DNA dimerizes by formation of guanine tetrads between hairpin loops," *Nature*, vol. 342, no. 6251, pp. 825–829, 1989.

[4] E. H. Blackburn, "Telomeres: No end in sight," *Cell*, vol. 77, no. 5. Cell Press, pp. 621–623, 1994.

[5] J. T. Davis, "G-quartets 40 years later: From 5'-GMP to molecular biology and supramolecular chemistry," *Angewandte Chemie - International Edition*, vol. 43, no. 6. Wiley Online Library, pp. 668–698, 2004.

[6] W. E. Wright, V. M. Tesmer, K. E. Huffman, S. D. Levene, and J. W. Shay, "Normal human chromosomes have long G-rich telomeric overhangs at one end," *Genes Dev.*, vol. 11, no. 21, pp. 2801–2809, 1997.

[7] G. Biffi, D. Tannahill, J. McCafferty, and S. Balasubramanian, "Quantitative visualization of DNA G-quadruplex structures in human cells," *Nat. Chem.*, vol. 5, no. 3, pp. 182–186, 2013.

[8] J. R. Williamson, M. K. Raghuraman, and T. R. Cech, "Monovalent cation-induced structure of telomeric DNA: The G-quartet model," *Cell*, vol. 59, no. 5, pp. 871–880, 1989.

[9] A. L. Moye *et al.*, "Telomeric G-quadruplexes are a substrate and site of localization for human telomerase," *Nat. Commun.*, vol. 6, p. 7643, 2015.

[10] D. M. Feldser and C. W. Greider, "Short telomeres limit tumor progression in vivo by inducing senescence," *Cancer Cell*, vol. 11, no. 5, pp. 461–469, 2007.

[11] J. W. Shay and S. Bacchetti, "A survey of telomerase activity in human cancer," *Eur. J. Cancer*, vol. 33, no. 5, pp. 787–791, 1997.

[12] B. Pan, Y. Xiong, K. Shi, J. Deng, and M. Sundaralingam, "Crystal Structure of an RNA Purine-Rich Tetraplex Containing Adenine Tetrads: Implications for Specific Binding in RNA Tetraplexes," *Structure*, vol. 11, no. 7, pp. 815–823, 2003.

[13] D. Zhang, T. Huang, P. S. Lukeman, and P. J. Paukstelis, "Crystal structure of a DNA/Ba2+ G-quadruplex containing a water-mediated C-tetrad," *Nucleic Acids Res.*, vol. 42, no. 21, pp. 13422–13429, 2014.

[14] C. Creze, B. Rinaldi, R. Haser, P. Bouvet, and P. Gouet, "Structure of a d(TGGGGT) quadruplex crystallized in the presence of Li^+ ions," *Acta Crystallogr. Sect. D*, vol. 63, no. 6, pp. 682–688, Jun. 2007.

[15] A. S. Rose, A. R. Bradley, Y. Valasatava, J. M. Duarte, A. Prlić, and P. W. Rose, "NGL Viewer: Web-based molecular graphics for large complexes," *Bioinformatics*, vol. 34, no. 21, pp. 3755–3758, 2018.

[16] J. T. Davis and G. P. Spada, "Supramolecular architectures generated by self-assembly of guanosine derivatives," *Chem. Soc. Rev.*, vol. 36, no. 2, pp. 296–313, 2007.

[17] A. Ciesielski, M. El Garah, S. Masiero, and P. Samorì, "Self-assembly of natural and unnatural nucleobases at surfaces and interfaces," *Small*, vol. 12, no. 1, pp. 83–95, 2016.

[18] Y. P. Yurenko, J. Novotný, V. Sklenář, and R. Marek, "Exploring non-covalent interactions in guanine- and xanthine-based model DNA quadruplex structures: a comprehensive quantum chemical approach," *Phys. Chem. Chem. Phys.*, vol. 16, no. 5, pp. 2072–2084, 2014.

[19] C. Fonseca Guerra, H. Zijlstra, G. Paragi, and F. M. Bickelhaupt, "Telomere structure and stability: covalency in hydrogen bonds, not resonance assistance, causes cooperativity in guanine quartets," *Chem. – A Eur. J.*, vol. 17, no. 45, pp. 12612–12622, 2011.

[20] T. van Mourik and A. J. Dingley, "Characterization of the monovalent ion position and hydrogen-bond network in guanine quartets by DFT calculations of NMR parameters," *Chem. – A Eur. J.*, vol. 11, no. 20, pp. 6064–6079, 2005.

[21] A. K. Jissy, U. P. M. Ashik, and A. Datta, "Nucleic acid G-quartets: Insights into diverse patterns and optical properties," *J. Phys. Chem. C*, vol. 115, no. 25, pp. 12530–12546, 2011.

[22] G. Louit, A. Hocquet, M. Ghomi, M. Meyer, and J. Sühnel, "Guanine tetrads interacting with metal ions. An AIM topological analysis of the electronic density," *PhysChemComm*, vol. 6, no. 1, pp. 1–5, 2003.

[23] G. Paragi and C. Fonseca Guerra, "Cooperativity in the self-assembly of the guanine nucleobase into quartet and ribbon structures on surfaces," *Chem. – A Eur. J.*, vol. 23, no. 13, pp. 3042–3050, 2017.

[24] S. Balasubramanian, L. H. Hurley, and S. Neidle, "Targeting G-quadruplexes in gene promoters: A novel anticancer strategy?," *Nat. Rev. Drug Discov.*, vol. 10, no. 4, pp. 261–275, 2011.

[25] A. K. Thazhathveetil, M. A. Harris, R. M. Young, M. R. Wasielewski, and F. D. Lewis, "Efficient charge transport via DNA G-quadruplexes," *J. Am. Chem. Soc.*, vol. 139, no. 5, pp. 1730–1733, 2017.

[26] Y.-L. Wu *et al.*, "Tunable crystallinity and charge transfer in two-dimensional G-quadruplex organic frameworks," *Angew. Chemie - Int. Ed.*, vol. 57, no. 15, pp. 3985–3989, 2018.

[27] Y.-L. Wu *et al.*, "G-quadruplex organic frameworks," *Nat. Chem.*, vol. 9, no. 5, pp. 466–472, 2017.

[28] N. E. Powers-Riggs, X. Zuo, R. M. Young, and M. R. Wasielewski, "Solvent independent symmetry-breaking charge separation in terrylenediimide guanine-quadruplex nanoparticles," *J. Chem. Phys.*, vol. 153, no. 20, p. 204302, 2020.

[29] N. E. Powers-Riggs, X. Zuo, R. M. Young, and M. R. Wasielewski, "Symmetry-breaking charge separation in a nanoscale terrylenediimide guanine-quadruplex assembly," *J. Am. Chem. Soc.*, vol. 141, no. 44, pp. 17512–17516, 2019.

[30] Y.-L. Wu, K. E. Brown, D. M. Gardner, S. M. Dyar, and M. R. Wasielewski, "Photoinduced hole injection into a self-assembled π-extended G-quadruplex," *J. Am. Chem. Soc.*, vol. 137, no. 11, pp. 3981–3990, 2015.

[31] Y.-L. Wu, K. E. Brown, and M. R. Wasielewski, "Extending photoinduced charge separation lifetimes by using supramolecular design: Guanine–perylenediimide G-quadruplex," *J. Am. Chem. Soc.*, vol. 135, no. 36, pp. 13322–13325, 2013.

[32] C.-W. Liu, C.-C. Huang, and H.-T. Chang, "Highly selective DNA-based sensor

for Lead(II) and Mercury(II) ions," *Anal. Chem.*, vol. 81, no. 6, pp. 2383–2387, 2009.

[33] M. Debnath, S. Chakraborty, Y. P. Kumar, R. Chaudhuri, B. Jana, and J. Dash, "Ionophore constructed from non-covalent assembly of a G-quadruplex and liponucleoside transports K^+-ion across biological membranes," *Nat. Commun.*, vol. 11, no. 1, p. 469, 2020.

[34] F. W. Kotch, J. C. Fettinger, and J. T. Davis, "A lead-filled G-quadruplex: Insight into the G-quartet's sSelectivity for Pb^{2+} over K^+," *Org. Lett.*, vol. 2, no. 21, pp. 3277–3280, 2000.

[35] W. Liu *et al.*, "Kinetics and mechanism of G-quadruplex formation and conformational switch in a G-quadruplex of PS2.M induced by Pb^{2+}," *Nucleic Acids Res.*, vol. 40, no. 9, pp. 4229–4236, 2012.

[36] A. D. Becke, "Density-functional thermochemistry. III. The role of exact exchange," *J. Chem. Phys.*, vol. 98, no. 7, pp. 5648–5652, 1993.

[37] C. Lee, W. Yang, and R. G. Parr, "Development of the Colle-Salvetti correlation-energy formula into a functional of the electron density," *Phys. Rev. B*, vol. 37, no. 2, pp. 785–789, Jan. 1988.

[38] T. Yanai, D. P. Tew, and N. C. Handy, "A new hybrid exchange–correlation functional using the Coulomb-attenuating method (CAM-B3LYP)," *Chem. Phys. Lett.*, vol. 393, no. 1, pp. 51–57, 2004.

[39] Y. Zhao and D. G. Truhlar, "The M06 suite of density functionals for main group thermochemistry, thermochemical kinetics, noncovalent interactions, excited states, and transition elements: Two new functionals and systematic testing of four M06-class functionals and 12 other function," *Theor. Chem. Acc.*, vol. 120, no. 1–3, pp. 215–241, 2008.

[40] J. P. Perdew, K. Burke, and M. Ernzerhof, "Generalized gradient approximation made simple," *Phys. Rev. Lett.*, vol. 77, no. 18, pp. 3865–3868, Oct. 1996.

[41] S. Grimme, J. Antony, S. Ehrlich, and H. Krieg, "A consistent and accurate ab initio parametrization of density functional dispersion correction (DFT-D) for the 94 elements H-Pu," *J. Chem. Phys.*, vol. 132, no. 15, p. 154104, 2010.

[42] S. Grimme, S. Ehrlich, and L. Goerigk, "Effect of the damping function in dispersion correcffted density functional theory," *J. Comput. Chem.*, vol. 32, no. 7, pp. 1456–1465, 2011.

[43] P. Su and H. Li, "Energy decomposition analysis of covalent bonds and intermolecular interactions," *J. Chem. Phys.*, vol. 131, no. 1, p. 14102, 2009.

[44] A. Klamt and G. Schüürmann, "COSMO: a new approach to dielectric screening in solvents with explicit expressions for the screening energy and its gradient," *J. Chem. Soc. Perkin Trans. 2*, no. 5, pp. 799–805, 1993.

[45] A. Schäfer, A. Klamt, D. Sattel, J. C. W. Lohrenz, and F. Eckert, "COSMO Implementation in TURBOMOLE: Extension of an efficient quantum chemical code towards liquid systems," *Phys. Chem. Chem. Phys.*, vol. 2, no. 10, pp. 2187–2193, 2000.

[46] M. J. Frisch *et al.*, "Gaussian 09 Revision D.01." .

[47] M. J. Frisch *et al.*, "Gaussian 16 Revision C.01." .

[48] "TURBOMOLE V7.5 2020, a development of University of Karlsruhe and Forschungszentrum Karlsruhe GmbH, 1989-2007, TURBOMOLE GmbH, since 2007; available from https://www.turbomole.org." .

[49] J. VandeVondele, M. Krack, F. Mohamed, M. Parrinello, T. Chassaing, and

J.Hutter, “QUICKSTEP: Fast and accurate density functional calculations using a mixed gaussian and plane waves approach,” *Comput. Phys. Commun.*, vol. 167, no. 2, pp. 103–128, 2005.

[50] J. C. Phillips *et al.*, “Scalable molecular dynamics on CPU and GPU architectures with NAMD,” *J. Chem. Phys.*, vol. 153, no. 4, p. 44130, 2020.

[51] D. A. Case *et al.*, “AMBER 2018, University of California, San Francisco.” .

[52] B. Hourahine *et al.*, “DFTB+, A software package for efficient approximate density functional theory based atomistic simulations,” *J. Chem. Phys.*, vol. 152, no. 12, p. 124101, 2020.

[53] E. Artacho *et al.*, “The SIESTA method: Developments and applicability,” *J. Phys. Condens. Matter*, vol. 20, no. 6, p. 64208, 2008.

[54] W. Humphrey, A. Dalke, and K. Schulten, “VMD: Visual molecular dynamics,” *J. Mol. Graph.*, vol. 14, no. 1, pp. 33–38, 1996.

[55] M. Brehm, M. Thomas, S. Gehrke, and B. Kirchner, “TRAVIS—A free analyzer for trajectories from molecular simulation,” *J. Chem. Phys.*, vol. 152, no. 16, p. 164105, 2020.

[56] M. Brehm and B. Kirchner, “TRAVIS - A free analyzer and visualizer for Monte Carlo and molecular dynamics trajectories,” *J. Chem. Inf. Model.*, vol. 51, no. 8, pp. 2007–2023, 2011.

[57] “Chemcraft - graphical software for visualization of quantum chemistry computations. https://www.chemcraftprog.com.” .

[58] T. Lu and F. Chen, “Multiwfn: A multifunctional wavefunction analyzer,” *J. Comput. Chem.*, vol. 33, no. 5, pp. 580–592, 2012.

[59] F. Plasser, “TheoDORE: A toolbox for a detailed and automated analysis of electronic excited state computations,” *J. Chem. Phys.*, vol. 152, no. 8, p. 84108, 2020.

[60] A. Wong, R. Ida, X. Mo, Z. Gan, J. Poh, and G. Wu, “Solid-state ^{25}Mg NMR spectroscopic and computational studies of organic compounds. square-pyramidal magnesium(II) ions in aqua(magnesium) phthalocyanine and chlorophyll a,” *J. Phys. Chem. A*, vol. 110, pp. 10084–10090, 2006.

[61] S. Lesage, H. Xu, and L. Durham, “The occurrence and roles of porphyrins in the environment: possible implications for bioremediation,” *Hydrol. Sci. J.*, vol. 38, no. 4, pp. 343–354, 1993.

[62] J. Jusélius and D. Sundholm, “The aromatic character of magnesium porphyrins,” *J. Org. Chem.*, vol. 65, no. 17, pp. 5233–5237, 2000.

[63] X. Jiang, Y. Gao, R. Lal, J. Hu, and B. Song, “Asymmetry induces Q-band split in the electronic excitations of magnesium porphyrin,” *Mol. Phys.*, vol. 116, no. 13, pp. 1697–1705, 2018.

[64] M. E. Druyan, J. R. Norris, and J. J. Katz, “Electron spin resonance of [^{25}Mg]chlorophyll a,” *J. Am. Chem. Soc.*, vol. 95, no. 5, pp. 1682–1683, 1973.

[65] S. G. Boxer, G. L. Closs, and J. J. Katz, “Effect of magnesium coordination on the carbon-13 and nitrogen-15 magnetic resonance Spectra of chlorophyll a. Relative energies of nitrogen nπ* states as deduced from a complete assignment of chemical shifts,” *J. Am. Chem. Soc.*, vol. 96, no. 22, pp. 7058–7066, 1974.

[66] J. R. Black, Q. zh. Yin, J. R. Rustad, and W. H. Casey, “Magnesium isotopic equilibrium in chlorophylls,” *J. Am. Chem. Soc.*, vol. 129, no. 28, pp. 8690–8691, 2017.

[67] A. R. Battersby, “Tetrapyrroles: the pigments of life,” *Nat. Prod. Rep.*, vol. 17,

pp. 507–526, 2000.

[68] J. Barrett, "Photo-oxidation of magnesium porphyrins and formation of protobiliviolin," *Nature*, vol. 215, pp. 733–735, 1967.

[69] M. Etinski, M. Petković, and M. M. Ristić, "A study of the low-lying singlet and triplet electronic states of chlorophyll a and b," *J. Serbian Chem. Soc.*, vol. 78, no. 11, pp. 1775–1787, 2013.

[70] M. Etinski, M. Petković, M. M. Ristić, and C. M. Marian, "Electron-vibrational coupling and fluorescence spectra of tetra-, penta-, and hexacoordinated chlorophylls c1 and c2," *J. Phys. Chem. B*, vol. 119, no. 32, pp. 10156–10169, 2015.

[71] M. Rubio and B. O. Roos, "Theoretical study of the electronic spectrum of magnesium-porphyrin," *J. Chem. Phys.*, vol. 110, p. 7202, 1999.

[72] J. S. Lindsey and J. N. Woodford, "A simple method for preparing magnesium porphyrins," *Inorg. Chem.*, vol. 34, no. 5, pp. 1063–1069, 1995.

[73] K. D. Borah and J. Bhuyan, "Magnesium porphyrins with relevance to chlorophylls," *Dalt. Transactions*, vol. 46, no. 20, pp. 6497–6509, 2017.

[74] I. Alkorta, J. Elguero, A. M. S. Silva, and A. C. Tomé, "A theoretical study of the conformation of meso-tetraphenylporphyrin (TPPH2), its anions, cations and metal complexes (Mg^{2+}, Ca^{2+} and Zn^{2+})," *J. Porphyr. Phthalocyanines*, vol. 14, no. 07, pp. 630–638, 2010.

[75] J. B. Allison and R. S. Becker, "Metalloporphyrins. Electronic spectra and nature of perturbations. III. absorption spectra and solute-solvent interactions," *J. Phys. Chem.*, vol. 67, no. 12, pp. 2675–2679, 1963.

[76] L. Bonomo, M.-L. Lehaire, E. Solari, R. Scopelliti, and C. Floriani, "The first crystalline calcium porphyrin and tetrakis (tert-butylphenyl) porphyrinato calcium (II): its synthesis, structure, and binding properties towards alkali and alkaline earth metal salts," *Angew. Chemie*, vol. 113, no. 4, pp. 793–796, 2001.

[77] G. Jia, Z. Feng, C. Wei, J. Zhou, X. Wang, and C. Li, "Dynamic insight into the interaction between porphyrin and G-quadruplex DNAs: Time-resolved fluorescence anisotropy study," *J. Phys. Chem. B*, vol. 113, no. 50, pp. 16237–16245, Dec. 2009.

[78] P. Zhao *et al.*, "Shedding light on the interactions of guanine quadruplexes with tricationic metalloporphyrins," *Spectrochim. Acta Part A Mol. Biomol. Spectrosc.*, vol. 108, pp. 1–7, 2013.

[79] T. L. Ruan *et al.*, "Lowering the overall charge on TMPyP4 improves its selectivity for G-quadruplex DNA," *Biochimie*, vol. 132, pp. 121–130, 2017.

[80] E. Boschi *et al.*, "Interaction of a cationic porphyrin and its metal derivatives with G-quadruplex DNA," *J. Phys. Chem. B*, vol. 120, no. 50, pp. 12807–12819, Dec. 2016.

[81] H. Yaku, T. Murashima, D. Miyoshi, and N. Sugimoto, "Specific binding of anionic porphyrin and phthalocyanine to the G-quadruplex with a variety of in vitro and in vivo applications," *Molecules*, vol. 17, no. 9, pp. 10586–10613, 2012.

[82] X. Yao *et al.*, "Interaction between G-quadruplex and zinc cationic porphyrin: The role of the axial water," *Sci. Rep.*, vol. 7, no. 1, p. 10951, 2017.

[83] A. T. Krummel and M. T. Zanni, "DNA vibrational coupling revealed with two-dimensional infrared spectroscopy: Insight into why vibrational spectroscopy is sensitive to DNA structure," *J. Phys. Chem. B*, vol. 110, no. 28, pp. 13991–14000, Jul. 2006.

[84] M. Azargun and T. D. Fridgen, "Guanine tetrads: an IRMPD spectroscopy,

energy resolved SORI-CID, and computational study of M(9-ethylguanine)$^{4+}$ (M = Li, Na, K, Rb, Cs) in the gas phase," *Phys. Chem. Chem. Phys.*, vol. 17, no. 39, pp. 25778–25785, 2015.

[85] V. Gabelica *et al.*, "Infrared signature of DNA G-quadruplexes in the gas phase," *J. Am. Chem. Soc.*, vol. 130, no. 6, pp. 1810–1811, Feb. 2008.

[86] C. Fraschetti, M. Montagna, L. Guarcini, L. Guidoni, and A. Filippi, "Spectroscopic evidence for a gas-phase librating G-quartet-Na^+ complex," *Chem. Commun.*, vol. 50, no. 94, pp. 14767–14770, 2014.

[87] S. S. Iyengar, "Computing vibrational properties in hydrogen-bonded systems using quantum wavepacket ab initio molecular dynamics," *Int. J. Quantum Chem.*, vol. 109, no. 15, pp. 3798–3810, 2009.

[88] F. Rosu, V. Gabelica, E. De Pauw, R. Antoine, M. Broyer, and P. Dugourd, "UV spectroscopy of DNA duplex and quadruplex structures in the gas phase," *J. Phys. Chem. A*, vol. 116, no. 22, pp. 5383–5391, Jun. 2012.

[89] A. C. Fyfe, P. W. Dunten, M. M. Martick, and W. G. Scott, "Structural variations and solvent structure of r(UGGGGU) quadruplexes stabilized by Sr^{2+} ions," *J. Mol. Biol.*, vol. 427, no. 12, pp. 2205–2219, 2015.

[90] J. Deng, Y. Xiong, and M. Sundaralingam, "X-ray analysis of an RNA tetraplex $(UGGGGU)_4$ with divalent Sr^{2+} ions at subatomic resolution (0.61 Å)," *Proc. Natl. Acad. Sci.*, vol. 98, no. 24, pp. 13665–13670, 2001.

[91] I. C. M. Kwan, Y.-M. She, and G. Wu, "Nuclear magnetic resonance and mass spectrometry studies of 2′,3′,5′-O-triacetylguanosine self-assembly in the presence of alkaline earth metal ions (Ca^{2+}, Sr^{2+}, Ba^{2+})," *Can. J. Chem.*, vol. 89, no. 7, pp. 835–844, 2011.

[92] B. Milovanović, A. Stanojević, M. Etinski, and M. Petković, "Intriguing intermolecular interplay in guanine quartet complexes with alkali and alkaline earth cations," *J. Phys. Chem. B*, vol. 124, no. 15, pp. 3002–3014, Aug. 2020.

[93] F. Zaccaria, S. C. C. van der Lubbe, C. Nieuwland, T. A. Hamlin, and C. Fonseca Guerra, "How divalent cations interact with the internal channel site of guanine quadruplexes," *ChemPhysChem*, vol. 22, no. 22, pp. 2286–2296, 2021.

[94] R. Ida and G. Wu, "Direct NMR detection of alkali metal ions bound to G-quadruplex DNA," *J. Am. Chem. Soc.*, vol. 130, no. 11, pp. 3590–3602, Mar. 2008.

[95] C. Detellier and P. Laszlo, "Role of alkali metal and ammonium cations in the self-assembly of the 5′-guanosine monophosphate dianion," *J. Am. Chem. Soc.*, vol. 102, no. 3, pp. 1135–1141, Jan. 1980.

[96] F. M. Chen, "Strontium^{2+} facilitates intermolecular G-quadruplex formation of telomeric sequences," *Biochemistry*, vol. 31, no. 15, pp. 3769–3776, Apr. 1992.

[97] A. Wong and G. Wu, "Selective binding of monovalent cations to the stacking G-quartet structure formed by guanosine 5′-monophosphate: A solid-state NMR study," *J. Am. Chem. Soc.*, vol. 125, no. 45, pp. 13895–13905, Nov. 2003.

[98] T. J. Pinnavaia, C. L. Marshall, C. M. Mettler, C. L. Fisk, H. T. Miles, and E. D. Becker, "Alkali metal ion specificity in the solution ordering of a nucleotide, 5′-guanosine monophosphate," *J. Am. Chem. Soc.*, vol. 100, no. 11, pp. 3625–3627, May 1978.

[99] F. Zaccaria, G. Paragi, and C. Fonseca Guerra, "The role of alkali metal cations in the stabilization of guanine quadruplexes: why K^+ is the best," *Phys. Chem. Chem. Phys.*, vol. 18, no. 31, pp. 20895–20904, 2016.

[100] C. C. Hardin, T. Watson, M. Corregan, and C. Bailey, "Cation-dependent transition between the quadruplex and Watson-Crick hairpin forms of

d(CGCG3GCG)," *Biochemistry*, vol. 31, no. 3, pp. 833–841, Jan. 1992.

[101] N. Gresh, S. Naseem-Khan, L. Lagardère, J.-P. Piquemal, J. E. Sponer, and J. Sponer, "Channeling through two stacked guanine quartets of one and two alkali cations in the Li+, Na+, K+, and Rb+ series. Assessment of the accuracy of the SIBFA anisotropic polarizable molecular mechanics potential," *J. Phys. Chem. B*, vol. 121, no. 16, pp. 3997–4014, Apr. 2017.

[102] K. Gkionis, H. Kruse, J. A. Platts, A. Mládek, J. Koča, and J. Šponer, "Ion binding to quadruplex DNA stems. Comparison of MM and QM descriptions reveals sizable polarization effects not included in contemporary simulations," *J. Chem. Theory Comput.*, vol. 10, no. 3, pp. 1326–1340, Mar. 2014.

[103] C. Nieuwland, F. Zaccaria, and C. Fonseca Guerra, "Understanding alkali metal cation affinities of multi-layer guanine quadruplex DNA," *Phys. Chem. Chem. Phys.*, vol. 22, no. 37, pp. 21108–21118, 2020.

[104] E. Zavyalova, G. Tagiltsev, R. Reshetnikov, A. Arutyunyan, and A. Kopylov, "Cation coordination alters the conformation of a thrombin-binding G-quadruplex DNA aptamer that affects inhibition of thrombin," *Nucleic Acid Ther.*, vol. 26, no. 5, pp. 299–308, 2016.

[105] J. Seo, E. S. Hong, H.-J. Yoon, and S. K. Shin, "Specific and nonspecific bindings of alkaline-earth metal ions to guanine-quadruplex thrombin-binding aptamer DNA," *Int. J. Mass Spectrom.*, vol. 330–332, pp. 262–270, 2012.

[106] S. D. Patil and D. G. Rhodes, "Influence of divalent cations on the conformation of phosphorothioate oligodeoxynucleotides: a circular dichroism study," *Nucleic Acids Res.*, vol. 28, no. 12, pp. 2439–2445, 2000.

[107] B. I. Kankia and L. A. Marky, "Folding of the thrombin aptamer into a G-quadruplex with Sr^{2+}: stability, heat, and hydration," *J. Am. Chem. Soc.*, vol. 123, no. 44, pp. 10799–10804, Nov. 2001.

[108] M. Vairamani and M. L. Gross, "G-quadruplex formation of thrombin-binding aptamer detected by electrospray ionization mass spectrometry," *J. Am. Chem. Soc.*, vol. 125, no. 1, pp. 42–43, Jan. 2003.

[109] X. Shi, J. C. Fettinger, and J. T. Davis, "Homochiral G-quadruplexes with Ba^{2+} but not with K^{+}: The cation programs enantiomeric self-recognition," *J. Am. Chem. Soc.*, vol. 123, no. 27, pp. 6738–6739, Jul. 2001.

[110] T. Li, E. Wang, and S. Dong, "Potassium−lead-switched G-quadruplexes: A new class of DNA logic gates," *J. Am. Chem. Soc.*, vol. 131, no. 42, pp. 15082–15083, Oct. 2009.

[111] C. Wang, Y. Li, G. Jia, Y. Liu, S. Lu, and C. Li, "Enantioselective Friedel–Crafts reactions in water catalyzed by a human telomeric G-quadruplex DNA metalloenzyme," *Chem. Commun.*, vol. 48, no. 50, pp. 6232–6234, 2012.

[112] I. C. M. Kwan, Y.-M. She, and G. Wu, "Trivalent lanthanide metal ions promote formation of stacking G-quartets," *Chem. Commun.*, no. 41, pp. 4286–4288, 2007.

[113] O. A. Stasyuk, M. Solà, M. Swart, C. Fonseca Guerra, T. M. Krygowski, and H. Szatylowicz, "Effect of alkali metal cations on length and strength of hydrogen bonds in DNA base pairs," *ChemPhysChem*, vol. 21, no. 18, pp. 2112–2126, 2020.

[114] G. I. Livshits *et al.*, "Long-range charge transport in single G-quadruplex DNA molecules," *Nat. Nanotechnol.*, vol. 9, no. 12, pp. 1040–1046, 2014.

[115] R. Sha *et al.*, "Charge splitters and charge transport junctions based on guanine quadruplexes," *Nat. Nanotechnol.*, vol. 13, no. 4, pp. 316–321, 2018.

[116] F. Pu, L. Wu, X. Ran, J. Ren, and X. Qu, "G-quartet-based nanostructure for mimicking light-harvesting antenna," *Angew. Chemie - Int. Ed.*, vol. 54, no. 3, pp.

892–896, 2015.

[117] M. R. Wasielewski, “Self-Assembly strategies for integrating light harvesting and charge separation in artificial photosynthetic systems,” *Acc. Chem. Res.*, vol. 42, no. 12, pp. 1910–1921, Dec. 2009.

[118] M. P. H. Lee, G. N. Parkinson, P. Hazel, and S. Neidle, “Observation of the coexistence of sodium and calcium ions in a DNA G-quadruplex ion channel,” *J. Am. Chem. Soc.*, vol. 129, no. 33, pp. 10106–10107, 2007.

[119] I. C. M. Kwan, A. Wong, Y.-M. She, M. E. Smith, and G. Wu, “Direct NMR evidence for Ca^{2+} ion binding to G-quartets,” *Chem. Commun.*, no. 6, pp. 682–684, 2008.

[120] C. J. Lech, A. T. Phan, M.-E. Michel-Beyerle, and A. A. Voityuk, “Influence of base stacking geometry on the nature of excited states in G-quadruplexes: A Time-Dependent DFT study,” *J. Phys. Chem. B*, vol. 119, no. 9, pp. 3697–3705, Mar. 2015.

[121] F.-A. Miannay, A. Banyasz, T. Gustavsson, and D. Markovitsi, “Excited states and energy transfer in G-quadruplexes,” *J. Phys. Chem. C*, vol. 113, no. 27, pp. 11760–11765, Jul. 2009.

[122] P. Changenet-Barret *et al.*, “Optical properties of guanine nanowires: Experimental and theoretical study,” *J. Phys. Chem. C*, vol. 114, no. 34, pp. 14339–14346, Sep. 2010.

[123] A. Dumas and N. W. Luedtke, “Cation-mediated energy transfer in G-quadruplexes revealed by an internal fluorescent probe,” *J. Am. Chem. Soc.*, vol. 132, no. 51, pp. 18004–18007, Dec. 2010.

[124] Y. Hua *et al.*, “Cation effect on the electronic excited states of guanine nanostructures studied by time-resolved fluorescence spectroscopy,” *J. Phys. Chem. C*, vol. 116, no. 27, pp. 14682–14689, Jul. 2012.

[125] Y. Hua, P. Changenet-Barret, T. Gustavsson, and D. Markovitsi, “The effect of size on the optical properties of guanine nanostructures: a femtosecond to nanosecond study,” *Phys. Chem. Chem. Phys.*, vol. 15, no. 19, pp. 7396–7402, 2013.

[126] C. J. Lech, A. T. Phan, M.-E. Michel-Beyerle, and A. A. Voityuk, “Electron-hole transfer in G-quadruplexes with different tetrad stacking geometries: A combined QM and MD study,” *J. Phys. Chem. B*, vol. 117, no. 34, pp. 9851–9856, Aug. 2013.

[127] P. Changenet-Barret, Y. Hua, and D. Markovitsi, “Electronic excitations in guanine quadruplexes,” in *Photoinduced Phenomena in Nucleic Acids II: DNA Fragments and Phenomenological Aspects*, M. Barbatti, A. C. Borin, and S. Ullrich, Eds. Cham: Springer International Publishing, 2015, pp. 183–201.

[128] R. Improta, “Quantum mechanical calculations unveil the structure and properties of the absorbing and emitting excited electronic states of guanine quadruplex,” *Chem. – A Eur. J.*, vol. 20, no. 26, pp. 8106–8115, 2014.

[129] E. Balanikas, A. Banyasz, G. Baldacchino, and D. Markovitsi, “Deprotonation dynamics of guanine radical cations,” *Photochem. Photobiol.*, no. Just Accepted, 2021.

[130] T. Gustavsson and D. Markovitsi, “Fundamentals of the intrinsic DNA fluorescence,” *Acc. Chem. Res.*, vol. 54, no. 5, pp. 1226–1235, Mar. 2021.

[131] A. Banyasz *et al.*, “Absorption of low-energy UV radiation by human telomere G-quadruplexes generates long-lived guanine radical cations,” *J. Am. Chem. Soc.*, vol. 139, no. 30, pp. 10561–10568, Aug. 2017.

[132] E. Balanikas, A. Banyasz, T. Douki, G. Baldacchino, and D. Markovitsi, "Guanine radicals induced in DNA by low-energy photoionization," *Acc. Chem. Res.*, vol. 53, no. 8, pp. 1511–1519, Aug. 2020.

[133] D. Avagliano, S. Tkaczyk, P. A. Sánchez-Murcia, and L. González, "Enhanced rigidity changes ultraviolet absorption: effect of a merocyanine binder on G-quadruplex photophysics," *J. Phys. Chem. Lett.*, vol. 11, no. 23, pp. 10212–10218, Dec. 2020.

[134] L. Martínez-Fernández, A. Banyasz, D. Markovitsi, and R. Improta, "Topology controls the electronic absorption and delocalization of electron holes in guanine quadruplexes," *Chem. – A Eur. J.*, vol. 24, no. 57, pp. 15185–15189, 2018.

[135] L. Martínez-Fernández, P. Changenet, A. Banyasz, T. Gustavsson, D. Markovitsi, and R. Improta, "Comprehensive study of guanine excited state relaxation and photoreactivity in G-quadruplexes," *J. Phys. Chem. Lett.*, vol. 10, no. 21, pp. 6873–6877, Nov. 2019.

[136] B. Behmand *et al.*, "Potassium ions enhance guanine radical generation upon absorption of low-energy photons by G-quadruplexes and modify their reactivity," *J. Phys. Chem. Lett.*, vol. 11, no. 4, pp. 1305–1309, Feb. 2020.

[137] A. Banyasz *et al.*, "Radicals generated in tetramolecular guanine quadruplexes by photoionization: Spectral and dynamical features," *J. Phys. Chem. B*, vol. 123, no. 23, pp. 4950–4957, Jun. 2019.

[138] L. Martínez-Fernández, L. Esposito, and R. Improta, "Studying the excited electronic states of guanine rich DNA quadruplexes by quantum mechanical methods: main achievements and perspectives," *Photochem. Photobiol. Sci.*, vol. 19, no. 4, pp. 436–444, 2020.

[139] E. Balanikas, L. Martínez-Fernández, R. Improta, P. Podbevšek, G. Baldacchino, and D. Markovitsi, "The structural duality of nucleobases in guanine quadruplexes controls their low-energy photoionization," *J. Phys. Chem. Lett.*, vol. 12, no. 34, pp. 8309–8313, Sep. 2021.

[140] H. Asha *et al.*, "Early steps of oxidative damage in DNA quadruplexes are position-dependent: Quantum mechanical and molecular dynamics analysis of human telomeric sequence containing ionized guanine," *Int. J. Biol. Macromol.*, 2021.

[141] C. Huang, S. Barlow, and S. R. Marder, "Perylene-3,4,9,10-tetracarboxylic acid diimides: Synthesis, physical properties, and use in organic electronics," *J. Org. Chem.*, vol. 76, no. 8, pp. 2386–2407, Apr. 2011.

[142] W. Jiang, Y. Li, and Z. Wang, "Tailor-made rylene arrays for high performance n-channel semiconductors," *Acc. Chem. Res.*, vol. 47, no. 10, pp. 3135–3147, Oct. 2014.

[143] O. Ostroverkhova, "Organic optoelectronic materials: Mechanisms and applications," *Chem. Rev.*, vol. 116, no. 22, pp. 13279–13412, Nov. 2016.

[144] G. P. Neupane, W. Ma, T. Yildirim, Y. Tang, L. Zhang, and Y. Lu, "2D organic semiconductors, the future of green nanotechnology," *Nano Mater. Sci.*, vol. 1, no. 4, pp. 246–259, 2019.

[145] H. Lee, S. Kim, Y. Kim, and S. Jung, "Structural characterization of glycerophosphorylated and succinylated cyclic β-(1→2)-d-glucan produced by sinorhizobium mliloti 1021," *Polymers (Basel).*, vol. 12, no. 9, 2020.

[146] L. Schmidt-Mende, A. Fechtenkötter, K. Müllen, E. Moons, R. H. Friend, and J. D. MacKenzie, "Self-organized discotic liquid crystals for high-efficiency organic photovoltaics," *Science (80-.).*, vol. 293, no. 5532, pp. 1119–1122, 2001.

[147] X. Zhan *et al.*, "Rylene and related diimides for organic electronics," *Adv. Mater.*, vol. 23, no. 2, pp. 268–284, 2011.

[148] A. del Prado, D. González-Rodríguez, and Y.-L. Wu, "Functional systems derived from nucleobase self-assembly," *ChemistryOpen*, vol. 9, no. 4, pp. 409–430, 2020.

[149] S. Pieraccini *et al.*, "Solvent-induced switching between two supramolecular assemblies of a guanosine–terthiophene conjugate," *Org. Biomol. Chem.*, vol. 8, no. 4, pp. 774–781, 2010.

[150] S. Sabury, T. J. Adams, M. Kocherga, S. M. Kilbey, and M. G. Walter, "Synthesis and optoelectronic properties of benzodithiophene-based conjugated polymers with hydrogen bonding nucleobase side chain functionality," *Polym. Chem.*, vol. 11, no. 36, pp. 5735–5749, 2020.

[151] M. El Garah *et al.*, "Guanosine-based hydrogen-bonded 2D scaffolds: metal-free formation of G-quartet and G-ribbon architectures at the solid/liquid interface," *Chem. Commun.*, vol. 51, no. 58, pp. 11677–11680, 2015.

[152] R. Bou Zerdan *et al.*, "Synthesis, optical properties, and electronic structures of nucleobase-containing π-conjugated oligomers," *J. Org. Chem.*, vol. 80, no. 3, pp. 1828–1840, Feb. 2015.

[153] D. González-Rodríguez *et al.*, "Persistent, well-defined, monodisperse, π-conjugated organic nanoparticles via G-quadruplex self-assembly," *J. Am. Chem. Soc.*, vol. 132, no. 13, pp. 4710–4719, Apr. 2010.

[154] F. Li, Y. Zhang, L. Zhou, X. Zhang, and Z. Chen, "Synthesis and aggregation properties of boron-dipyrromethene dyes conjugated with guanine units," *J. Porphyr. Phthalocyanines*, vol. 22, no. 09n10, pp. 944–952, Jul. 2018.

[155] X. Liu, I. C. M. Kwan, S. Wang, and G. Wu, "G-quartet formation from an N2-modified guanosine derivative," *Org. Lett.*, vol. 8, no. 17, pp. 3685–3688, Aug. 2006.

[156] J. Wong *et al.*, "High photovoltaic quantum efficiency in ultrathin van der Waals heterostructures," *ACS Nano*, vol. 11, no. 7, pp. 7230–7240, Jul. 2017.

[157] D. Jariwala, A. R. Davoyan, J. Wong, and H. A. Atwater, "Van der Waals materials for atomically-thin photovoltaics: Promise and outlook," *ACS Photonics*, vol. 4, no. 12, pp. 2962–2970, Dec. 2017.

[158] B. L. *et al.*, "Strong light-matter interactions in heterostructures of atomically thin films," *Science (80-.).*, vol. 340, no. 6138, pp. 1311–1314, Jun. 2013.

[159] Z. Yuan *et al.*, "Processable rylene diimide dyes up to 4 nm in length: Synthesis and STM visualization," *Chem. – A Eur. J.*, vol. 19, no. 36, pp. 11842–11846, 2013.

Биографија

Бранислав Ж. Миловановић је рођен 11. октобра 1993. године у Аранђеловцу где је завршио основну школу и гимназију. Дипломирао је на Факултету за физичку хемију Универзитета у Београду 2016. године. На истом факултету 2017. године стиче звање мастер физикохемичар а потом уписује и докторске студије. Од јуна 2018. године је запослен као истраживач-приправник на Факултету за физичку хемију где од августа исте године ради и као асистент. Као асистент је ангажован у настави на неколико предмета из групације опште физичке хемије као и на предмету Статистичка термодинамика. У току израде дисертације је ангажован на једном националном, два билатерална и једном NATO-SPS пројекту и аутор је седамнаест научних радова и неколико научних саопштења (до 05. 01. 2021.). Област ужег научног интересовања му је квантна хемија са акцентом на проучавање побуђених стања биомолекулских система у циљу разумевања фундаменталних процеса у којима учествују. Поред тога, бави се и проучавањем примене биомолекула у оквиру нанотехнологије. Осим науке, редовно се бави и популаризацијом науке кроз различите манифетације.

Библиографија

1. Научни радови објављени у часописима међународног значаја:

1.1. У врхунским часописима међународног значаја (M_{21}):

1.1.1. Branislav Milovanović, Milena Petković, Mihajlo Etinski, Alkaline Earth Cations Binding Mode Tailors Excited-State Charge Transfer Properties of Guanine Quadruplex: A TDDFT Study, *Spectrochim. Acta A*, **2022**, 267 (Part 2), pp 120584.
https://doi.org/10.1016/j.saa.2021.120584 *IF(2020) 4,098*

1.1.2. Branislav Milovanović, Mihajlo Etinski, Igor Popov, Self-Assembly of Rylene-Decorated Guanine Ribbons on Graphene Surface for Optoelectronic Applications: A Theoretical Study, *Nanotechnology*, **2021**, 32 (43), pp 435405.
https://doi.org/10.1088/1361-6528/ac162c *IF(2020) 3,874*

1.1.3. Branislav Milovanović, Jurica Novak, Mihajlo Etinski, Wolfgang Domcke, Nadja Došlić, Simulation of UV Absorption Spectra and Relaxation Dynamics of Uracil and Uracil-Water Clusters, *Phys. Chem. Chem. Phys.*, **2021**, 23, pp 2594-2604.
https://doi.org/10.1039/D0CP05618A *IF(2020) 3,676*

1.1.4. Ana Stanojević, Branislav Milovanović, Ivana M. Stanković, Mihajlo Etinski, Milena Petković, The Significance of the Metal Cation in Guanine-Quartet – Metalloporphyrin Complexes, *Phys. Chem. Chem. Phys.*, **2021**, 23, pp 574-584.
https://doi.org/10.1039/D0CP05798C *IF(2020) 3,676*

1.1.5. Branislav Milovanović, Ivana M. Stanković, Milena Petković, Mihajlo Etinski, Elucidating Solvent Effects on Strong Intramolecular Hydrogen Bond: DFT-MD Study of Dibenzoylmethane in Methanol Solution, *ChemPhysChem*, **2019**, 20 (21), pp 2852-2859.
https://doi.org/10.1002/cphc.201900704 *IF(2020) 3,102*

1.1.6. Branislav Milovanović, Marko Kojić, Milena Petković, Mihajlo Etinski, New Insight into Uracil Stacking in Water from *ab initio* Molecular Dynamics, *J. Chem. Theory Comput.*, **2018**, 14 (5), pp 2621–2632.
https://doi.org/10.1021/acs.jctc.8b00139 *IF(2020) 6,006*

1.1.7. Branislav Milovanović, Milan Milovanović, Suzana Veličković, Filip Veljković, Aleksandra Perić-Grujić, Stanka Jerosimić, Theoretical and Experimental Investigation of Geometry and Stability of Small Potassium-Iodide K_nI (n = 2–6) Clusters, *Int. J. Quantum Chem.*, **2019**, 119 (22), pp e26009.
https://doi.org/10.1002/qua.26009 *IF(2020) 2,444*

1.1.8. Ivana Petrović, Branislav Milovanović, Mihajlo Etinski, Milena Petković, Theoretical Scrutinization of Nine Benzoic Acid Dimers: Stability and Energy Decomposition Analysis, *Int. J. Quantum Chem.*, **2019**, 119 (13), pp e25918.
https://doi.org/10.1002/qua.25918 *IF(2020) 2,444*

1.2. У истакнутим часописима међународног значаја (M_{22}):

1.2.1. Branislav Milovanović, Milena Petković, Mihajlo Etinski, Igor Popov, Water-Mediated Interactions Enhance Alkaline Earth Cation Chelation in Neighboring Cavities of a Cytosine Quartet in the DNA Quadruplex, *J. Phys. Chem. B*, **2021**, 125 (43), pp 11996-12005. https://doi.org/10.1021/acs.jpcb.1c05598 *IF(2020) 2,991*

1.2.2. Branislav Milovanović, Ivana M. Stanković, Milena Petković, Mihajlo Etinski, Modulating Excited Charge Transfer States of G-Quartet Self-Assemblies by Earth Alkaline Cations and Hydration, *J. Phys. Chem. A*, **2020**, 124 (40), pp 8101-8111. https://doi.org/10.1021/acs.jpca.0c05022 *IF(2020) 2,781*

1.2.3. Branislav Milovanović, Ana Stanojević, Mihajlo Etinski, Milena Petković, Intriguing Inter–Molecular Interplay in Guanine Quartet Complexes with Alkali and Alkaline Earth Cations, *J. Phys. Chem. B*, **2020**, 124 (15), pp 3002-3014. https://doi.org/10.1021/acs.jpcb.0c01165 *IF(2020) 2,991*

1.2.4. Branislav Milovanović, Jelica Ilić, Ivana M. Stanković, Milana Popara, Milena Petković, Mihajlo Etinski, A Simulation of Free Radicals Induced Oxidation of Dopamine in Aqueous Solution, *Chem. Phys.*, **2019**, 524, pp 26-30. https://doi.org/10.1016/j.chemphys.2019.05.001 *IF(2020) 2,348*

1.2.5. Marko Kojić, Igor Lyskov, Branislav Milovanović, Christel Maria Marian, Mihajlo Etinski, The UVA Response of Enolic Dibenzoylmethane: Beyond the Static Approach, *Photochem. Photobiol. Sci.*, **2019**, 17 (6), pp 1324-1332. https://doi.org/10.1039/C9PP00005D *IF(2020) 3,982*

1.2.6. Miroslav Ristić, Milena Petković, Branislav Milovanović, Jelena Belić, Mihajlo Etinski, New Hybrid Cluster-Continuum Model for pKa Values Calculations: Case Study of Neurotransmitters' amino Group Acidity, *Chem. Phys.*, **2019**, 516, pp 55-62. https://doi.org/10.1016/j.chemphys.2018.08.022 *IF(2020) 2,348*

1.2.7. Branislav Milovanović, Milena Petković, Mihajlo Etinski, Raman Spectra of Aqueous Uracil Stacked Dimer: First Principle Molecular Dynamics Simulation, *Chem. Phys. Lett.*, **2018**, 713, pp 15-20. https://doi.org/10.1016/j.cplett.2018.10.015 *IF(2020) 2,328*

1.3. У међународним часописима (M_{23}):

1.3.1. Branislav Milovanović, Milena Petković, Mihajlo Etinski, Properties of the Excited Electronic States of Guanine Quartet Complexes with Alkali Metal Cations, *J. Serb. Chem. Soc.*, **2020**, 85 (8), pp 1021-1032. https://doi.org/10.2298/JSC191025140M *IF(2020) 1,240*

1.3.2. Branislav Milovanović, Mihajlo Etinski, Milena Petković, Hydrogen Transfer Reaction: Bond Formation and Bond Cleavage Through the Eyes of Interacting Quantum Atoms, *J. Serb. Chem. Soc.*, **2019**, 84 (8), pp 891-900. https://doi.org/10.2298/JSC190226034M *IF(2020) 1,240*

2. Научна саопштења:

2.1. На међународним скуповима штампана у књигама радова:

2.1.1. У облику кратког извода (M_{34}):

2.1.1.1. Branislav Milovanović, Milena Petković, Mihajlo Etinski, Significant Modulation of Charge-transfer States Properties in the Biological Assembly of the d(TG4T) Sequence in Crystal Form, *Nineteenth Young Researchers' Conference - Materials Science and Engineering*, pp 46, Book of Abstracts ISBN 978-86-80321-36-3, Belgrade, Serbia, December 1-3, **2021**.

2.1.1.2. Branislav Milovanović, Milena Petković, Mihajlo Etinski, Alkali Metal Cations Impact on the Excited States Properties of the Guanine Quartet, *11th Symposium on Computing π-Conjugated Compounds*, pp 42, Book of Abstracts (https://cpic-society.com), Zagreb, Croatia, January 30 – February 1, **2020**.

2.1.1.3. Branislav Milovanović, Ivana M. Stanković, Milena Petković, Mihajlo Etinski, Tuning Charge Transfer States in the G-octet-metal Ion Complexes for the Potential Nanotechnological Applications, *Eighteenth Young Researchers' Conference - Materials Science and Engineering*, pp 25, Book of Abstracts ISBN 978-86-80321-35-6, Belgrade, Serbia, December 4-6, **2019**.

2.1.1.4. Branislav Milovanović, Ivana M. Stanković, Milena Petković, Mihajlo Etinski, Influence of the Metal Ions on the Charge Transfer States in the G-octet-metal Ion Complexes, *Seventh Conference of Young Chemists of Serbia*, pp 153, Book of Abstracts ISBN 978-86-7132-076-4, Belgrade, Serbia, November 2, **2019**.

2.1.1.5. Branislav Milovanović, Milena Petković, Mihajlo Etinski, Discussing Aqueous Uracil Aggregation with First Principle Molecular Dynamics Simulations, *Sixth Conference of Young Chemists of Serbia*, pp 109-109, Book of Abstracts ISBN 978-86-7132-072-6, Belgrade, Serbia, October 27, **2018**.

2.1.1.6. Branislav Milovanović, Milan Milovanović, Suzana Veličković, Filip Veljković, Aleksandra Perić-Grujić, Stanka Jerosimić, Ionization Energies of KnI (n = 2, 3) Clusters Theoretical and Experimental Evaluation, N-1-P, Physical Chemistry 2018, *14th International Conference on Fundamental and Applied Aspects of Physical Chemistry*, Belgrade, Serbia, Sept 24-28, **2018**.

2.1.1.7. Branislav Milovanović, Milena Petković, Mihajlo Etinski, On the Importance of π-π Stacking and Hydrogen Bonding Cooperativity on Aqueous Uracil Aggregation, *Protein electrostatics*, pp 59, Book of Abstracts ISBN 978-86-7220-093-5, Belgrade, Serbia, June 25-28, **2018**.

2.2. На скуповима националног значаја штампана у књигама радова:

2.2.1. У облику кратког извода (M_{64}):

2.2.1.1. Branislav Milovanović, Milana Popara, Milena Petković, Mihajlo Etinski, *Ab initio* Molecular Dynamics Insights on How Dopamine Disarms Hydroxyl Radical, *55th Meeting of the Serbian chemical society*, pp 104, Book of Abstracts ISBN 978-86-7132-069-6, Novi Sad, Serbia, June 8-9, **2018**.

Прилози

Прилог 1 – *The Significance of the Metal Cation in Guanine-Quartet – Metalloporphyrin Complexes*

Објављени научни рад (категорија научног часописа M_{21}):

Ana Stanojević, Branislav Milovanović, Ivana M. Stanković, Mihajlo Etinski, Milena Petković, The Significance of the Metal Cation in Guanine-Quartet – Metalloporphyrin Complexes, *Phys. Chem. Chem. Phys.*, **2021**, 23, 574-584.

https://doi.org/10.1039/D0CP05798C *IF(2020) 3,676*

Ауторска права код издавача (приступљено дана 15.12.2021.):

The significance of the metal cation in guanine-quartet – metalloporphyrin complexes

A. Stanojević, B. Milovanović, I. Stanković, M. Etinski and M. Petković, *Phys. Chem. Chem. Phys.*, 2021, **23**, 574 **DOI:** 10.1039/D0CP05798C

To request permission to reproduce material from this article, please go to the Copyright Clearance Center request page.

If you are **an author contributing to an RSC publication, you do not need to request permission** provided correct acknowledgement is given.

If you are **the author of this article, you do not need to request permission to reproduce figures and diagrams** provided correct acknowledgement is given. If you want to reproduce the whole article in a third-party publication (excluding your thesis/dissertation for which permission is not required) please go to the Copyright Clearance Center request page.

Read more about how to correctly acknowledge RSC content.

PCCP

ROYAL SOCIETY OF CHEMISTRY

PAPER

View Article Online
View Journal | View Issue

Cite this: *Phys. Chem. Chem. Phys.*, 2021, **23**, 574

The significance of the metal cation in guanine-quartet – metalloporphyrin complexes

Ana Stanojević, [a] Branislav Milovanović, [a] Ivana Stanković, [b] Mihajlo Etinski [a] and Milena Petković *[a]

Received 6th November 2020,
Accepted 1st December 2020

DOI: 10.1039/d0cp05798c

rsc.li/pccp

The planarity and the appropriate size of the porphyrin ring make porphyrin derivatives ideal ligands for stacking to guanine quartets and they could thus be used as anti-cancer drugs. In this contribution we analyzed complexes of a guanine quartet with a porphyrin molecule, magnesium porphyrin and calcium porphyrin. As magnesium and calcium ions are located in the center and above the porphyrin ring, respectively, the two metalloporphyrins are expected to have different impacts on the target. The optimized structures of the three systems revealed geometrical changes in the guanine quartet upon complexation: while stacking of porphyrin and magnesium porphyrin does not induce significant changes, calcium porphyrin considerably distorts the quartet's structure, which has significant implications for the binding properties among guanine molecules. *Ab initio* molecular dynamics simulations revealed that the systems perform small fluctuations around the equilibrium structures. The largest atom displacements are performed by the calcium ion. The interacting quantum atoms methodology enabled analysis of the binding properties in the studied complexes. Interestingly, although the proximity of the calcium ion is responsible for the quartet's pronounced deformation and weakening of guanine–guanine binding, it also enables stronger binding of the metal ion to the quartet, resulting in a more stable complex. These results imply that metalloporphyrin-like ligands with out-of-plane central ions might represent promising drug candidates in anti-tumor treatment.

1 Introduction

More than three decades ago, Sena and Gilbert[1] suggested that guanine molecules in guanine rich telomeres are prone to self-organization into larger assemblies than Watson–Crick base pairing. The ability to form quartets (composed of four guanine molecules) and quadruplexes (two or more stacked quartets) was soon recognized as a convenient property for these species to serve as anti-cancer pharmaceutical targets[2] as binding of the drug to the quartet would prevent the DNA chain from unfolding. The quartet's flat structure implied that planar ligands might represent suitable drug candidates as they could be stacked to the target.[3–15] Porphyrin-like compounds possess necessary properties that enable their successful stacking to a guanine quartet: the ring is flat, it is of comparable size to the quartet, and the presence of carefully selected substituents might enhance its interaction with the target. In a series of experiments, porphyrin's methyne hydrogen atoms were substituted with anionic[4,16] or more often with cationic groups,[5,17–24] while the central hydrogen atoms (the two protons) were replaced with metal ions.[23,25–31] The porphyrin ring and the central metal ion interact with the guanine molecules themselves, whereas lateral substituent groups communicate with the DNA backbone. So far, four guanine quartet–porphyrin derivative binding modes have been identified: (i) end stacking,[19,21–25,28,31] (ii) intercalation,[5,19,22,23,25,28,31] (iii) sandwich formation,[5,32] and (iv) external binding.[18,21,28]

In this work, only the end stacking binding mode is considered: we focused on the nature and the strength of the guanine quartet (G_4) – porphyrin derivative (PM) interaction, as well as on the role of the porphyrin ring and the metal ion in metalloporphyrins in the hydrogen bond properties in the quartet. Three drug models were studied: the porphyrin molecule (PH_2), magnesium porphyrin (PMg) and calcium porphyrin (PCa). We recently analyzed the influence of alkaline earth cations on hydrogen bond cooperativity in guanine quartets[33] and demonstrated that the metal cation considerably deforms the guanine quartet, which results in its large deformation energy, but at the same time enhances the interaction among guanine molecules. Herein, we extend that analysis to the impact of porphyrin stacking, along with the synergetic effect of the porphyrin ring and the alkaline earth cation on the quartet's hydrogen bond strength.

[a] *University of Belgrade – Faculty of Physical Chemistry, Studentski trg 12-16, 11 158 Belgrade, Serbia. E-mail: milena@ffh.bg.ac.rs*
[b] *Institute of Chemistry, Technology and Metallurgy, Njegoševa 12, 11 000 Belgrade, Serbia*

Since life, as we know it, could not exist without magnesium porphyrins, these species have been thoroughly investigated both experimentally and theoretically.[34–46] In addition to naturally occurring products, synthetic analogues have also attracted attention.[47,48] On the other hand, publications involving calcium porphyrins are scarce.[49–52] While substitution of the central protons with a magnesium cation results in a planar porphyrin derivative, the calcium ion is located above the porphyrin plane. When calcium porphyrin is stacked to another planar ligand, Ca^{2+} is found between the two planes, forming a so-called double-decker structure (see ref. 50 and references therein). Since both cations are doubly charged, their distinct positions in the two metalloporphyrins enabled us to access the influence of the ion's radius on the quartet–metalloporphyrin interaction. The conclusions are drawn from results obtained by employing the interacting quantum atoms approach, which has so far been used for analysis of numerous different systems, unraveling the nature and the strength of various inter- and intramolecular interactions.[33,53–68] The energy decomposition investigation presented in this work was performed *in vacuo*.

The manuscript is organized as follows. First, the computational details are presented. In the following section, the structural parameters of the three complexes are analyzed. Subsequently, a detailed investigation of interaction energies among different fragments is presented and the corresponding binding energies are analyzed. The results are summarized in the final section.

2 Computational details

Quantum-chemical calculations were performed with the Gaussian software[69] by employing the M06-2X functional[70] in conjunction with the 6-31+G(d) and 6-311+G(d) basis sets[71–75] and an ultrafine integration grid. It is well known that the M06-2X functional is able to provide a reliable description of non-covalent interactions,[33,64,76–83] while diffuse and polarization functions on carbon, nitrogen and oxygen atoms are expected to adequately model stacking interactions. The importance of including solvent effects was tested with the Polarizable Continuum Model (PCM) as implemented in the Gaussian software.[84] All optimized complexes have only real frequencies and thus represent stable species. We considered Bader charges, which were computed with the AIMAll software.[85]

Density functional based molecular dynamics simulations of the three complexes (PH_2, PMg and PCa) were performed with the CP2K program package.[86] We employed the GGA BLYP functional[87,88] corrected with the D3 scheme for dispersion interactions.[89] The mixed Gaussian and plane wave (GPW) method[90] was used to describe the system's electron density. We used the DZVP basis set for localized functions and plane waves for delocalized functions (with the cutoff and the relative cutoff set to 350 Ry and 50 Ry, respectively) to describe valence electrons, while core electrons were described with GTH type pseudopotentials.[91] The SCF convergence threshold was set to 5.0×10^{-7} a.u. All systems were equlibrated during a 2 ps long run with a timestep of 0.5 fs for integrating the classical equations of motion within a nonperiodic cubic box of a 25 Å cell constant and under the *NVT* ensemble. We employed the CSVR thermostat[92] to equlibrate the systems at 300 K. Production runs lasted 10 ps under the same conditions after equlibration. The power spectra of the C═O stretching vibration were computed from 10 ps long *NVE* trajectories initiated from the last *NVT* configurations. The power spectra were determined by the TRAVIS program.[93,94] We also computed those spectra for G_4–G_4, G_4–Mg–G_4 and G_4–Ca–G_4 quadruplexes by using the same computational procedures as for the porphyrin complexes. The *NVE* trajectories were initiated from the *NVT* trajectories examined in our previous work.[95]

2.1 Interacting quantum atoms

The energy partitioning methodology known as Interacting Quantum Atoms[53,54] (IQA) is based on Bader's quantum theory of atoms in molecules,[96,97] according to which a molecule can be divided into atomic subspaces. Selected atoms form fragments $\mathscr{F}$; the interaction energy between fragments $\mathscr{F}_i$ and $\mathscr{F}_j$, $E_{\mathrm{int}}^{\mathscr{F}_i\mathscr{F}_j}$, is an additive property composed of the interaction energies among each pair of atoms I (that belongs to $\mathscr{F}_i$) and J (that belongs to $\mathscr{F}_j$):

$$\begin{aligned} E_{\mathrm{int}}^{\mathscr{F}_i\mathscr{F}_j} &= 1/2 \sum_{\mathrm{I}\in\mathscr{F}_i} \sum_{\mathrm{J}\in\mathscr{F}_j} V_{\mathrm{inter}}^{\mathrm{IJ}} = 1/2 \sum_{\mathrm{I}\in\mathscr{F}_i} \sum_{\mathrm{J}\in\mathscr{F}_j} \left(V_{\mathrm{cl}}^{\mathrm{IJ}} + V_{\mathrm{xc}}^{\mathrm{IJ}}\right) \\ &= E_{\mathrm{int}}^{\mathscr{F}_i\mathscr{F}_j} + E_{\mathrm{xc}}^{\mathscr{F}_i\mathscr{F}_j} \end{aligned} \tag{1}$$

In the above equation, the interaction energy among each pair of atoms $V_{\mathrm{inter}}^{\mathrm{IJ}}$ is written as a sum of its classical $V_{\mathrm{cl}}^{\mathrm{IJ}}$ and its non-classical $V_{\mathrm{xc}}^{\mathrm{IJ}}$ contribution, which constitute analogue energy components that describe the fragment–fragment interaction ($E_{\mathrm{cl}}^{\mathscr{F}_i\mathscr{F}_j}$ and $E_{\mathrm{xc}}^{\mathscr{F}_i\mathscr{F}_j}$).

A fragment's deformation energy $E_{\mathrm{def}}^{\mathscr{F}_i}$ is defined with respect to its reference state, which is an isolated fragment with the geometry it adopts in the complex. The sum of the interaction and deformation energies defines the IQA binding energy:

$$E_{\mathrm{IQA}}^{\mathrm{bind}} = 1/2 \sum_i \sum_j E_{\mathrm{int}}^{\mathscr{F}_i\mathscr{F}_j} + \sum_i E_{\mathrm{def}}^{\mathscr{F}_i}. \tag{2}$$

The number of fragments depends on the phenomenon of interest. In the current manuscript we employed several fragmentation schemes for the guanine quartet – metalloporphyrin complex, and they are based on: (i) two fragments (G_4 and PH_2/PMg/PCa), (ii) three fragments (G_4, P and H_2/Mg/Ca) and (iii) five fragments (four guanine molecules and PH_2/PMg/PCa). IQA analysis was performed with the AIMAll program[85] by employing the promega5 basin integration method. The precision of this approach, when applied on the system of interest, can be accessed by comparing the IQA binding energy $E_{\mathrm{IQA}}^{\mathrm{bind}}$ to

the SCF binding energy E_{SCF}^{bind}:

$$E_{SCF}^{bind} = E_{SCF}^{system} - \sum_i E_{SCF}^{\mathscr{F}_i}. \quad (3)$$

Let us consider, for example, G_4–PCa composed of six fragments: four guanine molecules, the porphyrin ring and the calcium ion. The IQA and SCF binding energies amount to −1336 and −1310 kJ mol^{-1}, respectively. Such a deviation is a consequence of numerical integrations: this system contains 101 atoms, therefore $101 \times (101 - 1)/2 = 5050$ pair interactions are considered. Although the absolute value of the deviation equals 26 kJ mol^{-1}, it represents only 2% of the SCF binding energy. We can also analyze those results from another perspective: if we consider just the quartet, the difference between the IQA and SCF binding energies equals 11 kJ mol^{-1}. Since the quartet is composed of four identical units, there are six pairs of guanine molecules (four neighboring and two diagonal pairs). If we neglect interactions among diagonal molecules and only consider neighbors, the average deviation of the binding energy per guanine–guanine pair is below 3 kJ mol^{-1}, which is acceptable for the current analysis.

3 Results and discussion

We start the analysis by inspecting the optimized geometries of the three complexes, which paves the way to the study of the interactions among different fragments.

3.1 Basis set convergence and solvent effect

Let us first analyze the quality of the employed level of theory. We will use the term complexation energy $E_{complex}$ for the energy difference between the optimized structure of the complex and the optimized structures of the target and the ligand (note that the term binding energy refers to the value computed by taking the geometries of the target and the ligand that they adopt in the complex). Complexation energies computed at different levels of theory are summarized in Table 1. The M06-2X functional was employed in all cases. First, we will consider the results obtained by optimizing the structures with different basis sets, which are presented in the upper part of the table. Taking the 6-31+G(d) basis set and performing calculations *in vacuo* gives for G_4–PH_2, G_4–PMg, and G_4–PCa complexation energies of −128, −137, and −332 kJ mol^{-1}, respectively. Employment of the 6-311+G(d) basis set results in values that are larger (*i.e.* more negative) by 10 and 7 kJ mol^{-1} for G_4–PH_2 and G_4–PMg, and weaker (less negative) by 23 kJ mol^{-1} for G_4–PCa. Almost identical $E_{complex}$ values are obtained at the 6-311+G(d)//6-31+G(d) level, which confirms that the double-zeta basis provides reliable geometries of the ligand, the target and the complex. Finally, let us consider solvent effects by taking the double-zeta geometries and performing triple-zeta single point energy calculations in the presence of the solvent included through the Polarizable Continuum Model (PCM) as implemented in the Gaussian software.[84] The complexation energy is only 3 and 9 kJ mol^{-1} lower for G_4–PH_2 and G_4–PMg compared to the 6-31+G(d) *in vacuo* values, but it is as much as 82 kJ mol^{-1} lower for G_4–PCa. The presented results indicate less significant importance of solvent inclusion in the absence of metal ions and in the case when the metal ion is shielded by the porphyrin ring, as well as its significance if the metal ion does not lie in the plane of the porphyrin ring. However, the $E_{complex}$ values computed at each level of theory presented in Table 1 are significantly larger in G_4–PCa with respect to the other two complexes. These results demonstrate that neglection of the solvent does not alter the qualitative picture and that the IQA procedure (in which solvent effects have not been implemented yet) offers a reliable description of the studied systems. Additionally, since the 6-311+G(d) basis set only slightly alters the 6-31+G(d) geometries and complexation energy values, IQA analysis was performed with the double-zeta basis set.

Table 1 Complexation energy $E_{complex}$ (in kJ mol^{-1}) computed with different basis sets *in vacuo* and by including implicit solvent for G_4–PH_2, G_4–PMg, and G_4–PCa

	$E_{complex}$		
Basis set & vacuum or solvent	G_4–PH_2	G_4–PMg	G_4–PCa
6-31+G(d)	−128	−137	−332
6-311+G(d)	−138	−144	−309
6-311+G(d)//6-31+G(d)	−138	−144	−310
6-311+G(d)(PCM)//6-31+G(d)	−125	−128	−250

3.2 Geometric considerations

Optimized structures of the three complexes are presented in Fig. 1. The area of the porphyrin ring is slightly smaller than the one of the quartet. Both species are essentially planar, which enables effective stacking. The small size of the magnesium cation allows its settlement in the center of the porphyrin ring. Consequently, substitution of the two central porphyrin protons with Mg^{2+} does not significantly alter the quartet–porphyrin complex geometry. However, the larger radius of the calcium cation compared to its analogue with fewer electrons disables its residence in the center of the porphyrin ring and is responsible for the ion's location between G_4 and P. Such a structure enables simultaneous compensation of the negative charge located in the porphyrin ring and on guanine oxygen atoms.

The fact that smaller cations fit in a certain cavity while larger ones are not able to do so is a well-known fact for metal ion complexes with guanine quartets: while Na^+ is able to accommodate itself between the oxygen atoms of the four guanine molecules, K^+ is located above the quartet.[33,98–102] Marek and coworkers[102] demonstrated that stacking G_4–Na to another guanine quartet pulls the metal ion into the cavity between the quartets, enabling it to stabilize the structure through the compensation of the negative charge of all eight oxygen atoms in the quadruplex. While in G_4–K–G_4 the cation is positioned at the midpoint between the quartets, the sodium ion in G_4–Na–G_4 can be found at two equivalent positions closer to either of the two G_4 systems, as analyzed by van Mourik and Dingley.[101] This is to be contrasted with the situation in magnesium porphyrin, as its stacking to G_4 does

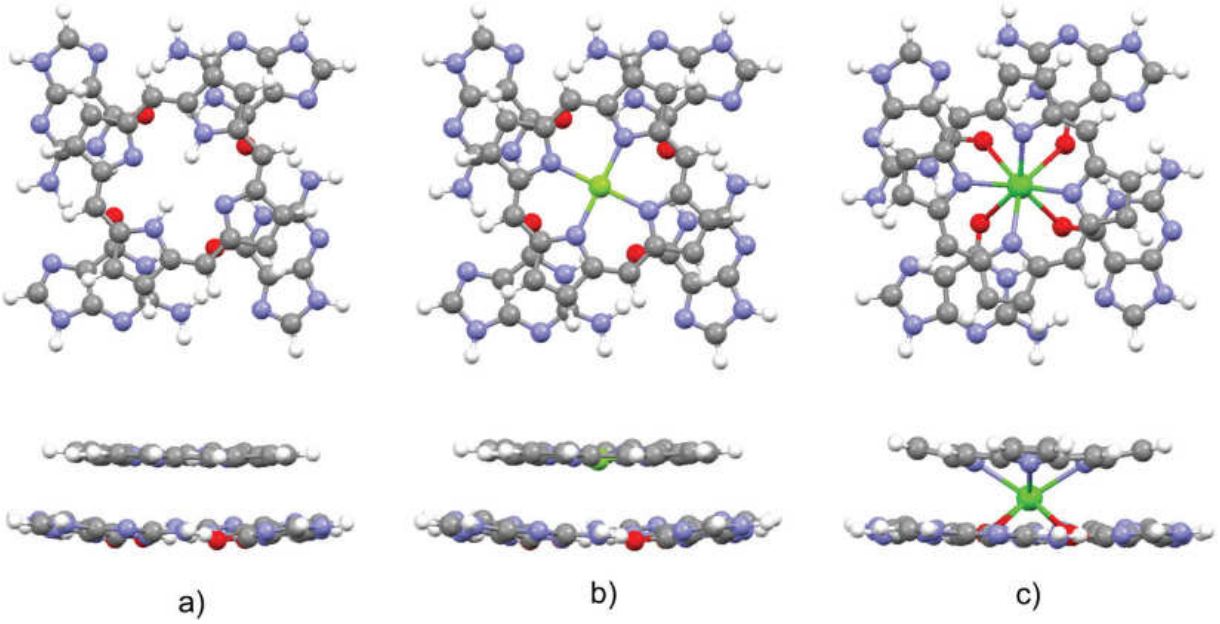

Fig. 1 Optimized structures of the complexes (top and side view) formed by G_4 and (a) PH_2, (b) PMg and (c) PCa.

not withdraw Mg^{2+} from the porphyrin ring: since the ring is charged, unlike the quartet, it does not allow significant displacement of the cation.

In order to obtain evidence of whether the structure of the guanine quartet is deformed upon complex formation, the geometry of the free quartet is overlapped with its analogues from each of the three complexes, Fig. 2. Oxygen atoms were used to orient the quartets. Let us label them O_1, O_2, O_3 and O_4 in the monomers down-left, down-right, up-right and up-left, respectively. O_1 is set as the origin of the coordinate system, and the *x*-axis is formed by O_1 and O_2, whereas O_1, O_2 and O_3 define the *xy*-plane. While PH_2 and PMg do not generate significant distortion in G_4, calcium's proximity causes electron redistribution in the quartet, which is reflected in the decrease of the oxygen–oxygen distance from 4.165 Å in unbound G_4, 4.168 Å in G_4–PH_2 (average value) and 4.104 Å in G_4–PMg, to only 3.111 Å in G_4–PCa. This simple analysis implies that metal–porphyrin complexes do not significantly perturb the quartet, provided that the size of the divalent metal cation is small enough to fit in the center of the porphyrin ring.

As can be seen in Fig. 2, each oxygen atom might form hydrogen bonds with hydrogen atoms of both amino and imino groups of the neighbor. The question of whether bifurcated hydrogen bonds exist in G_4 was analyzed by various authors[103,104] (see the discussion in ref. 33). The M06-2X functional in free G_4 favors the structure with bifurcated hydrogen bonds. The average $O\cdots H_{amino}$ distance in G_4, G_4–PH_2, G_4–PMg, and G_4–PCa equals 2.037, 2.010, 2.044 and 3.445 Å, respectively, while the average electron density at the $O\cdots H_{amino}$ bond critical points in G_4, G_4–PH_2, and G_4–PMg amounts to 0.023, 0.024, and 0.021 a.u., respectively, suggesting the existence of bifurcated hydrogen bonds in these three

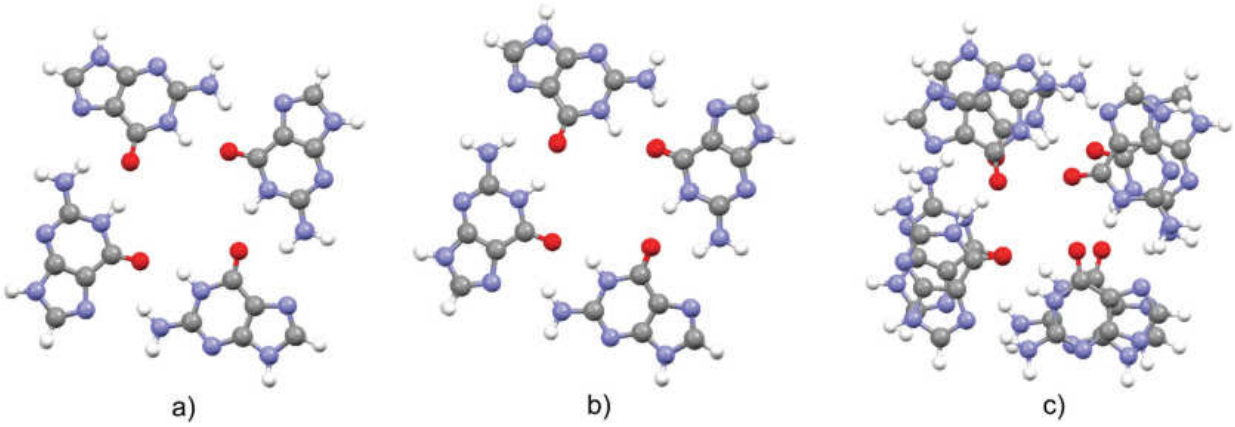

Fig. 2 Overlapped structures of a guanine quartet in free G_4 with the quartet structures in its complexes with (a) PH_2, (b) PMg and (c) PCa (see the text for details).

complexes and comparable O···H_{amino} hydrogen bond strength. On the other hand, the O···H_{amino} bond critical point in G_4–PCa does not exist. Thus, the calcium ion causes vanishing of bifurcated hydrogen bonds in the guanine quartet.

3.3 Are thermal fluctuations in G_4–PM complexes significant?

Insight into the system's flexibility can be gained from *ab initio* molecular dynamics simulations. The changes of the G_4^{COM}–P^{COM}, G_4^{COM}–Mg/Ca and Mg/Ca–P^{COM} distances (the abbreviation COM is used for a center of mass) in the three systems are displayed in Fig. 3, while their average values are shown in Table 2. The metal cation does not significantly alter the average G_4^{COM}–P^{COM} distance. Its most pronounced fluctuations are observed in G_4–PCa. As expected, the G_4^{COM}–Mg separation is significantly larger compared to $d(G_4^{COM}$–Ca), but it is characterized by considerably smaller variations. Finally, the average Mg–P^{COM} distance is almost four times smaller compared to the calcium analogue. Interestingly, the curves that correspond to the G_4^{COM}–Ca and Ca–P^{COM} distances are out of phase, which indicates calcium's oscillation between two negatively charged regions. The time evolution of selected distances in the analyzed complexes implies small geometry changes due to the thermal motion.

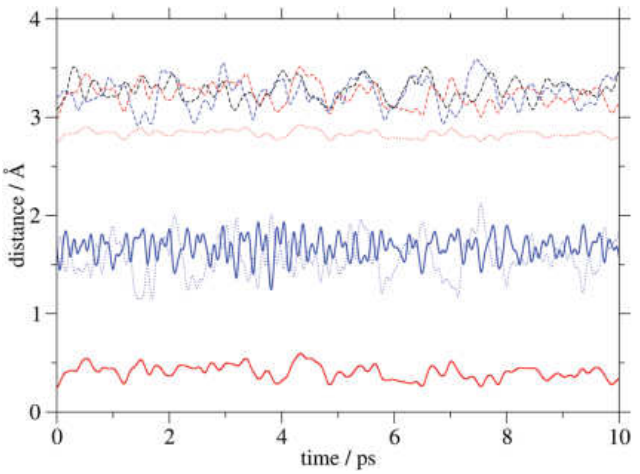

Fig. 3 Distances (COM stands for a center of mass) between G_4^{COM} and P^{COM} (dashed lines), G_4^{COM} and Mg/Ca (dotted lines), and Mg/Ca and P^{COM} (full lines) in PH_2 (black), PMg (red) and PCa (blue).

Table 2 Average distances and their standard deviations (in Å) between G_4^{COM} and P^{COM}/G_4^{COM}, G_4^{COM} and Mg/Ca, and Mg/Ca and P^{COM}/G_4^{COM} in G_4–PH_2/G_4–G_4, G_4–PMg/G_4–Mg–G_4, and G_4–PCa/G_4–Ca–G_4 (COM represents center of mass)

	$d(G_4^{COM}$–$P^{COM})$	$d(G_4^{COM}$–Mg/Ca)	d(Mg/Ca–P^{COM})
G_4–PH_2	3.280 ± 0.101		
G_4–PMg	3.233 ± 0.107	2.832 ± 0.036	0.405 ± 0.072
G_4–PCa	3.248 ± 0.145	1.571 ± 0.187	1.676 ± 0.115
	$d(G_4^{COM}$–$G_4^{COM})$	$d(G_4^{COM}$–Mg/Ca)	d(Mg/Ca–G_4^{COM})
G_4–G_4	4.110 ± 0.355		
G_4–Mg–G_4	3.809 ± 0.109	1.751 ± 0.056	2.068 ± 0.054
G_4–Ca–G_4	3.404 ± 0.120	1.684 ± 0.142	1.727 ± 0.162

3.4 Intermolecular interactions and binding energies

Let us now turn to intermolecular interactions. We will analyze the following: (i) the impact of the ligand on the guanine–guanine interaction, (ii) the porphyrin ring – metal cation interaction, (iii) the ligand – target interaction, and finally (iv) the deformation and binding energies.

3.4.1 Guanine–guanine interaction. Interaction energies among guanine molecules $\mathscr{G}$ are compiled in Table 3. In the absence of the ligand, E_{int} amounts to −253 and −20 kJ mol^{-1} between neighboring and diagonal molecules, respectively. Around 40% of the interaction energy among the neighbors is due to Coulomb interactions, whereas the interaction between diagonal guanines is entirely classical. Stacking of the porphyrin molecule PH_2 does not significantly perturb the guanine–guanine interaction, which is also the case with magnesium porphyrin. A similar situation was encountered in guanine quadruplexes as it was demonstrated that the energies of N–H···O and N–H···N hydrogen bonds do not significantly change upon stacking of two guanine quartets.[102] While sole alkaline earth cations weaken the guanine–guanine interaction,[33] PMg has a negligible influence on the quartet's building blocks due to Mg's position in the center of the porphyrin ring, which keeps it distanced from G_4 (Fig. 3 and Table 2). This is not the case with PCa and the proximity of the calcium ion is reflected in slight strengthening of the $\mathscr{G}$–$\mathscr{G}$ interaction. Interestingly, Ca^{2+} decreases the classical component and increases the exchange–correlation term between the neighbors. On the other hand, the interaction among diagonal terms remains completely electrostatic and is basically negligible. This behavior differs from the one in Na^+ and K^+ sandwiched between two quartets[102] – while the sodium ion does not significantly affect the guanine–guanine interaction due to the more pronounced G_4 planarity in the presence of the cation, the potassium ion weakens the hydrogen bonds in G_4 as a result of the stronger oxygen–cation interaction. The opposite influence of K^+ and Ca^{2+} is most likely due to different charges, as the calcium ion causes pronounced quartet distortion, which results in the decrease of the guanine–guanine distance, Fig. 2, and consequently stronger intermolecular interactions in G_4. This finding is in accord with the results presented by van Mourik and Dingley[101] who analyzed complexes of guanine quartets and alkali cations, and demonstrated that the cation

Table 3 Interaction energies E_{int} with their classical E_{cl} and non-classical E_{xc} components in kJ mol^{-1} between neighboring and diagonal guanine molecules in G_4, G_4–PH_2, G_4–PMg and G_4–PCa

	Neighboring			Diagonal		
Fragments	E^{int}	E^{cl}	E^{xc}	E^{int}	E^{cl}	E_{xc}
G_4	−253	−107	−146	−20	−20	0
G_4–PH_2	−258	−108	−150	−20	−20	0
G_4–PMg	−258	−108	−150	−20	−20	0
G_4–PCa	−278	−88	−190	−8	−8	0

decreases the distance between the oxygen atoms. The decrease in the O–O distance is even more pronounced in the presence of alkaline earth cations.

The carbonyl group stretching vibration is a sensitive probe for non-covalent interactions in quadruplexes. This mode exhibits in a quadruplex a significant spectral red-shift with respect to a single strand structure due to the hydrogen bonding with other guanine bases, as well as the interaction with a cation located between the quartets.[105] In order to understand to what extent thermal motion alters the conclusions from the static calculations, we computed the C═O stretching power spectra for the examined systems, Fig. 4. The most intense peak in each spectrum is due to the C═O stretching, whereas the two peaks on the red side of the spectra arise from vibrational couplings to other modes. The substitution of two porphyrin protons with Mg^{2+} results in the C═O stretching mode's small red-shift of 11 cm^{-1}. This is in accordance with our analysis of the optimized geometries of the G_4–PH_2 and G_4–PMg complexes in which we demonstrated that the magnesium ion has a negligible influence on the guanine–guanine interaction. On the other hand, Ca^{2+} strengthens the *G*-*G* interaction, which is reflected in the red-shift of the C═O stretching frequency by 56 cm^{-1} relative to G_4–PH_2. Therefore, thermal fluctuations do not modify the conclusions drawn from the analysis performed at the optimized geometries.

The C═O stretching power spectra of a stacked guanine quartet G_4–G_4 and its two analogues with sandwiched magnesium and calcium ions are also displayed in Fig. 4. The average distances of the two quartets in the quadruplexes are larger than the average distances between the quartet and the porphyrin ligands, Table 2. Unlike G_4–PM complexes in which Mg^{2+} is located within the ligand, whereas Ca^{2+} is not, both cations are located between the quartets in both quadruplexes, analogously to quadruplexes with Na^+ and K^+.[102] Note that the Mg^{2+} cation is closer to one of the quartets, Table 2, similarly to Na^+.[101] The fact that Ca^{2+} is closer to the quartet in G_4–PCa compared to G_4–Ca–G_4 is reflected in a more pronounced red shift of the C═O stretching mode in the complex with calcium porphyrin.

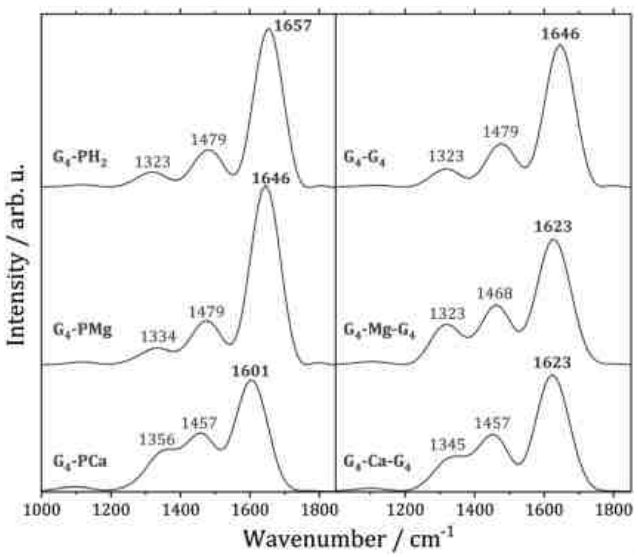

Fig. 4 Power spectra of the C═O stretching vibration. Left: G_4–PM complexes (M = H_2, Mg, Ca). Right: Guanine quadruplex G_8 and its sandwiches with Mg and Ca ions.

Marek and coworkers[106] studied Na^+ and K^+ ions stacked in artificial DNA quadruplexes (8-halo-9-dezaxanthines) and demonstrated that the metal ions are responsible for the electron density redistribution in both quartets, with the smaller ion causing significant electron polarization towards the cation, while the larger ion shows a tendency of electron sharing with the quartet. The delocalization indices for O–Mg bonds in G_4–PMg and O–Ca bonds in G_4–PCa amount to 4×10^{-4} and 0.077 a.u., respectively. The significantly more pronounced electron sharing with the heavier cation can in the case of the porphyrin ligands be ascribed to the nature of the metal ion, as its larger radius is responsible for its proximity to the quartet, which results in larger delocalization indices.

3.4.2 The two metalloporphyrins: porphyrin ring–cation interaction. We demonstrated that the nature of the ion affects the guanine–guanine interaction. Inversely, the proximity of the quartet also influences the interaction between the metal ion and the porphyrin ring, Table 4. G_4 weakens the P–Mg and P–Ca interaction roughly by 50 and 500 kJ mol^{-1}, respectively. In the case of magnesium porphyrin, it is entirely due to the charge transfer, which diminishes Coulomb interactions, whereas in calcium porphyrin the quartet noticeably affects both the E_{cl} and the E_{xc} term.

3.4.3 Target–ligand interaction. We now turn to the interactions between the quartet and the ligand, the quartet and the porphyrin ring and the quartet and the central cation. The results are summarized in Table 5. The interaction between G_4 and PH_2, as well as between G_4 and PMg, is predominantly non-classical. Substitution of the central protons with Mg^{2+} slightly strengthens the stacking. However, the G_4–PCa interaction is roughly two times stronger compared to the other two analogues. Replacement of Mg^{2+} with Ca^{2+} increases the exchange–correlation term by more than 35% and the Coulomb term by 20 times. These results reflect differences in the system properties that arise from the distinct distances between Mg and Ca cations and the quartet's center of mass. In the optimized structures they amount to 2.713 and 1.337 Å, respectively, and are responsible for significant strengthening of the Ca^{2+}–quartet interaction compared to its smaller counterpart. While the Mg^{2+}–G_4 interaction is basically purely electrostatic, the non-classical term of the Ca^{2+}–G_4 interaction amounts to almost −170 kJ mol^{-1}, which represents close to 20% of

Table 4 Interaction energies E_{int} with their classical E_{cl} and non-classical E_{xc} components in kJ mol^{-1} between P and M (M = Mg and Ca) in PM and G_4–PM

	P & M in PM			P & M in G_4–PM		
Fragments	E_{int}	E_{cl}	E_{xc}	E_{int}	E_{cl}	E_{xc}
PMg	−3107	−2710	−396	−3051	−2660	−391
PCa	−2664	−2202	−462	−2155	−1857	−298

Table 5 Interaction energies E_{int} with their classical E_{cl} and non-classical E_{xc} components in kJ mol^{-1} between G_4 and PM, G_4 and M, and G_4 and P (M = H_2, Mg, and Ca)

	G_4 & PM			G_4 & M			G_4 & P		
Fragments	E_{int}	E_{cl}	E_{xc}	E_{int}	E_{cl}	E_{xc}	E_{int}	E_{cl}	E_{xc}
G_4–PH_2	−697	−16	−681	−57	−57	0	−640	41	−681
G_4–PMg	−714	−19	−695	−128	−127	−1	−586	108	−694
G_4–PCa	−1357	−412	−945	−908	−741	−167	−449	329	−778

the overall metal–quartet interaction. This finding is consistent with results obtained for the interaction of the pure metal with the guanine quartet.[33] It results from more pronounced electron sharing with the heavier metal (see Section 3.4.1) as discovered in artificial DNA quadruplexes with stacked Na^+ and K^+ ions.[106] According to the results presented in Table 1, the solvent reduces the difference in the G_4–PCa and G_4–PMg complexation energies by 30%. Since $E_{int}^{G_4-PCa} \approx 2 \times E_{int}^{G_4-PMg}$, the corresponding term in a solvent is also expected to be significantly larger for calcium porphyrin.

Concerning the interaction between the quartet and the porphyrin ring, it weakens in the order PH_2, PMg, PCa. This behavior is a consequence of the accumulation of the negative charge in the porphyrin ring (−0.971 *e*, −1.638 *e* and −1.629 *e*, respectively), whereas the charges of the quartet change in the order −0.072 *e*, −0.083 *e* and −0.114 *e*. Consequently, the electrostatic repulsion is significantly increased on going from PH_2 to PCa, despite the system's stabilization through non-classical interactions. The charges of the two central protons, the magnesium ion and the calcium ion equal +1.051 *e*, +1.728 *e* and +1.749 *e*, respectively, which is reflected in the corresponding E_{cl} term.

3.4.4 Deformation and binding energies. At this point we are able to analyze the deformation and binding energies of the investigated species, Table 6.

First, consider a two-fragment ligand–target complex. The small adjustment of the ligand's structure upon complexation is the reason behind the comparable deformation energies of PH_2 and PMg. $E_{def}^{G_4}$ and E_{bind}^{IQA} in G_4–PH_2 and G_4–PMg are essentially the same, which is not surprising as the geometry of the quartet and the interaction energies between G_4 and PM are quite similar in the two complexes. On the other hand, the considerable distortion of the target and the ligand in G_4–PCa is reflected in significantly larger deformation energies of both fragments. The strong interaction between the quartet and calcium porphyrin is, however, responsible for the significantly stronger binding between this ligand and the target compared to the other two analogues.

In order to get a closer look at the importance of the size of the metal ions, we will artificially separate the cation from the porphyrin ring. We want to compare the roles of the magnesium and the calcium ion, while the results for PH_2 are presented for consistency (in this case M stands for the two hydrogens). Since the Mg–P interaction is almost 50% stronger than the Ca–P interaction in the corresponding complexes, Table 4, the deformation energy of the porphyrin skeleton and the metal ion is much larger in PMg. Note that the porphyrin ring has a stabilizing effect on the cation, which results in the ion's negative deformation energy. Taking into account the deformation and interaction energies between the three particles leads to larger binding energy in G_4–P–Mg with respect to G_4–P–Ca by almost 300 kJ mol^{-1}.

Finally, let us address the following questions: how does the ligand affect the binding among guanine molecules and what is the overall binding energy between the five molecules that constitute the complex (four guanine molecules and the metalloporphyrin)? We analyzed the ligand's influence on the guanine–guanine interaction energy but so far we did not consider the $\mathscr{G}$ deformation energies. The deformation energies of a single guanine molecule in G_4, G_4–PH_2, G_4–PMg and G_4–PCa amount to 170, 247, 247 and 332 kJ mol^{-1}, respectively. It should be emphasized that the deformation energy of a guanine molecule is not equal to a quarter of the quartet's deformation energy due to different fragment partitioning (*i.e.* four isolated guanine molecules as compared to a quartet). Note the significantly larger $\mathscr{G}$ deformation energy in G_4–PCa with respect to its two counterparts, while all of them notably exceed $E_{def}^{\mathscr{G}}$ in a non-stacked quartet. The binding energies between guanine molecules in G_4 and in the three complexes equal −372, −84, −84 and +152 kJ mol^{-1}, respectively. These results signify that all three ligands weaken the binding among $\mathscr{G}$'s: G_4–PH_2 and G_4–PMg have basically identical impact, while complexation to PCa leads to a positive binding energy among the quartet's constituents. Further, we will estimate the binding energies in a five-particle quartet–metalloporphyrin system, treating the complex G_4–PM as being composed of four guanine molecules and a metalloporphyrin ligand. The values for G_4–PMg and G_4–PCa amount to −495 and −741 kJ mol^{-1}, respectively. Hence, although the calcium ion distorts the quartet and is responsible for the guanines' large deformation energy, it slightly enhances the $\mathscr{G}$–$\mathscr{G}$ interaction, Table 3, and as the $\mathscr{G}$–Ca interaction is substantial, the result is strong binding between the five fragments (particles).

Table 6 Deformation E_{def} and binding E_{bind}^{IQA} energies in kJ mol^{-1} when considering two (G_4 and PM) or three (G_4, P and M) fragments in G_4–PM complexes (M = H_2, Mg and Ca)

	E_{def}				E_{bind}^{IQA}	
Fragments	G_4	PM	P	M	G_4 & PM	G_4 & P & M
G_4–PH_2	291	298	585	−2203	−108	−4119
G_4–PMg	295	302	788	−339	−117	−3021
G_4–PCa	472	465	454	−148	−420	−2734

The binding energies presented in Table 6 are estimated by considering the geometries the fragments adopt in the complexes. On the other hand, the complexation energy for G_4–PH_2 (computed by considering two optimized species, G_4 and PH_2) equals −128 kJ mol^{-1}, Table 1, which represents approximately 13 kJ mol^{-1} weaker binding compared to two stacked quartets.[102] In other words, two planar aromatic ligands of similar size bind with comparable strength to the guanine quartet. These results

imply that fine tuning of the interaction between a specific planar ligand (with similar shape and dimensions to G_4) and the guanine quartet can be achieved by a careful choice of the metal cation. This conclusion is in agreement with the results of Meyer *et al.*[107] who showed that the most significant interaction in G_4–M–G_4 complexes (M = Na^+, K^+) is the one between the quartet and the metal ion. Pratviel and coworkers[26] performed experimental analysis of binding metalloporphyrins to G_4 and concluded that the ligand's metal does not significantly affect the binding energy. They employed four metal ions: Ni^{2+}, Mn^{3+}, Co^{3+}, and Au^{3+}. Their ionic radii amount to 0.69, 0.64/0.58 (high/low spin), 0.61/0.54 (high/low spin), and 0.85 Å, respectively, whereas the corresponding values for Mg^{2+} and Ca^{2+} equal 0.72 and 1.00 Å (in all cases six-coordinated ions were considered).[108] Due to their small size, all four metal ions considered in the experiments are located in the center of the porphyrin ring, as is the case with the magnesium analogue. In accordance with our results, their impact on the ligand's binding energy is expected to be small.

4 Conclusions

In this contribution we analyzed stacking of porphyrin (PH_2), magnesium porphyrin (PMg) and calcium porphyrin (PCa) to a guanine quartet (G_4) in the gas phase from the viewpoint of interacting quantum atoms. The guanine quartet is regarded as an anti-cancer pharmaceutical target that can be aimed at with a porphyrin-like (PM) ligand. While the magnesium ion is located in the center of the porphyrin ring, the calcium ion is sandwiched between G_4 and PM. The reason for choosing Mg^{2+} and Ca^{2+} is twofold: (i) since the impact of these two ions on the quartet had already been established,[33] G_4–PM study made it possible to assess the cooperative effect of these metal cations and the porphyrin ring on the properties of the quartet; and (ii) due to the distinct position of the divalent metal ion with respect to the porphyrin ring, this investigation enabled us to evaluate the significance of the ion's radius (which dictates the cation's position) to the ligand's binding affinity to the target.

Complexation of G_4 with PH_2 and PMg does not significantly alter the quartet's geometry, which results in a negligible change of the guanine–guanine ($\mathscr{G}$–$\mathscr{G}$) interaction. This is to be contrasted with the G_4–PCa formation, which intensifies the interaction among guanine monomers. Namely, the small radius of Mg^{2+} is responsible for the planar PMg structure with a strong P–Mg interaction where the ring acts as a shield, preventing the cation from engaging in significant interactions with the target. On the other hand, the large radius of the Ca^{2+} ion forbids its settlement within the porphyrin ring, which results in a smaller G_4–Ca^{2+} distance in G_4–PCa. Consequently, the guanine–guanine interaction is stronger in the complex with calcium porphyrin, as is the quartet–ion interaction.

In order to access the complex stability, we computed binding energies $E_{\mathrm{bind}}^{\mathrm{IQA}}$ according to three fragmentation schemes. First, the fragments were chosen to be G_4 and PM, in which case $E_{\mathrm{bind}}^{\mathrm{IQA}}$ of G_4–PCa is more than three times larger than the one for G_4–PMg. According to the second scheme, the fragments are the quartet, the porphyrin ring and the metal cation. Due to the large P–Mg interaction, the binding energy with the magnesium ion is almost 10% larger compared to the calcium analogue. Finally, we used a five fragment system composed of four guanine molecules and PM (M = Mg, Ca). This fragmentation strategy takes into account the fact that guanine molecules are held through non-covalent interactions. In this case, the binding energy is around 50% larger for the complex that contains the calcium ion. Although Ca^{2+} is responsible for the larger deformation energy of the guanine molecules, it strengthens their mutual interaction, while its proximity to the quartet results in a strong guanine–Ca^{2+} interaction. Consequently, the binding in the ($\mathscr{G}$–$\mathscr{G}$–$\mathscr{G}$–$\mathscr{G}$)–PCa system is significantly more pronounced compared to the Mg counterpart.

The computed complexation energies are considerably larger for the complex with calcium porphyrin compared to the one with magnesium porphyrin, both in a vacuum and in water. In this case the solvent does not alter the qualitative picture, and the energy decomposition analysis was performed in a vacuum. Moreover, the presence of the DNA backbone and the closest bases was not taken into account as the model would be far too large for quantum chemical calculations. On the other hand, *ab initio* molecular dynamics simulations demonstrated that the system does not undergo large amplitude motion during a 10 ps run, which confirms that results from static calculations represent a reliable description of the phenomenon we are interested in, *i.e.* binding of the ligand to the target. The presented results imply that metalloporphyrins with larger metal ions, which are not coplanar with the porphyrin ring, are liable to form more strongly bound complexes compared to the planar analogues and thus might represent superior candidates for anti-cancer drugs. As the number of metal ions that fulfill this condition is limited, further research might be aimed at the synthesis of a porphyrin-like substrate with an out-of-plane central metal cation.

Conflicts of interest

There are no conflicts to declare.

Acknowledgements

This work was financially supported by the Ministry of Education, Science, and Technological Development of the Republic of Serbia within the framework of contract number: 451-03-68/2020-14/200146. Numerical simulations were run on the PARADOX cluster at the Scientific Computing Laboratory of the Institute of Physics, Belgrade, supported in part by the Ministry of Education, Science, and Technological Development of the Republic of Serbia. The research leading to these results has been co-funded by the European Commission under the H2020 Research Infrastructures contract no. 675121 (project VI-SEEM).

References

1 D. Sen and W. Gilbert, *Nature*, 1988, **334**, 364–366.

2 S. Neidle and M. A. Read, *Biopolymers*, 2001, **56**, 195–208.
3 C. A. Hunter and J. K. M. Sanders, *J. Am. Chem. Soc.*, 1990, **112**, 5525–5534.
4 Y. Li, C. R. Geyer and D. Sen, *Biochemistry*, 1996, **35**, 6911–6922.
5 N. V. Anantha, M. Azam and R. D. Sheardy, *Biochemistry*, 1989, **37**, 2709–2714.
6 F. J. M. Hoeben, P. Jonkheijm, E. W. Meijer and A. P. H. J. Schenning, *Chem. Rev.*, 2005, **105**, 1491–1546.
7 Y. Qi and L. G. Hector Jr., *Appl. Phys. Lett.*, 2007, **90**, 081922.
8 J. Antony and S. Grimme, *Phys. Chem. Chem. Phys.*, 2008, **10**, 2722–2729.
9 R. Podeszwa and K. Szalewicz, *Phys. Chem. Chem. Phys.*, 2008, **10**, 2735–2746.
10 M. Birowska, K. Milowska and J. A. Majewski, *Acta Phys. Pol.*, 2011, **120**, 845–848.
11 G. V. Janjić, P. V. Petrović, D. B. Ninković and S. D. Zarić, *J. Mol. Model.*, 2011, **17**, 2083–2092.
12 X. Qian, Y. Wang, W. Li, J. Lu and J. Li, *2D Mater.*, 2015, **2**, 032003.
13 R. Nozawa, H. Tanaka, W. Cha, Y. Hong, I. Hisaki, S. Shimizu, J.-Y. Shin, T. Kowalczyk, S. Irle, D. Kim and H. Shinokubo, *Nat. Commun.*, 2016, **7**, 13620.
14 D. N. Sredojević, P. V. Petrović, G. V. Janjić, E. N. Brothers, M. B. Hall and S. D. Zarić, *J. Mol. Model.*, 2014, **22**, 30.
15 M. Durec, F. Zaccaria, C. Foncesca Guerra and R. Marek, *Chem. – Eur. J.*, 2016, **22**, 10912–10922.
16 H. Yaku, T. M. D. Miyoshi and N. Sugimoto, *Molecules*, 2012, **17**, 10586–10613.
17 F. X. Han, R. T. Wheelhouse and L. H. Harley, *J. Am. Chem. Soc.*, 1999, **121**, 3561–3570.
18 T. Yamashita, T. Uno and Y. Ishikawa, *Bioorg. Med. Chem.*, 2005, **13**, 2423–2430.
19 C. Wei, G. Jia, J. Yuan, Z. Feng and C. Li, *Biochemistry*, 2006, **45**, 6681–6691.
20 P. Zhao, L.-C. Xu, J.-W. Huang, B. Fu, H.-C. Yu and L.-N. Ji, *Dyes Pigm.*, 2009, **83**, 81–87.
21 C. Wei, L. Wang, G. Jia, J. Zhou, G. Han and C. Li, *Biophys. Chem.*, 2009, **143**, 79–84.
22 V. H. Le, N. Nagesh and E. A. Lewis, *PLoS One*, 2013, **8**, e72462.
23 E. Boschi, S. Davis, S. Taylor, A. Butterworth, L. A. Chirayath, V. Purohit, L. K. Siegel, J. Buenaventura, A. H. Sheriff, R. Jin, R. Sheardy, L. A. Yatsunyk and M. Azam, *J. Phys. Chem. B*, 2016, **120**, 12807–12819.
24 T. L. Ruan, S. J. Davis, B. M. Powell, C. P. Harbeck, J. Habdas, P. Habdas and L. A. Yatsunyk, *Biochemie*, 2017, **132**, 121–130.
25 L. R. Keating and V. A. Szalai, *Biochemistry*, 2004, **43**, 15891–15900.
26 C. Romera, O. Bombarde, R. Bonnet, D. Gomez, P. Dumy, P. Calsou, J.-F. Gwan, J.-H. Lin, E. Defrancq and G. Pratviel, *Biochemie*, 2011, **93**, 1310–1317.
27 J. K. Choi, A. D'Urso and M. Balaz, *J. Inorg. Biochem.*, 2013, **127**, 1–6.
28 P. Zhao, J.-Z. Lu, F.-Y. Hong, B.-H. Ou, F.-D. Zhang, L.-N. Ma and H.-M. Guo, *Spectrochim. Acta, Part A*, 2013, **108**, 1–7.
29 Y.-H. Kim, C. Lee, S. K. Kim and S. C. Jeoung, *Biophys. Chem.*, 2014, **190–191**, 17–24.
30 J. Dejeu, T. Lavergne, J. D. Nora, E. Defrancq and G. Pratviel, *Inorg. Chim. Acta*, 2016, **452**, 98–103.
31 X. Yao, D. Song, T. Qin, C. Yang, Z. Ye, X. Li, K. Liu and H. Su, *Sci. Rep.*, 2017, **7**, 10951.
32 D. Song, W. Yang, T. Qin, L. Wu, K. Liu and H. Su, *J. Phys. Chem. Lett.*, 2014, **5**, 2259–2266.
33 B. Milovanović, A. Stanojević, M. Etinski and M. Petković, *J. Phys. Chem. B*, 2020, **124**, 3002–3014.
34 S. J. Baum, B. F. Burnham and R. A. Plane, *Proc. Natl. Acad. Sci. U. S. A.*, 1964, **52**, 1439–1442.
35 J. Barrett, *Nature*, 1967, **215**, 733–735.
36 M. E. Druyan, J. R. Norris and J. J. Katz, *J. Am. Chem. Soc.*, 1973, **95**, 1682–1683.
37 S. G. Boxer, G. L. Closs and J. J. Katz, *J. Am. Chem. Soc.*, 1974, **96**, 7058–7066.
38 S. Lesage, H. Xu and L. Durham, *Hydrol. Sci. J.*, 1993, **38**, 343–354.
39 M. Rubio and B. O. Roos, *J. Chem. Phys.*, 1999, **110**, 7202.
40 A. R. Battersby, *Nat. Prod. Rep.*, 2000, **17**, 507–526.
41 J. Jusélius and D. Sundholm, *J. Org. Chem.*, 2000, **65**, 5233–5237.
42 A. Wong, R. Ida, X. Mo, Z. Gan, J. Poh and G. Wu, *J. Phys. Chem. A*, 2006, **110**, 10084–10090.
43 J. R. Black, Q. Yin, J. R. Rustad and W. H. Casey, *J. Am. Chem. Soc.*, 2017, **129**, 8690–8691.
44 M. Etinski, M. Petković and M. M. Ristić, *J. Serb. Chem. Soc.*, 2013, **78**, 1775–1787.
45 M. Etinski, M. Petković, M. M. Ristić and C. M. Marian, *J. Phys. Chem. B*, 2015, **119**, 10156–10169.
46 X. Jiang, Y. Gao, R. Lal, J. Hu and B. Song, *Mol. Phys.*, 2018, **116**, 1697–1705.
47 J. S. Lindsey and J. N. Woodford, *Inorg. Chem.*, 1995, **34**, 1063–1069.
48 K. D. Borah and J. Bhuyan, *Dalton Trans.*, 2017, **46**, 6497–6509.
49 J. B. Allison and R. S. Becker, *J. Phys. Chem.*, 1963, **67**, 2675–2679.
50 L. Bonomo, M.-L. Lehaire, E. Solari, R. Scopelliti and C. Floriani, *Angew. Chem., Int. Ed.*, 2001, **40**, 771–774.
51 I. Alkorta, J. Elguero, A. M. S. Silva and A. C. Tomé, *J. Porphyrins Phthalocyanines*, 2010, **14**, 631–638.
52 F. Feixas, J. Poater, E. Matito and M. Solá, *Aromaticity of Organic and Inorganic Heterocycles*, Springer, Berlin, Heidelberg, 2014, pp. 129–160.
53 M. A. Blanco, A. M. Pendás and E. Francisco, *J. Chem. Theory Comput.*, 2005, **1**, 1096–1109.
54 A. M. Pendás, M. A. Blanco and E. Francisco, *J. Comput. Chem.*, 2007, **28**, 161–184.
55 D. Tiana, E. Francisco, M. A. Blanco, P. Macchi, A. Sironi and A. M. Pendás, *J. Chem. Theory Comput.*, 2010, **6**, 1064–1074.

56 P. Dem'yanov and P. M. Polestshuk, *Chem. – Eur. J.*, 2013, **19**, 10945–10957.
57 Z. Badri, C. Foroutan-Nejad, J. Kozelka and R. Marek, *Phys. Chem. Chem. Phys.*, 2015, **17**, 26183–26190.
58 C. Foroutan-Nejad, Z. Badri and R. Marek, *Phys. Chem. Chem. Phys.*, 2015, **17**, 30670–30679.
59 Z. Badri and C. Foroutan-Nejad, *Phys. Chem. Chem. Phys.*, 2016, **18**, 11693–11699.
60 I. Alkorta, J. C. R. Thacker and P. L. A. Popelier, *J. Comput. Chem.*, 2018, **39**, 546–556.
61 J. L. Casalz-Sainz, J. Manuel-Vela, E. Francisco, T. Rocha-Rinza and A. M. Pendás, *ChemPhysChem*, 2017, **18**, 3553–3561.
62 N. Javadi, M. Najafi and S. Yourdkhani, *Int. J. Quantum Chem.*, 2017, **117**, e25379.
63 M. Petković, Đ. Nakarada and M. Etinski, *J. Comput. Chem.*, 2018, **39**, 1868–1877.
64 I. Petrović, B. Milovanović, M. Etinski and M. Petković, *Int. J. Quantum Chem.*, 2019, **119**, e25918.
65 J. C. R. Thacker and P. L. A. Popelier, *J. Phys. Chem. A*, 2018, **122**, 1439–1450.
66 J. C. R. Thacker, M. A. Vincent and P. L. A. Popelier, *Chem. – Eur. J.*, 2018, **24**, 11200–11210.
67 N. Orangi, K. Eskandari, J. C. R. Thacker and P. L. A. Popelier, *ChemPhysChem*, 2019, **20**, 1922–1930.
68 J. L. Casalz-Sainz, J. Manuel-Vela, E. Francisco, T. Rocha-Rinza and A. M. Pendás, *J. Comput. Chem.*, 2020, **41**, 1234–1241.
69 M. J. Frisch, G. W. Trucks, H. B. Schlegel, G. E. Scuseria, M. A. Robb, J. R. Cheeseman, G. Scalmani, V. Barone, B. Mennucci, G. A. Petersson, H. Nakatsuji, M. Caricato, X. Li, H. P. Hratchian, A. F. Izmaylov, J. Bloino, G. Zheng, J. L. Sonnenberg, M. Hada, M. Ehara, K. Toyota, R. Fukuda, J. Hasegawa, M. Ishida, T. Nakajima, Y. Honda, O. Kitao, H. Nakai, T. Vreven, J. A. Montgomery, Jr., J. E. Peralta, F. Ogliaro, M. Bearpark, J. J. Heyd, E. Brothers, K. N. Kudin, V. N. Staroverov, T. Keith, R. Kobayashi, J. Normand, K. Raghavachari, A. Rendell, J. C. Burant, S. S. Iyengar, J. Tomasi, M. Cossi, N. Rega, J. M. Millam, M. Klene, J. E. Knox, J. B. Cross, V. Bakken, C. Adamo, J. Jaramillo, R. Gomperts, R. E. Stratmann, O. Yazyev, A. J. Austin, R. Cammi, C. Pomelli, J. W. Ochterski, R. L. Martin, K. Morokuma, V. G. Zakrzewski, G. A. Voth, P. Salvador, J. J. Dannenberg, S. Dapprich, A. D. Daniels, O. Farkas, J. B. Foresman, J. V. Ortiz, J. Cioslowski and D. J. Fox, *Gaussian 09 Revision D.01*, Gaussian Inc., Wallingford CT, 2009.
70 Y. Zhao and D. G. Truhlar, *Theor. Chem. Acc.*, 2008, **120**, 215–241.
71 A. D. McLean and G. S. Chandler, *J. Chem. Phys.*, 1980, **72**, 5639–5648.
72 R. Krishnan, J. S. Binkley, R. Seeger and J. A. Pople, *J. Chem. Phys.*, 1980, **72**, 650–654.
73 T. Clark, J. Chandrasekhar, G. W. Spitznagel and P. v. R. Schleyer, *J. Comput. Chem.*, 1983, **4**, 294–301.
74 M. J. Frisch, J. A. Pople and J. S. Binkley, *J. Chem. Phys.*, 1984, **80**, 3265–3269.
75 J. Blaudeau, *J. Chem. Phys.*, 1997, **107**, 5016–5021.
76 A. Ruiz, H. Perez, C. Morera-Boado, L. Almagro, C. C. P. da Silva, J. Ellena, J. M. G. de la Vega, R. Martinez-Alvarez, M. Suarez and N. Martin, *CrystEngComm*, 2014, **16**, 7802–7814.
77 S. E. Kochanek, T. M. Clymer, V. S. Pakkala, S. P. Hebert, K. Reeping, S. M. Firestine and J. D. Evanseck, *J. Phys. Chem. B*, 2015, **119**, 1184–1191.
78 S. W. L. Hogan and T. van Mourik, *J. Comput. Chem.*, 2016, **37**, 763–770.
79 A. Motahari and A. Fattahi, *New J. Chem.*, 2017, **41**, 15110–15119.
80 A. Mortazavifat, H. Raissi and M. Shahabi, *J. Biomol. Struct. Dyn.*, 2019, **37**, 4852–4862.
81 I. Iribarren, M. M. Montero-Campillo, I. Alkorta, J. Elguero and D. Quiñonero, *Phys. Chem. Chem. Phys.*, 2019, **21**, 5796–5802.
82 Y. Itoh, Y. Nakashima, S. Tsukamoto, T. Kurohara, M. Suzuki, Y. Sakae, M. Oda, Y. Okamoto and T. Suzuki, *Sci. Rep.*, 2019, **9**, 767.
83 G. Lv, X. Sun, C. Zhang and M. Li, *Atmos. Chem. Phys.*, 2019, **19**, 2833–2844.
84 J. Tomasi, B. Mennucci and R. Cammi, *Chem. Rev.*, 2005, **105**, 2999–3093.
85 T. A. Keith, *AIMAll (Version 19.10.12, Professional)*, TK Gristmill Software, Overland Park KS, USA, 2019 (aim.tkgristmill.com).
86 J. VandeVondele, M. Krack, F. Mohamed, M. Parrinello, T. Chassaing and J. Hutter, *Comput. Phys. Commun.*, 2005, **167**, 103–128.
87 A. D. Becke, *Phys. Rev. A: At., Mol., Opt. Phys.*, 1988, **38**, 3098–3100.
88 C. T. Lee, W. T. Yang and R. G. Parr, *Phys. Rev. B: Condens. Matter Mater. Phys.*, 1988, **37**, 785–789.
89 S. Grimme, J. Antony, S. Ehrlich and H. Krieg, *J. Chem. Phys.*, 2010, **132**, 154104.
90 G. Lippert, J. Hutter and M. Parrinello, *Mol. Phys.*, 1997, **92**, 477–487.
91 S. Goedecker, M. Teter and J. Hutter, *Phys. Rev. B: Condens. Matter Mater. Phys.*, 1996, **54**, 1703–1710.
92 G. Bussi, D. Donadio and M. Parrinello, *J. Chem. Phys.*, 2007, **126**, 014101.
93 M. Brehm and B. Kirchner, *J. Chem. Inf. Model.*, 2011, **51**, 2007–2023.
94 M. Thomas, M. Brehm, R. Fligg, P. Voehringer and B. Kirchner, *Phys. Chem. Chem. Phys.*, 2013, **15**, 6608–6622.
95 B. Milovanović, I. Stanković, M. Petković and M. Etinski, *J. Phys. Chem. A*, 2020, **124**, 8101–8111.
96 R. F. W. Bader, *Atoms in Molecules: A Quantum Theory*, Oxford University Press, 1990.
97 *The Quantum Theory of Atoms in Molecules: From Solid State to DNA and Drug Design*, ed. C. F. Matta and R. J. Boyd, Wiley-VCH, Weinheim, 2007.
98 M. Meyer, T. Steinke, M. Brandl and J. Sühnel, *J. Comput. Chem.*, 2001, **22**, 109–124.
99 G. Louit, A. Hocquet, M. Ghomi, M. Meyer and J. Sühnel, *PhysChemComm*, 2003, **6**, 1–5.

100 M. Meyer and J. Sühnel, *J. Biomol. Struct. Dyn.*, 2003, **20**, 507–517.
101 T. van Mourik and A. J. Dingley, *Chem. – Eur. J.*, 2005, **11**, 6064–6079.
102 Y. P. Yurenko, J. Novotný, V. Sklenář and R. Marek, *Phys. Chem. Chem. Phys.*, 2014, **16**, 2072–2084.
103 M. Meyer, M. Brandl and J. Sühnel, *J. Phys. Chem. A*, 2001, **105**, 8223–8225.
104 A. K. Jissy, U. P. M. Ashik and A. Datta, *J. Phys. Chem. C*, 2011, **115**, 12530–12546.
105 V. Gabelica, F. Rosu, E. D. Pauw, J. Lemaire, J.-C. Gillet, J.-C. Poully, F. Lecomte, G. Grégoire, J.-P. Schermann and C. Desfrançois, *J. Am. Chem. Soc.*, 2008, **130**, 1810–1811.
106 Y. P. Yurenko, J. Novotný, M. P. Mitoraj, V. Sklenář, A. Michalak and R. Marek, *J. Chem. Theory Comput.*, 2014, **10**, 5353–5365.
107 M. Meyer, A. Hocquet and J. Sühnel, *J. Comput. Chem.*, 2005, **26**, 352–364.
108 R. D. Shannon, *Acta Crystallogr., Sect. A: Cryst. Phys., Diffr., Theor. Gen. Crystallogr.*, 1976, **32**, 751–767.

Прилог 2 – *Water-Mediated Interactions Enhance Alkaline Earth Cation Chelation in Neighboring Cavities of a Cytosine Quartet in the DNA Quadruplex*

Објављени научни рад (категорија научног часописа M_{22}):

Branislav Milovanović, Milena Petković, Mihajlo Etinski, Igor Popov, Water-Mediated Interactions Enhance Alkaline Earth Cation Chelation in Neighboring Cavities of a Cytosine Quartet in the DNA Quadruplex, *J. Phys. Chem. B*, **2021**, 125 (43), pp 11996-12005.

https://doi.org/10.1021/acs.jpcb.1c05598 *IF(2020) 2,991*

Ауторска права код издавача (приступљено дана 15.12.2021.):

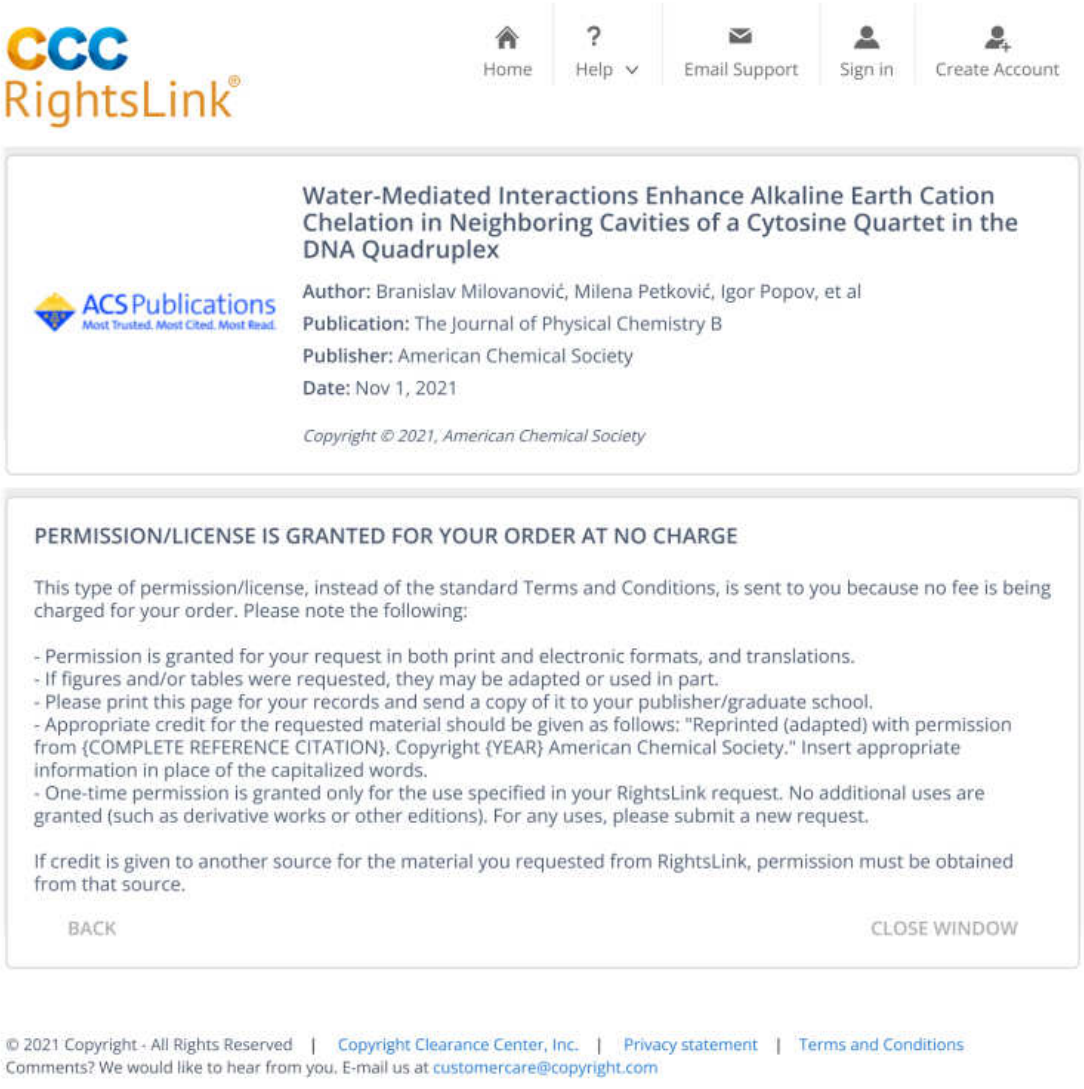

THE JOURNAL OF PHYSICAL CHEMISTRY B
A JOURNAL OF THE AMERICAN CHEMICAL SOCIETY

pubs.acs.org/JPCB

Article

Water-Mediated Interactions Enhance Alkaline Earth Cation Chelation in Neighboring Cavities of a Cytosine Quartet in the DNA Quadruplex

Branislav Milovanović, Milena Petković, Igor Popov, and Mihajlo Etinski*

Cite This: https://doi.org/10.1021/acs.jpcb.1c05598

Read Online

ACCESS | Metrics & More | Article Recommendations | Supporting Information

ABSTRACT: Larger Coulombic repulsion between divalent cations compared to the monovalent counterparts dictates the cation−cation distance in the central ion channel of quadruplexes. In this work, density functional theory and a continuum solvation model were employed to study bond energies of alkaline earth cations in adjacent cavities of the central ion channel. Four crystallized tetramolecular quadruplexes with various geometric constraints and structural motifs available in the Protein Data Bank were examined in order to understand how the cation binding affinities could be increased in aqueous solution. A cytosine quartet sandwiched between guanine quartets has a larger bond energy of the second alkaline earth cation in comparison with guanine and uracil quartets. Four highly conserved hydrogen-bonded water molecules in the center of the cytosine quartet are responsible for a higher electrostatic interaction with the cations in comparison with guanines' carbonyl groups. The reported findings are valuable for the design of synthetic quadruplexes templated with divalent cations for optoelectronic applications.

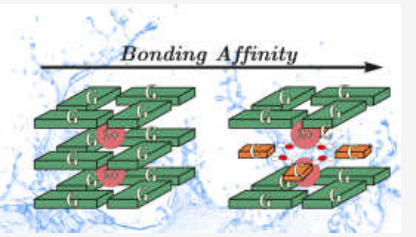

INTRODUCTION

The stability of nucleic acids' structures is determined by nucleobase-specific interactions that allow strands to adopt energetically favorable forms. A larger diversity of these nanostructures is achieved by noncanonical nucleobase pairing.[1] Particularly intriguing is the guanine quadruplex due to its stability under physiological conditions. It consists of stacked guanine quartets, in which guanine units are connected by four hydrogen bonds formed between complementary Watson−Crick and Hoogsteen edges of neighboring units. Unlike in other nucleic acid structures, guanines in quadruplexes interact directly with monovalent and divalent cations via inner sphere coordination in order to increase the stability of the overall structure.[2] While monovalent cations occupy all quadruplex vacancies in the central ion channel, divalent cations tend to avoid adjacent vacancies.[3−7]

The interactions between chelated cations and guanines provides an opportunity to modulate the electronic properties of quadruplexes by different cation types.[8−13] This can be achieved by using cations with different ionic radii and charges. Larger mobility of smaller than larger cations is favorable for trapping relaxed charge transfer excitons.[10] These collective excitations are also stabilized to a greater degree by divalent than monovalent cations.[13] Electric fields created by several divalent cations positioned in consecutive vacancies will likely stabilize charge transfer excitations below bright states. Considering the importance of these excited electronic states for nanotechnology applications, it is desirable to understand how divalent cations in the central ion channel might be stabilized with the same spacing as monovalent cations.

Several theoretical studies have addressed the stabilizing interactions between monovalent cations and a quadruplex scaffold.[2,14−18] Energy decomposition analysis (EDA) revealed that the interaction between an alkali cation and guanines in a two-layer quadruplex is overwhelmingly electrostatic.[2] The orbital interaction contribution is found to be twice smaller. This energy term mainly results from the donation of electron density from the highest occupied orbitals of guanines' oxygen atoms to the lowest unoccupied orbitals of the alkali cation. By adding the second and the third alkali cation in quadruplexes with one and two cations, respectively, Nieuwland et al. showed that electrostatic energies of the added cations decrease as a result of the electrostatic repulsion between the cations, whereas the orbital interaction does not change.[18] In the case of two alkali cations, the electrostatic interaction between the second cation and a quadruplex scaffold chelated with the first cation is slightly larger than the orbital interaction of the second cation. By adding the third alkali cation, the orbital interaction energy of this cation becomes larger than its electrostatic energy. Destabilizing the electrostatic repulsion between the hosted alkali cations is counterbalanced by electronic screening and solvation effects so that the magnitude

Received: June 24, 2021
Revised: September 30, 2021

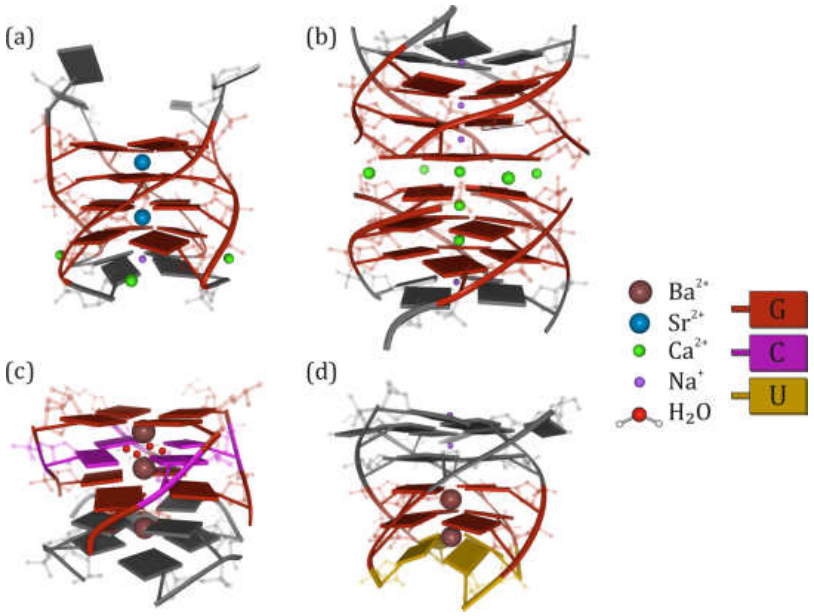

Figure 1. Crystal structures of quadruplexes coordinated with at least two alkaline earth cations: (a) $r(UG_4U)_4$,[3] (b) two end-to-end stacked $d(TG_4T)_4$,[19] (c) $d(GCGTGG)_4$[20] (thymines do not form a quartet and are not shown), and (d) $r(GAGGU)_4$.[21] The coloring scheme is adjusted to highlight the reduced computational model used in this work. Nucleobases that are not considered in the model are colored in gray.

of the energy needed for binding consecutive alkali cations remains unaltered.

Alkaline earth cations have a two times larger charge than alkali cations, and if they have been coordinated with a similar spacing along the central axis of a quadruplex as alkali cations, they experience a 4 times larger electrostatic repulsion between them. This results in a high energy penalty for alkaline earth cations binding between consecutive guanine quartets. Solution NMR faces difficulties to probe the direct response of alkaline earth cations since their spectral signatures originate from exotic nuclei such as ^{43}Ca, ^{87}Sr, and ^{137}Ba.[22,23] Due to this, the existence of two alkaline earth cations positioned in neighboring vacancies of the central ion channel has not been experimentally observed in aqueous solutions. Inspection of the Protein Data Bank (PDB) reveals three crystal quadruplex structures with at least two alkaline earth cations coordinated between successive guanine or other nucleobase quartets[19−21] (Figure 1). Two of them contain a pair of Ba^{2+} cations positioned between three consecutive layers, one of which is a pyrimidine nucleobase quartet. In the $r(GAGGU)_4$ quadruplex, a tandem of guanine quartets interacts with one Ba^{2+} cation, whereas the second Ba^{2+} cation is positioned between the guanine and uracil quartets.[21] Since the uracil quartet is at the 3′-terminus of the quadruplex, it exhibits out-of-plane deformation, which enables approximately 1 Å longer distance between the Ba^{2+} cations than those found between other cations in the quadruplex. The second structure with two Ba^{2+} cations is found in a tetramolecular quadruplex formed from a decameric oligonucleotide $d(CCA^{CNV}KGCGTGG)$ (^{CNV}K is 3-cyanovinylcarbazole) sequence.[20] The quadruplex contains a cytosine quartet, which is stabilized by four highly conserved water molecules positioned in the middle of the quartet. The oxygens of the water molecules are in the same location as the O6 of the guanines in a typical guanine quartet. In this case, a large energy penalty due to electrostatic repulsion between Ba^{2+} cations is avoided by water coordination of the cations. The oxygen atoms of four hydrogen-bonded water molecules in the interior of the cytosine quartet have enhanced electron densities relative to those in the guanine's oxygen atom, which facilitates screening of Ba^{2+} cations.[20] Lee et al. crystallized a tetramolecular $d(TG_4T)_4$ quadruplex in a mixed Na^+ and Ca^{2+} environment and found an arrangement involving both cations in the central channel.[19] The crystallographic unit contains two end-to-end stacked quadruplexes asymmetrically populated by Na^+ and Ca^{2+} cations. One quadruplex is templated with three Na^+ cations, whereas the other one has one Na^+ and two Ca^{2+} cations. There is also one Ca^{2+} cation coordinated at the interface between the quadruplexes.

The three crystallized quadruplexes[19−21] provide us with the opportunity to examine electronic energies of chelated cations for structures in aqueous solutions. As reference systems, we also study tetramolecular quadruplexes coordinated with Sr^{2+} cations between every other layer and one coordinated with Na^+ cations. Our goal is to provide insights into the importance of structural motifs and geometric constraints for enhancing chelation affinity of alkaline earth cations in neighboring vacancies. To this end, we performed EDA of the interaction energy for binding the first and the second cation and examined many-body and solvation effects in model quadruplexes consisting of three and four layers. We also determined the energy needed to exchange two Na^+ by two Ca^{2+} cations in tetramolecular quadruplexes with GGG and GCG sequences. The present results offer a comparison between the binding energies of alkaline earth cations in adjacent positions with those in systems with vacant cavities and energies of alkali cations. The computations reveal that the cytosine quartet stacked between guanine quartets has a much higher propensity for binding alkaline earth cations than the pure guanine quadruplex. This finding reveals that the design of synthetic tetramolecular quadruplexes with divalent cations in adjacent chelating sites in aqueous solutions benefits from selection of the GCG sequence motif.

https://doi.org/10.1021/acs.jpcb.1c05598
J. Phys. Chem. B XXXX, XXX, XXX−XXX

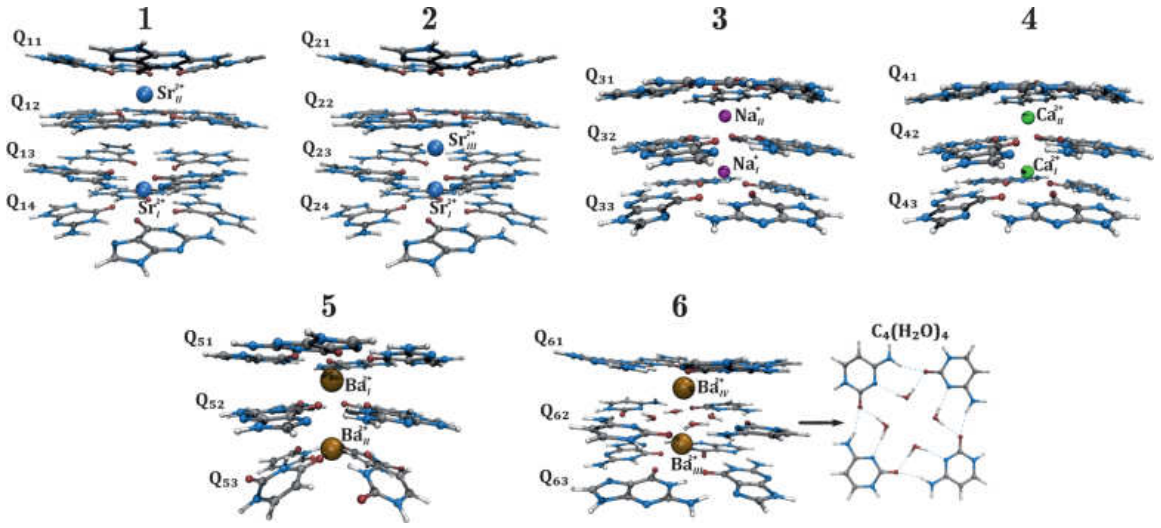

Figure 2. Geometries of quadruplexes and labels used in the present work.

METHODS

In order to make this study computationally feasible, we used a reduced quadruplex model in which the sugar−phosphate backbone is neglected. Previous computational studies showed that the presence of the backbone does not considerably alter alkali cation binding energies.[2,18] The geometries of the six examined structures are given in Figure 2, whereas cation labels and PDB IDs of quadruplexes from which atomic positions were extracted are collected in Table 1. Quadruplex **2** was created from **1** by shifting the Sr_I^{2+} cation to the midway position between the Sr_I^{2+} and Sr_{II}^{2+} cations (the new cation label is Sr_{III}^{2+}). Crystallographic positions of waters' hydrogen atoms are not given for structure **6**. Their positions were determined by performing partial optimization at the level of theory used for electronic structure calculations in this work.

Table 1. Structures, Cation Labels, and PDB IDs of Quadruplexes from Which Atomic Positions Were Extracted

structure	cation labels	PDB ID
1	G_4-Sr_I^{2+}-G_4-G_4-Sr_{II}^{2+}-G_4	1J8G[3]
2	G_4-Sr_I^{2+}-G_4-Sr_{III}^{2+}-G_4-G_4	1J8G[3]
3	G_4-Na_I^{+}-G_4-Na_{II}^{+}-G_4	2GW0[19]
4	G_4-Ca_I^{2+}-G_4-Ca_{II}^{2+}-G_4	2GW0[19]
5	G_4-Ba_I^{2+}-G_4-Ba_{II}^{2+}-U_4	1J6S[21]
6	G_4-Ba_{III}^{2+}-$C_4(H_2O)_4$-Ba_{IV}^{2+}-G_4	4U92[20]

All calculations were performed with the Turbomole program package.[24] We used density functional theory with the B-LYP functional[25,26] and Grimmes's D3 correction[27] for calculations of electronic energies. Kohn−Sham molecular orbitals were expended in the def2-TZVPP basis set.[28] Multipole accelerated resolution-of-identity was used to accelerate the calculation of the electronic Coulomb interaction. This combination of density functional and valence triple-zeta polarization basis set has been used often to study guanine self-assemblies.[2,29−32] Atomic charges were computed by using natural population analysis.[33] Solvent effects were taken into account by employing the continuum solvation model (COSMO)[34,35] with the dielectric constant of water (ϵ = 78.5). The cation radii used in the COSMO model were recalculated to reproduce experimental solvation energies of the cations.[36] The recalculated values were 1.8161, 1.9819, 2.1890, and 1.8685 Å, for Ca^{2+}, Sr^{2+}, Ba^{2+}, and Na^{+}, respectively.

The bond energy ΔE_{bond} represents the energy needed to chelate a cation to a quadruplex in aqueous solution. It was computed using structures depicted in Figure 3. In order to understand the contribution of various stabilizing and destabilizing energy terms, we decomposed the bond energy into

$$\Delta E_{bond} = \Delta E_{desolv} + \Delta E_{int} + \Delta E_{solv} \quad (1)$$

ΔE_{desolv}, ΔE_{solv}, and ΔE_{int} are the energies of desolvation, solvation, and interaction energy, respectively (see Figure 3). The desolvation and solvation energies are related to energy differences between the gas phase and aqueous solution energies. Note that binding a cation to a quadruplex results in deformation of quadruplex's geometry. The related preparation energy is relatively small (<10 kcal/mol)[18] and not accounted for in bond energies since we employed the experimental geometries. One- and two-cation interaction energies, ΔE_{int}, are decomposed by using EDA.[37] This method decomposes the electronic energy into electrostatic (ΔE_{ele}), exchange (ΔE_{ex}), repulsion (ΔE_{rep}), polarization and orbital interaction (ΔE_{pol}), and dispersion (sum of correlation and D3 dispersion energies) (ΔE_{disp}) terms. The energy needed to exchange two Na^{+} by two Ca^{2+} cations was calculated by the thermodynamic cycle shown in Figure 3. It contains the desolvation ΔE_{desolv}, solvation ΔE_{solv}, and preparation energy ΔE_{prep}, as well as two-cation interaction energies $\Delta E_{int,2Na^+}$ and $\Delta E_{int,2Ca^{2+}}$ with Na^{+} and Ca^{2+} cations, respectively.

Let us summarize approximations employed in this work. In the first place, we used molecular geometries determined for quadruplexes in a crystal environment. These structures are slightly different from those in the aqueous solution. This choice of geometries was dictated by difficulties related to geometry optimization of quadruplexes with more than two stacked quartets. Bond energies are determined in fixed molecular geometries without geometry relaxation upon cation chelation. The sugar−phosphate backbone is not taken into account, and solvent effects were modeled by a continuum model. Since cation radii are chosen to reproduce experimental free hydration energies, the computed bond energies also

https://doi.org/10.1021/acs.jpcb.1c05598
J. Phys. Chem. B XXXX, XXX, XXX−XXX

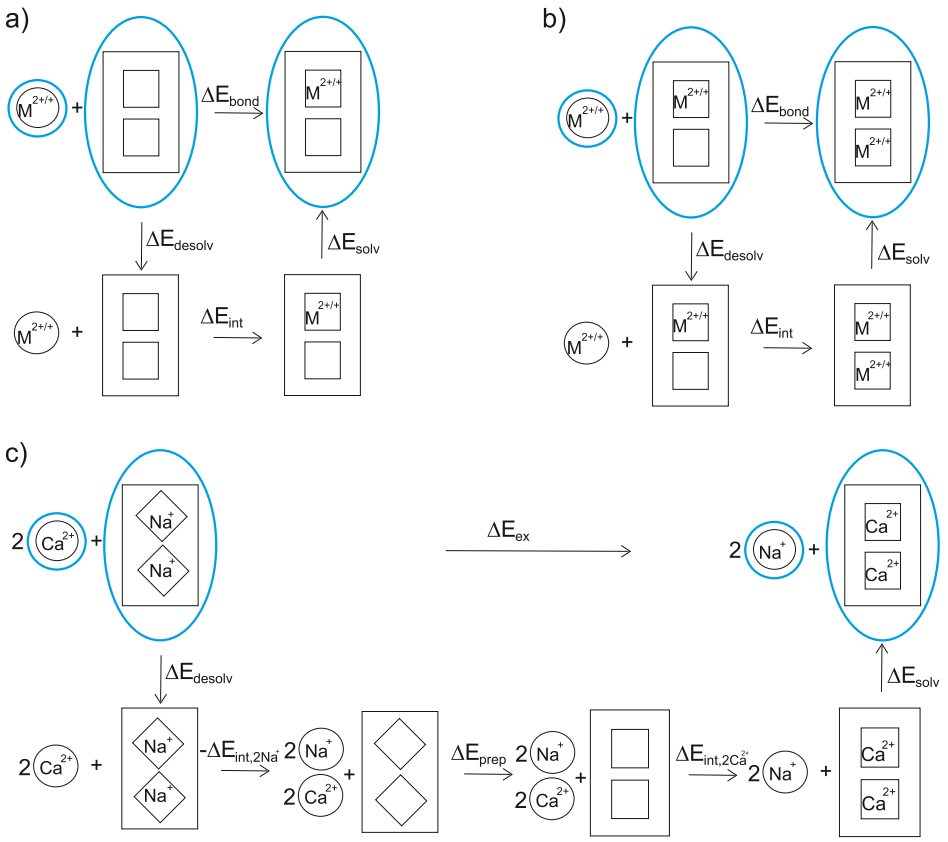

Figure 3. Thermodynamic cycles for the calculation of the bond energy [for the first (a) and the second (b) cation] and the energy needed to exchange two Na^+ by two Ca^{2+} cations (c). The fragments encircled by blue lines were computed in aqueous solutions.

Table 2. Partitioning of the Bond Energy (in kcal/mol)

quadruplex	1		2		3	
cation	Sr_I^{2+}	Sr_{II}^{2+}	Sr_I^{2+}	Sr_{III}^{2+}	Na_I^+	Na_{II}^+
E_{desolv}	456.9	516.1	456.9	516.1	191.5	197.9
E_{solv}	−186.2	−382.5	−186.2	−405.6	−110.6	−159.2
$E_{desolv} + E_{solv}$	270.7	133.5	270.7	110.5	80.9	38.4
E_{int}	−388.2	−234.9	−388.2	−129.1	−157.6	−111.8
E_{bond}	−117.4	−101.4	−117.4	−18.6	−76.7	−73.2
quadruplex	4		5		6	
cation	Ca_I^{2+}	Ca_{II}^{2+}	Ba_I^{2+}	Ba_{II}^{2+}	Ba_{III}^{2+}	Ba_{IV}^{2+}
E_{desolv}	464.9	530.7	395.1	458.7	403.3	467.0
E_{solv}	−171.0	−395.4	−159.9	−407.4	−168.2	−386.6
$E_{desolv} + E_{solv}$	293.9	135.3	235.2	51.3	235.1	80.3
E_{int}	−368.4	−158.9	−327.6	−28.9	−392.5	−167.4
E_{bond}	−74.5	−23.7	−92.4	22.4	−157.4	−87.0

implicitly take into account thermal effects of cation hydration. Nevertheless, the bond energies are not free energies since the quadruplex's scaffold thermal effects are not included. Free energies might be determined by employing molecular dynamics with polarizable force fields or approximate theories such as quasi-chemical theory.[38,39] In order to estimate the importance of entropy for binding affinities, we optimized guanine octets chelated with Na^+ and Ca^{2+} cations. Although these systems have 381 normal modes, the zero-point vibrational energy and entropy differences were found to be only 983 cm^{-1} and 4.3 kcal/mol (at 298 K), respectively, at the B-LYP-D3/def2-SVP level. This implies that quadruplexes are stiff systems toward cation exchange and that the cation−nucleobase interaction energy dominates the relative free energy difference.[40]

RESULTS AND DISCUSSION

Bond Energies. The sum of desolvation and solvation energies of a quadruplex scaffold and cations in water is positive for binding one and two cations. Since water is a more polarizable environment than crystals, cation binding in the aqueous solution will be weaker than in the solid state. The Gibbs energies of hydration for Ca^{2+}, Sr^{2+}, and Ba^{2+} cations amount to −1505, −1380, and −1250 kcal/mol,[36] respectively. These energies are much higher than those for Na^+ (−365 kcal/mol), K^+ (−295 kcal/mol), and Rb^+ (−275 kcal/mol).[36]

https://doi.org/10.1021/acs.jpcb.1c05598
J. Phys. Chem. B XXXX, XXX, XXX−XXX

At first sight, it appears that the bond energies of alkaline earth cations are smaller in comparison with alkali cation energies. However, alkaline earth cations also interact more strongly with the quadruplex scaffold than alkali cations, which compensates the solvation effects.

Bond energies and their partition into desolvation, interaction, and solvation energies are given in Table 2. Comparison between bond energies of cations from different quadruplexes is only possible if the quadruplexes have the same chemical makeup or the cations are of the same type or have similar radii. The bond energies for chelation of the first cation in every quadruplex were strongly negative, irrespective of the cation type. By comparing bond energies of the Ca_I^{2+}, Sr_I^{2+} and Ba_I^{2+} cations chelated between guanine quartets, we found that the most strongly bound cation was Sr_I^{2+}, followed by Ba_I^{2+} and Ca_I^{2+}. This stabilization ordering is in accordance with experimental findings of Venczel and Sen,[41] although we examined both RNA and DNA quadruplexes. Ba_I^{2+} had the lowest sum of solvation and desolvation energies, but its interaction energy was considerably smaller than that of Sr_I^{2+}. Chelation of Na_I^{+} was 2.2 kcal/mol stronger than that of Ca_I^{2+} with a similar ionic radius. This unexpectedly small energy difference indicates that an increase in Ca^{2+} concentration may lead to the exchange of one Na^+ by the Ca^{2+} cation in aqueous solutions. Yet, the difference in entropic terms computed from the optimized geometries (4.3 kcal/mol at 298 K) additionally stabilizes chelation of Na^+ over the Ca^{2+} cation.

The bond energy of the Ba^{2+} cation between guanine and cytosine quartets is much higher than that between two guanine quartets. The sum of solvation and desolvation energies of the Ba_{III}^{2+} cation is equal to that of the Ba_I^{2+} cation, implying that these contributions are robust against the influence of geometric constraints and different structural motif contributions for binding of the first cation. On the other hand, we find that the solvation effects for chelating the second cation were approximately 30 kcal/mol more favorable in quadruplex **5** than in **6** due to the larger cation−cation distance.

The energy needed for binding the Na_{II}^{+} cation was almost equal to the energy of the Na_I^{+}, as has been found previously.[18] A somewhat larger energy difference is noticed for the Sr_I^{2+} and Sr_{II}^{2+} cations, but still the bond energy of Sr_{II}^{2+} was sufficiently negative to allow strong chelation of Sr_{II}^{2+} two cavities away from already occupied cavity. If the second Sr^{2+} cation is chelated in the adjacent vacancy, its bond energy is −19 kcal/mol. This value was 83 kcal/mol higher than the energy needed for chelation in every other cavity. Since electrostatic interaction has a long-range character, the third consecutive Sr^{2+} cation and every following cation would experience even larger Coulomb repulsion than the second one. Their energies would decrease and eventually become positive, which prevents chelation of the Sr^{2+} cation in the adjacent cavities of the guanine quadruplex. Therefore, alkaline earth cations prefer alternating occupation of cavities of the guanine quadruplex in the aqueous solution.

Similar to the binding of Sr^{2+} to quadruplex **2**, the bond energy of the second Ca^{2+} cation was much lower than that of the first cation. It amounted to −24 kcal/mol, which is 49 kcal/mol smaller than that for the second Na^+ cation. Hence, although chelation of two alkaline earth cations in neighboring quadruplexes' binding sites is energetically possible, their small bond energies indicate that these quadruplexes are not as stable as those templated with monovalent cations. In order to further reveal the difference in binding affinities of Na^+ and Ca^{2+} cations, we computed the energy needed to exchange two Na^+ cations in quadruplex **3** by two Ca^{2+} cations in quadruplex **4**. The exchange energy amounted to 49 kcal/mol, that is, the cation exchange was not spontaneous in the aqueous solution. The desolvation and solvation contributions were 878.6 and −570.1 kcal/mol, respectively, and their sum was 308.5 kcal/mol. The large discrepancy between the absolute values of these terms is due to the fact that water hydrates double-positive charge of the Ca^{2+} cation more strongly than a single charge of the Na^+ cation. The interaction energies $-E_{int,2Na^+}$ and $E_{int,2Ca^+}$ are 269.5 and −527.5 kcal/mol, respectively. Their sum (−258 kcal/mol) is negative since Ca^{2+} cations are more tightly bound to the quadruplex than Na^+ cations. The preparation energy term was very small (−1.5 kcal/mol), reflecting similar quadruplex scaffolds for structures with Ca^{2+} and Na^+ cations. Overall, the cation exchange in the aqueous solution was not spontaneous even when the entropic contribution would be taken into account and was dominated by the solvation penalty. In a crystallizing solution, high ion concentrations decrease the dielectric constant, which makes Ca^{2+} cations easier to desolvate than in water. As a result, there are three Ca^{2+} cations in the adjacent vacancies of the crystallized stacked guanine quadruplex.[19]

The bond energy of the second Ba^{2+} cation in quadruplex **5** was positive due to small interaction energy, implying that the constrained geometry of this quadruplex is only stable under crowding conditions in the crystal and not in the aqueous solution. The cytosine quartet sandwiched between two guanine quartets exhibits much stronger affinity for binding the second cation than the guanine quartet stacks. The bond energy of the Ba_{IV}^{2+} cation is equal to −87 kcal/mol, which was only 5 kcal/mol lower than the energy needed for binding the first Ba^{2+} cation in the guanine quadruplex.

We can indirectly compare the bond energy of the Ba_{IV}^{2+} cation with those of alkali cations. In the first place, Ba^{2+} and K^+ cations have radii which only differ by 0.02 Å. In addition, the bond energies of Na^+ and K^+ cations are up to approximately 1 kcal/mol.[2] Taking into account that the bond energy of the Ba_{IV}^{2+} cation is 14 kcal/mol higher than the energy of the second Na^+ cation in guanine quadruplex **3**, we conclude that it is plausible that the Ba_{IV}^{2+} cation is more tightly bound than alkali cations in guanine quadruplexes. We also suggest that two Ba^{2+} cations are sufficiently strongly coordinated in the tetramolecular quadruplex segment with the GCG sequence being stable in the aqueous solution.

Affinity of the $(GCG)_4$ Quadruplex toward Na^+ and Ca^{2+} Cations. The unusually high affinity of the cytosine quartet sandwiched between guanine quartets for Ba^{2+} cations might indicate that it will also hold true for other divalent cations. Yet, Liu et al. showed that this motif in a solution of Pb^{2+} and several monovalent cations bound only one Pb^{2+} cation—the cation in the adjacent vacancy was found to be Na^+.[42] Since two chelation sites of the $(GCG)_4$ quadruplex have distinct coordination geometries (bipyramidal antiprismatic and nearly square prismatic), Liu et al. argued that Pb^{2+} coordination might depend on the quartet orientation.[42] This observation motivated us to examine bond energies of Na^+ and Ca^{2+} cations in the $(GCG)_4$ quadruplex. We computed these energies at the geometries of Ba^{2+} cations in quadruplex **6**. This procedure is justified by similar ionic radii of Na^+ and Ca^{2+} cations (0.97 and 0.99 Å) and very small preparation energy for exchange of two Na^+ by two Ca^{2+} cations in the guanine

https://doi.org/10.1021/acs.jpcb.1c05598
J. Phys. Chem. B XXXX, XXX, XXX−XXX

quadruplex. In addition, it was found that the optimized guanine quartet chelated by Na^+ and Ca^{2+} cations also had similar oxygen-cation distances, 2.26 and 2.27 Å,[17] respectively.

Table 3 contains bond energies of Na^+ and Ca^{2+} cations chelated in vacancies of quadruplex **6** and their partitioning to desolvation, solvation, and interaction energy contributions. Both the first and second bond energy of Na^+ cations were larger than those in the guanine quadruplex. Nevertheless, the larger decrease of the bond energy from the first to the second Na^+ cation in comparison with the guanine quadruplex was found. The bond energies of Ca^{2+} cations were similar to those of the Ba^{2+} cation, implying that alkaline earth cations are likely coordinated in both vacancies of this motif. Besides bond energies, we also calculated the energy needed for exchange of two Na^+ by two Ca^{2+} cations. The desolvation and solvation energies for this process were 878.6 and −561.3 kcal/mol, respectively. These values are almost equal to those for pure guanine quadruplex, that is, solvation and desolvation costs are independent of structural motifs. On the other hand, the interaction energies $-E_{int,2Na^+}$ and $E_{int,2Ca^+}$ were 330.6 and −671.4 kcal/mol, respectively, giving an exchange energy of −23.5 kcal/mol. Thus, the water-stabilized cytosine quartet stacked between guanine quartets acts as a selective ionophore for chelation of alkaline earth over alkali cations in the adjacent positions. This conclusion is based on the electronic energy contributions to the free energy.

Table 3. Partitioning of the Bond Energies of Na^+ and Ca^{2+} Cations Chelated in Vacancies of Quadruplex 6 (in kcal/mol)[a]

cation	Na_{III}^+	Na_{IV}^+	Ca_{III}^{2+}	Ca_{IV}^{2+}
E_{desolv}	191.8	200.7	464.2	527.8
E_{solv}	−113.4	−159.2	−168.1	−386.6
$E_{desolv} + E_{solv}$	78.4	41.6	296.0	141.3
E_{int}	−190.5	−140.1	−442.4	−229.0
E_{bond}	−112.0	−98.6	−146.4	−87.7

[a]The cations Na_{III}^+/Ca_{III}^{2+} and Na_{IV}^+/Ca_{IV}^{2+} are positioned in the place of the cations Ba_{III}^{2+} and Ba_{IV}^{2+}, respectively.

Structural Properties. The size of a central cavity between the quadruplex layers overwhelmingly influences the interaction between a cation and quadruplex scaffold. This property is reflected by oxygen-cation distances. Besides, coordinating oxygen atoms in quadruplexes with pyrimidine bases might have different charges than those of guanine's oxygens. Zhang et al. noticed that cytosine's N3 and O2 atoms form hydrogen bonds with water molecules in quadruplex **6**, which likely results in a rise of the electron density at the water oxygen's lone pairs.[20] Here, we analyze geometric and structural properties which determine the interaction between cations and ligands.

Table 4 shows the average oxygen-cation distances for each layer, their average values for both layers, and their differences between the layers. It also contains cation−cation distances. Quantum chemical calculations showed that an occupied cavity tends to adapt its size when a cation is hosted in the adjacent position.[18] The most frequent oxygen-cation distance was in the range 2.7−2.8 Å. This observation also includes waters' oxygens in the cytosine quartet. Deviations form these lengths indicate that there is distortion in the quadruplex scaffold. Sr^{2+} cations in quadruplex **1** with four layers were found to be symmetrically positioned between the layers. Guanine carbonyl groups were distorted toward the cations, which resulted in average oxygen-cation distances equal to 2.6 Å. In quadruplex **2**, the Sr_{III}^{2+} cation was inserted in the vacancy next to the one of the Sr_I^{2+} cation, but its oxygen-cation distances were not relaxed. The obtained average O6−Sr_{III}^{2+} length was 0.3 Å longer than the relaxed value. Quadruplexes **3** and **4** exhibited asymmetric positions of cations relative to the upper and lower quartets. This was particularly pronounced for Ca_I^{2+} and Na_{II}^+ cations. The asymmetry might originate from relatively small radii of these cations, which allow flexibility in their positions within the cavity. One consequence of this asymmetry was that the average distance between a cation and oxygens of the closer quartet was 2.5 Å. Note that average distances between oxygens of both quartets and Ca^{2+} cations were 2.8 Å, as found in other quadruplexes. In quadruplex **5**, the Ba_{II}^{2+} cation was much closer to the uracil than to the guanine quartet. The shortest and longest distance between the cations in the adjacent cavities was found in quadruplexes **2** and **5**, respectively. The distance between two Ba^{2+} cations in quadruplex **6** was 0.5 Å shorter than in quadruplex **5**.

Figure 4 shows the average oxygens' charges for each quartet. Guanine's oxygen charges were in the range from −0.57*e* to −0.76*e*. It is clearly noticeable that there was a redistribution of charges within different quartets. In the case of quadruplexes **3** and **4**, the oxygens of the central layer showed decreased electron density, whereas in the case of quadruplex **1**, every other quartet had the same average charge. Oxygens of the uracil quartet did not exhibit significantly different values than on average guanines. On the other hand, water oxygens in the cytosine quartet had in average −1.09*e*. This highly negative charge enables strong electrostatic interaction between the cations and water molecules.

Energy Decomposition Analysis. The interaction between cations and biological molecules is characterized by

Table 4. Average Distances (in Å) between the Oxygen Atoms of Guanine Quartets (Water Molecules in Structure 6) and Cations in the Quadruplexes[a]

quadruplex	1		2	3		4		5		6	
cation	Sr_I^{2+}	Sr_{II}^{2+}	Sr_{III}^{2+}	Ca_I^{2+}	Ca_{II}^{2+}	Na_I^+	Na_{II}^+	Ba_I^{2+}	Ba_{II}^{2+}	Ba_{III}^{2+}	Ba_{IV}^{2+}
lower quartet	2.61	2.60	2.90	2.53	2.68	2.75	3.10	2.74	2.35	2.66	2.82
upper quartet	2.61	2.60	2.90	3.13	2.93	2.54	2.48	2.77	3.64	2.76	2.68
average	2.61	2.60	2.90	2.83	2.80	2.64	2.79	2.76	3.00	2.71	2.75
difference	0.00	0.00	0.00	0.60	0.25	−0.21	−0.62	0.03	1.29	0.10	−0.14
d_{CC}	6.37		3.19[b]	3.59		3.49		4.39		3.86	

[a]The differences and averages are given between the values for upper and lower quartets. d_{CC} is the distance (in Å) between the cations. [b]Distance between the Sr_I^{2+} and Sr_{III}^{2+} cations.

https://doi.org/10.1021/acs.jpcb.1c05598
J. Phys. Chem. B XXXX, XXX, XXX−XXX

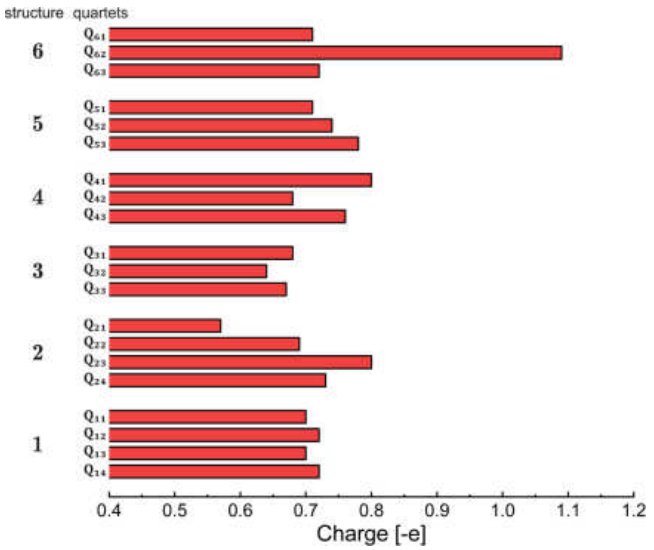

Figure 4. Average oxygens' charges for each quartet. See Figure 2 for quartet labels.

large contributions of both additive and nonadditive (many-body) polarization. Recently, Jing et al. argued that the selectivity of calcium-binding proteins for Ca^{2+} over the Mg^{2+} cation stems from the energetic cost due to the many-body polarization effect.[43] They revealed that many-body polarization is sensitive to the number and spatial arrangement of charged residues surrounding the cation. By employing the EDA, we examine to what extent polarization contributes to interaction between cations and the quadruplex scaffold. Besides, we provide insights into decreased stability of the Ba_{II}^{2+} cation.

Table 5 contains the EDA of interaction energies for binding one and two cations, cation−cation energies, and many-body effects (MBEs). Polarization contributed to a greater extent to the interaction energy for alkaline earth than alkali cations. In the former case, it amounted to around 50% of the one-cation interaction energy, whereas for alkali cations, this term was about 25%. The situation was even more drastic for the two-cation interaction energy: the sum of all other terms for quadruplexes **2** and **5** was positive, implying that their stability originated completely from the polarization energy. For other quadruplexes, polarization contributed to 70−90% of the interaction energy. Note that approximately one-third of the cation−cation Coulomb repulsion of alkaline earth cations in neighboring sites is reduced by many-body polarization energy. As expected, many-body contributions of other energy components were strictly or nearly pairwise additive.

The atomic coordinates of the quadruplex scaffold around the Sr_{III}^{2+} cation were not relaxed, so that the interaction energy of this cation was 27 kcal/mol weaker than the one of the Sr_{I}^{2+} cation. Note that interaction energies of adjacent cations in other quadruplexes can vary by up to 10 kcal/mol. Hence, we predicted that the interaction energy of the Sr_{III}^{2+} cation is approximately 20 kcal/mol underestimated. Nevertheless, this energy value does not modify the conclusions about Sr^{2+} cation chelation in the adjacent cavities of guanine quadruplexes.

Two Ba^{2+} cations in quadruplex **5** were separated by an around 1 Å larger distance than those found for other cations in the $r(GAGGU)_4$ quadruplex.[21] This resulted in 90 kcal/mol lower Coulomb repulsion between the cations. On the other hand, the Ba_{II}^{2+} is coordinated by a distorted uracil quartet whose oxygen atoms are closer to the Ba_{II}^{2+} cation than those of guanines. As a consequence of these close oxygen-cation distances, the Ba_{II}^{2+} cation experienced 150 kcal/mol larger repulsion energy than the Ba_{I}^{2+} cation. Taking into account other energy components, it was 100 kcal/mol less stable than the Ba_{I}^{2+} cation. Hence, all energy gain from longer cation−cation distance was compensated by the repulsion energy due to proximity of the uracil quartet.

Table 5. Partitioning of Cation−Cation, One- and Two-Cation Interaction Energies, and MBE (in kcal/mol)

	1-Sr_I^{2+}	**1**-Sr_{II}^{2+}	Sr_I^{2+}-Sr_{II}^{2+}	**1**-Sr_I^{2+}-Sr_{II}^{2+}	MBE
ΔE_{int}	−388.2	−384.6	205.4	−623.1	−55.7
ΔE_{ele}	−252.6	−248.8	208.5	−293.0	0.0
ΔE_{ex}	−4.3	−4.1	0.0	−8.4	0.0
ΔE_{rep}	95.2	92.6	0.0	188.3	0.5
ΔE_{pol}	−185.8	−184.1	−0.7	−429.1	−58.5
ΔE_{disp}	−40.6	−40.2	−2.4	−80.9	2.3
	2-Sr_I^{2+}	**2**-Sr_{III}^{2+}	Sr_I^{2+}-Sr_{III}^{2+}	**2**-Sr_I^{2+}-Sr_{III}^{2+}	MBE
ΔE_{int}	−388.2	−361.1	405.6	−517.3	−173.6
ΔE_{ele}	−252.6	−207.4	416.4	−43.7	0.0
ΔE_{ex}	−4.3	2.0	0.5	−2.0	−0.2
ΔE_{rep}	95.2	34.3	1.1	133.5	3.0
ΔE_{pol}	−185.8	−154.9	−11.1	−526.9	−175.1
ΔE_{disp}	−40.6	−35.0	−1.2	−78.1	1.2
	3-Na_I^{+}	**3**-Na_{II}^{+}	Na_I^{+}-Na_{II}^{+}	**3**-Na_I^{+}-Na_{II}^{+}	MBE
ΔE_{int}	−157.6	−167.4	94.1	−269.5	−38.5
ΔE_{ele}	−111.2	−118.7	95.1	−134.8	0.0
ΔE_{ex}	0.6	1.2	0.0	1.7	0.0
ΔE_{rep}	16.7	15.2	0.0	32.2	0.3
ΔE_{pol}	−39.6	−41.5	−0.4	−120.9	−39.4
ΔE_{disp}	−24.1	−23.5	−0.7	−47.7	0.6
	4-Ca_I^{2+}	**4**-Ca_{II}^{2+}	Ca_I^{2+}-Ca_{II}^{2+}	**4**-Ca_I^{2+}-Ca_{II}^{2+}	MBE
ΔE_{int}	−368.4	−376.6	364.7	−527.4	−147.0
ΔE_{ele}	−214.5	−215.3	369.8	−60.0	0.0
ΔE_{ex}	−0.3	1.5	0.1	1.3	0.0
ΔE_{rep}	43.4	29.3	0.0	73.9	1.2
ΔE_{pol}	−166.5	−162.9	−4.0	−482.1	−148.7
ΔE_{disp}	−30.6	−29.2	−1.1	−60.4	0.5
	5-Ba_I^{2+}	**5**-Ba_{II}^{2+}	Ba_I^{2+}-Ba_{II}^{2+}	**5**-Ba_I^{2+}-Ba_{II}^{2+}	MBE
ΔE_{int}	−327.6	−224.0	296.3	−356.6	−101.2
ΔE_{ele}	−216.1	−179.7	302.7	−93.2	0.0
ΔE_{ex}	−6.7	−30.8	0.1	−37.5	−0.1
ΔE_{rep}	114.6	264.5	0.0	382.3	3.2
ΔE_{pol}	−175.5	−231.0	−5.7	−517.4	−105.2
ΔE_{disp}	−43.8	−47.1	−0.9	−90.8	0.9
	6-Ba_{III}^{2+}	**6**-Ba_{IV}^{2+}	Ba_{III}^{2+}-Ba_{IV}^{2+}	**6**-Ba_{III}^{2+}-Ba_{IV}^{2+}	MBE
ΔE_{int}	−392.5	−397.7	335.0	−559.9	−104.7
ΔE_{ele}	−286.8	−297.8	344.5	−240.1	0.0
ΔE_{ex}	−8.6	−11.6	0.5	−20.1	−0.3
ΔE_{rep}	125.2	145.0	0.4	272.3	1.6
ΔE_{pol}	−174.7	−184.0	−9.5	−475.1	−106.9
ΔE_{disp}	−47.6	−49.3	−0.9	−96.9	0.9

Structure−Property Relations. Although examined quadruplexes have various geometric parameters and are chelated with different alkaline earth cation types, the cation coordination by oxygen atoms provides structure−property relations for two most stabilizing interaction energy terms: electrostatic interaction between a cation and quadruplex scaffold and the electronic shielding of cations due to many-

https://doi.org/10.1021/acs.jpcb.1c05598
J. Phys. Chem. B XXXX, XXX, XXX−XXX

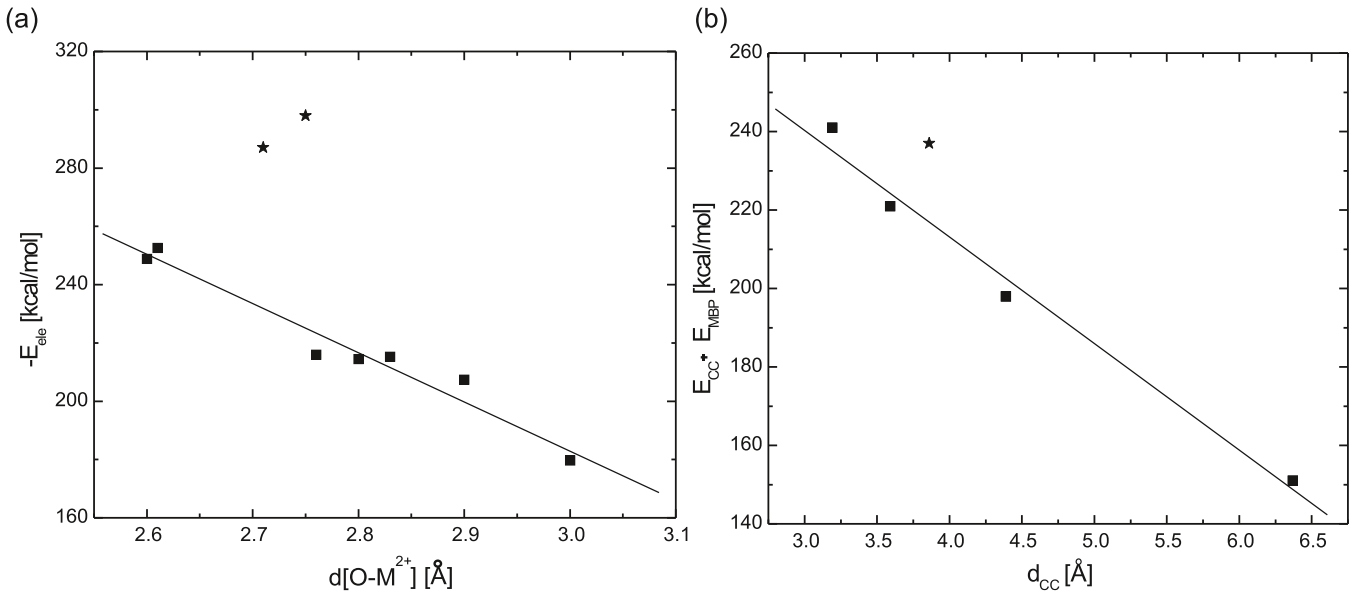

Figure 5. (a) Plot of the one-cation electrostatic energy (E_{ele}) vs the average oxygen-cation distance for both layers and (b) plot of the sum of the cation−cation Coulomb repulsion (E_{CC}) and many-body polarization energy (E_{MBP}) vs the cation−cation distance for each quadruplex. Straight lines represent linear regressions for all alkaline earth cations excluding those related to a cytosine quartet (depicted by star symbols).

body polarization. These relations hold for quadruplexes with the same chemical composition, irrespective of the chelated cations. By studying these relations, we provide insights into the excess interaction energy of the cytosine-containing quadruplex **6** relative to guanine quadruplexes.

Figure 5 shows the one-cation electrostatic energy and the sum of the cation−cation Coulomb repulsion and many-body polarization energy as functions of the average oxygen-cation and the cation−cation distance, respectively, for quadruplexes with alkaline earth cations. Both energy terms exhibited a linear correlation with the selected geometric parameters. The correlation coefficient was slightly lower for the one-cation electrostatic energy (−0.979) than for the sum of the cation−cation Coulomb repulsion and many-body polarization energy (−0.992). Note that the electrostatic energy of the Ba_{II}^{2+} cation which interacts with the uracil quartet was also nicely correlated with the energies of the other cations. The electrostatic energies of the Ba_{III}^{2+} and Ba_{IV}^{2+} cations were ≈60 kcal/mol larger than expected from the linear regression. This is a consequence of the increased water's oxygen charge relative to those of carbonyl groups. On the other hand, these cations and quadruplex **6** exhibited lower many-body polarization energy than guanine systems by 20 kcal/mol. Due to this weaker cation shielding, there is a larger decrease of the bond energy from the first to the second cation of the $(GCG)_4$ quadruplex relative to that of the guanine quadruplexes. Overall, the binding of the second Ba^{2+} cation benefits ≈40 kcal/mol from waters' oxygens in comparison with values expected from O6 oxygens.

CONCLUSIONS

The most common mode of alkaline earth cation binding to quadruplexes is the sandwich type with alternating cations and vacancies.[3−7] The goal of this study was to understand how another binding mode related to chelation in adjacent positions can be enhanced in aqueous solutions. We examined four crystallized tetramolecular quadruplexes,[19−21] two of which are associated with pyrimidine quartets. EDA of interaction energies between quadruplex scaffold and cations revealed that the binding of the second cation in a consecutive position is due to additive and many-body polarization. Solvation effects were found to be robust for different structural motifs. The common feature of all quadruplexes was that the bond energy of the second alkaline earth cation was considerably smaller than that of the first one, unlike for quadruplexes with alkali cations and alkaline earth cations in every other cavity. This indicates that each subsequent cation chelation will be even more difficult and that it is likely that only two alkaline earth cations can be bound in adjacent vacancies of hydrated quadruplexes.

Quadruplexes consisting of guanine quartets had negative energy of chelation of the second cation but these values were much smaller compared to those of alkaline cations. The energy needed to exchange two Na^{2+} by two Ca^{2+} cations is 49 kcal/mol, which shows that cation substitution is not possible in water. Could quartets composed of pyrimidine bases increase the bond energy of the second cation? Flexibility of the end-stacked uracil quartet allows elongation of the cation−cation distance by approximately 1 Å in the crystallized quadruplex. Yet, the reduced Coulomb repulsion between the cations is compensated by the large repulsion energy between uracils' oxygens and the chelated cation. Larger cation desolvation energies in water than in the crystallizing environment is responsible for positive bond energy of the cation coordinated by the uracil quartet. On the other hand, the bond energy of the second cation in the vacancy created by cytosine and guanine quartets is sufficiently large to be stable in aqueous solutions. The energy increase originates from water-mediated contacts between the cations. The increased charge of water's relative to guanine's oxygen results in stronger electrostatic attraction with cations, whereas electronic shielding is somewhat reduced. We tentatively propose that the cytosine quartet stacked between two guanine quartets has higher affinity for alkaline earth than alkali cations in water. This suggests that different structural motifs might be used to

https://doi.org/10.1021/acs.jpcb.1c05598
J. Phys. Chem. B XXXX, XXX, XXX−XXX

synthesize quadruplexes with an unusual cation bonding mode for nanotechnology applications.

■ ASSOCIATED CONTENT

Supporting Information

The Supporting Information is available free of charge at https://pubs.acs.org/doi/10.1021/acs.jpcb.1c05598.

Cartesian coordinates of all examined systems (PDF)

■ AUTHOR INFORMATION

Corresponding Author

Mihajlo Etinski − *Faculty of Physical Chemistry, University of Belgrade, 11000 Belgrade, Serbia;* orcid.org/0000-0003-0342-7045; Phone: +381113336632; Email: etinski@ffh.bg.ac.rs

Authors

Branislav Milovanović − *Faculty of Physical Chemistry, University of Belgrade, 11000 Belgrade, Serbia*

Milena Petković − *Faculty of Physical Chemistry, University of Belgrade, 11000 Belgrade, Serbia;* orcid.org/0000-0001-6180-1854

Igor Popov − *Institute for Multidisciplinary Research, University of Belgrade, 11030 Belgrade, Serbia; Institut of Physics, University of Belgrade, 11080 Belgrade, Serbia;* orcid.org/0000-0002-2030-3530

Complete contact information is available at: https://pubs.acs.org/10.1021/acs.jpcb.1c05598

Notes

The authors declare no competing financial interest.

■ ACKNOWLEDGMENTS

The research leading to these results has been cofunded by the European Commission under the H2020 Research Infrastructures contract no. 675121 (project VI-SEEM). B.M., M.P., and M.E. acknowledge the financial support by the Ministry of Education, Science and Technological Development of Republic of Serbia contract no: 451-03-9/2021-14/200146. I.P. acknowledges the financial support from the Ministry for Education, Science and Technological development of the Republic of Serbia, contract with the Institute for Multidisciplinary Research, University of Belgrade 451-03-9/2021-14/200053, and Qatar National Research Fund (QNRF), cycle eleven, grant no NPRP11S-1126-170033.

■ REFERENCES

(1) Yatsunyk, L. A.; Mendoza, O.; Mergny, J.-L. "Nano-oddities": Unusual Nucleic Acid Assemblies for DNA-Based Nanostructures and Nanodevices. *Acc. Chem. Res.* **2014**, *47*, 1836−1844.

(2) Zaccaria, F.; Paragi, G.; Fonseca Guerra, C. The Role of Alkali Metal Cations in the Stabilization of Guanine Quadruplexes: Why K^+ is the Best. *Phys. Chem. Chem. Phys.* **2016**, *18*, 20895−20904.

(3) Deng, J.; Xiong, Y.; Sundaralingam, M. X-Ray Analysis of an RNA Tetraplex $(UGGGGU)_4$ with Divalent Sr^{2+} Ions at Subatomic Resolution (0.61 Å). *Proc. Natl. Acad. Sci. U.S.A.* **2001**, *98*, 13665−13670.

(4) Shi, X.; Fettinger, J. C.; Davis, J. T. Ion-Pair Recognition by Nucleoside Self-Assembly: Guanosine Hexadecamers Bind Cations and Anions. *Angew. Chem. Int. Ed.* **2001**, *40*, 2827−2831.

(5) Hud, N. V.; Plavec, J. *Quadruplex Nucleic Acids*; Neidle, S., Balasubramanian, S., Eds.; RSC Publishing: Cambridge, U.K., 2006, Chapter 4; pp 100−130.

(6) Fyfe, A. C.; Dunten, P. W.; Martick, M. M.; Scott, W. G. Structural Variations and Solvent Structure of r(UGGGGU) Quadruplexes Stabilized by Sr^{2+} Ions. *J. Mol. Biol.* **2015**, *427*, 2205−2219.

(7) Plank, T. N.; Skala, L. P.; Davis, J. T. Supramolecular Hydrogels for Environmental Remediation: G4-Quartet Gels that Selectively Absorb Anionic Dyes from Water. *Chem. Commun.* **2017**, *53*, 6235−6238.

(8) Dumas, A.; Luedtke, N. W. Cation-Mediated Energy Transfer in G-Quadruplexes Revealed by an Internal Fluorescent Probe. *J. Am. Chem. Soc.* **2010**, *132*, 18004−18007.

(9) Jissy, A. K.; Ashik, U. P. M.; Datta, A. Nucleic Acid G-quartets: Insights into Diverse Patterns and Optical Properties. *J. Phys. Chem. C* **2011**, *115*, 12530−12546.

(10) Hua, Y.; Changenet-Barret, P.; Improta, R.; Vayá, I.; Gustavsson, T.; Kotlyar, A. B.; Zikich, D.; Šket, P.; Plavec, J.; Markovitsi, D. Cation Effect on the Electronic Excited States of Guanine Nanostructures Studied by Time-Resolved Fluorescence Spectroscopy. *J. Phys. Chem. C* **2012**, *116*, 14682−14689.

(11) Changenet-Barret, P.; Hua, Y.; Markovitsi, D. Electronic Excitations in Guanine Quadruplexes. *Top. Curr. Chem.* **2014**, *356*, 183−201.

(12) Behmand, B.; Balanikas, E.; Martinez-Fernandez, L.; Improta, R.; Banyasz, A.; Baldacchino, G.; Markovitsi, D. Potassium Ions Enhance Guanine Radical Generation upon Absorption of Low-Energy Photons by G-Quadruplexes and Modify Their Reactivity. *J. Phys. Chem. Lett.* **2020**, *11*, 1305−1309.

(13) Milovanović, B.; Stanković, I.; Petković, M.; Etinski, M. Modulating Excited Charge-Transfer States of G-Quartet Self-Assemblies by Earth Alkaline Cations and Hydration. *J. Phys. Chem. A* **2020**, *124*, 8101−8111.

(14) Gkionis, K.; Kruse, H.; Platts, J. A.; Mládek, A.; Koča, J.; Šponer, J. Ion Binding to Quadruplex DNA Stems. Comparison of MM and QM Descriptions Reveals Sizable Polarization Effects Not Included in Contemporary Simulations. *J. Chem. Theory Comput.* **2014**, *10*, 1326−1340.

(15) Gresh, N.; Naseem-Khan, S.; Lagardère, L.; Piquemal, J.-P.; Sponer, J. E.; Sponer, J. Channeling through Two Stacked Guanine Quartets of One and Two Alkali Cations in the Li^+, Na^+, K^+, and Rb^+ Series. Assessment of the Accuracy of the SIBFA Anisotropic Polarizable Molecular Mechanics Potential. *J. Phys. Chem. B* **2017**, *121*, 3997−4014.

(16) Milovanović, B.; Petković, M.; Etinski, M. Properties of the Excited Electronic States of Guanine Quartet Complexes with Alkali Metal Cations. *J. Serb. Chem. Soc.* **2020**, *85*, 1021−1032.

(17) Milovanović, B.; Stanojević, A.; Etinski, M.; Petković, M. Intriguing Intermolecular Interplay in Guanine Quartet Complexes with Alkali and Alkaline Earth Cations. *J. Phys. Chem. B* **2020**, *124*, 3002−3014.

(18) Nieuwland, C.; Zaccaria, F.; Fonseca Guerra, C. Understanding Alkali Metal Cation Affinities of Multi-layer Guanine Quadruplex DNA. *Phys. Chem. Chem. Phys.* **2020**, *22*, 21108−21118.

(19) Lee, M. P. H.; Parkinson, G. N.; Hazel, P.; Neidle, S. Observation of the Coexistence of Sodium and Calcium Ions in a DNA G-Quadruplex Ion Channel. *J. Am. Chem. Soc.* **2007**, *129*, 10106−10107.

(20) Zhang, D.; Huang, T.; Lukeman, P. S.; Paukstelis, P. J. Crystal Structure of a DNA/Ba^{2+} G-Quadruplex Containing a Water-Mediated C-Tetrad. *Nucleic Acids Res.* **2014**, *42*, 13422−13429.

(21) Pan, B.; Xiong, Y.; Shi, K.; Deng, J.; Sundaralingam, M. Crystal Structure of an RNA Purine-Rich Tetraplex Containing Adenine Tetrads: Implications for Specific Binding in RNA Tetraplexes. *Structure* **2003**, *11*, 815−823.

(22) Kwan, I. C. M.; Wong, A.; She, Y.-M.; Smith, M. E.; Wu, G. Direct NMR Evidence for Ca^{2+} Ion Binding to G-Quartets. *Chem. Commun.* **2008**, *2008*, 682−684.

(23) Kwan, I. C. M.; She, Y.-M.; Wu, G. Nuclear Magnetic Resonance and Mass Spectrometry Studies of 2',3',5'-O-Triacetylgua-

nosine Self-Assembly in the Presence of Alkaline Earth Metal Ions (Ca^{2+}, Sr^{2+}, Ba^{2+}). *Can. J. Chem.* **2011**, *89*, 835−844.
(24) *TURBOMOLE*, version 7.0; TURBOMOLE GmbH: Karlsruhe, Germany, 2015.
(25) Becke, A. D. Density-Functional Exchange-Energy Approximation with Correct Asymptotic-Behavior. *Phys. Rev. A: At., Mol., Opt. Phys.* **1988**, *38*, 3098−3100.
(26) Lee, C.; Yang, W.; Parr, R. G. Development of the Coll-Salvetti Correlation-Energy Formula into a Functional of the Electron-density. *Phys. Rev. B: Condens. Matter Mater. Phys.* **1988**, *37*, 785−789.
(27) Grimme, S.; Antony, J.; Ehrlich, S.; Krieg, H. A Consistent and Accurate Ab Initio Parametrization of Density Functional Dispersion Correction (DFT-D) for the 94 Elements H-Pu. *J. Chem. Phys.* **2010**, *132*, 154104.
(28) Weigend, F.; Ahlrichs, R. Balanced Basis Sets of Split Valence, Triple Zeta Valence and Quadruple Zeta Valence Quality for H to Rn: Design and Assessment of Accuracy. *Phys. Chem. Chem. Phys.* **2005**, *7*, 3297−3305.
(29) Guerra, C. F.; Zijlstra, H.; Paragi, G.; Bickelhaupt, F. M. Telomere Structure and Stability: Covalency in Hydrogen Bonds, not Resonance Assistance, Causes Cooperativity in Guanine Quartets. *Chem.—Eur. J.* **2011**, *17*, 12612−12622.
(30) Wolters, L. P.; Smits, N. W. G.; Guerra, C. F. Covalency in Resonance-Assisted Halogen Bonds Demonstrated with Cooperativity in N-Halo-Guanine Quartets. *Phys. Chem. Chem. Phys.* **2015**, *17*, 1585−1592.
(31) Paragi, G.; Kupihár, Z.; Endre, G.; Fonseca Guerra, C.; Kovács, L. The Evaluation of 5-Amino-and 5-Hydroxyuracil Derivatives as Potential Quadruplex-forming Agents. *Org. Biomol. Chem.* **2017**, *15*, 2174−2184.
(32) Paragi, G.; Guerra, C. F. Cooperativity in the Self-Assembly of the Guanine Nucleobase into Quartet and Ribbon Structures on Surfaces. *Chem.—Eur. J.* **2017**, *23*, 3042−3050.
(33) Reed, A. E.; Weinstock, R. B.; Weinhold, F. Natural Population Analysis. *J. Chem. Phys.* **1985**, *83*, 735−746.
(34) Klamt, A.; Schüürmann, G. COSMO: a New Approach to Dielectric Screening in Solvents with Explicit Expressions for the Screening Energy and its Gradient. *J. Chem. Soc., Perkin Trans. 2* **1993**, *5*, 799−805.
(35) Schäfer, A.; Klamt, A.; Sattel, D.; Lohrenz, J. C. W.; Eckert, F. COSMO Implementation in TURBOMOLE: Extension of an Efficient Quantum Chemical Code Towards Liquid Systems. *Phys. Chem. Chem. Phys.* **2000**, *2*, 2187−2193.
(36) Marcus, Y. Thermodynamics of Solvation of Ions Part 5. Gibbs Free Energy of Hydration at 298.15 K. *J. Chem. Soc., Faraday Trans.* **1991**, *87*, 2995−2999.
(37) Su, P.; Li, H. Energy Decomposition Analysis of Covalent Bonds and Intermolecular Interactions. *J. Chem. Phys.* **2009**, *131*, 014102.
(38) Asthagiri, D.; Dixit, P. D.; Merchant, S.; Paulaitis, M. E.; Pratt, L. R.; Rempe, S. B.; Varma, S. Ion Selectivity from Local Configurations of Ligands in Solutions and Ion Channels. *Chem. Phys. Lett.* **2010**, *485*, 1−7.
(39) Asthagiri, D. N.; Paulaitis, M. E.; Pratt, L. R. Thermodynamics of Hydration from the Perspective of the Molecular Quasichemical Theory of Solutions. *J. Phys. Chem. B* **2021**, *125*, 8294−8304.
(40) Yu, H.; Noskov, S. Y.; Roux, B. Two Mechanisms of Ion Selectivity in Protein Binding Sites. *Proc. Natl. Acad. Sci. U.S.A.* **2010**, *107*, 20329−20334.
(41) Venczel, E. A.; Sen, D. Parallel and Antiparallel G-DNA Structures from a Complex Telomeric Sequence. *Biochemistry* **1993**, *32*, 6220−6228.
(42) Liu, H.; et al. High-Resolution DNA Quadruplex Structure Containing all the A-, G-, C-, T-Tetrads. *Nucleic Acids Res.* **2018**, *46*, 11627−11638.
(43) Jing, Z.; Liu, C.; Qi, R.; Ren, P. Many-Body Effect Determines the Selectivity for Ca^{2+} and Mg^{2+} in Proteins. *Proc. Natl. Acad. Sci. U.S.A.* **2018**, *115*, E7495−E7501.

https://doi.org/10.1021/acs.jpcb.1c05598
J. Phys. Chem. B XXXX, XXX, XXX−XXX

Прилог 3 – *Properties of the Excited Electronic States of Guanine Quartet Complexes with Alkali Metal Cations*

Објављени научни рад (категорија научног часописа M_{23}):

Branislav Milovanović, Milena Petković, Mihajlo Etinski, Properties of the Excited Electronic States of Guanine Quartet Complexes with Alkali Metal Cations, *J. Serb. Chem. Soc.*, **2020**, 85 (8), pp 1021-1032.

https://doi.org/10.2298/JSC191025140M *IF(2020) 1,240*

Ауторска права код издавача (приступљено дана 15.12.2021.):

Copyright Notice

Authors who publish with this journal agree to the following terms:

Authors retain copyright and grant the journal right of first publication with the work simultaneously licensed under a Creative Commons Attribution License (http://creativecommons.org/licenses/by/3.0/) that allows others to share the work with an acknowledgement of the work's authorship and initial publication in this journal.

Authors grant to the Publisher the following rights to the manuscript, including any supplemental material, and any parts, extracts or elements thereof:

- the right to reproduce and distribute the Manuscript in printed form, including print-on-demand;
- the right to produce prepublications, reprints, and special editions of the Manuscript;
- the right to translate the Manuscript into other languages;
- the right to reproduce the Manuscript using photomechanical or similar means including, but not limited to photocopy, and the right to distribute these reproductions;
- the right to reproduce and distribute the Manuscript electronically or optically on any and all data carriers or storage media – especially in machine readable/digitalized form on data carriers such as hard drive, CD-Rom, DVD, Blu-ray Disc (BD), Mini-Disk, data tape – and the right to reproduce and distribute the Article via these data carriers;
- the right to store the Manuscript in databases, including online databases, and the right of transmission of the Manuscript in all technical systems and modes;
- the right to make the Manuscript available to the public or to closed user groups on individual demand, for use on monitors or other readers (including e-books), and in printable form for the user, either via the internet, other online services, or via internal or external networks.

Journal of the Serbian Chemical Society
JSCS-info@shd.org.rs • www.shd.org.rs/JSCS
J. Serb. Chem. Soc. *85* (8) 1021–1032 (2020)
JSCS–5356
UDC 547.857.7:532.14+546.311+
544.354–128.4:533.912
Original scientific paper

Properties of the excited electronic states of guanine quartet complexes with alkali metal cations

BRANISLAV Ž. MILOVANOVIĆ#, MILENA M. PETKOVIĆ#
and MIHAJLO R. ETINSKI*#

University of Belgrade, Faculty of Physical Chemistry, Studentski trg 12–16, 11158 Belgrade, Serbia

(Received 25 October, revised 2 December, accepted 24 December 2019)

Abstract: G-quartets are supra-molecular structures that consist of four guanine molecules connected by eight hydrogen bonds. They are additionally stabilized by metal cations. In this contribution, the excited states of G-quartet and its complexes with lithium, sodium and potassium were studied by employing time-dependent density functional theory. The findings indicate that vertical excitations from the optimized ground state involve transitions from several bases, whereas excitations from the optimized lowest excited state include transitions from one base. The charge-transfer character of these states was analyzed. It was shown that the cations are able to modify positions of the maxima of the fluorescence spectra of the complexes.

Keywords: density functional theory; G-quadruplex; fluorescence.

INTRODUCTION

Self-assembly of guanines leads to formation of square planar G-quartets (G_4) which might further stack into G-quadruplexes. These supramolecular structures allow binding of metal cations into the central cavity that results in more stable cation-templated structures. The molecular structure of a G-quartet/metal cation complex is displayed in Fig. 1. The stability of the complex is largely determined by cation–guanine interaction and Hoogsteen and/or bifurcated hydrogen bonding between hydrogen bond donating and accepting groups. It is believed that hydrogen bonding accounts for 50 % of the energy responsible for internal stability of these structures.[1]

G-quartets are highly selective towards metal cations. In an aqueous solution, alkali metal stabilization is in the order: $Cs^+ > Rb^+ > K^+ > Na^+ > Li^+$, while in the gas phase, the affinities are in the reversed order.[2] This is a con-

* Corresponding author. Email: etinski@ffh.bg.ac.rs
# Serbian Chemical Society member.
https://doi.org/10.2298/JSC191025140M

sequence of the increasing alkali metal dehydration as going from Li^+ to Cs^+.[2,3] It is additionally due to the fact that smaller cations have stronger electrostatic interactions and thus they reduce the repulsion between oxygen atoms of the guanines.[4] Zaccaria and Fonseca Guerra argued that this mutual repulsion of the oxygens appears to be a secondary effect and thus the cation is primarily required for the enthalpic stabilization of these complexes.[5] Some authors[6,7] considered cation–oxygen interaction to be mostly electrostatic in nature whereas others[1,8] considered it to be covalent.

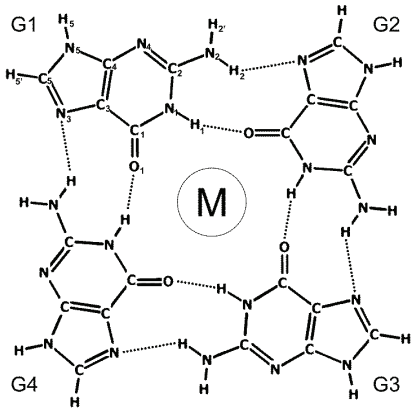

Fig. 1. Atomic and fragment numbering of the G_4–M complex.

Although excited states of G-quadruplexes were investigated both experimentally[9–13] and theoretically,[14,15] not much is known about how cations tune their properties. Hua and co-workers showed that alkali metal cations (Na^+ and K^+) play an important role in modulating decay pathways of G-quadruplexes.[12] In the presence of a potassium cation, G-quadruplex emission stems from excitonic $\pi\pi^*$ states, whereas in the presence of a sodium cation, the emission originates from charge-transfer (CT) states. Hua and coworkers argued that such difference is not due to the original excited electronic states but is a consequence of different mobility of potassium and sodium cations during electronic relation. Improta studied the excited states of the G-quartet with two potassium cations at the M05-2X/6-31G(d) level of theory.[14] He found that the lowest absorption peak of hydrated guanosine monophosphate at approximately 4.90 eV originates from two $\pi\pi^*$ states. The lowest energy transition assigned to the L_a state originates from HOMO to LUMO transition, whereas the higher energy state is the L_b state, which stems from HOMO to LUMO+1 excitation. Although the energy difference and relative intensities of these two states were correctly reproduced with the M05-2X functional, there was a blue-shift of 0.86 eV with respect to the experimental energies. This energy difference was attributed to the employed basis set and the lack of solvent–solute interaction as well as vibronic effects in the employed computational model.

In this contribution, the extent to which alkali metal cations modulate low--lying excited singlet electronic states and their charge-transfer character in G-quartet complexes with metal cations were systematically examined. The goal was to determine whether various monovalent metal cations might change the charge-transfer content of the lowest excited singlet state in its minimum. To this end, the ground and lowest excited singlet electronic states of G-quartet complexes with lithium, sodium and potassium cations were optimized and a detailed analysis of their charge-transfer character performed.

COMPUTATIONAL DETAILS

The ground state geometries of the G_4–M complexes were optimized with the M06-2X functional,[16] which correctly describes the dispersion interactions important for hydrogen bond description. The excited states were computed using the time-dependent density functional theory with a long-range corrected CAM-B3LYP functional.[17,18] This functional provides a balance description of local and charge-transfer states. It also outperforms the M06-2X functional in the energy values of the excited state.[19] Split valence 6-31+G(d,p) and 6-31G basis sets[20–24] were employed for the ground and excited state optimizations, respectively. Vertical excitation spectra were calculated with cc-pVDZ correlation consistent basis set[25] for guanines and TZVP basis set[26] for the metal cations. Geometry optimizations were performed without symmetry restrictions. All electronic structure calculations were realized using the Gaussian 16 program package.[27]

Characterization of excited state properties was performed by employing the Multiwfn program.[28,29] The interfragment charge transfer (IFCT) methodology was applied and the natural transition orbitals (NTOs) computed. The IFCT method is based on the analysis of the transition density matrix. This matrix is used to obtain the interfragment charge transfer matrix *M*, the diagonal elements of which represent the magnitude of electron redistribution on a particular atom in the corresponding excited state upon excitation from the ground state. The off-diagonal elements represent the magnitude of the electron redistribution between different atoms (*i.e.*, fragments if block matrices are considered). By summing up certain values of these matrix elements, the local excitation and charge-transfer content (in fractions) for predefined fragments in the system could be estimated for each excited state. Thus, the following descriptor was defined:

$$X = \frac{\sum_{i,j\in(G_k,M\rightarrow G_l,M)} M_{ij}}{\sum_{i,j} M_{ij}} \quad (1)$$

The sum in the denominator in Eq. (1) runs over all matrix elements while the sum in the numerator defines the quantity *X* as follows: *X* represents local excitation (LE) content if *i* and *j* run over block diagonal matrices that represent only the contribution of excitations within each fragment (single guanine unit, G_l, G_k = 1, 2, 3, 4; see Fig 1.) and metal ion (M), *i.e.*, G1→G1, G2→G2, G3→G3, G4→G4 and M→M; X represents the charge-transfer content if summing all block non-diagonal elements, for example, contribution from G1→M or G4→G3. The charge-transfer content can be divided into three parts: $CT_{neighbor}$, if only charge-transfer excitation contributions between the neighboring fragments are considered, *i.e.*, G1→G2, G1→G4; $CT_{diagonal}$ if contributions are only between diagonal guanine frag-

ments G1, G3 and G2, G4; CT_{metal} depicting the charge transfer between guanines and metal ion. The descriptors satisfy the following equation:

$$LE + CT = LE + CT_{neighbour} + CT_{diagonal} + CT_{metal} = 1 \quad (2)$$

RESULTS AND DISCUSSION

The ground state geometry

The optimized structures of G_4, G_4–Li^+, G_4–Na^+, G_4–K^+ are presented in Fig. 2 (additional data are given as Supplementary material to this paper). Their most important geometrical parameters are collected in Table I. The G_4 structure is almost planar and it has the C_{4h} symmetry group. The average distance between oxygen atoms and their geometrical center is 2.95 Å. The N_1–$H_1\cdots O_1$ and N_2–$H_2\cdots N_3$ hydrogen bond lengths amount to 1.91 and 2.46 Å, respectively. Alkali metal cations have a significant impact on the structure of the complexes. The presence of the cations decreases the repulsion between the oxygen atoms and thus decreases the lengths of the hydrogen bond. The later effect results in stronger hydrogen bonds. In addition, different cationic radii are responsible for different geometrical parameters of the complexes. The G_4–Li^+ geometry is close to the S_4 symmetry group. The average distance between the oxygen atom and lithium cation is 1.99 Å. The N_1–$H_1\cdots O_1$ and N_2–$H_2\cdots N_3$ hydrogen bond lengths are equal to 1.99 and 1.83 Å, respectively.

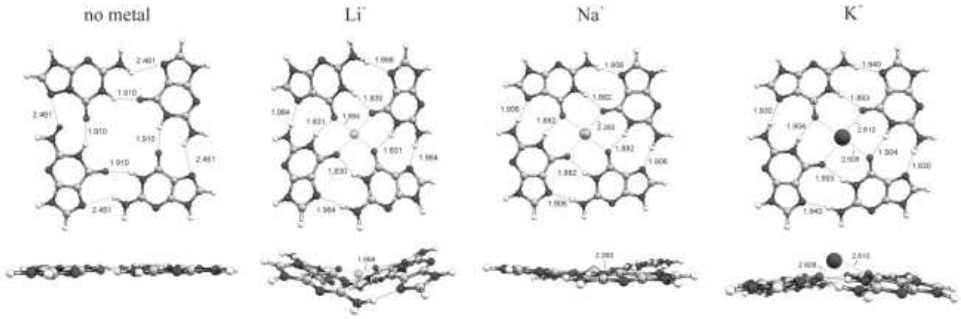

Fig. 2. The G_4 and G_4–M (M = Li^+, Na^+, K^+) structures with top and side view. The indicated hydrogen bond lengths and O_1–M distances are given in Å.

The dihedral angle between the oxygen atoms has a value of 35.2°, indicating a highly twisted structure. The G_4–Na^+ structure is much less distorted compared to the G_4–Li^+ one and it has approximately S_4 group symmetry. Dihedral angle between the oxygen atoms is equal to 0.4°. The N_1–$H_1\cdots O_1$ and N_2–$H_2\cdots N_3$ bond lengths increase and decrease relative to those of the complex with lithium cation, respectively. The structure with potassium cation has similar properties to those of the complex with sodium cation. The symmetry of the G_4-K^+ geometry is close to that of the C_4 group. Smaller ionic radius of Li^+ and

Na^+ allow these ions to be positioned in or near the center of the G_4 structure, whereas K^+ is located out of the plane defined by the G_4 structure (see Fig. 2).

TABLE I. Geometrical parameters for G_4 and G_4–M (M=Li^+, Na^+, K^+) structures

Structure	Bond distance, Å			Bond angle, °		
	d[O_1–M][a]	N_1–H_1···O_1[b]	N_2–H_2···N_3[c]	∠$N_1H_1O_1$[d]	∠$N_2H_2N_3$[e]	dih_{OOOO}[f]
G_4	2.95	1.91	2.46	151.7	131.8	0.4
G_4–Li^+	1.99	1.83	1.96	152.6	167.7	35.2
G_4–Na^+	2.26	1.88	1.91	161.8	176.2	0.4
G_4–K^+	2.61	1.90	1.93	168.1	170.4	1.1

[a]Average distance between four oxygen atoms and alkali metal ion. For an empty G_4 scaffold, the average distance of the O_1-geometrical center is taken; [b]average inner hydrogen bond distance; [c]average outer hydrogen bond distance; [d]average inner hydrogen bond angle; [e]average outer hydrogen bond angle; [f]dihedral angle defined by the four O_1 oxygen atoms

Vertical excitation spectrum

Vertical excitation energies, oscillatory strengths, excited state descriptors and fragment contributions to excitations of the first eight states of G_4 and G_4–M complexes are collected in Table II. Electronic coupling and degeneracy of the excited states of the multiple guanine bases in the examined systems is responsible for presence of the delocalized states in these supramolecular structures. Many different canonical orbitals contribute to electronic transitions and thus it is difficult to understand how the electron density is modified upon excitations. On the other hand, natural transition orbitals provide a compact description of the electronic excitations and a small number of orbitals are needed to describe the transitions. The lowest four states are the combination of different monomer-like L_a transitions, whereas the next four states belong to monomer-like L_b transitions. Although the transitions include charge-transfer, there is no net charge separation.

The G_4 absorption spectrum has two distinct maxima located at 5.22 and 5.65 eV. The exciton coupling is found to be less than 0.01 eV. Only the first state of the L_a transition is stabilized by 0.04 eV with respect to the other three states. The lowest absorption band originates from transitions to the bright S_2 and S_3 states, which are delocalized over the diagonal guanine monomers G1, G3 and G2, G4, respectively. Local excitations contribute to half of all the transitions. The dominant CT contributions are diagonal, whereas the excitations between neighboring guanine monomers account for only 7 %. The S_1 and S_4 states are dark states and thus do not contribute to this absorption band. These two states stem from the orbitals that are delocalized over all the guanine monomers. Their excitations have mostly neighboring CT character. The four L_b states have similar properties to those of the L_a states but in this case, the dark states are the third and four states in the L_b group.

TABLE II. Vertical excitation energies, oscillator strengths, excited state descriptors and fragment contributions to excitations of G_4 and G_4–M (M = Li^+, Na^+, K^+) complexes

Complex	State	E / eV	f	LE	CT	$CT_{neighbour}$	$CT_{diagonal}$	CT_{metal}	Fragment contributions
G_4	S_1	5.19	0.00	0.250	0.750	0.500	0.250	–	20% G1234 →G1234 + 24% G13→G13 + 24% G24→G24 + 27% G1234→G1234
	S_2	5.23	0.36	0.465	0.535	0.070	0.465	–	46% G1→G1 + 46% G3→G3
	S_3	5.23	0.36	0.465	0.535	0.070	0.465	–	46% G2→G2 + 46% G4→G4
	S_4	5.23	0.00	0.250	0.750	0.500	0.250	–	22% G1234 →G1234 + 24% G24→G24 + 24% G13→G13 + 26% G1234→G1234
	S_5	5.65	0.80	0.370	0.630	0.261	0.370	–	41% G4→G4 + 42% G2→G2
	S_6	5.65	0.80	0.370	0.630	0.260	0.370	–	41% G1→G1 + 42% G3→G3
	S_7	5.65	0.00	0.250	0.750	0.500	0.250	–	22% G1234→G1234 + 24% G13→G13 + 24% G24→G24 + 26% G1234→G1234
	S_8	5.66	0.00	0.250	0.750	0.500	0.250	–	22% G1234→G1234 + 24% G13→G13 + 24% G24→G24 + 26% G1234→G1234
G_4–Li^+	S_1	5.03	0.02	0.248	0.752	0.495	0.247	0.010	21% G1234→G1234 + 23% G24→G24 + 23% G13→G13 + 28% G1234→G1234
	S_2	5.06	0.29	0.466	0.534	0.058	0.466	0.010	45% G13→G13 + 49% G13→G13
	S_3	5.06	0.29	0.466	0.534	0.058	0.466	0.010	45% G24→G24 + 49% G24→G24
	S_4	5.14	0.00	0.248	0.752	0.495	0.248	0.009	21% G1234→G1234 + 23% G13→G13 + 23% G24→G24 + 28% G1234→G1234
	S_5	5.64	0.00	0.249	0.751	0.498	0.249	0.003	24% G1234→G1234 + 24% G13→G13 + 24% G24→G24 + 25% G1234→G1234
	S_6	5.69	0.66	0.472	0.528	0.052	0.472	0.003	47% G24→G24 + 47% G24→G24
	S_7	5.69	0.66	0.472	0.528	0.052	0.472	0.003	45% G13→G13 + 49% G13→G13
	S_8	5.73	0.13	0.249	0.751	0.498	0.249	0.003	21% G1234→G1234 + 24% G24→G24 + 24% G13→G13 + 26% G1234→G1234

TABLE II. Continued

Complex	State	E / eV	f	LE	CT	$CT_{neighbour}$	$CT_{diagonal}$	CT_{metal}	Fragment contributions
G_4–Na^+	S_1	5.00	0.01	0.244	0.756	0.488	0.244	0.022	20% G1234→G1234 + 22% G13→G13 + 22% G24→G24 + 32% G1234→G1234
	S_2	5.03	0.30	0.474	0.526	0.029	0.473	0.023	44% G13→G13 + 52% G13→G13
	S_3	5.03	0.30	0.474	0.526	0.029	0.473	0.023	44% G24→G24 + 52% G24→G24
	S_4	5.10	0.00	0.245	0.755	0.489	0.245	0.020	19% G1234→G1234 + 22% G13→G13 + 22% G24→G24 + 32% G1234→G1234
	S_5	5.64	0.00	0.249	0.751	0.497	0.249	0.005	23% G1234→G1234 + 24% G13→G13 + 24% G24→G24 + 25% G1234→G1234
	S_6	5.69	0.76	0.272	0.728	0.450	0.272	0.005	16% G13→G13 + 22% G13→G13 + 31% G24→G24 + 32% G24→G24
	S_7	5.69	0.76	0.272	0.728	0.450	0.272	0.005	16% G24→G24 + 22% G24→G24 + 31% G13→G13 + 32% G13→G13
	S_8	5.73	0.00	0.249	0.751	0.497	0.249	0.005	19% G1234→ G1234 + 22% G13→G13 + 22% G24→G24 + 32% G1234→G1234
G_4–K^+	S_1	5.02	0.01	0.241	0.759	0.480	0.240	0.035	20% G1234→G1234 + 23% G24→G24 + 23% G13→G13 + 30% G1234→G1234
	S_2	5.04	0.28	0.466	0.534	0.032	0.463	0.036	45% G13→G13 + 50% G13→G13
	S_3	5.04	0.30	0.466	0.534	0.030	0.464	0.038	45% G24→G24 + 50% G24→G24
	S_4	5.09	0.01	0.241	0.759	0.478	0.239	0.038	18% G1234→G1234 + 22% G13→G13 + 22% G24→G24 + 32% G1234→G1234
	S_5	5.63	0.01	0.246	0.754	0.489	0.245	0.018	23% G13→G13 + 24% G24→G24 + 24% G1234→G1234 + 25% G1234→G1234
	S_6	5.68	0.77	0.474	0.526	0.046	0.474	0.006	47% G24→G24 + 48% G24→G24
	S_7	5.68	0.75	0.474	0.526	0.043	0.473	0.008	47% G13→G13 + 47% G13→G13
	S_8	5.71	0.00	0.245	0.755	0.486	0.244	0.020	20% G1234→G1234 + 22% G13→G13 + 24% G24→G24 + 29% G1234→G1234

The presence of alkali metal cations in G-quartet results in a red-shift of the lower energy absorption band. This spectral displacement amounts to 0.17, 0.20 and 0.18 eV for the G4–Li^+, G4–Na^+ and G4–K^+ complexes, respectively. Thus, the cation radiuses are not correlated with the band shift of the L_a state. On the other hand, the cation radiuses correlate with the contribution of the guanine to metal excitations. These contributions are approximately 1, 2 and 3.5 % for the G_4–Li^+, G_4–Na^+ and G_4–K^+ complexes, respectively.

The CT_{metal} contributions mostly arise at the expense of $CT_{neighbour}$ content making the *LE* and $CT_{diagonal}$ components almost unchanged. The L_b states undergo a blue-shift which amounts to less than 0.05 eV in all three cases. Similarly to the L_a states, these shifts are not correlated with the cation radii. The CT_{metal} contribution to L_b states accounts by less than 0.5 % in the G_4–Li^+ and G_4–Na^+ systems and by less than 2.0 % in the G_4–K^+. Metal ions change the ordering of the bright and dark L_b states compared to the empty quartet scaffold. The S_6 and S_7 states become bright states responsible for the high-energy absorption band. The *LE* content is comparable to the one of the L_a states except for the G_4–Na^+ system that has a different character of the S_6 and S_7. The S_6 and S_7 bright L_b states of the G_4–Na^+ system exhibit a high *CT* content that amounts to 72.8 %. The characters of the S_5 and S_8 states are not significantly influenced by the alkali metal ions in the G_4–M complexes and they remain dark with a CT content of 75 %.

The first excited state

The properties of the first excited singlet state are not only important due to their relation with fluorescence but they might also provide insight into the electronic relaxation of the molecule. Hua and co-workers argued that the fluorescence of G-quadruplexes in the presence of sodium and potassium cations originates from states with different charge-transfer properties.[12] It is questionable whether these properties remain for isolated G-quartets, or are a consequence of G-quartet stacking. Adiabatic and vertical excitation energies, oscillator strengths, excited state descriptors and fragment contributions to the S_1 state of G_4 and G_4–M complexes are presented in Table III. The vertical excitation energies correspond to the energy differences between the S_1 and ground state at the optimized geometry of the S_1 state. The optimized geometries of the S_1 states of G_4 and G_4–M complexes are given in Fig. 3, whereas the most important geometric parameters are collected in Table IV. Natural transition orbitals reveal that the electronic excitation is localized on a single guanine fragment so that the transition mostly involves a local excitation. The charge transfer character is very small and it does not change upon cation substitution. Thus, it was concluded that the properties of the S_1 states of G-quartet and G-quadruplex are different. It is proposed that the relaxation of the excited state of G-quartets proceeds *via* guan-

ine monomers and does not include all bases. It is likely that the lifetime of the excited state of the G-quartet is similar to that of an isolated guanine.

TABLE III. Adiabatic and vertical excitation energies, oscillator strengths, excited state descriptors and fragment contributions to the S_1 state of G_4 and G_4–M (M = Li^+, Na^+, K^+) complexes

Structure	E_A eV	E_V eV	f	LE	CT	$CT_{neighbour}$	$CT_{diagonal}$	CT_{metal}	Fragment contributions
G_4	4.97	3.47	0.11	0.979	0.021	0.018	0.003	–	98% G3→G3
G_4–Li^+	4.97	4.43	0.17	0.939	0.061	0.042	0.008	0.010	96% G4→G4
G_4–Na^+	4.96	4.35	0.17	0.938	0.062	0.034	0.007	0.021	97% G2→G2
G_4–K^+	4.89	3.25	0.10	0.944	0.056	0.023	0.005	0.028	99% G2→G2

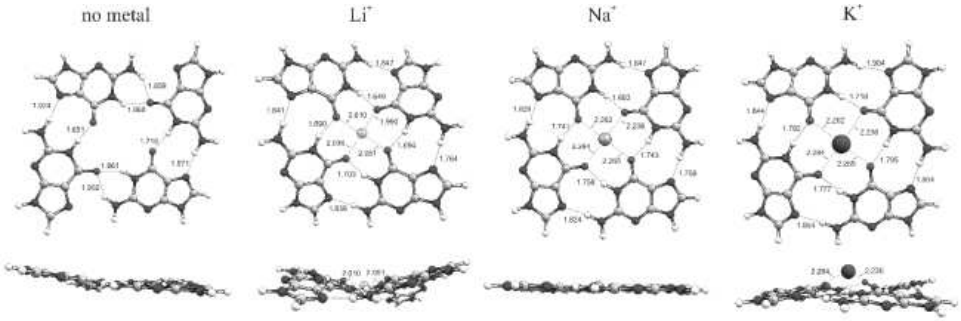

Fig. 3. The structures of G_4 and G_4–M (M = Li^+, Na^+, K^+) of the optimized state of S_1 with top and side view. The indicated hydrogen bond lengths and O1–M distances are given in Å.

The adiabatic energies of G_4, and the G_4–Li^+ and G_4–Na^+ complexes amount to approximately 5 eV. The complex with potassium cation has 0.07–0.08 eV lower adiabatic energy than the other three systems. On the other hand, the vertical excitation energies drastically vary with the cation species. The lowest value (3.25 eV) is found in the complex with potassium cation. The vertical excitation energy of the G_4 complex is 0.22 eV higher. The complexes with lithium and sodium cations have vertical energies that are approximately equal to 4.4 eV.

Therefore, there is a large difference in the maxima of the fluorescence spectra between the examined complexes. These discrepancies are correlated with the differences between optimized geometries of the ground and the first excited states. In addition to Hoogsteen hydrogen bonds, the G_4 structure also exhibits bifurcated hydrogen bonds in the S_1 state, *i.e.*, the O_1 atom is the hydrogen bond acceptor for two bonds. The G_4 geometry loses its planarity in the excited state. The average distance between oxygen atoms and their geometric centers decreases in the excited state by 0.25 Å. Thus, the ground state energy of the G_4 structure is strongly destabilized at the S_1 state optimized geometry. The

complexes with the cations exhibit smaller geometrical changes in the optimized S_1 state than the G_4 structure. Yet, the largest distortions between these complexes are found for the structure with potassium cation – its dihedral angle between the oxygen atoms changes by 5.8 degrees.

TABLE IV. Geometrical parameters for G_4 and G_4–M (M = Li^+, Na^+, K^+) structures in the S_1 optimized state

Structure	Bond distance, Å			Bond angle, °		
	d[O1–M][a]	N1–H1···O1[b]	N2–H2···N3[c]	∠N1H1O1[d]	∠N2H2N3[e]	dih_{OOOO}[f]
G_4	2.70	1.77	2.21	160.6	148.5	–1.6
G_4–Li^+	2.04	1.69	1.82	158.4	170.5	31.5
G_4–Na^+	2.26	1.74	1.81	165.4	174.6	–1.2
G_4–K^+	2.61	1.77	1.85	168.8	170.8	–4.7

[a]Average distance between four oxygen atoms and alkali metal ion. For empty G_4 scaffold average distance of O_1-geometrical center is taken; [b]average inner hydrogen bond distance; [c]average outer hydrogen bond distance; [d]average inner hydrogen bond angle; [e]average outer hydrogen bond angle; [f]dihedral angle defined by the four O_1 oxygen atoms

CONCLUSIONS

G-quartet complexes with alkali metal cations are supramolecular structures stabilized by cation–guanine interaction and hydrogen bonding. Smaller cations are positioned in or close to the plane defined by G-quartet, whereas larger cations are located out of the plane. Due to the degeneracy caused by multiple guanines, the vertical excitations of G-quartet complexes are not localized on one but involve several guanines. It was found that electronic transitions have local excitation and charge-transfer character that includes neighbor and diagonal contributions. Although the transitions include charge-transfer, there is no net charge separation. The lowest four states are found to be the combination of monomer-like L_a excitations, whereas the next four states have monomer-like L_b excitations. In the presence of the alkali cations, the L_a and L_b transitions exhibit red- and blue-shifts, respectively. The shifts are not sensitive to the nature of the cation. The lowest excited singlet state at its minimum is localized on one guanine monomer and its charge-transfer character is approximately equal for all complexes with the cations. The existence of localized excitation implies that the excited state lifetime of the G-quartet is similar to that of an isolated guanine monomer. Although all examined complexes have very similar adiabatic energies, their vertical excitation energies at the S_1 minimum differ considerably. These differences are attributed to distortions of the complex geometries at the S_1 minimum. Consequently, alkali metal cations tune the fluorescence spectra maxima of the G-quartet complexes.

SUPPLEMENTARY MATERIAL

Additional data are available electronically at the pages of journal website: https://www.shd-pub.org.rs/index.php/JSCS/index, or from the corresponding author on request.

Acknowledgements. The research leading to these results was co-funded by the European Commission under the H2020 Research Infrastructures contract No. 675121 (project VI-SEEM). The authors acknowledge the Ministry of Education, Science, and Technological Development of the Republic of Serbia (Contract No. 451-03-68/2020-14/200146) for financial support. We thank Dr. Nađa Došlić for providing a part of computational time. B. Ž. M. acknowledges the Municipality of Arandjelovac (Youth Office) for the financial support.

ИЗВОД

СВОЈСТВА ПОБУЂЕНИХ ЕЛЕКТРОНСКИХ СТАЊА КОМПЛЕКСА КВАРТЕТА ГУАНИНА СА КАТЈОНИМА АЛКАЛНИХ МЕТАЛА

БРАНИСЛАВ Ж. МИЛОВАНОВИЋ, МИЛЕНА. М. ПЕТКОВИЋ и МИХАЈЛО Р. ЕТИНСКИ

Универзитет у Београду – Факултет за физичку хемију, Студентски трг 12–16, 11158 Београд

G-квартети су супра-молекулске структуре које се састоје од четири гунанина повезана помоћу осам водоничних веза. Оне су додатно стабилизоване металним катјонима. У овом раду проучавамо побуђена стања G-квартета и њихових комплекса са литијумом, натријумом и калијумом користећи временски зависну теорију функционала електронске густине. Наши резултати указују да вертикална побуђивања из оптимизованог основног стања укључују прелазе између неколико база, док побуђивања из оптимизованог најниже побуђеног стања укључују прелазе са једне базе. Анализиран је удео преноса наелектрисања у тим стањима. Показали смо да катјони могу да модификују положаје максимума флуоросцентних спектара комплекса.

(Примљено 25. октобра, ревидирано 2. децембра, прихваћено 24. децембра 2019)

REFERENCES

1. Y. P. Yurenko, J. Novotny, V. Sklenávr, R. Marek, *Phys. Chem. Chem. Phys.* **16** (2014) 2072 (https://dx.doi.org/10.1039/C3CP53875C)
2. J. Gu, J. Leszczynski, *J. Phys. Chem., A* **106** (2002) 529 (https://dx.doi.org/10.1021/jp012739g)
3. F. Zaccaria, G. Paragi, C. Fonseca Guerra, *Phys. Chem. Chem. Phys.* **18** (2016) 20895 (https://dx.doi.org/10.1039/C6CP01030J)
4. M. T. Rodgers, P. B. Armentrout, *J. Am. Chem. Soc.* **122** (2000) 8548–8558 (https://dx.doi.org/10.1021/ja001638d)
5. F. Zaccaria, C. Fonseca Guerra, *Chem. - A Eur. J.* **24** (2018) 16315 (https://dx.doi.org/10.1002/chem.201803530)
6. G. Louit, A. Hocquet, M. Ghomi, M. Meyer, J. Sühnel, *PhysChemComm* **6** (2003) 1 (https://dx.doi.org/10.1039/B210911E)
7. J. Gu, J. Leszczynski, M. Bansal, *Chem. Phys. Lett.* **311** (1999) 209 (https://dx.doi.org/10.1016/S0009-2614(99)00821-0)
8. W. S. Ross, C. C. Hardin, *J. Am. Chem. Soc.* **116** (1994) 6070 (https://dx.doi.org/10.1021/ja00093a003)
9. F. Rosu, V. Gabelica, E. De Pauw, R. Antoine, M. Broyer, P. Dugourd, *J. Phys. Chem., A* **116** (2012) 5383 (https://dx.doi.org/10.1021/jp302468x)

10. L. Martinez-Fernández, A. Banyasz, D. Markovitsi, R. Improta, *Chem. - A Eur. J.* **24** (2018) 15185 (https://dx.doi.org/10.1002/chem.201803222)
11. M. E. Sherlock, C. A. Rumble, C. K. Kwok, J. Breffke, M. Maroncelli, P. C. Bevilacqua, *J. Phys. Chem., B* **120** (2016) 5146 (https://dx.doi.org/10.1021/acs.jpcb.6b03790)
12. Y. Hua, P. Changenet-Barret, R. Improta, I. Vayá, T. Gustavsson, A. B. Kotlyar, D. Zikich, P. Šket, J. Plavec, D. Markovitsi, *J. Phys. Chem., C* **116** (2012) 14682 (https://dx.doi.org/10.1021/jp303651e)
13. A. Banyasz, L. Martinez-Fernandez, C. Balty, M. Perron, T. Douki, R. Improta, D. Markovitsi, *J. Am. Chem. Soc.* **139** (2017) 10561 (https://dx.doi.org/10.1021/jacs.7b05931)
14. R. Improta, *Chem. Eur. J.* **20** (2014) 8106–8115 (https://dx.doi.org/10.1002/chem.201400065)
15. C. J. Lech, A. T. Phan, M.-E. Michel-Beyerle, A. A. Voityuk, *J. Phys. Chem., B* **119** (2015) 3697 (https://dx.doi.org/10.1021/jp512767j)
16. Y. Zhao, D. G. Truhlar, *Theor. Chem. Acc.* **120** (2008) 215 (https://dx.doi.org/10.1007/s00214-007-0401-8
17. T. Yanai, D. P. Tew, N. C. Handy, *Chem. Phys. Lett.* **393** (2004) 51 (https://dx.doi.org/10.1016/j.cplett.2004.06.011)
18. A. D. Becke, *J. Chem. Phys.* **98** (1993) 5648 (https://dx.doi.org/10.1063/1.464913)
19. D. Jacquemin, E. A. Perpete, I. Ciofini, C. Adamo, R. Valero, Y. Zhao, D. G. Truhlar, *J. Chem. Theory Comput.* **6** (2010) 2071 (https://dx.doi.org/10.1021/ct100119e)
20. G. A. Petersson, A. Bennett, T. G. Tensfeldt, M. A. Al-Laham, W. A. Shirley, J. Mantzaris, *J. Chem. Phys.* **89** (1988) 2193 (https://dx.doi.org/10.1063/1.455064)
21. A. D. McLean, G. S. Chandler, *J. Chem. Phys.* **72** (1980) 5639 (https://dx.doi.org/10.1063/1.438980)
22. G. A. Petersson, M. A. Al-Laham, *J. Chem. Phys.* **94** (1991) 6081 (https://dx.doi.org/10.1063/1.460447)
23. R. Krishnan, J. S. Binkley, R. Seeger, J. A. Pople, *J. Chem. Phys.* **72** (1980) 650 (https://dx.doi.org/10.1063/1.438955)
24. M. J. Frisch, J. A. Pople, J. S. Binkley, *J. Chem. Phys.* **80** (1984) 3265 (https://dx.doi.org/10.1063/1.447079)
25. T. H. Dunning Jr, *J. Chem. Phys.* **90** (1989) 1007 (https://dx.doi.org/10.1063/1.456153)
26. A. Schäfer, H. Horn, R. Ahlrichs, *J. Chem. Phys.* **97** (1992) 2571 (https://dx.doi.org/10.1063/1.463096)
27. *Gaussian 09, Revision A.02*, Gaussian, Inc., Wallingford, CT, 2016
28. T. Lu, F. Chen, *J. Comput. Chem.* **33** (2012) 580 (https://dx.doi.org/10.1002/jcc.22885)
29. T. Lu, F. Chen, *J. Mol. Graph. Model.* **38** (2012) 314 (https://dx.doi.org/10.1016/j.jmgm.2012.07.004).

Прилог 4 – *Modulating Excited Charge Transfer States of G-Quartet Self-Assemblies by Earth Alkaline Cations and Hydration*

Објављени научни рад (категорија научног часописа M_{22}):

Branislav Milovanović, Ivana M. Stanković, Milena Petković, Mihajlo Etinski, Modulating Excited Charge Transfer States of G-Quartet Self-Assemblies by Earth Alkaline Cations and Hydration, *J. Phys. Chem. A*, **2020**, 124 (40), pp 8101-8111.

https://doi.org/10.1021/acs.jpca.0c05022 *IF(2020) 2,781*

Ауторска права код издавача (приступљено дана 15.12.2021.):

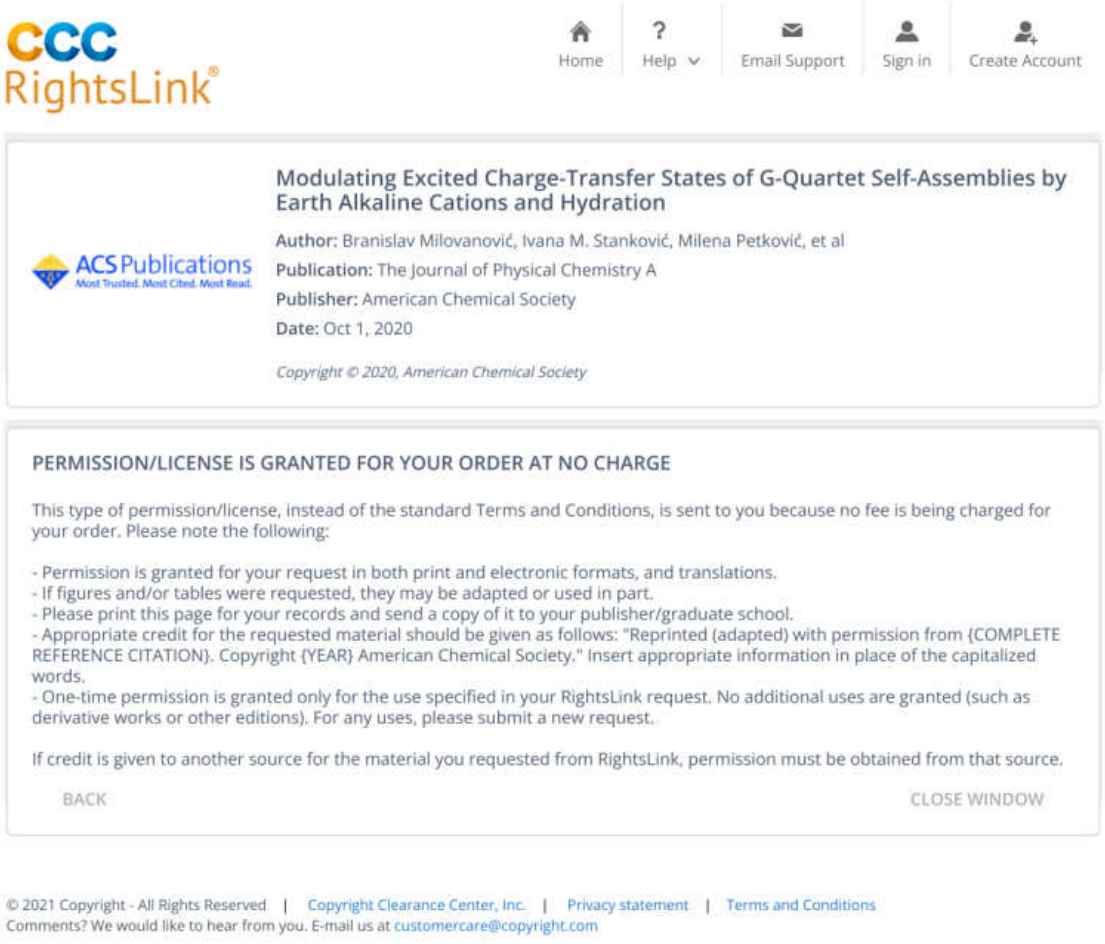

THE JOURNAL OF PHYSICAL CHEMISTRY A

pubs.acs.org/JPCA Article

Modulating Excited Charge-Transfer States of G-Quartet Self-Assemblies by Earth Alkaline Cations and Hydration

Branislav Milovanović, Ivana M. Stanković, Milena Petković, and Mihajlo Etinski*

Cite This: J. Phys. Chem. A 2020, 124, 8101−8111 Read Online

ACCESS | Metrics & More | Article Recommendations | Supporting Information

ABSTRACT: Guanine self-assemblies are promising supramolecular platforms for optoelectronic applications. The study (Hua *et al., J. Phys. Chem. C* **2012**, *116*, 14,682−14,689) reported that alkaline cations cannot modulate the electronic absorption spectrum of G-quadruplexes, although a cation effect is observable during electronic relaxation due to different mobility of Na^+ and K^+ cations. In this work, we theoretically examined whether divalent Mg^{2+} and Ca^{2+} cations and hydration might shift excited charge-transfer states of a cation-templated stacked G-quartet to the absorption red tail. Our results showed that earth alkaline cations blue-shifted nπ^* states and stabilized charge-transfer $\pi\pi^*$ states relative to those of complexes with alkaline cations, although the number of charge-separation states was not significantly modified. Earth alkaline cations were not able to considerably increase the amount of charge-transfer states below the L_b excitonic states. Hydration shifted charge-transfer states of the Na^+-coordinated G-octet to the absorption red tail, although this part of the spectrum was still dominated by monomer-like excitations. We found G-octet electron detachment states at low excitation energies in aqueous solution. These states were distributed over a broad range of excitation energies and could be responsible for oxidative damage observed upon UV irradiation of biological G-quadruplexes.

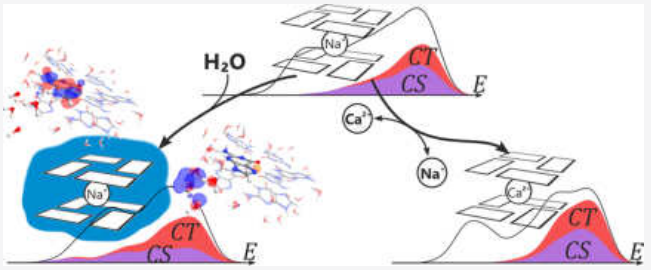

INTRODUCTION

Guanine (G) and its derivatives are able to self-assemble into ribbons and macrocycles formed by four monomers (quartets). In both structures, monomers are connected by four hydrogen bonds formed between complementary Watson−Crick and Hoogsteen edges of neighboring units, but their relative stability depends on the experimental conditions.[1] Particularly, monovalent and divalent cations dictate the self-assembly of guanines into a cation-templated G-quartet structure (see Figure 1). The stability of this supramolecular structure is determined by cooperative hydrogen bonding, the size of the cation, and its hydration energy.[2−9]

Stacking of G-quartets into columnar aggregates gives rise to G-quadruplexes in which cations are sandwiched between two G-quartets or between every other G-quartet pair as in the case of the Sr^{2+} cation.[10] The latter binding mode likely occurs due to unfavorable electrostatic repulsion between double positive charges. Among monovalent cations, K^+ has the strongest ability to govern 5′-guanosine monophosphate self-assembly into G-quadruplexes followed by Na^+ and Rb^+.[11] Generally, divalent cations are known to be more effective in stabilization of G-quadruplexes than alkaline cations.[12,13] Kwan *et al.* found that the divalent cation ability to promote formation of a guanosine derivative self-assembly follows the ordering of ionic radii found for monovalent alkaline cations ($Sr^{2+} \gg Ba^{2+} > Ca^{2+}$).[14] G-quadruplexes are also found in guanine-rich DNA and RNA sequences and have important biological functions.[15,16] It is possible to form superstructures called G-wires by polimerization of short biological G-quadruplex sequences using gel electrophoresis in the presence of K^+, Na^+, or Mg^{2+} cations.[17]

Self-assembly of functional building blocks into nanometer-sized structures is found to be a more efficient approach for optoelectronic applications than covalent syntheses.[18] Guanine absorbs light in the UV spectral region and it is not suitable for solar radiation absorption. For photovoltaic applications, it might be functionalized with a dye molecule. Wasielewski and co-workers exploited a G-quadruplex decorated with π-chromophores as a supramolecular platform for photochemical charge separation.[19−21] The core−shell columnar architecture of these systems favors photoinduced charge separation over a long distance, which demonstrates that G-quadruplexes can serve as effective hole conduits in these assemblies. Pu *et al.* used Sr^{2+}-templated G-quartet self-assembly of guanosine 5′-monophosphate intercalated with dye molecules as a light-harvesting antenna.[22] This nanostructure showed good light-harvesting properties both in solution and in the solid state

Received: June 3, 2020
Revised: September 16, 2020
Published: September 16, 2020

https://dx.doi.org/10.1021/acs.jpca.0c05022
J. Phys. Chem. A 2020, 124, 8101−8111

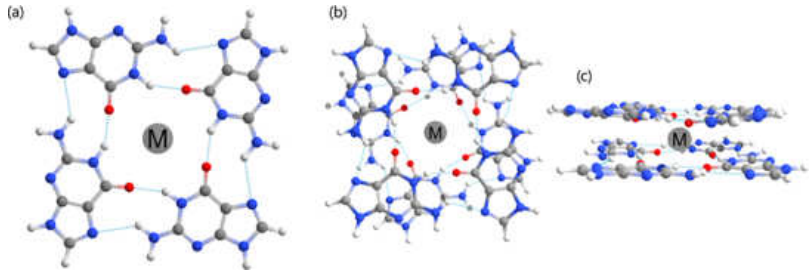

Figure 1. (a) Structure of G-quartet coordinated with a metal cation. (b) Top and (c) side views of stacked G-quartet coordinated with a metal cation.

indicating the potential for application as a photoelectric device.

Given the growing interest in G-quadruplex-based optoelectronic devices, it is necessary to examine how structural parameters modulate absorption and electronic relaxation of these supramolecular structures. Previous experimental and theoretical studies examined biological G-quadruplexes and G-wires templated with Na^+ and K^+ cations.[23−38] These studies found that their photophysics depends on the number of stacked G-quartets, relative orientation between neighboring G-quartets, and a templating cation. Absorption spectra of G-quadruplexes are dominated by collective excitations,[23] which include Frenkel excitons and charge-transfer states.[32] Excitons are found to be more strongly coupled between stacked guanines than between hydrogen-bonded guanines.[31,32]

Although the G-quadruplex structure is necessary for promoting intramolecular energy transfer, the templating cations are also needed for the unusually efficient energy-transfer reactions within the G-quadruplex.[25] Hua *et al.* studied the absorption and emission spectra of a short DNA sequence containing G-quadruplexes templated with Na^+ and K^+ cations.[26] Two-dimensional NMR experiments could not detect any differences in the relative positions of guanine moieties, indicating that the overall structure is not affected by the cation type. Also, the absorption spectra did not exhibit significant differences in either shape or intensity. On the other hand, the fluorescence spectra showed remarkable differences since they were dominated by emission from charge transfer and Frenkel excitons for Na^+- and K^+-templated structures, respectively. These findings were related to different mobility of Na^+ and K^+ cations in the central vacancies of G-quadruplexes. More mobile Na^+ cations stabilized charge-transfer states during electronic relaxation, whereas this decay channel is obstructed by the less mobile K^+ cation.

In this work, we examined to what extent the absorption spectra of G-quadruplexes templated with divalent cations differ from those of alkaline cations. Excited charge-transfer states are sensitive to environment polarity and double positive charges of divalent cations might stabilize them to a greater extent than those of monovalent cations. It is particularly intriguing whether earth alkaline cations are able to shift charge-transfer states below the first bright state since this might result in a more efficient photoinduced charge separation. We also studied the hydration effects on the excited state properties of G-quadruplexes. To this end, we simulated the electronic absorption spectra of stacked G-quartets (G-octet) templated with divalent earth alkaline cations Mg^{2+} and Ca^{2+} in the gas phase. As a reference, we also examined structures with monovalent alkaline cations Li^+, Na^+, and K^+ as well as the structure without a cation. These systems represent a minimal model of G-quartet self-assemblies, which is at the same time feasible for computational studies. The lack of a sugar-phosphate backbone enables G-quartets to exhibit various close-energy conformers and hydrogen-bonding patterns.[4] Hence, we computed the ground-state nuclear ensemble by employing classical density functional theory-based molecular dynamics. Subsequently, the excited states and their properties were calculated using time-dependent density functional theory. The hydration effects on the excited states were examined by comparing the density of states of G-octets templated with a sodium cation in the gas phase and in the microhydrated environment.

The paper is organized as follows. In the next section, we discuss various computational methods that were employed in this work. In the following section, we present and discuss results related to the relative arrangements of guanines in the G-octets as well as the cation and hydrogen-bonding interactions with the carbonyl group. Also, we discuss the density of excited states, charge-transfer character, absorption spectra, and hydration effects. Finally, we draw conclusions from our study.

METHODS

Density functional theory-based molecular dynamics simulations were performed with the CP2K program package.[39] We employed the BLYP functional[40,41] and Grimme's D3 correction for dispersion interaction.[42] The electron density was expanded using a mixed Gaussian and plane wave method[43] with a DZVP basis set for the localized functions and a cutoff of 320 Ry for the plane waves. GTH pseudopotentials[44] were used to replace core electrons, whereas the valence electrons were correlated. The simulation was performed in a cubic box with an edge size of 25 Å under nonperiodic conditions. The SCF convergence was set to 5.0×10^{-7} au. The nuclei were propagated on the Born−Oppenheimer surface of the electronic ground state using a time step of 0.5 fs. The CSVR thermostat[45] was employed in order to simulate a canonical ensemble at 300 K. The initial geometries for equlibriation were choosen to be the anti/anti partial 5/6 ring structure (see Figure 1), which was reported to be the most common stacking geometry within the G-quadruplex core.[46] The structures were equilibriated for 2 ps and subsequently propagated for 14 ps in the NVT ensemble.

Electronic absorption spectrum was simulated within the semiclassical approximation in which it is proportional to an ensemble average of vertical electronic excitations:

$$A(\omega) \approx \left\langle \sum_n f_{n,0}\, g(\omega - \omega_{n,0}) \right\rangle \quad (1)$$

https://dx.doi.org/10.1021/acs.jpca.0c05022
J. Phys. Chem. A 2020, 124, 8101−8111

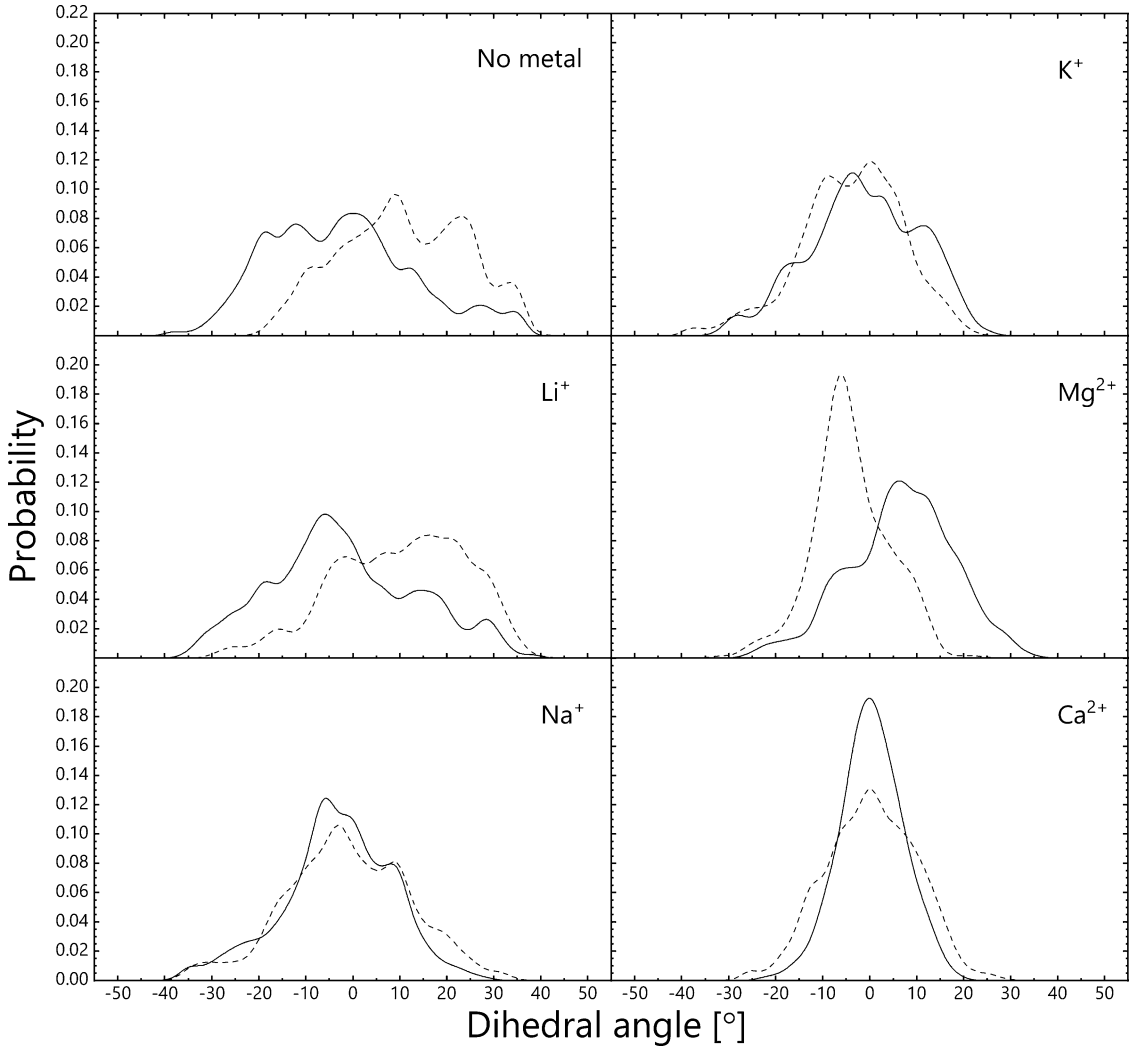

Figure 2. Probability distributions of the dihedral angles between the carbonyl oxygen atoms for each G-quartet (full and dashed lines).

where $f_{n,0}$ and $\omega_{n,0}$ are the oscillator strength and frequency of the electronic transition to the nth electronic state, respectively, and g is a line-broadening function with the Gaussian shape.

$$g(\omega) = \sqrt{\frac{2}{\pi\delta^2}} \exp(-2\omega^2/\delta^2) \tag{2}$$

We used a large broadening value δ = 0.2 eV, which enables us to remove statistical noise. The nuclear distribution in the ground electronic state was prepared by molecular dynamics simulation. The density of transition was determined by taking eq 1 and substituting $f_{n,0}$ = 1. Excited electronic states were computed by employing linear response time-dependent density functional theory with the long-range corrected CAM-B3LYP functional[47] and split valence 6-31G(d) basis set. We calculated 32 excited electronic states at 10 sampled configurations separated by 1 ps for each G-octet. The excited state calculations were carried out using the Gaussian software package.[48] Analysis of the excited states was conducted using the TheoDORE program,[49] which evaluates the one-electron transition density matrix[50,51] and natural transition orbitals.[52,53] Excited states of multichromophoric G-octet systems might be monomer-like excited states, delocalized Frenkel excitons, and charge-transfer states. Charge-transfer states involve transitions between orbitals localized on different guanines. Charge-separation states are a subset of charge-transfer states in which there is a net charge transfer from one group of guanines to the other. In this work, we only consider charge-separation states arising from excitations from one to the other G-quartet. In order to distinguish between locally excited and charge-transfer states, we used a CT descriptor implemented in the TheoDORE program, which gives a fraction of the charge transferred between guanines—a value of 1 for the pure charge-transfer state and 0 for locally excited state. The point from which the locally excited state turns into the charge-transfer state has to be chosen arbitrary and in this work, we chose a threshold value of 0.5. Charge-separation states were determined by analyzing a CT_{net} descriptor and two fragments, each consisted of one G-quartet. We also used a threshold value of 0.5 for assigning charge-separation character. Delocalization of electronic transitions (the number of guanines that participate in the excitation) was computed by employing the DEL descriptor in the TheoDORE program. This descriptor provided a real value from one up to the number of guanine fragments (eight). The computed values were rounded to the nearest integer.

The configurations of the microsolvated cluster used to elucidate the hydration effect were generated by the following

https://dx.doi.org/10.1021/acs.jpca.0c05022
J. Phys. Chem. A 2020, 124, 8101−8111

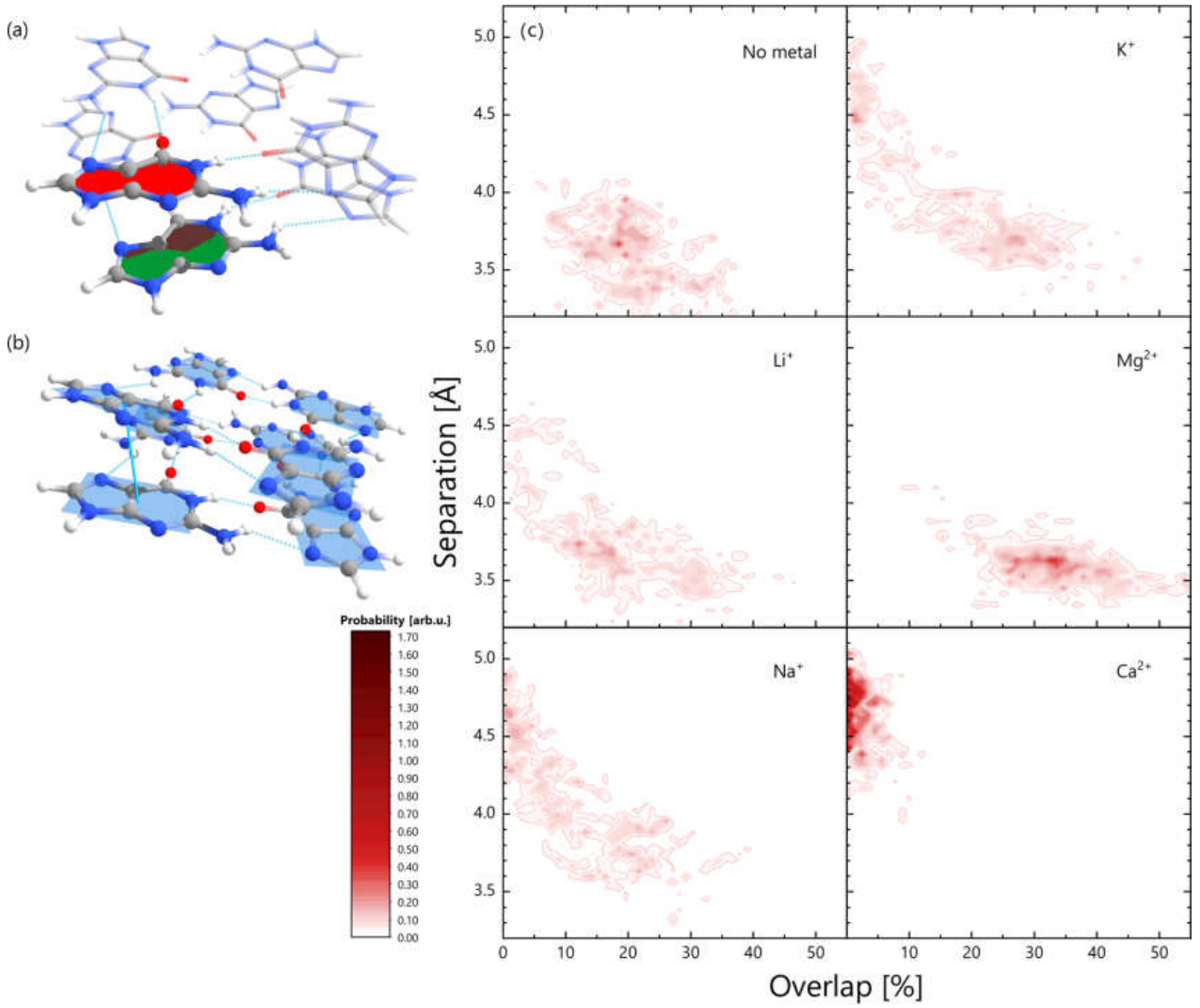

Figure 3. (a) Schematic display of overlap between the surfaces enclosed with purine ring atoms within a guanine dimer (brown surface). (b) Guanine separation coordinate. (c) Probability distribution of guanine separation and overlap coordinates.

procedure. The 10 previously selected structures of Na^+-coordinated G-octet were selected for molecular dynamics simulations in aqueous solution. Each structure was placed in the center of the orthorhombic box and solvated by water molecules using AmberTools20.[54,55] Edges of the box were expanded to a distance of 10 Å away in all directions from the solute, resulting in a box size of around 40, 40, and 31 Å along the *x*, *y*, and *z* directions, respectively. The box was filled with 1150 TIP3P[56] water molecules on average. We added one Cl^- ion to maintain the system electrostatically neutral. The G-octet was described using generalized AMBER force field (GAFF)[57] while Na^+ and Cl^- were described using the TIP3P model. The energy of the system was initially minimized by 1000 steps. After minimization, we carried out a 1 ns long classical NVT molecular dynamics run by using the NAMD program.[58] The temperature was kept constant at 298 K by means of the Langevin dynamics method.[59] During the minimization and dynamics, coordinates of the G-octet and Na^+ cation were kept fixed to preserve DFT-MD geometries. This was necessary since GAFF does not preserve the G-octet structure. The time step for integrating classical equations of motion was 1 fs. A cutoff of 12 Å with a smooth switching function starting at 10 Å was used to describe van der Waals forces, whereas electrostatic forces were treated via the particle mesh Ewald method.[60] A microsolvated cluster was created by taking the G-octet structure with 57 closest water molecules from the last configuration of the molecular dynamics run.

RESULTS AND DISCUSSION

Ground-State Properties. The lack of a sugar-phosphate backbone in stacked G-quartets gives larger flexibility in relative arrangements of guanine moieties than those in biological G-quadruplexes. These arrangements determine dipolar coupling among guanines, which influences the absorption lineshape. A theoretical study[61] found that the coordination number of the Li^+ cation in optimized stacked G-quartets differs from those of other alkaline cations as Li^+ is positioned in the middle of one G-quartet and it coordinates only four oxygens. This was attributed to the small ionic radius that prevents coordination of all oxygen atoms.[61] In our molecular dynamics simulations, we observed that Li^+ might interact with both G-quartets. Its most probable coordination numbers were four and five. We also noticed that Mg^{2+} strongly interacted with six oxygen atoms of which three belong to one G-quartet. Na^+, K^+, and Ca^{+2} cations were found

https://dx.doi.org/10.1021/acs.jpca.0c05022
J. Phys. Chem. A 2020, 124, 8101−8111

to be coordinated with eight oxygen atoms, so oxygen atoms formed a square antiprismatic molecular geometry.

Having discussed the coordination of the cations, let us proceed to the relative orientation of guanines in the G-octets. The probability distribution of dihedral angles defined between the carbonyl oxygen atoms is presented in Figure 2. It reflects a deviation of G-quartet from planarity (dihedral angle equals to 0°). The structures with Na^+, K^+, and Ca^{+2} exhibit planar G-quartets, with Ca^{+2} having the least deviations. The G-octets coordinated with Li^+ and Mg^{2+} cations and without a cation have G-quartets, which are nonplanar. The broad probability distributions of these systems indicate that they possess a shallow potential energy surface along the dihedral angle. Pronounced asymmetry of the distributions for G-quartets with Li^+ and Mg^{2+} cations is due to the flexibility of noncoordinated guanines.

Azargun et al. failed to produce a 9-ethylguanine octet coordinated with a Li^+ cation in the gas phase, although other alkaline cations easily formed the complexes.[62] We believe that the instability of Li^+-coordinated G-octets originates from the inability of the Li^+ cation to coordinate all oxygen atoms and subsequently the lack of G-quartet rigidity, which is crucial for G-quartet stacking. In the case of the Mg^{2+} cation, the stability might be even more reduced since it was previously shown that G-quartets with earth alkaline cations only exist because of strong cation−guanine attraction[9] and this cation also does not coordinate all oxygen atoms. We will show below that the earth alkaline cations even reduce the strengths of the inner hydrogen bonds in the G-octets relative to those of G-octets coordinated with alkaline cations.

G-quartet arrangements, which have a high degree of 5/6 ring overlap in G-quadruplexes, exhibit exceptional electron−hole transfer rates and charge-transfer properties.[29,32] In order to examine to what extent cations modify guanine stacking in the G-octets, we studied the following two coordinates: (1) guanine overlap coordinate, defined as an average overlap between the surfaces enclosed with purine ring atoms obtained by projecting a ring of one quartet on its counterpart and expressed in percents and (2) guanine separation coordinate, defined as a minimal distance between geometrical centers of purine rings in one quartet and their analogues in the other quartet. The probability distribution of these coordinates is given in Figure 3. It can be noticed that G-octets with alkaline cations have similar distributions, although the average base separation coordinate is smaller for the Li^+-templating structure than for the other two structures. In these cases, the guanine overlap coordinates take values from 0 to 40%, with larger values indicating smaller separation. The structure without a metal cation preserves the guanine overlap better than the structures with alkaline cations. The highest guanine overlap is found for the Mg^{2+}-templating G-octet with an average value of 35%. On the other hand, the Ca^{2+} cation disrupts the base overlap since it does not allow small separations between the bases. These data might indicate that the Mg^{2+}-containing G-octet would have a higher degree of exciton delocalization than other G-octets. Yet, we will later show that this is not the case since nonplanar G-quartets in the presence of a Mg^{2+} cation prevent exciton delocalization.

The carbonyl group plays an important role in low-lying electronic excitations of G-octets since these transitions originate from nonbonding n and bonding π orbitals localized on this group. The electron density of carbonyl is perturbed by inner hydrogen bonds and oxygen−cation interaction. Although the latter interaction is dominated by electrostatics,[6,9] it also has a partially covalent nature. Selected geometrical parameters related to these interactions are collected in Table 1. Similarly, as for the guanine overlap−separation probability distribution, we find that G-octets with alkaline cations have comparable geometrical parameters. The inner hydrogen bonds of alkaline cation-coordinated G-octets amount to 1.82−1.84 Å, whereas their angles are in the range of 160−165°. In the case of earth alkaline cations, the hydrogen bond length is found to be longer. This implies that G-octets in complexes with earth alkaline cations have weaker inner hydrogen bonds relative to the alkaline analogues. Particularly, the Mg^{2+}-coordinated structure has a 0.23 Å longer inner hydrogen bond than the one in the G-octet without the cation. On the other hand, earth alkaline cations make the oxygen−cation distance even shorter than the alkaline cations, which is favorable for electrostatic interaction between lone pairs of the oxygens and cation. This interaction results in elongation of the oxygen lone pair toward the metal cation and subsequent stabilization of the oxygen *n* orbital. Hence, the excitations from the oxygen *n* orbitals will have higher energies in G-octets with earth alkaline than with alkaline cations.

Table 1. Selected Distances (in Å) and Angles (in °)[a]

cation	$O\cdots M^{+/2+}$	$\delta[WC_{LP}\cdots O]$	N − H···O	N−H−O
no metal	3.51	0.000	1.96	153
Li^+	2.96	0.011	1.84	160
Na^+	2.77	0.009	1.82	163
K^+	2.93	0.007	1.84	165
Mg^{2+}	2.63	0.028	2.19	146
Ca^{2+}	2.60	0.024	1.88	158

[a] $O\cdots M^{+/2+}$ is the oxygen−cation distance (in the case without a cation, it is the distance between the geometrical center of eight oxygen atoms and oxygen atoms), $\delta[WC_{LP}\cdots O]$ is the distance between a Wannier center of the oxygen lone pair (directed toward the cation) and oxygen nucleus relative to the value for the G-octet without a cation, N−H···O is the inner hydrogen bond length, and N−H−O is the inner hydrogen bond angle.

Density of Excited States. Assigning the diabatic character of excited electronic states from each configuration in a nuclear ensemble is a difficult task. A recently proposed procedure for automatic spectral assignment[63] is not applicable due to large discrepancies between the selected reference geometry and other geometries in the ensemble that result from G-octets' pronounced flexibility. Yet, we were able to assign $n\pi^*$ and $\pi\pi^*$ transitions by visual inspection of natural transition orbitals.

The density of states for examined G-octets are given in Figure 4. There is a correlation between the ground-state properties of the G-octets and those densities. As we already discussed, the ground-state properties of the G-octets with alkaline cations are similar. The same is valid for their densities of states. The situation is somewhat different with earth alkaline cations. This is in line with a finding of Jissy *et al.* who showed that electronic properties of a G-quartet are more sensitive to cation radii in the case of earth alkaline cations than in the case of alkaline cations.[4] Note that the density of states for the Mg^{2+}-coordinated G-octet exhibits a long tail at the low-energy side likely due to insufficient sampling in the nuclear ensemble.

https://dx.doi.org/10.1021/acs.jpca.0c05022
J. Phys. Chem. A 2020, 124, 8101−8111

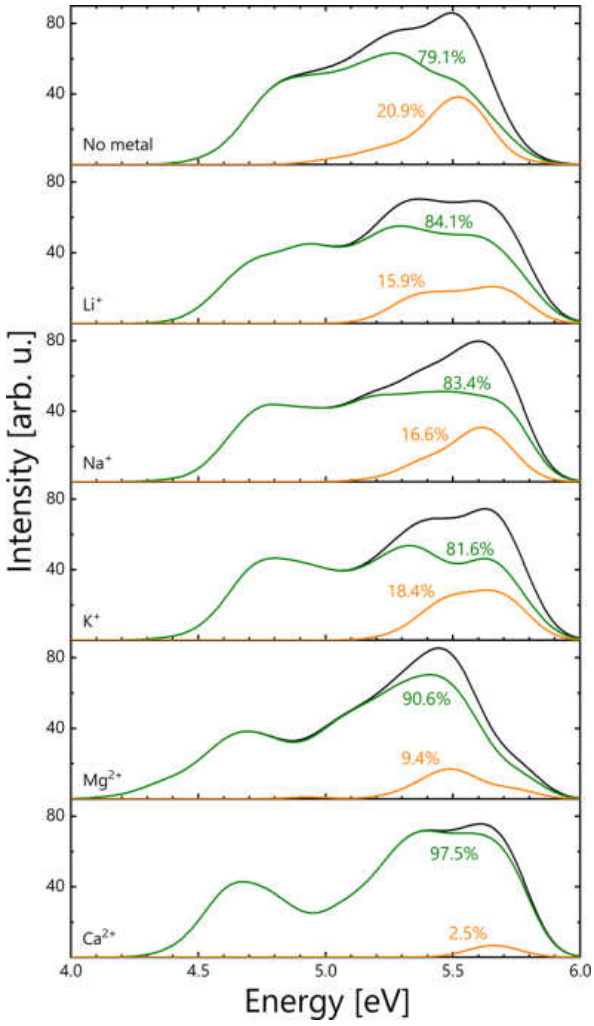

Figure 4. Density of states (black line) decomposed on the $\pi\pi^*$ (green line) and $n\pi^*$ (orange line) contributions.

In all analyzed systems, most of the first 32 computed excited states belong to $\pi\pi^*$ excitations. The first two $\pi\pi^*$ states of guanine are well-known L_a and L_b states. By using the semiclassical approximation, Sapunar *et al.* estimated their energies to be 4.57 and 5.22 eV, respectively, in the gas phase at the ADC(2)/aug-cc-pVDZ level of theory.[63] From the shoulder of the $\pi\pi^*$ density of states, we find that L_a states are positioned at 4.40 eV in the empty G-octet. The presence of the alkaline and earth alkaline cations red-shifts these states by 0.15 and 0.20−0.25 eV, respectively. The energy of the L_b states amounts to 5.25 eV in the empty G-octet. The complexation of the G-octet with alkaline and earth alkaline cations blue-shifts the L_b states by 0.05−0.10 and 0.10 eV, respectively. Interestingly, the L_a and L_b states in aqueous solution[63] have the opposite energy shift relative to those due to the cation complexation in G-quadruplexes. The L_a and L_b states are followed with two close-energy groups of $\pi\pi^*$ states,[63] which are difficult to resolve in our density of states.

$n\pi^*$ transitions are found above the L_a states. Their ratio in the first 32 states decreases from 21% in the empty G-octet to 16−18% in G-octets coordinated with alkaline cations and 9 and 2% for Mg^{2+}- and Ca^{2+}-coordinated complexes, respectively. This is a consequence of the stabilization of the oxygens' n orbitals due to hydrogen bonding and interaction with a cation, which results in higher excitation energies of $n\pi^*$ states. These states are shifted above the first 32 states and at the same time, higher $\pi\pi^*$ states are lowered to their positions. In order to understand the origin of the latter effect, we examined charge-transfer and charge-separation characters of the excited states. Their contributions to the density of states are displayed in Figure 5. Only $\pi\pi^*$ states above the L_a states

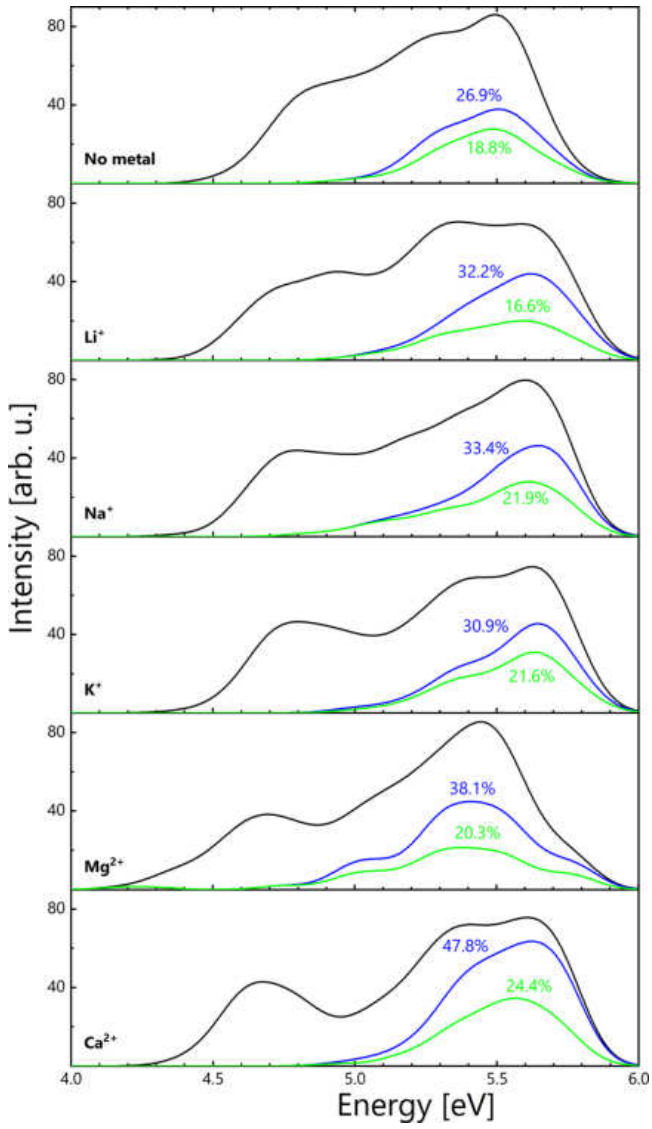

Figure 5. Density of states (black line) and its charge transfer (blue line) and charge separation (green line) contributions.

exhibit a significant charge-transfer character. Their contribution for energies below 5 eV is less than 1%. The exception is the Mg^{2+}-coordinated G-octet, which has approximately 4% of charge-transfer states. The contribution of charge-transfer states to density of states of the empty G-octet is 27%. It increases to 31−33% for the G-octets with alkaline cations, which again confirms that Franck−Condon states of these G-octets have very similar properties. An even larger increase is found in the systems coordinated with earth alkaline cations, with 38 and 48% for Mg^{2+} and Ca^{2+}, respectively. Stabilization of these $\pi\pi^*$ charge-transfer states is due to the cation electrostatic field. Contrary to charge-transfer states, the total number of charge separation states does not considerably

https://dx.doi.org/10.1021/acs.jpca.0c05022
J. Phys. Chem. A 2020, 124, 8101−8111

depend on the cation type. The largest number of charge-transfer states is observed in the G-octet coordinated with the Ca^{2+} cation—only 2% more than the G-octets with Na^+ and K^+ cations. Thus, it is not possible to employ earth alkaline cations to significantly modulate charge separation in the vertical electronic excitation spectrum. In addition, this finding reveals that additional charge-transfer states due to a cation coordination do not have net transfer of charge but are formed from the mutual charge relocations between guanines.

Charge-transfer states are typically characterized with low oscillatory strengths. Let us now discuss the absorption spectra and their charge-transfer contribution (Figure 6). The

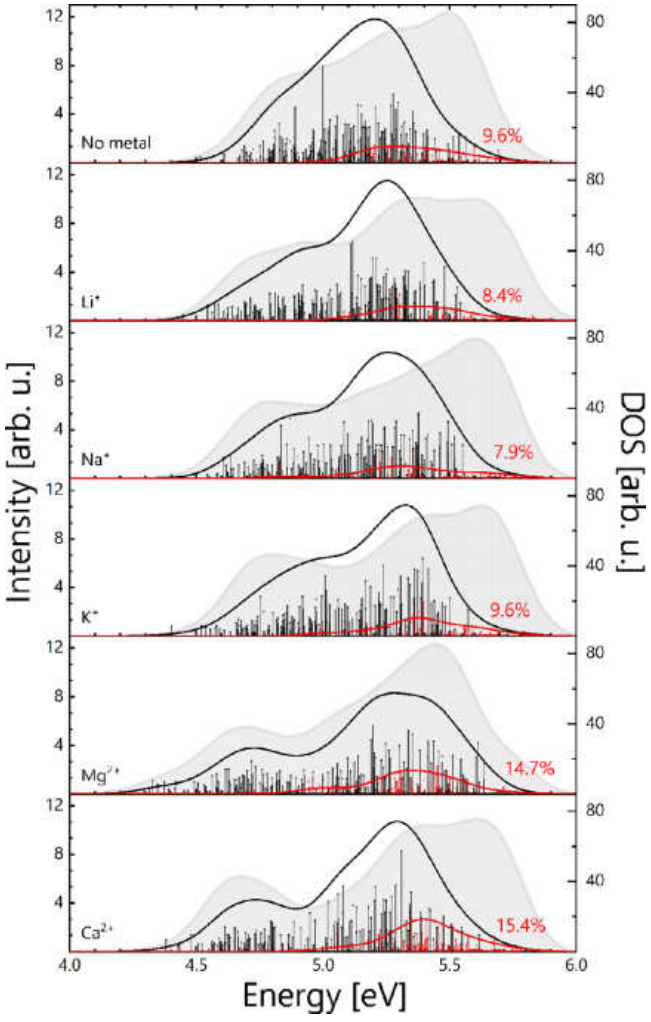

Figure 6. Computed absorption convoluted and stick spectra (black lines), their CT contributions (red lines), and density of states (gray shaded area).

absorption spectrum consists of two peaks due to the L_a and L_b transitions. These two peaks converge into a single broad peak with a shoulder in the case of the empty G-octet. On the other hand, the gap between them is larger for earth alkaline than for alkaline cations. UV light-absorbing charge-transfer states are positioned at somewhat higher energies than the maximum of the L_b band. The contribution of these states to absorption of the empty G-octet is 10%. Alkaline cations have negligible effects on the charge-transfer state absorption, whereas earth alkaline cations increase this contribution by 50%. These results demonstrate that photoabsorption leads to a more pronounced population of charge-transfer states of earth alkaline complexes compared to their alkaline analogues. Decompositions of the absorption spectra according to excited state delocalization are given in Figure S1 in the Supporting Information. The absorption is dominated by excited states delocalized on two guanines. The contribution of states delocalized on three guanines is larger than those of monomer-like states. The latter states contribute at most to the absorption in the red tail, similarly as in single-stranded polyadenine.[64] We find that that delocalization does not considerably vary with the cation type. This implies that intramolecular energy transfer occurring upon photoexcitation of these systems has similar initial dynamics.

Hydration Effects. Charge-transfer states in aqueous solution exhibit strong solvatochromism due to dipole electric field caused by the hydration shell. Yin *et al.* found that the lowest charge-transfer state of stacked adenine in water is red-shifted by 0.7−1.0 eV relative to the value in the gas phase.[65] The charge-transfer state is found to be positioned below bright states in the absorption red tail. Motivated by this finding, we studied hydration effects on charge-transfer states of G-octets templated with the Na^+ cation.

Figure 7 displays the absorption spectra, density of states, and their decomposition for the system in the gas phase and aqueous solution. Both charge-transfer and charge-separation states are considerably stabilized in water relative to the gas phase. They appear in the absorption red tail but their density is lower than that of monomer-like states. In the blue part of the spectrum, charge-transfer density of states also increases, whereas $n\pi^*$ states are blue-shifted. It is interesting that delocalization of excited states in water is larger than in the gas phase. Particularly, there are two times less monomer-like states and three times more states that are delocalized on three guanines.

In addition to charge-transfer states localized on the G-octet, we also found charge-transfer states that include electron transfer for the G-octet to water molecules. These electron detachment states have a very broad distribution that begins at 4.4 eV. Their contribution to the total density of states amounts to 7.5%, which points to their probable population upon photoexcitation. In Figure 7, we also provide natural transition orbitals for one such transition. This is a long-range electron transfer, i. e., an electron is transferred from a guanine to water molecules that are not in its vicinity.

Note that unlike other nucleobases, guanine is very weakly soluble in water. It has to be functionalized with hydrophilic moieties such as the sugar-phosphate group in order to become more soluble. Yet, it is not clear to what extent these moieties screen guanines from water electric field. Nogueira *et al.* showed that charge-transfer states of single-stranded poly-adenine in aqueous solution are not located in the red side of the absorption spectrum.[64] They argued that the sugar-phosphate backbone prevents water molecules to interact directly with nucleobases and thus, small cluster models with hydrated nucleobases do not appropriately describe hydration of biological self-assemblies.

Recently, Markovitsi and co-workers reported that photo-ionization of biological G-quadruplexes occurs at much lower energies than for guanine mononucleotide.[37,66] This process is found to be operative in a very broad excitation energy range. Since the cation effect was noticed,[37] these authors argued that photoionization of G-quadruplexes does not proceed vertically but occurs in a series of steps that start from the population of

https://dx.doi.org/10.1021/acs.jpca.0c05022
J. Phys. Chem. A 2020, 124, 8101−8111

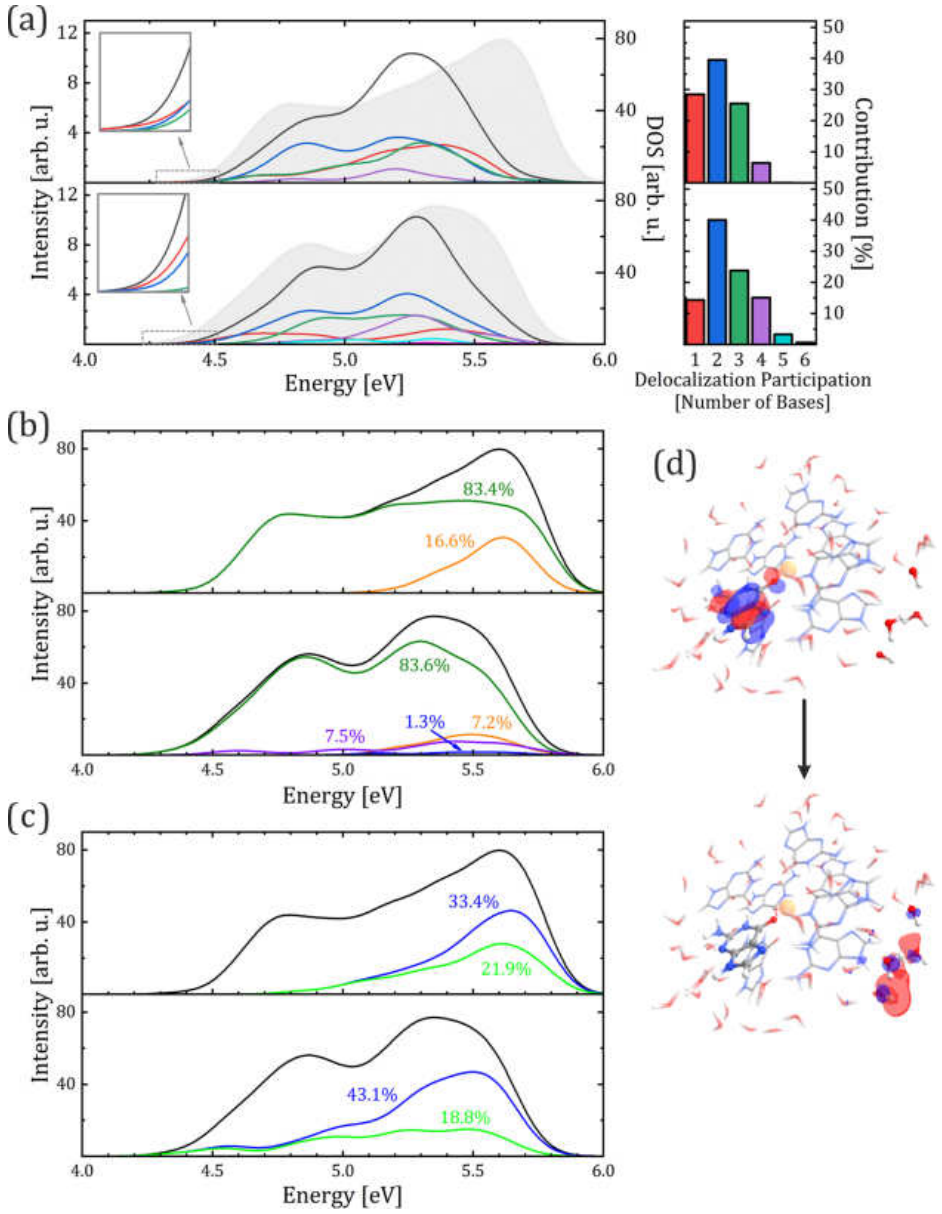

Figure 7. Excited-state properties of of the G-octet templating with the Na^+ cation in the gas phase (upper plots) and aqueous solution (lower plots): (a) Left: decomposition of the absorption spectra (black lines) according to excited-state delocalization: DEL = 1 (red lines), DEL = 2 (blue lines), DEL = 3 (green lines), DEL = 4 (purple lines), DEL = 5 (cyan lines), and DEL = 6 (yellow lines). The insets show the decomposition of the absorption red tail. Density of states is represented by the gray shaded area. Right: histograms of DEL contributions to the spectrum (the same coloring code as in the spectrum plots). (b) Density of states (black line) decomposed on the $\pi\pi^*$ (green line) and $n\pi^*$ (orange line) states, charge-transfer states between the G-octet and water (purple line), and transitions localized on water molecules (blue line). (c) Density of states (black line) and its charge-transfer (blue line) and charge-separation (green line) states localized on the G-octet. (d) Natural transition orbitals involved in a selected charge transfer from the G-octet to water molecules.

G-quadruplex charge-transfer states. The similarity between properties of electron detachment states observed in our simulation and experimentally detected photoionization states of biological G-quadruplexes[37,66] led us to tentatively propose that G-quadruplex oxidative damage upon UV light absorption might also take place in a single step.

CONCLUSIONS

In this work, the cation and hydration effects on low-energy excited states of G-quartet self-assemblies in the Franck–Condon region were studied. We employed a minimal model consisting of two stacked G-quartets coordinated with alkaline Li^+, Na^+, K^+, and earth alkaline Mg^{2+} and Ca^{2+} cations. The lack of a sugar-phosphate backbone in these systems resulted in larger conformational flexibility of guanine molecules. Generally, all alkaline cation-coordinated G-octets had similar ground-state properties. The exception was the lower coordination number of the Li^+ cation, which enabled larger distortions of G-quartets. Also, the complex with the Na^+ cation had a somewhat shorter oxygen–cation distance and stronger inner hydrogen bonds than the complexes with other alkaline cations. On the other hand, the G-octets coordinated with earth alkaline cations exhibited larger variations in guanine arrangements and inner hydrogen bond strength. Interestingly, it was found that stacked guanine molecules in

https://dx.doi.org/10.1021/acs.jpca.0c05022
J. Phys. Chem. A 2020, 124, 8101–8111

the Mg^{2+}-containing G-octet experience more pronounced overlap than those in any other G-octet.

G-octets coordinated with divalent earth alkaline cations had slightly different excited-state properties compared to their alkaline counterparts. Apart from the larger L_a-L_b gaps, the presence of earth alkaline cations blue-shifted $n\pi^*$ states and stabilized charge-transfer $\pi\pi^*$ states. Yet, the number of states that resulted in charge separation between G-quartets was not considerably modified upon cation exchange. The ratio of charge-transfer states lower than 5 eV was below 1% in all G-octets except for the Mg^{2+}-coordinated one, which had approximately 4%. Therefore, earth alkaline cations are not able to increase the density of charge-transfer states in the absorption red tail. The present study unraveled a complex relation between the properties of the metal cation and the electronic absorption spectra of G-quadruplexes that might be exploited in the design of novel nanostructures with adjustable optical properties. In this respect, it would be interesting to study the effects that may arise from the coordination with trivalent lanthanide metal ions[67] or two divalent cations coordinated between consecutive G-quartets.

Hydration shifted charge-transfer states to the absorption red tail. However, this spectral range was dominated by monomer-like excitations as in the gas phase. We found a broad density of states related to electron transfer from G-octet to water molecules. These electron detachment states might also be present in biological G-quadruplexes, although the sugar-phosphate backbone screens guanines from water electric field. We tentatively proposed that these states are responsible for oxidative damage of G-quadruplexes[37,66] upon UV photoexcitation.

■ ASSOCIATED CONTENT

Supporting Information

The Supporting Information is available free of charge at https://pubs.acs.org/doi/10.1021/acs.jpca.0c05022.

Decomposition of absorption spectra according to excited-state delocalization (PDF)

■ AUTHOR INFORMATION

Corresponding Author

Mihajlo Etinski − *Faculty of Physical Chemistry, University of Belgrade, Belgrade 11000, Serbia;* orcid.org/0000-0003-0342-7045; Phone: +381113336632; Email: etinski@ffh.bg.ac.rs

Authors

Branislav Milovanović − *Faculty of Physical Chemistry, University of Belgrade, Belgrade 11000, Serbia*

Ivana M. Stanković − *Institute of Chemistry, Technology and Metallurgy, University of Belgrade, Belgrade 11000, Serbia;* orcid.org/0000-0001-5790-5538

Milena Petković − *Faculty of Physical Chemistry, University of Belgrade, Belgrade 11000, Serbia;* orcid.org/0000-0001-6180-1854

Complete contact information is available at: https://pubs.acs.org/10.1021/acs.jpca.0c05022

Notes

The authors declare no competing financial interest.

■ ACKNOWLEDGMENTS

The research leading to these results has been cofunded by the European Commission under the H2020 Research Infrastructures contract no. 675121 (project VI-SEEM). B.M., M.P., and M.E. acknowledge the financial support by the Ministry of Education, Science and Technological Development of Republic of Serbia contract no, 451-03-68/2020-14/200146 B.M. acknowledges the Municipality of Arandjelovac (Youth Office) for the financial support. M.E. thanks Dr. Nađa Došlić(Ruđer Bošković Institute, Zagreb) for useful comments.

■ REFERENCES

(1) Davis, J. T.; Spada, G. P. Supramolecular Architectures Generated by Self-Assembly of Guanosine Derivatives. *Chem. Soc. Rev.* **2007**, *36*, 296−313.

(2) Louit, G.; Hocquet, A.; Ghomi, M.; Meyer, M.; Sühnel, J. Guanine Tetrads Interacting with Metal Ions. An AIM Topological Analysis of the Electronic Density. *PhysChemComm* **2003**, *6*, 1−5.

(3) van Mourik, T.; Dingley, A. J. Characterization of the Monovalent Ion Position and Hydrogen-Bond Network in Guanine Quartets by DFT Calculations of NMR Parameters. *Chem. − Eur. J.* **2005**, *11*, 6064−6079.

(4) Jissy, A. K.; Ashik, U. P. M.; Datta, A. Nucleic Acid G-quartets: Insights into Diverse Patterns and Optical Properties. *J. Phys. Chem. C* **2011**, *115*, 12530−12546.

(5) Guerra, C. F.; Zijlstra, H.; Paragi, G.; Bickelhaupt, F. M. Telomere Structure and Stability: Covalency in Hydrogen Bonds, not Resonance Assistance, Causes Cooperativity in Guanine Quartets. *Chem. − Eur. J.* **2011**, *17*, 12612−12622.

(6) Yurenko, Y. P.; Novotný, J.; Sklenář, V.; Marek, R. Exploring Non-covalent Interactions in Guanine-and Xanthine-based Model DNA Quadruplex Structures: A Comprehensive Quantum Chemical Approach. *Phys. Chem. Chem. Phys.* **2014**, *16*, 2072−2084.

(7) Paragi, G.; Guerra, C. F. Cooperativity in the Self-Assembly of the Guanine Nucleobase into Quartet and Ribbon Structures on Surfaces. *Chem. − Eur. J.* **2017**, *23*, 3042−3050.

(8) Milovanović, B. Ž.; Petković, M. M.; Etinski, M. R. Properties of the Excited Electronic States of Guanine Quartet Complexes with Alkali Metal Cations. *J. Serb. Chem. Soc.* **2020**, *85*, 1021−1032.

(9) Milovanović, B.; Stanojević, A.; Etinski, M.; Petković, M. Intriguing Intermolecular Interplay in Guanine Quartet Complexes with Alkali and Alkaline Earth Cations. *J. Phys. Chem. B* **2020**, *124*, 3002−3014.

(10) Deng, J.; Xiong, Y.; Sundaralingam, M. X-Ray Analysis of an RNA Tetraplex $(UGGGGU)_4$ with Divalent Sr^{2+} Ions at Subatomic Resolution (0.61 Å). *Proc. Natl. Acad. Sci. U. S. A.* **2001**, *98*, 13665−13670.

(11) Pinnavaia, T. J.; Marshall, C. L.; Mettler, C. M.; Fisk, C. L.; Miles, H. T.; Becker, E. D. Alkali Metal Ion Specicity in the Solution Ordering of a Nucleotide, 5′-Guanosine Monophosphate. *J. Am. Chem. Soc.* **1978**, *100*, 3625−3627.

(12) Chen, F. M. Sr^{2+} Facilitates Intermolecular G-Quadruplex Formation of Telomeric Sequences. *Biochemistry* **1992**, *31*, 3769−3776.

(13) Hardin, C. C.; Watson, T.; Corregan, M.; Bailey, C. Cation-Dependent Transition Between the Quadruplex and Watson-Crick Hairpin Forms of d(CGCG3GCG). *Biochemistry* **1992**, *31*, 833−841.

(14) Kwan, I. C. M.; She, Y.-M.; Wu, G. Nuclear Magnetic Resonance and Mass Spectrometry Studies of 2′,3′,5′-O-Triacetylguanosine Self-Assembly in the Presence of Alkaline Earth Metal Ions (Ca^{2+}, Sr^{2+}, Ba^{2+}). *Can. J. Chem.* **2011**, *89*, 835−844.

(15) Blackburn, E. H. Telomeres: No End in Sight. *Cell* **1994**, *77*, 621−623.

(16) Wright, W. E.; Tesmer, V. M.; Huffman, K. E.; Levene, S. D.; Shay, J. W. Normal Human Chromosomes Have Long G-rich Telomeric Overhangs At One End. *Genes Dev.* **1997**, *11*, 2801−2809.

(17) Davis, J. T. G-Quartets 40 Years Later: From 5'-GMP to Molecular Biology and Supramolecular Chemistry. *Angew. Chem., Int. Ed.* **2004**, *43*, 668−698.
(18) Wasielewski, M. R. Self-Assembly Strategies for Integrating Light Harvesting and Charge Separation in Artificial Photosynthetic Systems. *Acc. Chem. Res.* **2009**, *42*, 1910−1921.
(19) Wu, Y.-L.; Brown, K. E.; Wasielewski, M. R. Extending Photoinduced Charge Separation Lifetimes by Using Supramolecular Design: Guanine-Perylendiimide GQuadruplex. *J. Am. Chem. Soc.* **2013**, *135*, 13322−13325.
(20) Wu, Y.-L.; Brown, K. E.; Gardner, D. M.; Dyar, S. M.; Wasielewski, M. R. Photoinduced Hole Injection into a Self-Assembled π-Extended G-Quadruplex. *J. Am. Chem. Soc.* **2015**, *137*, 3981−3990.
(21) Powers-Riggs, N. E.; Zuo, X.; Young, R. M.; Wasielewski, M. R. Symmetry-Breaking Charge Separation in a Nanoscale Terrylenediimide Guanine-Quadruplex Assembly. *J. Am. Chem. Soc.* **2019**, *141*, 17512−17516.
(22) Pu, F.; Wu, L.; Ran, X.; Ren, J.; Qu, X. G-Quartet-Based Nanostructure for Mimicking Light-Harvesting Antenna. *Angew. Chem., Int. Ed.* **2015**, *54*, 892−896.
(23) Miannay, F.-A.; Banyasz, A.; Gustavsson, T.; Markovitsi, D. Excited States and Energy Transfer in G-Quadruplexes. *J. Phys. Chem. C* **2009**, *113*, 11760−11765.
(24) Changenet-Barret, P.; Emanuele, E.; Gustavsson, T.; Improta, R.; Kotlyar, A. B.; Markovitsi, D.; Vayá, I.; Zakrzewska, K.; Zikich, D. Optical Properties of Guanine Nanowires: Experimental and Theoretical Study. *J. Phys. Chem. C* **2010**, *114*, 14339−14346.
(25) Dumas, A.; Luedtke, N. W. Cation-Mediated Energy Transfer in G-Quadruplexes Revealed by an Internal Fluorescent Probe. *J. Am. Chem. Soc.* **2010**, *132*, 18004−18007.
(26) Hua, Y.; Changenet-Barret, P.; Improta, R.; Vayá, I.; Gustavsson, T.; Kotlyar, A. B.; Zikich, D.; Šket, P.; Plavec, J.; Markovitsi, D. Cation Effect on the Electronic Excited States of Guanine Nanostructures Studied by Time-Resolved Fluorescence Spectroscopy. *J. Phys. Chem. C* **2012**, *116*, 14682−14689.
(27) Rosu, F.; Gabelica, V.; De Pauw, E.; Antoine, R.; Broyer, M.; Dugourd, P. UV Spectroscopy of DNA Duplex and Quadruplex Structures in the Gas Phase. *J. Phys. Chem. A* **2012**, *116*, 5383−5391.
(28) Hua, Y.; Changenet-Barret, P.; Gustavsson, T.; Markovitsi, D. The Effect of Size on the Optical Properties of Guanine Nanostructures: A Femtosecond to Nanosecond Study. *Phys. Chem. Chem. Phys.* **2013**, *15*, 7396−7402.
(29) Lech, C. J.; Phan, A. T.; Michel-Beyerle, M.-E.; Voityuk, A. A. Electron-Hole Transfer in G-Quadruplexes with Different Tetrad Stacking Geometries: A Combined QM and MD Study. *J. Phys. Chem. B* **2013**, *117*, 9851−9856.
(30) Changenet-Barret, P.; Hua, Y.; Markovitsi, D. Electronic Excitations in Guanine Quadruplexes. *Top. Curr. Chem.* **2014**, *356*, 183−201.
(31) Improta, R. Quantum Mechanical Calculations Unveil the Structure and Properties of the Absorbing and Emitting Excited Electronic States of Guanine Quadruplex. *Chem. − Eur. J.* **2014**, *20*, 8106−8115.
(32) Lech, C. J.; Phan, A. T.; Michel-Beyerle, M.-E.; Voityuk, A. A. Inuence of Base Stacking Geometry on the Nature of Excited States in G-quadruplexes: A Time-Dependent DFT Study. *J. Phys. Chem. B* **2015**, *119*, 3697−3705.
(33) Banyasz, A.; Marténez-Fernández, L.; Balty, C.; Perron, M.; Douki, T.; Improta, R.; Markovitsi, D. Absorption of Low-Energy UV Radiation by Human Telomere G-Quadruplexes Generates Long-Lived Guanine Radical Cations. *J. Am. Chem. Soc.* **2017**, *139*, 10561−10568.
(34) Marténez-Fernández, L.; Banyasz, A.; Markovitsi, D.; Improta, R. Topology Controls the Electronic Absorption and Delocalization of Electron Holes in Guanine Quadruplexes. *Chem. − Eur. J.* **2018**, *24*, 15185−15189.
(35) Marténez-Fernández, L.; Changenet, P.; Banyasz, A.; Gustavsson, T.; Markovitsi, D.; Improta, R. Comprehensive Study of Guanine Excited State Relaxation and Photoreactivity in G-quadruplexes. *J. Phys. Chem. Lett.* **2019**, *10*, 6873−6877.
(36) Banyasz, A.; Balanikas, E.; Martinez-Fernandez, L.; Baldacchino, G.; Douki, T.; Improta, R.; Markovitsi, D. Radicals Generated in Tetramolecular Guanine Quadruplexes by Photoionization: Spectral and Dynamical Features. *J. Phys. Chem. B* **2019**, *123*, 4950−4957.
(37) Behmand, B.; Balanikas, E.; Martinez-Fernandez, L.; Improta, R.; Banyasz, A.; Baldacchino, G.; Markovitsi, D. Potassium Ions Enhance Guanine Radical Generation upon Absorption of Low-Energy Photons by G-Quadruplexes and Modify Their Reactivity. *J. Phys. Chem. Lett.* **2020**, *11*, 1305−1309.
(38) Marténez-Fernández, L.; Esposito, L.; Improta, R. Studying the Excited Electronic States of Guanine Rich DNA Quadruplexes by Quantum Mechanical Methods: Main Achievements and Perspectives. *Photochem. Photobiol. Sci.* **2020**, *19*, 436−444.
(39) VandeVondele, J.; Krack, M.; Mohamed, F.; Parrinello, M.; Chassaing, T.; Hutter, J. QUICKSTEP: Fast and Accurate Density Functional Calculations using a Mixed Gaussian and Plane Waves Approach. *J. Comp. Phys. Commun.* **2005**, *167*, 103−128.
(40) Becke, A. D. Density-Functional Exchange-Energy Approximation with Correct Asymptotic-Behavior. *Phys. Rev. A* **1988**, *38*, 3098−3100.
(41) Lee, C.; Yang, W.; Parr, R. G. Development of the Coll-Salvetti CorrelationEnergy Formula into a Functional of the Electron-density. *Phys. Rev. B* **1988**, *37*, 785−789.
(42) Grimme, S.; Antony, J.; Ehrlich, S.; Krieg, H. A Consistent and Accurate Ab Initio Parametrization of Density Functional Dispersion Correction (DFT-D) for the 94 Elements H-Pu. *J. Chem. Phys.* **2010**, *132*, 154104.
(43) Lippert, G.; Hutter, J.; Parrinello, M. A Hybrid Gaussian and Plane Wave Density Functional Scheme. *Mol. Phys.* **1997**, *92*, 477−487.
(44) Goedecker, S.; Teter, M.; Hutter, J. Separable Dual-Space Gaussian Pseudopotentials. *Phys. Rev. B* **1996**, *54*, 1703−1710.
(45) Bussi, G.; Donadio, D.; Parrinello, M. Canonical Sampling Through Velocity Rescaling. *J. Chem. Phys.* **2007**, *126*, No. 014101.
(46) Lech, C. J.; Heddi, B.; Phan, A. T. Guanine Base Stacking in G-quadruplex Nucleic Acids. *Nucleic Acids Res.* **2012**, *41*, 2034−2046.
(47) Yanai, T.; Tew, D. P.; Handy, N. C. A New Hybrid Exchange-Correlation Functional Using the Coulomb-Attenuating Method (CAM-B3LYP). *Chem. Phys. Lett.* **2004**, *393*, 51−57.
(48) Frisch, M. J.; Trucks, G. W.; Schlegel, H. B.; Scuseria, G. E.; Robb, M. A.; Cheeseman, J. R.; Scalmani, G.; Barone, V.; Mennucci, B.; Petersson, G. A.; et al.. *Gaussian 09*; Revision D.01. Gaussian Inc.: Wallingford CT, 2009.
(49) Plasser, F. TheoDORE: a Toolbox for a Detailed and Automated Analysis of Electronic Excited State Computations. *J. Chem. Phys.* **2020**, *152*, No. 084108.
(50) Plasser, F.; Lischka, H. Analysis of Excitonic and Charge Transfer Interactions from Quantum Chemical Calculations. *J. Chem. Theory Comput.* **2012**, *8*, 2777−2789.
(51) Plasser, F.; Wormit, M.; Dreuw, A. New Tools for the Systematic Analysis and Visualization of Electronic Excitations. I. Formalism. *J. Chem. Phys.* **2014**, *141*, No. 024106.
(52) Mai, S.; Plasser, F.; Dorn, J.; Fumanal, M.; Daniel, C.; González, L. Quantitative Wave Function Analysis for Excited States of Transition Metal Complexes. *Coord. Chem. Rev.* **2018**, *361*, 74−97.
(53) Plasser, F. Entanglement Entropy of Electronic Excitations. *J. Chem. Phys.* **2016**, *144*, 194107.
(54) Case, D.; Belfon, K.; Ben-Shalom, I.; Brozell, S.; Cerutti, D.; Cheatham, T.; Cruzeiro, V.; Darden, T.; Duke, R.; Giambasu, G.; et al.. *AMBER*; University of California: San Francisco, 2020.
(55) Salomon-Ferrer, R.; Case, D. A.; Walker, R. C. An Overview of the Amber Biomolecular Simulation Package. *WIREs Comput. Mol. Sci.* **2013**, *3*, 198−210.
(56) Jorgensen, W. L.; Chandrasekhar, J.; Madura, J. D.; Impey, R. W.; Klein, M. L. Comparison of Simple Potential Functions for Simulating Liquid Water. *J. Chem. Phys.* **1983**, *79*, 926−935.

https://dx.doi.org/10.1021/acs.jpca.0c05022
J. Phys. Chem. A 2020, 124, 8101−8111

(57) Wang, J.; Wolf, R. M.; Caldwell, J. W.; Kollman, P. A.; Case, D. A. Development and Testing of a General Amber Force Field. *J. Comput. Chem.* **2004**, *25*, 1157−1174.
(58) Phillips, J. C.; Braun, R.; Wang, W.; Gumbart, J.; Tajkhorshid, E.; Villa, E.; Chipot, C.; Skeel, R. D.; Kalé, L.; Schulten, K. Scalable Molecular Dynamics with NAMD. *J. Comput. Chem.* **2005**, *26*, 1781−1802.
(59) Martyna, G. J. Remarks on "Constant-Temperature Molecular Dynamics with Momentum Conservation". *Phys. Rev. E* **1994**, *50*, 3234.
(60) Darden, T.; York, D.; Pedersen, L. Particle Mesh Ewald: An N·log(N) Method for Ewald Sums in Large Systems. *J. Chem. Phys.* **1993**, *98*, 10089−10092.
(61) Zaccaria, F.; Paragi, G.; Fonseca Guerra, C. The Role of Alkali Metal Cations in the Stabilization of Guanine Quadruplexes: Why K^+ is the Best. *Phys. Chem. Chem. Phys.* **2016**, *18*, 20895−20904.
(62) Azargun, M.; Jami-Alahmadi, Y.; Fridgen, T. D. The Intrinsic Stabilities and Structures of Alkali Metal Cationized Guanine Quadruplexes. *Phys. Chem. Chem. Phys.* **2017**, *19*, 1281−1287.
(63) Sapunar, M.; Domcke, W.; Došlić, N. UV Absorption Spectra of DNA Bases in the 350-190 nm Range: Assignment and State Specic Analysis of Solvation Effects. *Phys. Chem. Chem. Phys.* **2019**, *21*, 22782−22793.
(64) Nogueira, J. J.; Plasser, F.; González, L. Electronic Delocalization, Charge Transfer and Hypochromism in the UV Absorption Spectrum of Polyadenine Unravelled by Multiscale Computations and Quantitative Wavefunction Analysis. *Chem. Sci.* **2017**, *8*, 5682−5691.
(65) Yin, H.; Ma, Y.; Mu, J.; Liu, C.; Rohlfing, M. Charge-Transfer Excited States in Aqueous DNA: Insights from Many-Body Green's Function Theory. *Phys. Rev. Lett.* **2014**, *112*, 228301.
(66) Balanikas, E.; Banyasz, A.; Douki, T.; Baldacchino, G.; Markovitsi, D. Guanine Radicals Induced in DNA by Low-Energy Photoionization. *Acc. Chem. Res.* **2020**, *53*, 1511−1519.
(67) Kwan, I. C. M.; She, Y.-M.; Wu, G. Trivalent Lanthanide Metal Ions Promote Formation of Stacking G-Quartets. *Chem. Commun.* **2007**, 4286−4288.

https://dx.doi.org/10.1021/acs.jpca.0c05022
J. Phys. Chem. A 2020, 124, 8101−8111

Прилог 5 – *Alkaline Earth Cations Binding Mode Tailors Excited-State Charge Transfer Properties of Guanine Quadruplex: A TDDFT Study*

Објављени научни рад (категорија научног часописа M_{21}):

Branislav Milovanović, Milena Petković, Mihajlo Etinski, Alkaline Earth Cations Binding Mode Tailors Excited-State Charge Transfer Properties of Guanine Quadruplex: A TDDFT Study, *Spectrochim. Acta A*, **2022**, 267 (Part 2), pp 120584.

https://doi.org/10.1016/j.saa.2021.120584 *IF(2020) 4,098*

Ауторска права код издавача (приступљено дана 15.12.2021.):

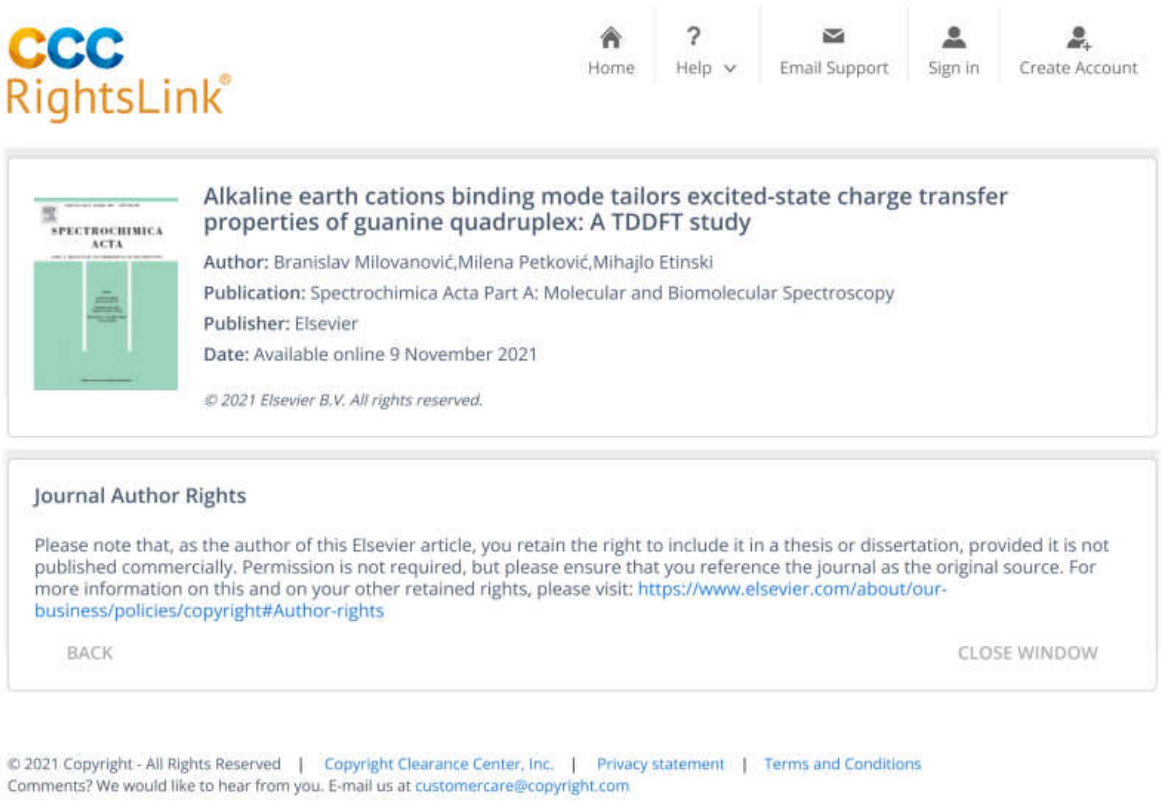

Spectrochimica Acta Part A: Molecular and Biomolecular Spectroscopy 267 (2022) 120584

Contents lists available at ScienceDirect

Spectrochimica Acta Part A: Molecular and Biomolecular Spectroscopy

journal homepage: www.elsevier.com/locate/saa

Alkaline earth cations binding mode tailors excited-state charge transfer properties of guanine quadruplex: A TDDFT study

Branislav Milovanović, Milena Petković, Mihajlo Etinski *

University of Belgrade, Faculty of Physical Chemistry, Studentski trg 12-16, Belgrade, Serbia

HIGHLIGHTS

- The cations bound at adjacent cavities of the quadruplex stabilize CT states.
- Increasing the number of the layers and cations in the quadruplex tends to redshift CT states.
- Stabilization of cations' *d* orbitals assists in redshifting of nucleobase-metal CT states.

GRAPHICAL ABSTRACT

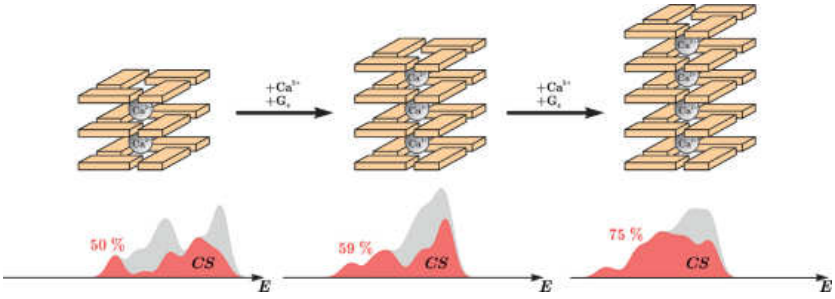

ARTICLE INFO

Article history:
Received 15 August 2021
Received in revised form 25 October 2021
Accepted 2 November 2021
Available online 9 November 2021

Keywords:
G-quadruplex
Charge separation
Electronics

ABSTRACT

Quadruplexes formed by nucleic acids and their derivates tend to chelate different monovalent and bivalent cations, which simultaneously affect their excited electronic states properties. Cation binding to every and every other cavity of the central ion channel could be exploited for tuning exited-state charge transfer properties. In this work we utilize set of descriptors constructed on the basis of the one-electron transition density matrix obtained using linear-response TDDFT to study excited states properties of four crystallized tetramolecular quadruplexes that chelate alkaline earth cations (Ca^{2+}, Sr^{2+} and Ba^{2+}). Here, we show that alkaline earth cations situated at adjacent vacancies promote existence of the nucleobase-metal charge separation (CS) states, contrary to the structures with cations that occupy every second available vacancy. We argued that stabilization of these CS states is due to the strong electric field that stabilizes *d* orbitals of the cations which accept an excited-electron. Moreover, CS content is increased and redshifted below the first bright transition when number of the chelated cations is increased. Hydration effects stabilized CS states and increased their relative content. We also identified electron detachment states in the broad energy range for the Ca^{2+} containing system. These findings are valuable for understanding and development of the novel nanostructures based on the quadruplex scaffold with adjustable optical properties.

Introduction

Within the purine rich telomeric regions of the DNA non-standard four-stranded structures can be formed via Hoogsteen-type hydrogen bonding of the guanine (G) bases called guanine quadruplexes (GQ), Fig. 1 [1–4]. GQs are made up of the layers called G-quartets or G-tetrads in which four guanines/guanosines are connected via hydrogen bonds. In the absence of the nucleic backbone, guanine/guanosine and their derivates are also able to self-assemble into square planar structures (G-quartets) and infinite hydrogen bonded ribbons (G-ribbons) [5]. Stabilization of GQ supra-molecular architectures is regulated by multiple factors:

* Corresponding author.
E-mail address: etinski@ffh.bg.ac.rs (M. Etinski).

https://doi.org/10.1016/j.saa.2021.120584
1386-1425/

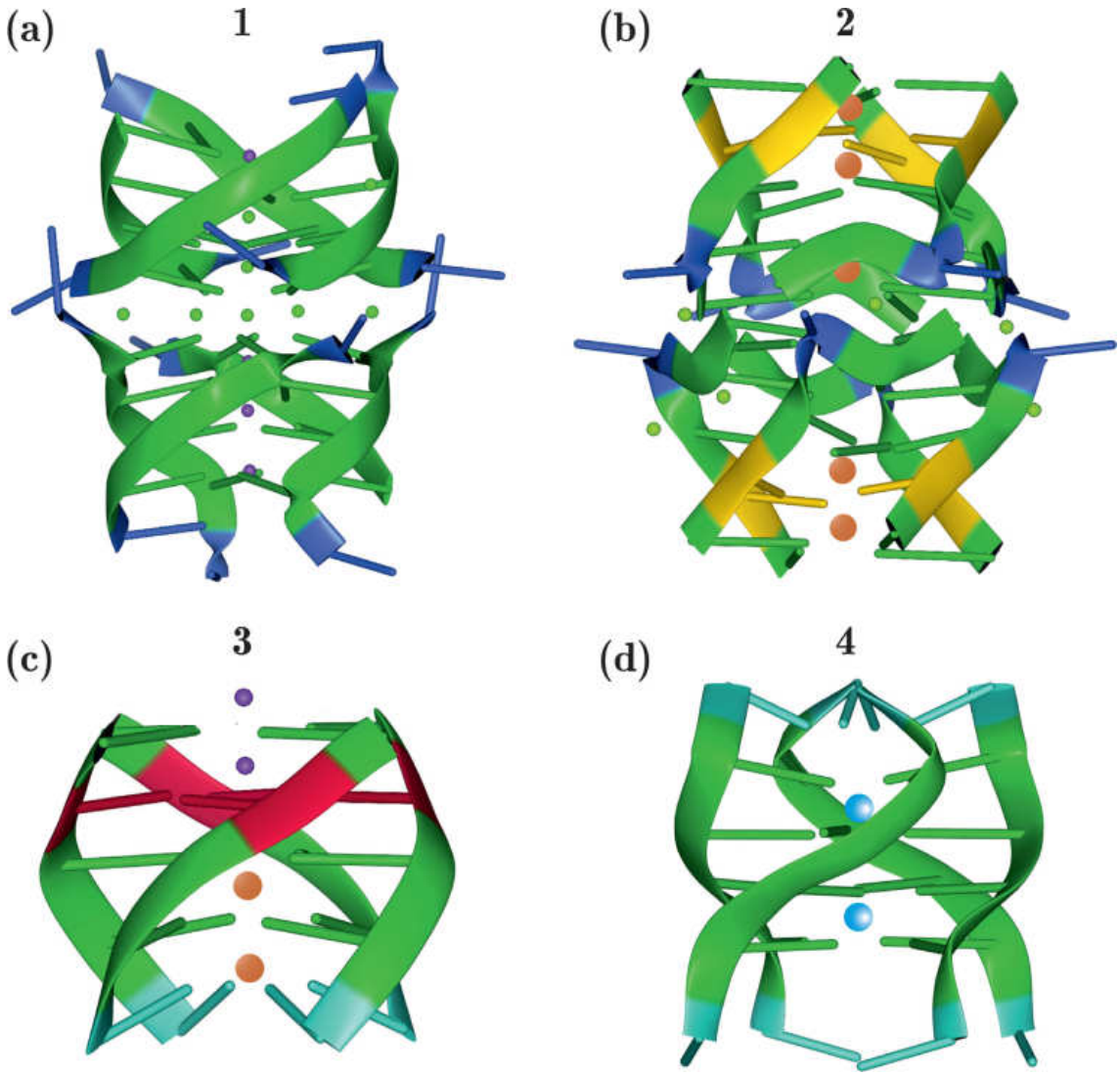

Fig. 1. Quadruplex structures used to extract computational model. Nucleobases and its sugar phosphate backbones are colored according to scheme: uracil (U) - cyan, thymine (T) - blue, cytosine (C) - yellow, adenine (A) - red and guanine (G) - green. Spheres represent ligands/cations within the quadruplex structures with coloring method: Na^+ - purple, Ca^{2+} - green, Ba^{2+} - orange and Sr^{2+} - blue. The biological assembly of: a) crystal structure of d(TGGGGT) sequence - Na^+ and Ca^{2+} complex (PDB ID: 2GW0) [52] consisted of two end-to-end stacked d(TGGGGT) molecules, upper (accommodating two Ca^{2+} and one Na^+) and lower (accommodating three Na^+) separated by five interface Ca^{2+} cations - abbreviated with **1**; b) crystal structure of a DNA/Ba^{2+} G-quadruplex containing a water-mediated C-tetrad (PDB ID: 4U92) [53] - abbreviated with **2**; c) crystal structure of an RNA tetraplex $(UGAGGU)_4$ with A-tetrads, G-tetrads and U-tetrads (PDB ID: 1J6S) [54] - abbreviated with **3**; d) RNA tetraplex $(UGGGGU)_4$ with divalent Sr^{2+} cations (PDB ID: 1J8G) [55] - abbreviated with **4**. Quadruplex structures are visualized using NGL Viewer at RCSB PDB [56,57].

(1) presence of the cation within its central cavity and its properties (charge and size); (2) cooperativity and efficiency of the hydrogen bonding between neighboring G units; and (3) solvation energy of the system. [6–13].

Preferences of GQs and G-quartets towards different alkaline and alkaline earth cations have been extensively investigated [6,13–23]. Alkaline metal cations can adopt positions between every or every second G-quartet layer within the GQ, while destabilizing electrostatic repulsion of the bivalent alkaline earth cations forces them to adopt positions between every second G-quartet, making this binding mode more favorable as in the case of the Sr^{2+} within the RNA tetraplex structure [16,24]. Recent work from Fonseca Guerra group emphasizes that destabilizing electrostatic repulsion is also apparent in the case of the alkaline metal cations as well as the counterbalance in the form of the stabilizing solvation effects [14]. Nevertheless, GQ affinity towards some bivalent cations is found to be even stronger compared to the alkaline cations under certain conditions [18–20,25–30]. Cations such as Be^{2+} [13] Mg^{2+} [13,19,27–29,31], Ca^{2+} [13,19,27–29,20,31], Sr^{2+} [16,18,20,26–30], Ba^{2+} [20,26–30,32], Mn^{2+} [26,28], Pb^{2+} [25,30,33] and Cu^{2+} [34] were considered as an alternative to the biologically abundant Na^+ and K^+ for both biologically occurring thrombine binding aptamer and isolated guanosine derivates nanostructures. As in the case of the alkaline cations, ionic radii play crucial role for enhanced stabilization of the GQs assembled via alkaline earth cations. From all bivalent cations investigated throughout the literature Sr^{2+} is found to elevate GQs structural stability upmost [18,20,29,30]. Alkaline earth cations stabilization trend of the 5'-guanosine monophosphate self-assemblies proposed by Kwan and coworkers [20] follows the trend: $Sr^{2+} \gg Ba^{2+} > Ca^{2+}$ which is similar to that found for the alkaline cations: $Cs^{2+} > Rb^+ \approx Na^{2+} > K^+$ with respect to the ionic radii [21–23]. Furthermore, it is found that smaller cations such as Li^+, Mg^{2+} and Mn^{2+} tend to destabilize GQs [26,28]. On the other hand, quite opposite effect of the smaller Li^+ cation is found for the canonical, i.e. standard hydrogen bonded DNA base pairs [35].

Beside the important biological functions, GQs can serve as building blocks for the bottom-up approach in constructing nanometer-sized structures using its self-assembly feature [5,36–38]. GQs find manifold of applications in the material science. For example, molecular G-wires are used for the long-range charge transport and can be formed via gel electrophoresis in the presence of the Na^+, K^+ and Mg^{2+} cations [39,40]. The molecular scale current splitters and charge transfer juctions designed using GQs are also reported [41]. When peripherally functionalized with dye molecules GQs provide guidance for the self-assembly of the structures that could be used for the optoelectronic applications as an efficient alternative to the covalent synthesis of such materials [42]. GQs can be exploited for crystalline 2D organic frameworks assembly when linked with rylene dye molecules such that G acts as an electron donor upon photoionization [43]. Photogenerated electron-holes and excited-electrons in these systems have long recombination lifetimes and thus favorable kinetics of the charge carriers. Few more interesting examples could be found in the literature such as core–shell columnar aggregates of dye decorated GQ where G moiety also serves as an electron-hole conduits upon photochemical charge separation [44–46]. By using self-assembly of the 5'-guanosine monophosphate decorated with thiazolium based dye in the presence of the Sr^{2+} cations Pu and coworkers managed to create nanofibers with similar properties to those of the light-harvesting antenna i.e. nanostructure that displays photocurrent upon visible light irradiation [47].

Cations coordinated within quadruplex structures provide solid ground for modulating their excited electronic states properties [8,48–51]. It has been demonstrated [50] that alkaline cations' size could affect charge-transfer exciton trapping ability of the quadruplex. Smaller and more mobile Na^+ cations favor conversion of the $\pi\pi^*$ excitons to the charge transfer states while larger and less mobile K^+ cations favor emission from the initially populated localized $\pi\pi^*$ excitons. On the other hand, a bivalent cation sandwiched between two G-quartets is not able to significantly modulate its absorption profiles compared to the monovalent cations [31]. Therefore, it is interesting to examine to which extent excited electronic states of multilayered quadruplex structures are modified in the presence of two bivalent cations, especially when cations are interposed between every consecutive quartet layer. It is expected that such cation arrangement leads to the stabilization of the charge transfer states due to the presence of the strong electric field within the central ion channel. To the best of our knowledge, no experimental data on the electronic absorption of the quadruplex structures accommodating doubly charged cations is currently available. Given the increasing interest for self-assembled system such as GQs for optoelectronic application, it is of great importance to investigate their excited electronic states in detail.

In this paper we focus on the excited electronic states properties of the quadruplex structures in which bivalent cations are interposed between every quartet layer. We found three experimentally obtained crystal structures [52–54] (see Fig. 1a-c) with such cation arrangement from which we extract our computational model. These crystal structures hold out against standard binding mode in which doubly charged cations are positioned between every other quartet layer due to their mutual electrostatic repulsion. For the sake of comparison, we also investigate one crystal structure containing two Sr^{2+} in the standard binding mode (see Fig. 1d) [55]. Impact of such cation arrangement on the electronic absorption of the quadruplex structures is investigated. Special attention is given to the charge transfer components of the electronic absorption spectra since we anticipate involvement of doubly charged cations on their properties.

The paper is organized in the following order: after introduction of the examined systems, theoretical methodology is presented. Then we proceed with the results and discussion section that includes excited states characterization, discussion of the electronic absorption and DOS profiles and hydration effects. At the end, conclusions are given.

Theoretical Methodology

Our computational model consists of up to five nucleobase layers/quartets and doubly charged cations inserted between every or every second consecutive layer. Since we are interested in the effects introduced by cations within the central cavity, our quadruplex model consists from nucleobases without accompanying sugar-phosphate backbone and is therefore computationally feasible to study. The geometries of six studied systems are presented in Fig. 2. Three structures are obtained from the quadruplex **1**: **1-Ca$_2$** by extracting three G-quartets and two Ca^{2+} coordinating cations from the upper d(TGGGGT) molecule. **1-Ca$_3$** is extended version of **1-Ca$_2$** with another G-quartet layer and Ca^{2+} cation. This cation is located at the interface between two end-to-end stacked d(TGGGGT) molecules in quadruplex **1** (see Fig. 1a). **1-Ca$_4$** computational model is obtained by replacing Na^+ cation closest to the interface layer with Ca^{2+} cation. This can be rationalized by the fact that both Na^+ and Ca^{2+} have similar and relatively small ionic radii. Average Ca^{2+}-oxygen distances in the upper d(TGGGGT) molecule amount to 2.83 and 2.80 Å while average Na^+-oxygen distance of the exchanged Na^+ cation is 2.65 Å. Remaining Na^+ cation in the lower d(TGGGGT) molecule has average Na^+-oxygen distance of 2.79 Å. This reflects flexible position of small cations within the central ion channel in the GQ structures. Computational models **2-Ba$_2$** and **3-Ba$_2$** are derived from the quadruplexes **2** and **3**, respectively. Both computational models containing Ba^{2+} cations have one pyrimidine nucleobase quartet. **2-Ba$_2$** has water mediated C-quartet in-between two Ba^{2+} cations while **3-Ba$_2$** has U-quartet as a terminal layer in the structure. This U-quartet is formed via 3'-ends of a RNA strand and therefore has an out-of-plane deformation which leads to greater separation between two Ba^{2+} cations within **2-Ba$_2$**. **4-Sr$_2$** is formed using standard four layered GQ designated as **4** and with two Sr^{2+} cations in the standard binding mode.

Electronic absorption spectrum for the studied systems is computed using linear response time-dependent density functional theory (LR-TDDFT) and the long-range corrected CAM-B3LYP functional [58] in conjunction with Grimme's D3 dispersion corrections [59]. Kohn–Sham orbitals were expanded using def2-SV(P) basis set [60,61]. All calculations were carried out using Gaussian09 [62]. For each nucleobase in the system we included four lowest lying singlet excited states (N). For example, in the case of the smallest systems with three nucleobase layers (**1-Ca$_2$**, **2-Ba$_2$** and **3-Ba$_2$**) we computed 48, while for the largest system **1-Ca$_4$** with five nucleobase layers we computed 80 lowest lying singlet excited states. Gaussian shaped function is used to broaden vertical electronic transitions at the given geometries. Electronic absorption spectrum is calculated according to:

$$A(E) \sim \sum_{j=1}^{N} \frac{f_j}{\sqrt{2\pi\sigma^2}} exp\left(-\frac{1}{2}\left(\frac{E-E_j}{\sigma}\right)^2\right) \quad (1)$$

where f_j and E_j is oscillator strength and energy of the j-th vertical electronic transition, respectively. Broadening parameter σ amounts to 0.2 eV in all cases. This value of broadening parameter is found to be optimal for resolving the absorption profiles. The density of excited states (DOS) is also computed using Eq. 1 but with f_j values set to 1 for each transition.

Excited states character is analyzed using TheoDORE program package [63–67] which relies on the analysis of the one-electron transition density matrix (1eTDE) and it is useful to resolve types

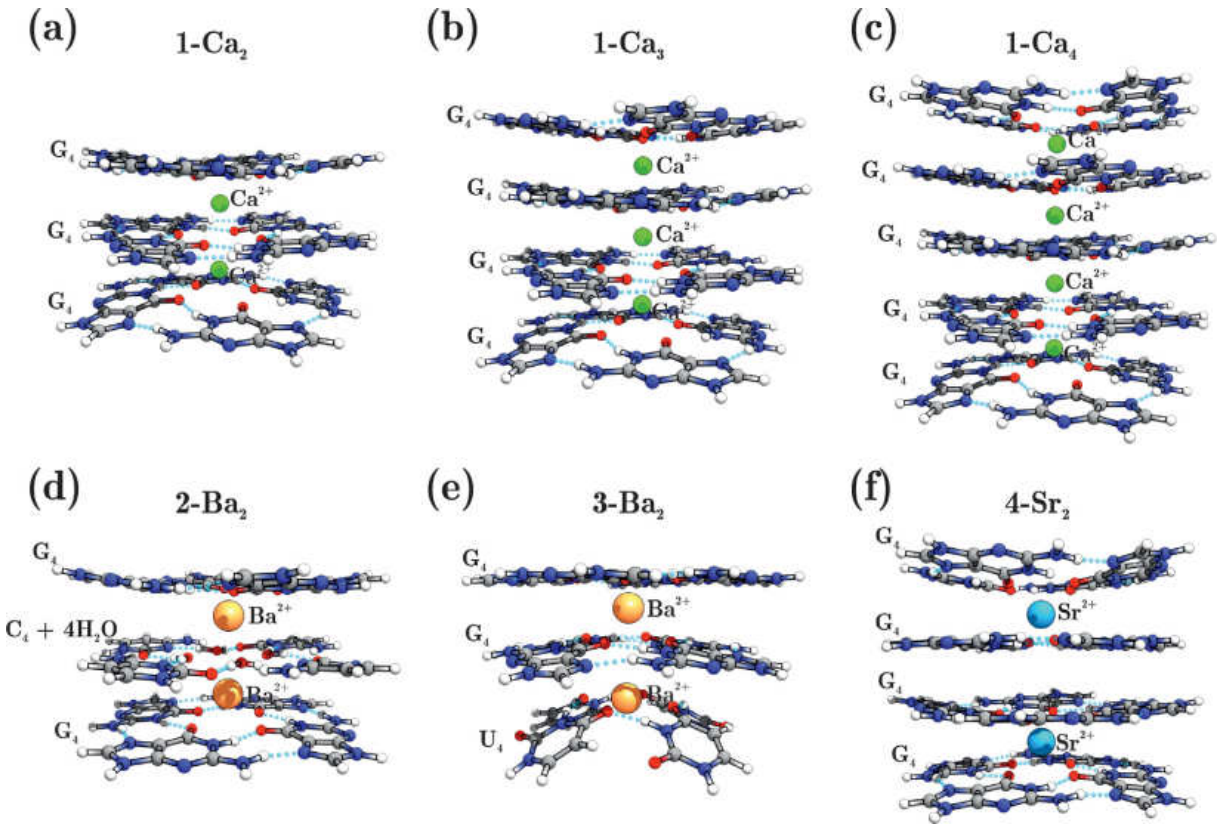

Fig. 2. Computational models extracted from quadruplex structures presented in Fig. 1. Three- four- and five-layered quadruplex structures accommodating Ca^{2+} cations are depicted on the panels (a), (b) and (c) and denoted as **1-Ca$_2$**, **1-Ca$_3$** and **1-Ca$_4$**, respectively. Two three-layered structures with Ba^{2+} cations within the central cavity are denoted as **2-Ba$_2$** and **3-Ba$_2$** and presented on the panels (d) and (e), respectively. Four layered quadruplex with two Sr^{2+} cations in the standard binding mode is denoted as **4-Sr$_2$**. Prefixes **1**, **2**, **3** and **4** indicate that structures originate from 2GW0, 4U92, 1J6S and 1J8G quadruplex sequences, respectively. G_4, U_4 and C_4+$4H_2O$ designate G-, U- and water mediated C-quartets.

of excitations in the systems of interacting chromophores. Excited states character is determined using two descriptors based on decomposition of the 1eTDE. First descriptor denoted with PR is calculated as arithmetic mean of the participation ratios of electron-hole and excited-electron, i.e. number of defined fragments on which they are delocalized at the moment of excitation. Second descriptor denoted with CT describes charge transfer character of the excited state, with the values ranging from zero (locally excited state) to one (charge transfer state). To test whether some of the encountered charge transfer states are charge resonance states or completely charge separation states we used additional descriptor denoted with PR_{NTO}. This descriptor is the measure of how many different natural transition orbitals (NTOs), i.e., how many transitions are required to describe examined state. In our case, PR_{NTO} is close to one for all states previously identified as charge transfer states which means these states can only be characterized as charge separation states. Therefore, in our case PR and CT descriptors are useful for distinction between localized, excimer and charge separation transitions. Detailed derivation of these descriptors from the 1eTDM could be found elsewhere [64]. Fragmentation of the system is important for this type of analysis and it is described in the following section. Multiwfn software [68] was used to derive NTOs and to inspect orbital composition of the molecular orbitals (MOs).

To account for the solvation effects, we generated microsolvated cluster using force-field molecular dynamics simulation. System was prepared using AmberTools20 [69,70]. For this purpose we selected the **1-Ca$_2$** structure which we placed in the center of the orthorhombic box and solvated with the 2698 water molecules and added four Cl^- ions in order to electrostatically neutralize system. This resulted in the simulation box size of 50.8, 50.4 and 44.3 Å along the *x*, *y* and *z* directions, respectively. Guanines were modeled using generalized AMBER force field (GAFF) [71], while water molecules, Ca^{2+} and Cl^- ions were described using TIP3P model [72]. Prior to the NVT production run, system's energy was minimized. **1-Ca$_2$** coordinates were fixed in order to preserve configuration and only water molecules were allowed to move. In this way we are able to elucidate solvation effects for the particular experimental quadruplex geometry. NVT production run lasted for 0.5 ns and was performed using CP2K [73]. CSVR thermostat [74] was used to equilibrate system to the temperature of 300 K. The cutoff radius for the nonbonded interactions was set to 10 Å and smooth particle mesh Ewald method [75] was used to treat the electrostatic forces. From the last frame of the molecular dynamic run we extracted microsolvated cluster by taking into account all water molecules within the 3 Å radius from the **1-Ca$_2$**. Using this procedure, we modeled the first solvation sphere that contains 79 water molecules which together with **1-Ca$_2$** yielded 431 atoms in total.

Results and Discussion

Excited States Characterization

To assign orbital character of the transitions we visually inspect NTOs. All transitions within studied energy window involved only π orbitals in the case of nucleobases and a mixture of different *d* orbitals in the case of the cations. Note that the final localization of the excited-electron is always situated at the cations when they

are involved into a transition. Schematic description of the excitations encountered for the computational models presented in Fig. 2 are depicted in Fig. 3. Three main types of excitations are encountered in our systems: localized, excimeric and charge separation (CS). Due to multichromophoric character of these assemblies three different fragmentation schemes must be employed in order to effectively distinguish between several subtypes of the excitations. In the first fragmentation scheme every nucleobase in the system and the cations are considered as separate fragments. Descriptors obtained in this way are denoted as CT_1 and PR_1. After defining certain threshold value, CT_1 is useful to determine whether excitations have local, excimeric or CS character. CT threshold values are chosen arbitrary in the way that excitations with $CT_1 < 0.2$ are considered as localized, with $0.2 < CT_1 < 0.8$ as excimeric and $CT_1 > 0.8$ as a pure CS states. PR_1 is used to distinguish between monomeric and excitonic localized transitions, i.e. transitions with $CT_1 < 0.2$. If the value of PR_1 is lower than 1.25 that transition is considered as localized monomeric. On the other hand, PR_1 values greater than 1.25 suggest that it is an excitonic state. Threshold value of 1.25 for PR_1 is chosen following the definition of this descriptor [64]. If the transition exhibits $PR_1 > 1.25$ it means that one quarter of the electron density is delocalized over more than one fragment defined in the system which in combination with $CT_1 < 0.2$ condition leads to the excimeric character designation for that transition. To anticipate involvement of the cations in the eximeric and CS transitions we defined fragments in the systems in two additional ways. Firstly, every nucleobase layer and every cation are defined as a separate fragment and secondly all nucleobases together and all cations together in the systems are defined as a separate fragment leading to only two fragments in total. CT descriptors defined via former fragmentation scheme are denoted as CT_2 and with the latter as CT_3. Transitions with $0.2 < CT_1 < 0.8$ are qualified as excimeric and furthermore as nucleobase-nucleobase or nucleobase-metal excimers if fulfilled $CT_3 < 0.2$ and $0.2 < CT_3 < 0.8$ conditions, respectively. In the similar fashion using last two fragmentation schemes we could differentiate between interlayer and nucleobase-metal CS transitions. When $CT_1 > 0.8$ is combined with $CT_2 > 0.8$ and $CT_3 < 0.2$ transition is regarded as interlayer nucleobase-nucleobase transition without direct involvement of the cations. On the other hand, $CT_2 > 0.8$ and $CT_3 > 0.2$ indicate that transition has nucleobase-metal CS character with the excited-electron localized on the mixture of *d* orbitals of the cations. Note that intralayer CS type of transitions are not encountered in studied systems in the gas phase and therefore its scheme is not presented in Fig. 3. These transitions would have $CT_1 > 0.8$, $CT_2 < 0.8$ and $CT_3 < 0.2$ combination of the descriptor values. Additional fragmentation scheme was employed to segregate electron detachment from the other transitions in the case of the **1-Ca$_2$** microsolvated cluster. Electron detachment transition forms hydrated electron [76,77] which can be treated as G-H_2O CS state. For this purpose, two fragments are defined: whole **1-Ca$_2$** system as the first fragment and all water molecules as the second. This fragmentation scheme defines CT_4 descriptor that takes values $CT_4 > 0.8$ if the transition is characterized as the electron detachment.

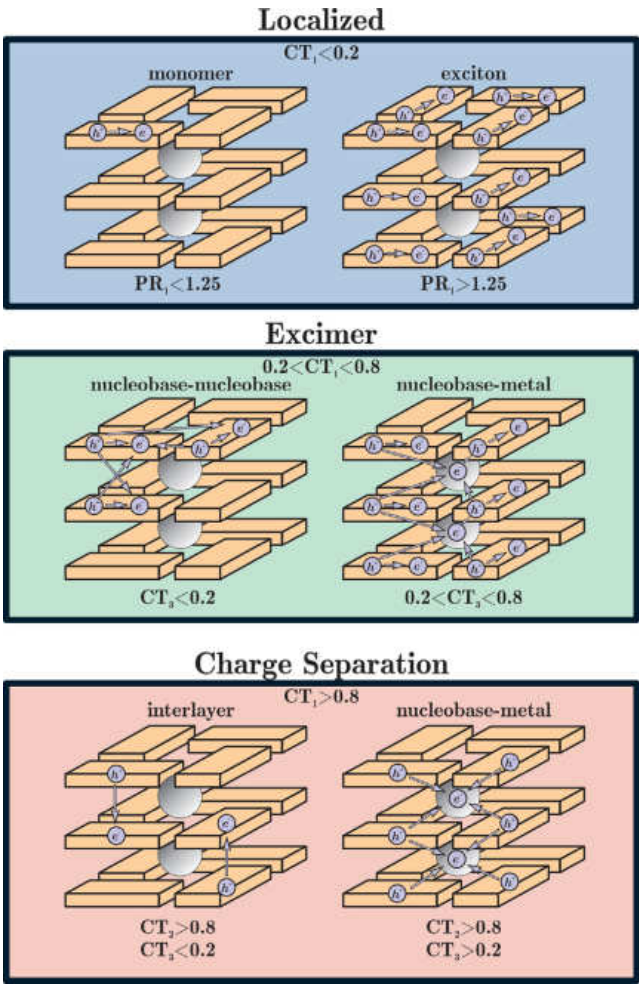

Fig. 3. Schematic depiction and names of the types of the excited states encountered for multilayered quadruplex structures with cations adopting positions between every consecutive quartet layer. Yellow cuboids represent nucleobases while grey spheres represent cations. h^+ and e^- illustrate electron-hole and excited-electron while arrows points from initial to the final localization of electron during excitation process. CT and PR descriptors thresholds are given for each excited state type. Note that not necessarily all of the excited states types must be present in the electronic absorption profile for all studied systems.

Electronic Absorption Spectra

Let us first discuss electronic absorption profiles presented in Figs. 4 and 5. All **3-Ba$_2$**, **2-Ba$_2$** and **4-Sr$_2$** electronic absorption profiles have the first peak positioned around 5 eV, i.e. 4.96, 4.97 and 5.02 eV, respectively. Character of these transitions is purely excitonic for **3-Ba$_2$** and **4-Sr$_2$** and mixed excitonic/excimeric for **2-Br$_2$**. Different spatial organization of guanines within the quadruplex assemblies can affect electronic absorption properties [78,79]. Less flexible quadruplex structures, i.e. having quartets with increased planarity should promote existence of the excimeric transitions [78]. Quartets forming **2-Ba$_2$** structure are exhibiting least deviation from the planarity with root-mean-square deviation (RMSD) of the atomic position amounting to 0.30 Å which is smaller than 0.38 Å and 0.58 Å RMSD values found for **4-Sr$_2$** and **3-Ba$_2$** quartets, respectively. Therefore, excimeric transitions for the **2-Ba$_2$** system appear in the wide range of the energies and contribute significantly to the electronic absorption intensity. Another interesting feature for the **2-Ba$_2$** system is the peak positioned at 5.34 eV originating from the two closely lying localized monomeric cytosine transitions. These transitions correspond to the S_1 state (HOMO–LUMO transition) of an isolated cytosine. At the similar level of theory (CAM-B3LYP-D3/6–31+G(d,p)) Yaghoubi-Jouybari *et al.* calculated this energy to be 5.00 eV [80]. The second peak for the **2-Ba$_2$** and **4-Sr$_2$** structures is found at 5.83 and 5.65 eV, respectively, both with mixed excitonic and excimeric character. For **3-Ba$_2$** the second peak is not observed within the studied energy window since we only included 48 excitations. This is due to the stabilization of the CS transitions which are now mostly below the first bright transition in the spectrum. Ca^{2+} containing GQs also exhibit similar first peak positions. They are found at 4.85, 4.77 and

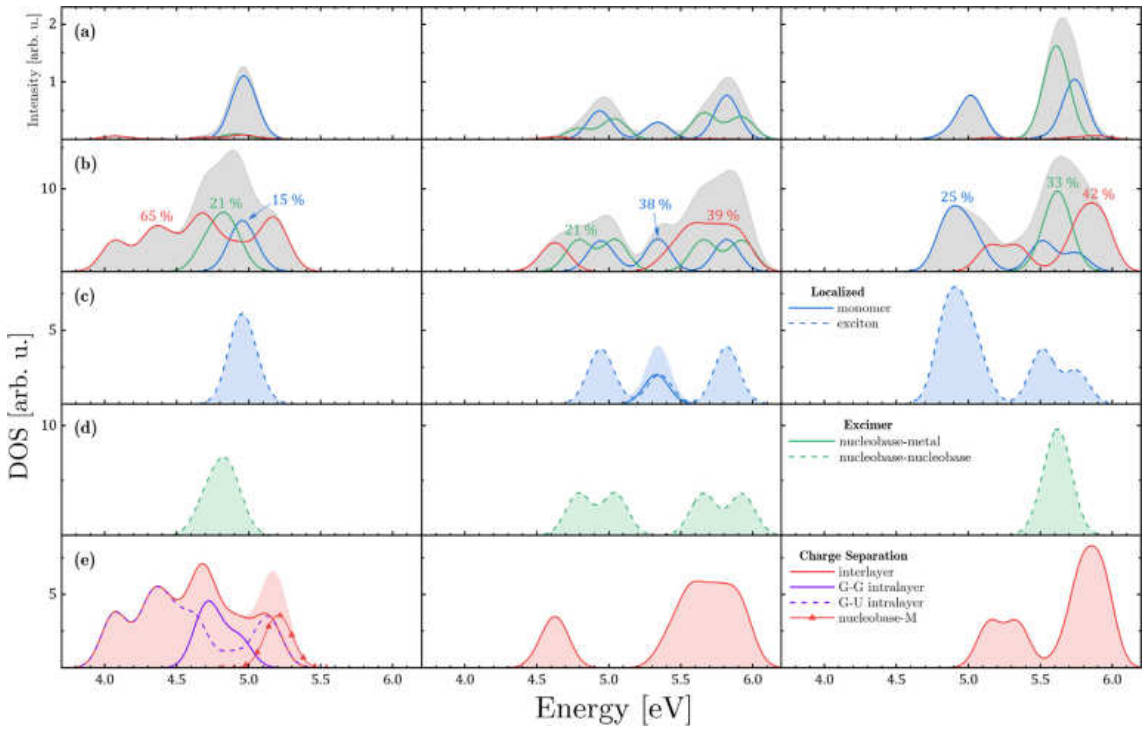

Fig. 4. Decomposition of (a) electronic absorption spectrum (shaded area) and (b) density of excited states (DOS) (shaded area) into the localized (blue lines), excimer (green lines) and charge separation (red lines) contributions. Percentage of each contribution to the DOS is indicated. Further decomposition of localized, excimer and charge separation contributions is presented on the panels (c), (d) and (e), respectively with the legend on the far right panels. **3-Ba$_2$** absorption profile is presented on the left, **2-Ba$_2$** in the middle and **4-Sr$_2$** on the right vertical panel. For excited states types see Fig. 3.

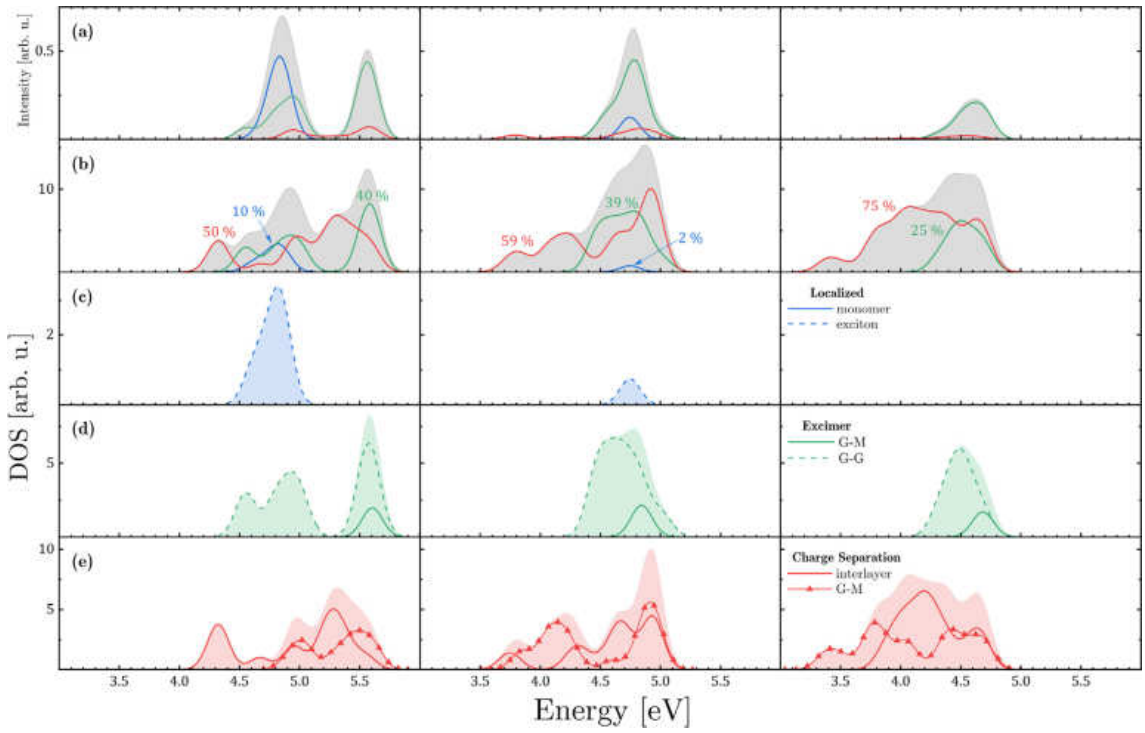

Fig. 5. Decomposition of (a) electronic absorption spectrum (shaded area) and (b) density of excited states (DOS) (shaded area) into the localized (blue lines), excimer (green lines) and charge separation (red lines) contributions. Percentage of each contribution to the DOS is indicated. Further decomposition of localized, excimer and charge separation contributions is presented on the panels (c), (d) and (e), respectively with the legend on the far right panels. **1-Ca$_2$** absorption profile is presented on the left, **1-Ca$_3$** in the middle and **1-Ca$_4$** on the right vertical panel. For excited states types see Fig. 3.

4.61 eV, together with peak shoulders located at 4.53, 4.52 and 4.32 eV for the **1-Ca$_2$**, **1-Ca$_3$** and **1-Ca$_4$**, respectively. The second peak is visible only for the **1-Ca$_2$** system due to the same reasons as for the Ba^{2+} and Sr^{2+} accommodating sequences. With increasing number of layers, i.e. number of interacting chromophores collective effects become more apparent. Localized excitonic contribution to the spectrum decreases, while excimeric contribution becomes dominant. Red shift of the first peak and accompanying shoulder peaks are also apparent. These effects were already emphasized by Markovitsi and coworkers in the systems with monovalent cations withing the central GQs cavity [49]. Also, CS states have noteworthy contribution to the electronic absorption spectra and therefore can be populated directly upon photoabsorption.

Density of Excited Electronic States

Analysis of the DOS profiles through decomposition to the different contributions provides valuable insights into arrangement and interplay of all and not just bright excited electronic states. Identifying energy range and participation of such usually dark CS states is useful from the aspects of application for the optoelectronic devices. DOS for studied systems are presented in Figs. 4 and 5. Excited states densities for the **4-Sr$_2$** assembly with the Sr^{2+} cations obeying standard binding mode have transitions roughly arranged with the respect to the excitation energy in the following way: localized < excimeric < CS. Main feature for the **4-Sr$_2$** system is that CS states are mostly localized on the high energy part of the DOS with the total contribution of 42 % while low energy part of the DOS is dominated with localized excimeric transitions contributing with 25 % of the total DOS. In-between these two regions excimeric transitions are dominant (33 %) together with smaller amount of latter contributions. Similar arrangement of the excited states is encountered for the smaller model systems i.e. two G-quartets with sandwiched Mg^{2+} and Ca^{2+} cations [31]. However, this is not the case for the Ba^{2+} containing systems. For both **2-Ba$_2$** and **3-Ba$_2$** CS states are stabilized below the first bright $\pi\pi^*$ transition. Stiffness of the quartets of **2-Ba$_2$** structure reflects on the DOS in the same way as for its absorption spectrum, i.e. excimeric transitions are delocalized over wide range of the energies. Participation of CS transitions in DOS is not significantly changed for **2-Ba$_2$** when compared to **4-Sr$_2$**, i.e. 39 % compared to the 42 %. Content of the localized transitions for **2-Ba$_2$** is slightly increased to 38 % due to the presence of two localized monomeric cytosine transitions. On the other hand, **3-Ba$_2$** DOS is abundant with CS transitions which cover 65 % of the examined DOS with most of these states located below the absorption maximum. In this case, localized and excimeric transitions participate with 15 % and 21 %, respectively. Further decomposition of the CS states yields interesting features. All of the CS states occurring between nucleobases are interlayer guanine-uracil (G-U) and guanine-guanine (G-G) CS. Majority of them are G-U type excitations, with the excited-electron always located at uracil. This can be rationalized with highest electron affinity of uracil [81] as well as the lowest ionization potential of guanine [82] among all nucleobases. Another interesting type of CS states is also encountered for **3-Ba$_2$** system and that is CS between nucleobases and cations with the excited-electron always located at the cation. Average value of CT_3 descriptor in this case is 0.57 which means that more than a half of excited-electron density is localized at the cations at the end of the excitation. These states could be exploited for the purposes of photoinduced charge transport in such systems [44–46]. Its Ba^{2+} binding mode in combination with low ionization potential of guanine and adjacent arrangement of G-quartets that causes stabilization of the nucleobase-cation CS states. It would be interesting to see whether these states could be stabilized bellow the first bright $\pi\pi^*$ transition. In order to investigate whether this is the case for the Ca^{2+} containing sequences we conducted the same type of analysis for **1-Ca$_2$**, **1-Ca$_3$** and **1-Ca$_4$** systems. With increasing number of layers and Ca^{2+} cations in the system, redshift of DOS becomes visible and CS content drastically changes. CS content increases gradually from 50 % to 59 % and to 75 % for **1-Ca$_2$**, **1-Ca$_3$** and **1-Ca$_4$**, respectively. While CS content is increased with increasing system size simultaneously content of the localized transitions reduces. It amounts to 10 % for **1-Ca$_2$**, only 2 % for **1-Ca$_3$** and drops to zero for the **1-Ca$_3$**. Owing to the spatial overlap of numerous identical chromophores, all of the localized transitions have excitonic character. Excimeric content originating at the high energy part of DOS is also reduced from 40 % to 39 % and to 25 % for **1-Ca$_2$**, **1-Ca$_3$** and **1-Ca$_4$**, respectively. Another type of excimeric states is encountered in these systems and that is nucleobase-metal, i.e. G-Ca^{2+} excimers. G-Ca^{2+} excimers are encountered at the blue part of the DOS and manifest in the studied energy region only in the systems where at least two Ca^{2+} are situated in the adjacent vacancies of three-layered GQ. In all three systems low lying CS states are bellow first electronic absorption band. Additional decomposition of the CS part of the spectrum reveals presence of the nucleobase-cation CS states similar to the **3-Ba$_2$** system (G-Ca^{2+} CS) as well as their appealing feature. With increasing system size these states become dominant in the red part of the DOS. Orbital composition of the MOs contributing the most to the electron-accepting NTOs of G-Ca^{2+} CS states is given in Table 1. Representative G-Ca^{2+} CS transitions are depicted in Fig. 6. Fraction of the MOs localization in the region of the Ca^{2+} cations is also given in Table 1. From the results compiled in Table 1 we can notice high degree of the Ca^{2+} *d* orbitals participation in the excited-electron accepting MOs for these systems. Moreover, *d* orbitals content and participation of Ca^{2+} atomic orbitals is further increased within these MOs when increasing system size. Interestingly, LUMO has among the largest participation of the *d* orbitals located on the Ca^{2+} cation along with some of the MOs with higher energies, i.e. LUMO + 4, LUMO + 8 and LUMO + 15 for the **1-Ca$_2$**, **1-Ca$_3$** and **1-Ca$_4$**, respectively. Spectral consequence of such orbital composition is that G-Ca^{2+} CS states are pushed to the red side of the DOS. Moreover, for the largest studied Ca^{2+} containing system

Table 1
MOs with major contribution (> 10 %) in the unoccupied excited-electron accepting NTOs. Percentage of the *d* orbitals and Ca^{2+} cations participation in the orbital composition of the selected MOs for Ca^{2+} containing systems is also indicated.

System	Dominant excited-electron accepting MOs	*d* orbitals participation	Ca^{2+} participarion
1-Ca$_2$	LUMO	18.3	30.6
	LUMO + 1	6.1	5.6
	LUMO + 2	6.5	6.4
	LUMO + 3	7.1	6.4
	LUMO + 4	22.7	23.3
1-Ca$_3$	LUMO	50.4	57.4
	LUMO + 1	9.6	26.9
	LUMO + 2	9.9	9.0
	LUMO + 3	6.5	6.3
	LUMO + 4	11.8	12.2
	LUMO + 6	10.3	11.7
	LUMO + 7	17.5	17.3
	LUMO + 8	26.7	34.5
1-Ca$_4$	LUMO	50.9	58.5
	LUMO + 1	34.9	41.0
	LUMO + 4	12.0	10.4
	LUMO + 5	15.2	41.6
	LUMO + 6	12.3	11.0
	LUMO + 8	12.7	16.8
	LUMO + 10	10.8	10.8
	LUMO + 12	20.8	20.0
	LUMO + 15	75.0	75.3

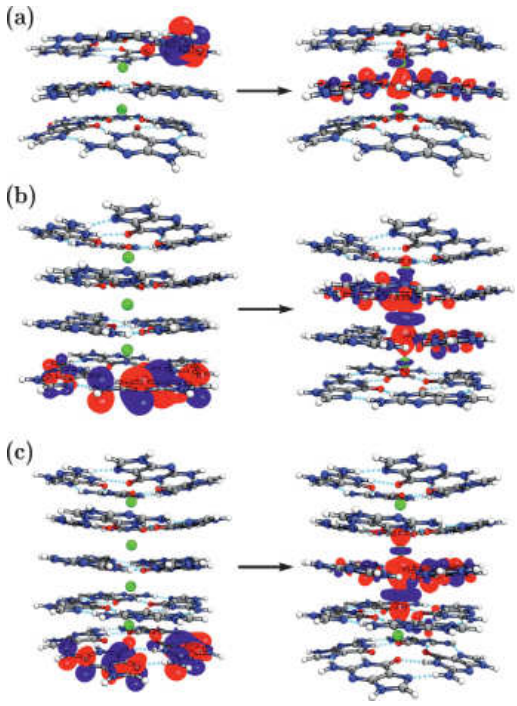

Fig. 6. Representative NTO pairs of the G-Ca^{2+} CS states for (a) **1-Ca_2** (S_{18}, E = 4.92 eV), (b) **1-Ca_3** (S_5, E = 4.02 eV) and (c) **1-Ca_4** (S_1, E = 3.36 eV) systems.

S_1 is identified as G-Ca^{2+} CS state (see Fig. 6c). This spectral characteristic could be explained by the mutual effect of the Ca^{2+} interaction with the guanine's coordinating oxygens' and unusual Ca^{2+} binding mode. Latter effect is previously characterized as predominantly electrostatic for the alkaline cations [6,13,31,83,84] while on the other hand there is evidence supporting strong orbital interaction between cations and coordinating oxygens [10,14,85]. This would depend on both cation size and charge. Strong electric field within the GQs central cavity induced by doubly charged Ca^{2+} cation provides solid ground for the stabilization of the *d* orbitals. This stabilization is even more enhanced with Ca^{2+} binding mode that causes delocalization of the *d* orbitals between adjacent Ca^{2+} cations and further decreases their energy.Thisleads to the increased participation of the Ca^{2+} *d* orbitals in the unoccupied frontier MOs tailoring spectral properties of studied GQs.

Hydration effects

CT states are prone to stabilize in the aqueous environment due to the presence of the electric field induced by the solvent. In the case of the stacked adenine dimer strong stabilization (≈1 eV) of the CT states is found [86]. Therefore, we performed additional calculation to inspect solvation effects on the CT states for the **1-Ca_2** system. We choose the smallest studied system since we use microsolvated water cluster to account for the hydration effects since this methodology drastically increases number of atoms in the system.

In the Fig. 7 comparison of the absorption spectrum, DOS and accompanying CS contributions to the DOS for the **1-Ca_2** in the gas phase and aqueous environment is presented. The position of the first absorption maximum remains unchanged (4.85 eV). However, underlying decomposition of the first absorption maximum suggests slight stabilization of the excimeric transition which partially possesses CT character. The absorption red-tail is dominated with excimeric transitions in both cases. At first glance, the hydration effect on the second absorption maximum is more apparent which is blueshifted by around 0.2 eV. However, slightly asymmetric shape of this peak can be observed and detailed examination of the transitions actually reveals that the position of the gas phase second absorption maximum is almost unchanged while blueshift seemingly originates from additional excimeric states that are now present since we included 32 more excited states in the calculation for the **1-Ca_2** with the microsolvated water cluster. Overall, bright states are not greatly influenced by the solvation. On the other hand, this is not the case for the CT component of the DOS. The composition of the DOS within the studied energy region remains almost unaltered. Slight increase by 5 % of the CS content is observed. At the same time excimeric content is reduced by 5 %. Contrary to the composition, positions of the CS peaks are highly affected and overall stabilized due the hydration. The first two excited states are identified as interlayer CS and G-Ca^{2+} CS states positioned at 3.93 and 4.38 eV, respectively. Beside the stabilization, we identified intralayer CS states at somewhat higher energies that were not present in the gas phase Ca^{2+} containing systems. In addition, we also observed transitions that include charge transfer from the G to the surrounding water molecules. These states were previously described as the electron detachment states [31,76,77] that could be responsible for the oxidative damage upon the absorption of the UV light, i.e. generation of the G radical [87–89]. These electron detachment states appear in the broad energy range as in the case of G-octets [31].

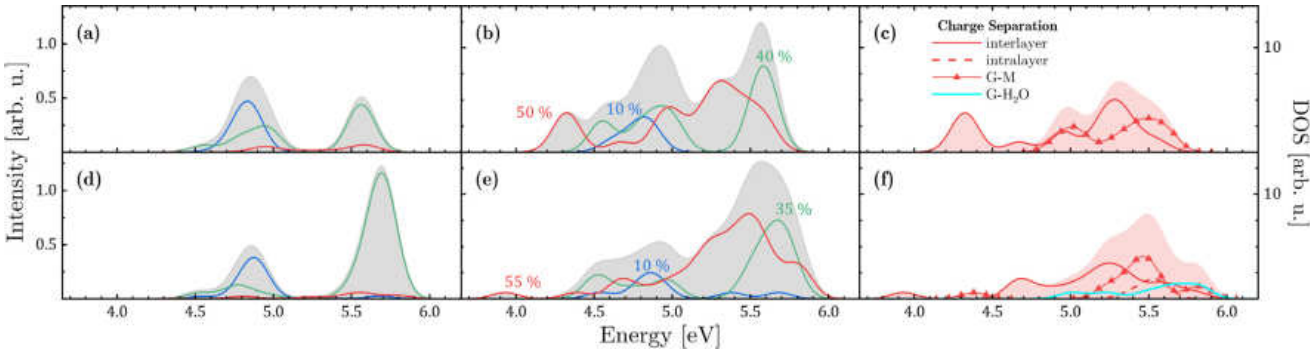

Fig. 7. Decomposition of (a), (d) electronic absorption spectrum (shaded area) and (b), (e) density of excited states (DOS) (shaded area) into the localized (blue lines), excimer (green lines) and charge separation (red lines) contributions. Percentage of each contribution to the DOS is indicated. Further decomposition of the charge separation contributions is presented on the panels (e) and (f) with the legend on the upper right panel. Upper panels ((a), (b) and (c)) and lower panels ((d), (e) and (f)) correspond to the **1-Ca_2** systems in the gas phase and in the aqueous environment, respectively.

Conclusions

Affinity of the GQs structures to chelate alkali cations within the central cavity is extensively investigated [6,13–15,17,21–23]. Alkali cations usually occupy cavities between every quartet layer which is referred as a standard binding mode. On the other hand, alkaline earth cations are rarely found in the standard binding mode arrangement but usually occupy every other available cavity [24,32,55,90]. The purpose of this study is to understand how altering between two binding modes of alkaline earth cations affects electronic absorption of GQs. To this end we used linear-response TDDFT method to examine four crystalized tetramolecular quadruplexes [52–55]. Three of them have alkaline earth cations defying standard binding mode of which two structures accommodate one pyrimidine quartet. Decomposing absorption spectra and corresponding DOS reveal several interesting conclusions. Excimeric and excitonic contributions rule the absorption profiles for all studied structures. Especially, excimeric contribution is dominant in the wide range of the energies when quadruplex's quartets experience small deviation from the planarity as found for **2-Ba$_2$**. Non-negligible absorption intensity for CS transitions is also encountered, especially for the Ca^{2+} containing sequences.

Special attention is devoted to the CS states and their properties dependence on the type of cation binding mode. We found that increasing the size of the quadruplex enhances collective effects as well as the redshift of the CS states. For quadruplexes having at least two adjacent G-quartets and two alkaline earth cations chelated at adjacent cavities CS states dominate DOS and most of them are found below the first bright transition. For instance, 75 % of the 80 lowest lying singlet states are identified as CS states for **1-Ca$_4$** system. This supramolecular design also promote existence of the G-Ca^{2+} CS states which also become dominant in the red part of the spectrum with increasing number of cations and layers. Presence of the G-Ca^{2+} CS states is ascribed to the favorable stabilization of Ca^{2+} *d* orbitals due to interaction of doubly charged cations with guanine's coordinating oxygens and *d* orbitals delocalization across Ca^{2+} situated at adjacent cavities of GQ. Such CS imprint is not observed for the **2-Ba$_2$** system where water mediated C-tetrad is sandwiched between two G-tetrads, nor in the **4-Sr$_2$** system in which two Sr^{2+} cations are chelated in the standard binding mode.

Hydration leads to the stabilization of the CS states among which interlayer and G-Ca^{2+} CS states are greatly stabilized and found to be lowest lying singlet states for the solvated **1-Ca$_2$** system. Furthermore, electron detachment states are identified in the broad energy range. These excited states may be responsible for the oxidative damage upon the UV light absorption within the biologically occurring quadruplexes.

Using robust computational approach we demonstrated interesting optical properties concerning CS states of the experimentally realized tetramolecular quadruplexes. We believe our findings could help utilize these CS states for the optoelectronic devices and help in designing novel nanostructures with adjustable optical properties.

Declaration of Competing Interest

The authors declare that they have no known competing financial interests or personal relationships that could have appeared to influence the work reported in this paper.

Acknowledgment

The research leading to these results has been co-funded by the European Commission under the H2020 Research Infrastructures contract No. 675121 (project VI-SEEM). Authors acknowledge the financial support by Ministry of Education, Science and Technological Development of Republic of Serbia Contract number: 451–03-9/2021–14/200146. B.M. acknowledges the Municipality of Arandjelovac (Youth Office) for the financial support.

References

[1] D.P.N. Gonçalves, S. Ladame, S. Balasubramanian, J.K.M. Sanders, Synthesis and g-quadruplex binding studies of new 4-n-methylpyridinium porphyrins, Org. Biomol. Chem. 4 (2006) 3337–3342, https://doi.org/10.1039/B608494J.
[2] M.L. Bochman, K. Paeschke, V.A. Zakian, Dna secondary structures: Stability and function of g-quadruplex structures, Nat. Rev. Genet 13 (11) (2012) 770–780, https://doi.org/10.1038/nrg3296.
[3] R. Hänsel-Hertsch, M. Di Antonio, S. Balasubramanian, Dna g-quadruplexes in the human genome: Detection, functions and therapeutic potential, Nat. Rev. Mol. Cell Biol. 18 (5) (2017) 279–284, https://doi.org/10.1038/nrm.2017.3.
[4] E. Henderson, C.C. Hardin, S.K. Walk, I. Tinoco Jr, E.H. Blackburn, Telomeric dna oligonucleotides form novel intramolecular structures containing guanine guanine base pairs, Cell 51 (6) (1987) 899–908, https://doi.org/10.1016/0092-8674(87)90577-0.
[5] J.T. Davis, G.P. Spada, Supramolecular architectures generated by self-assembly of guanosine derivatives, Chem. Soc. Rev. 36 (2007) 296, https://doi.org/10.1039/B600282J.
[6] G. Louit, A. Hocquet, M. Ghomi, M. Meyer, J. Sühnel, Guanine tetrads interacting with metal ions. an aim topological analysis of the electronic density, PhysChemComm 6 (2003) 1, https://doi.org/10.1039/B210911E.
[7] T. van Mourik, A.J. Dingley, Characterization of the monovalent ion position and hydrogen-bond network in guanine quartets by dft calculations of nmr parameters, Chem. - Eur. J. 11 (2005) 6064, https://doi.org/10.1002/chem.200500198.
[8] A.K. Jissy, U.P.M. Ashik, A. Datta, Nucleic acid g-quartets: Insights into diverse patterns and optical properties, J. Phys. Chem. C 115 (2011) 12530, https://doi.org/10.1021/jp202401b.
[9] C.F. Guerra, H. Zijlstra, G. Paragi, F.M. Bickelhaupt, Telomere structure and stability: Covalency in hydrogen bonds, not resonance assistance, causes cooperativity in guanine quartets, Chem. - Eur. J. 17 (2011) 12612, https://doi.org/10.1002/chem.201102234.
[10] Y.P. Yurenko, J. Novotný, V. Sklenář, R. Marek, Exploring non-covalent interactions in guanine- and xanthine-based model dna quadruplex structures: A comprehensive quantum chemical approach, Phys. Chem. Chem. Phys. 16 (2014) 2072–2084, https://doi.org/10.1039/C3CP53875C.
[11] G. Paragi, C.F. Guerra, Cooperativity in the self-assembly of the guanine nucleobase into quartet and ribbon structures on surfaces, Chem. - Eur. J. 23 (2017) 3042, https://doi.org/10.1002/chem.201604830.
[12] B. Milovanovic, M.M. Petkovic, M.R. Etinski, Properties of the excited electronic states of guanine quartet complexes with alkali metal cations, J. Serb. Chem. Soc. 85 (2020) 1021, https://doi.org/10.2298/JSC191025140M.
[13] B. Milovanovic, A. Stanojevic, M. Etinski, M. Petkovic, Intriguing intermolecular interplay in guanine quartet complexes with alkali and alkaline earth cations, J. Phys. Chem. B 124 (2020) 3002, https://doi.org/10.1021/acs.jpcb.0c01165.
[14] C. Nieuwland, F. Zaccaria, C. Fonseca Guerra, Understanding alkali metal cation affinities of multi-layer guanine quadruplex dna, Phys. Chem. Chem. Phys. 22 (2020) 21108–21118, https://doi.org/10.1039/D0CP03433A.
[15] F. Zaccaria, G. Paragi, C. Fonseca Guerra, The role of alkali metal cations in the stabilization of guanine quadruplexes: Why k^+ is the best, Phys. Chem. Chem. Phys. 18 (2016) 20895–20904, https://doi.org/10.1039/C6CP01030J.
[16] J. Deng, Y. Xiong, M. Sundaralingam, X-ray analysis of an rna tetraplex (uggggu)4 with divalent sr^{2+} ions at subatomic resolution (0.61 å), Proc. Natl. Acad. Sci. U.S.A. 98 (2001) 13665, https://doi.org/10.1073/pnas.241374798.
[17] T.J. Pinnavaia, C.L. Marshall, C.M. Mettler, C.L. Fisk, H.T. Miles, E.D. Becker, Alkali metal ion specicity in the solution ordering of a nucleotide, 5'-guanosine monophosphate, J. Am. Chem. Soc. 100 (1978) 3625, https://doi.org/10.1021/ja00479a070.
[18] F.M. Chen, Sr^{2+} facilitates intermolecular g-quadruplex formation of telomeric sequences, Biochemistry 31 (1992) 3769, https://doi.org/10.1021/bi00130a006.
[19] C.C. Hardin, T. Watson, M. Corregan, C. Bailey, Cation-dependent transition between the quadruplex and watson-crick hairpin forms of d(cgcg$_3$gcg), Biochemistry 31 (1992) 833, https://doi.org/10.1021/bi00118a028.
[20] I.C.M. Kwan, Y.-M. She, G. Wu, Nuclear magnetic resonance and mass spectrometry studies of 2',3',5'-o-triacetylguanosine self-assembly in the presence of alkaline earth metal ions (ca^{2+}, sr^{2+}, ba^{2+}), Can. J. Chem. 89 (2011) 835, https://doi.org/10.1139/v10-179.
[21] R. Ida, G. Wu, Direct nmr detection of alkali metal ions bound to g-quadruplex dna, J. Am. Chem. Soc. 130 (11) (2008) 3590–3602, pMID: 18293981. arXiv: https://doi.org/10.1021/ja709975z, doi:10.1021/ja709975z. doi: 10.1021/ja709975z.
[22] C. Detellier, P. Laszlo, Role of alkali metal and ammonium cations in the self-assembly of the 5'-guanosine monophosphate dianion, J. Am. Chem. Soc. 102 (3) (1980) 1135–1141. arXiv:https://doi.org/10.1021/ja00523a033, doi:10.1021/ja00523a033. doi: 10.1021/ja00523a033.
[23] A. Wong, G. Wu, Selective binding of monovalent cations to the stacking g-quartet structure formed by guanosine 5'-monophosphate: A solid-state nmr

study, J. Am. Chem. Soc. 125 (45) (2003) 13895–13905, pMID: 14599230. arXiv:https://doi.org/10.1021/ja0302174, doi:10.1021/ja0302174. doi: 10.1021/ja0302174.
[24] A.C. Fyfe, P.W. Dunten, M.M. Martick, W.G. Scott, Structural variations and solvent structure of r(uggggu) quadruplexes stabilized by sr2+ ions, Journal of Molecular Biology 427 (12) (2015) 2205–2219, https://doi.org/10.1016/j.jmb.2015.03.022.
[25] W. Liu, H. Zhu, B. Zheng, S. Cheng, Y. Fu, W. Li, T.-C. Lau, H. Liang, Kinetics and mechanism of g-quadruplex formation and conformational switch in a g-quadruplex of ps2.m induced by pb^{2+}, Nucleic Acids Res. 40 (9) (2012) 4229–4236. arXiv:https://academic.oup.com/nar/article-pdf/40/9/4229/3926497/gkr1310.pdf, doi:10.1093/nar/gkr1310. doi: 10.1093/nar/gkr1310.
[26] E. Zavyalova, G. Tagiltsev, R. Reshetnikov, A. Arutyunyan, A. Kopylov, Cation coordination alters the conformation of a thrombin-binding g-quadruplex dna aptamer that affects inhibition of thrombin, Nucleic Acid Ther. 26 (5) (2016) 299–308. arXiv:https://doi.org/10.1089/nat.2016.0606, doi:10.1089/nat.2016.0606. doi: 10.1089/nat.2016.0606.
[27] J. Seo, E.S. Hong, H.-J. Yoon, S.K. Shin, Specific and nonspecific bindings of alkaline-earth metal ions to guanine-quadruplex thrombin-binding aptamer dna, Int. J. Mass Spectrom. 330–332 (2012) 262–270, sI: Armentrout Honor Issue. doi: 10.1016/j.ijms.2012.09.002. http://www.sciencedirect.com/science/article/pii/S1387380612003430.
[28] S.D. Patil, D.G. Rhodes, Influence of divalent cations on the conformation of phosphorothioate oligodeoxynucleotides: A circular dichroism study, Nucleic Acids Res. 28 (12) (2000) 2439–2445. arXiv:https://academic.oup.com/nar/article-pdf/28/12/2439/9904585/282439.pdf, doi: 10.1093/nar/28.12.2439. https://doi.org/10.1093/nar/28.12.2439.
[29] B.I. Kankia, L.A. Marky, Folding of the thrombin aptamer into a g-quadruplex with sr^{2+}: Stability, heat, and hydration, J. Am. Chem. Soc. 123 (44) (2001) 10799–10804, https://doi.org/10.1021/ja010008o.
[30] M. Vairamani, M.L. Gross, G-quadruplex formation of thrombin-binding aptamer detected by electrospray ionization mass spectrometry, J. Am. Chem. Soc. 125 (1) (2003) 42–43, https://doi.org/10.1021/ja0284299.
[31] B. Milovanovic, I.M. Stankovic, M. Petkovic, M. Etinski, Modulating excited charge-transfer states of g-quartet self-assemblies by earth alkaline cations and hydration, J. Phys. Chem. A 124 (40) (2020) 8101–8111, https://doi.org/10.1021/acs.jpca.0c05022.
[32] X. Shi, J.C. Fettinger, J.T. Davis, Homochiral g-quadruplexes with ba^{2+} but not with k^{+}: The cation programs enantiomeric self-recognition, J. Am. Chem. Soc. 123 (27) (2001) 6738–6739, https://doi.org/10.1021/ja004330v.
[33] T. Li, E. Wang, S. Dong, Potassium-lead-switched g-quadruplexes: A new class of dna logic gates, J. Am. Chem. Soc. 131 (42) (2009) 15082–15083, https://doi.org/10.1021/ja9051075.
[34] C. Wang, Y. Li, G. Jia, Y. Liu, S. Lu, C. Li, Enantioselective friedel-crafts reactions in water catalyzed by a human telomeric g-quadruplex dna metalloenzyme, Chem. Commun. 48 (2012) 6232–6234, https://doi.org/10.1039/C2CC31320K.
[35] O.A. Stasyuk, M. Solà, M. Swart, C. Fonseca Guerra, T.M. Krygowski, H. Szatylowicz, Effect of alkali metal cations on length and strength of hydrogen bonds in dna base pairs, ChemPhysChem 21 (18) (2020) 2112–2126. doi: 10.1002/cphc.202000434.
[36] A. del Prado, D. González-Rodríguez, Y.-L. Wu, Functional systems derived from nucleobase self-assembly, ChemistryOpen 9 (4) (2020) 409–430, https://doi.org/10.1002/open.201900363.
[37] J.-L. Mergny, D. Sen, Dna quadruple helices in nanotechnology, Chemical Reviews 119 (10) (2019) 6290–6325, https://doi.org/10.1021/acs.chemrev.8b00629.
[38] B. Milovanovic, M. Etinski, I. Popov, Self-assembly of rylene-decorated guanine ribbons on graphene surface for optoelectronic applications: A theoretical study, Nanotechnologydoi:https://doi.org/10.1088/1361-6528/ac162c.
[39] J.T. Davis, G-quartets 40 years later: From 5'-gmp to molecular biology and supramolecular chemistry, Angew. Chem., Int. Ed. 43 (2004) 668, https://doi.org/10.1002/anie.200300589.
[40] G.I. Livshits, A. Stern, D. Rotem, N. Borovok, G. Eidelshtein, A. Migliore, E. Penzo, S.J. Wind, R. Di Felice, S.S. Skourtis, J.C. Cuevas, L. Gurevich, A.B. Koylyar, D. Porath, Long-range charge transport in single g-quadruplex dna molecules, Nat. Nanotechnol. 9 (12) (2014) 1040–1046, https://doi.org/10.1038/nnano.2014.246.
[41] R. Sha, L. Xiang, C. Liu, A. Balaeff, Y. Zhang, P. Zhang, Y. Li, D.N. Beratan, N. Tao, N.C. Seeman, Charge splitters and charge transport junctions based on guanine quadruplexes, Nat. Nanotechnol. 13 (4) (2018) 316–321, https://doi.org/10.1038/s41565-018-0070-x.
[42] M.R. Wasielewski, Self-assembly strategies for integrating light harvesting and charge separation in artificial photosynthetic systems, Acc. Chem. Res. 42 (2009) 1910, https://doi.org/10.1021/ar9001735.
[43] Y.-L. Wu, N.E. Horwitz, K.-S. Chen, D.A. Gomez-Gualdron, N.S. Luu, L. Ma, T.C. Wang, M.C. Hersam, J.T. Hupp, O.K. Farha, R.Q. Snurr, M.R. Wasielewski, G-quadruplex organic frameworks, Nature Chem. 9 (5) (2017) 466–472, https://doi.org/10.1038/nchem.2689.
[44] Y.-L. Wu, K.E. Brown, M.R. Wasielewski, Extending photoinduced charge separation lifetimes by using supramolecular design: Guanine-perylendiimide g-quadruplex, J. Am. Chem. Soc. 135 (2013) 13322, https://doi.org/10.1021/ja407648d.
[45] Y.-L. Wu, K.E. Brown, D.M. Gardner, S.M. Dyar, M.R. Wasielewski, Photoinduced hole injection into a self-assembled π-extended g-quadruplex, J. Am. Chem. Soc. 137 (2015) 3981, https://doi.org/10.1021/jacs.5b00977.
[46] N.E. Powers-Riggs, X. Zuo, R.M. Young, M.R. Wasielewski, Symmetry-breaking charge separation in a nanoscale terrylenediimide guanine-quadruplex assembly, J. Am. Chem. Soc. 141 (2019) 17512, https://doi.org/10.1021/jacs.9b10108.
[47] F. Pu, L. Wu, X. Ran, J. Ren, X. Qu, G-quartet-based nanostructure for mimicking light-harvesting antenna, Angew. Chem., Int. Ed. 54 (2015) 892, https://doi.org/10.1002/anie.201409832.
[48] L. Martínez-Fernández, L. Esposito, R. Improta, Studying the excited electronic states of guanine rich dna quadruplexes by quantum mechanical methods: Main achievements and perspectives, Photochem. Photobiol. Sci. 19 (2020) 436–444, https://doi.org/10.1039/D0PP00065E.
[49] P. Changenet-Barret, Y. Hua, D. Markovitsi, Electronic Excitations in Guanine Quadruplexes, Springer International Publishing, 2015, pp. 183–201, https://doi.org/10.1007/128_2013_511.
[50] Y. Hua, P. Changenet-Barret, R. Improta, I. Vayá, T. Gustavsson, A.B. Kotlyar, D. Zikich, P. Šket, J. Plavec, D. Markovitsi, Cation effect on the electronic excited states of guanine nanostructures studied by time-resolved fluorescence spectroscopy, The Journal of Physical Chemistry C 116 (27) (2012) 14682–14689, https://doi.org/10.1021/jp303651e.
[51] A. Dumas, N.W. Luedtke, Cation-mediated energy transfer in g-quadruplexes revealed by an internal fluorescent probe, Journal of the American Chemical Society 132 (51) (2010) 18004–18007, https://doi.org/10.1021/ja1079578.
[52] M.P.H. Lee, G.N. Parkinson, P. Hazel, S. Neidle, Observation of the coexistence of sodium and calcium ions in a dna g-quadruplex ion channel, J. Am. Chem. Soc. 129 (33) (2007) 10106–10107, pMID: 17661470. arXiv:https://doi.org/10.1021/ja0740869, doi:10.1021/ja0740869. doi: 10.1021/ja0740869.
[53] D. Zhang, T. Huang, P.S. Lukeman, P.J. Paukstelis, Crystal structure of a dna/ba^{2+} g-quadruplex containing a water-mediated c-tetrad, Nucleic Acids Res. 42 (21) (2014) 13422–13429. arXiv:https://academic.oup.com/nar/article-pdf/42/21/13422/14122432/gku1122.pdf, doi:10.1093/nar/gku1122. doi: 10.1093/nar/gku1122.
[54] B. Pan, Y. Xiong, K. Shi, J. Deng, M. Sundaralingam, Crystal structure of an rna purine-rich tetraplex containing adenine tetrads: Implications for specific binding in rna tetraplexes, Structure 11 (7) (2003) 815–823, https://doi.org/10.1016/S0969-2126(03)00107-2.
[55] J. Deng, Y. Xiong, M. Sundaralingam, X-ray analysis of an rna tetraplex (uggggu)_4 with divalent sr^{2+} ions at subatomic resolution (0.61 å), Proceedings of the National Academy of Sciences 98 (24) (2001) 13665–13670. arXiv:https://www.pnas.org/content/98/24/13665.full.pdf, doi:10.1073/pnas.241374798. https://www.pnas.org/content/98/24/13665.
[56] H.M. Berman, J. Westbrook, Z. Feng, G. Gilliland, T.N. Bhat, H. Weissig, I.N. Shindyalov, P.E. Bourne, The Protein Data Bank, Nucleic Acids Research 28 (1) (2000) 235–242. arXiv:https://academic.oup.com/nar/article-pdf/28/1/235/9895144/280235.pdf, doi:10.1093/nar/28.1.235. doi: 10.1093/nar/28.1.235.
[57] A.S. Rose, A.R. Bradley, Y. Valasatava, J.M. Duarte, A. Prlić, P.W. Rose, NGL viewer: Web-based Molecular Graphics for Large Complexes, Bioinformatics 34 (21) (2018) 3755–3758, https://doi.org/10.1093/bioinformatics/bty419.
[58] T. Yanai, D.P. Tew, N.C. Handy, A new hybrid exchange-correlation functional using the coulomb-attenuating method (cam-b3lyp), Chemical Physics Letters 393 (1) (2004) 51–57, https://doi.org/10.1016/j.cplett.2004.06.011.
[59] S. Grimme, J. Antony, S. Ehrlich, H. Krieg, A consistent and accurate ab initio parametrization of density functional dispersion correction (dft-d) for the 94 elements h-pu, The Journal of Chemical Physics 132 (15) (2010) 154104, https://doi.org/10.1063/1.3382344.
[60] F. Weigend, R. Ahlrichs, Balanced basis sets of split valence, triple zeta valence and quadruple zeta valence quality for h to rn: Design and assessment of accuracy, Physical Chemistry Chemical Physics 7 (2005) 3297–3305, https://doi.org/10.1039/B508541A.
[61] F. Weigend, Accurate coulomb-fitting basis sets for h to rn, Physical Chemistry Chemical Physics 8 (2006) 1057–1065, https://doi.org/10.1039/B515623H.
[62] M.J. Frisch, G.W. Trucks, H.B. Schlegel, G.E. Scuseria, M.A. Robb, J.R. Cheeseman, G. Scalmani, V. Barone, B. Mennucci, G.A. Petersson, H. Nakatsuji, M. Caricato, X. Li, H.P. Hratchian, A.F. Izmaylov, J. Bloino, G. Zheng, J.L. Sonnenberg, M. Hada, M. Ehara, K. Toyota, R. Fukuda, J. Hasegawa, M. Ishida, T. Nakajima, Y. Honda, O. Kitao, H. Nakai, T. Vreven, J.A. Montgomery, Jr., J.E. Peralta, F. Ogliaro, M. Bearpark, J.J. Heyd, E. Brothers, K.N. Kudin, V.N. Staroverov, T. Keith, R. Kobayashi, J. Normand, K. Raghavachari, A. Rendell, J.C. Burant, S.S. Iyengar, J. Tomasi, M. Cossi, N. Rega, J.M. Millam, M. Klene, J.E. Knox, J.B. Cross, V. Bakken, C. Adamo, J. Jaramillo, R. Gomperts, R.E. Stratmann, O. Yazyev, A.J. Austin, R. Cammi, C. Pomelli, J.W. Ochterski, R.L. Martin, K. Morokuma, V.G. Zakrzewski, G.A. Voth, P. Salvador, J.J. Dannenberg, S. Dapprich, A.D. Daniels, O. Farkas, J.B. Foresman, J.V. Ortiz, J. Cioslowski, D.J. Fox, Gaussian 09 Revision D.01, gaussian Inc., Wallingford CT 2009.
[63] F. Plasser, Theodore: A toolbox for a detailed and automated analysis of electronic excited state computations, The Journal of Chemical Physics 152 (8) (2020) 084108, https://doi.org/10.1063/1.5143076.
[64] F. Plasser, H. Lischka, Analysis of excitonic and charge transfer interactions from quantum chemical calculations, Journal of Chemical Theory and Computation 8 (8) (2012) 2777–2789, https://doi.org/10.1021/ct300307c.
[65] F. Plasser, M. Wormit, A. Dreuw, New tools for the systematic analysis and visualization of electronic excitations. i. formalism, The Journal of Chemical Physics 141 (2) (2014) 024106, https://doi.org/10.1063/1.4885819.
[66] S. Mai, F. Plasser, J. Dorn, M. Fumanal, C. Daniel, L. González, Quantitative wave function analysis for excited states of transition metal complexes, Coordination Chemistry Reviews 361 (2018) 74–97, https://doi.org/10.1016/j.ccr.2018.01.019.

[67] F. Plasser, Entanglement entropy of electronic excitations, The Journal of Chemical Physics 144 (19) (2016) 194107, https://doi.org/10.1063/1.4949535.
[68] T. Lu, F. Chen, Multiwfn: A multifunctional wavefunction analyzer, Journal of Computational Chemistry 33 (5) (2012) 580–592, https://doi.org/10.1002/jcc.22885.
[69] D. Case, K. Belfon, I. Ben-Shalom, S. Brozell, D. Cerutti, T.C. III, V. Cruzeiro, T. Darden, R. Duke, G. Giambasu, M. Gilson, H. Gohlke, A. Goetz, R. Harris, S. Izadi, S. Izmailov, K. Kasavajhala, A. Kovalenko, R. Krasny, T. Kurtzman, T. Lee, S. LeGrand, P. Li, C. Lin, J. Liu, T. Luchko, R. Luo, V. Man, K. Merz, Y. Miao, O. Mikhailovskii, G. Monard, H. Nguyen, A. Onufriev, F. Pan, S. Pantano, R. Qi, D. Roe, A. Roitberg, C. Sagui, S. Schott-Verdugo, J. Shen, C. Simmerling, N. Skrynnikov, J. Smith, J. Swails, R. Walker, J. Wang, L. Wilson, R. Wolf, X. Wu, Y. Xiong, Y. Xue, Amber 2020, university of California, San Francisco.
[70] R. Salomon-Ferrer, D.A. Case, R.C. Walker, An overview of the amber biomolecular simulation package, WIREs Computational Molecular Science 3 (2) (2013) 198–210. arXiv:https://wires.onlinelibrary.wiley.com/doi/pdf/10.1002/wcms.1121, doi: 10.1002/wcms.1121. https://wires.onlinelibrary.wiley.com/doi/abs/10.1002/wcms.1121.
[71] J. Wang, R.M. Wolf, J.W. Caldwell, P.A. Kollman, D.A. Case, Development and testing of a general amber force field, Journal of Computational Chemistry 25 (9) (2004) 1157–1174. arXiv:https://onlinelibrary.wiley.com/doi/pdf/10.1002/jcc.20035, doi: 10.1002/jcc.20035. https://onlinelibrary.wiley.com/doi/abs/10.1002/jcc.20035.
[72] D.J. Price, C.L. Brooks, A modified tip3p water potential for simulation with ewald summation, The Journal of Chemical Physics 121 (20) (2004) 10096–10103, https://doi.org/10.1063/1.1808117.
[73] J. VandeVondele, M. Krack, F. Mohamed, M. Parrinello, T. Chassaing, J. Hutter, QUICKSTEP: Fast and Accurate Density Functional Calculations using a Mixed Gaussian and Plane Waves Approach, J. Comp. Phys. Comm. 167 (2005) 103–128.
[74] G. Bussi, D. Donadio, M. Parrinello, Canonical sampling through velocity rescaling, The Journal of Chemical Physics 126 (1) (2007) 014101, https://doi.org/10.1063/1.2408420.
[75] U. Essmann, L. Perera, M.L. Berkowitz, T. Darden, H. Lee, L.G. Pedersen, A smooth particle mesh ewald method, The Journal of Chemical Physics 103 (19) (1995) 8577–8593, https://doi.org/10.1063/1.470117.
[76] A.L. Sobolewski, W. Domcke, Photoinduced electron and proton transfer in phenol and its clusters with water and ammonia, The Journal of Physical Chemistry A 105 (40) (2001) 9275–9283, https://doi.org/10.1021/jp011260l.
[77] I. Sandler, J.J. Nogueira, L. González, Solvent reorganization triggers photo-induced solvated electron generation in phenol, Phys. Chem. Chem. Phys. 21 (2019) 14261–14269, https://doi.org/10.1039/C8CP06656F.
[78] L. Martínez-Fernández, A. Banyasz, D. Markovitsi, R. Improta, Topology controls the electronic absorption and delocalization of electron holes in guanine quadruplexes, Chemistry - A European Journal 24 (57) (2018) 15185–15189, https://doi.org/10.1002/chem.201803222.
[79] D. Avagliano, S. Tkaczyk, P.A. Sánchez-Murcia, L. González, Enhanced rigidity changes ultraviolet absorption: Effect of a merocyanine binder on g-quadruplex photophysics, The Journal of Physical Chemistry Letters 11 (23) (2020) 10212–10218, https://doi.org/10.1021/acs.jpclett.0c03070.
[80] M. Yaghoubi Jouybari, Y. Liu, R. Improta, F. Santoro, Ultrafast dynamics of the two lowest bright excited states of cytosine and 1-methylcytosine: A quantum dynamical study, Journal of Chemical Theory and Computation 16 (9) (2020) 5792–5808. doi: 10.1021/acs.jctc.0c00455.
[81] A.K. Dutta, T. Sengupta, N. Vaval, S. Pal, Electron attachment to dna and rna nucleobases: An eomcc investigation, International Journal of Quantum Chemistry 115 (12) (2015) 753–764, https://doi.org/10.1002/qua.24892.
[82] D. Roca-Sanjuán, M. Rubio, M. Merchán, L. Serrano-Andrés, Ab initio determination of the ionization potentials of dna and rna nucleobases, The Journal of Chemical Physics 125 (8) (2006) 084302, https://doi.org/10.1063/1.2336217.
[83] J. Gu, J. Leszczynski, M. Bansal, A new insight into the structure and stability of hoogsteen hydrogen-bonded g-tetrad: An ab initio scf study, Chemical Physics Letters 311 (3) (1999) 209–214, https://doi.org/10.1016/S0009-2614(99)00821-0.
[84] M. Meyer, T. Steinke, M. Brandl, J. Sühnel, Density functional study of guanine and uracil quartets and of guanine quartet/metal ion complexes, Journal of Computational Chemistry 22 (1) (2001) 109–124, https://doi.org/10.1002/1096-987X(20010115)22:1<109::AID-JCC11>3.0.CO;2-5.
[85] W.S. Ross, C.C. Hardin, Ion-induced stabilization of the g-dna quadruplex: Free energy perturbation studies, Journal of the American Chemical Society 116 (14) (1994) 6070–6080, https://doi.org/10.1021/ja00093a003.
[86] H. Yin, Y. Ma, J. Mu, C. Liu, M. Rohlfing, Charge-transfer excited states in aqueous dna: Insights from many-body green's function theory, Phys. Rev. Lett. 112 (2014) 228301, https://doi.org/10.1103/PhysRevLett.112.228301.
[87] E. Balanikas, A. Banyasz, T. Douki, G. Baldacchino, D. Markovitsi, Guanine radicals induced in dna by low-energy photoionization, Accounts of Chemical Research 53 (8) (2020) 1511–1519, https://doi.org/10.1021/acs.accounts.0c00245.
[88] A. Banyasz, E. Balanikas, L. Martinez-Fernandez, G. Baldacchino, T. Douki, R. Improta, D. Markovitsi, Radicals generated in tetramolecular guanine quadruplexes by photoionization: Spectral and dynamical features, The Journal of Physical Chemistry B 123 (23) (2019) 4950–4957, https://doi.org/10.1021/acs.jpcb.9b02637.
[89] B. Behmand, E. Balanikas, L. Martinez-Fernandez, R. Improta, A. Banyasz, G. Baldacchino, D. Markovitsi, Potassium ions enhance guanine radical generation upon absorption of low-energy photons by g-quadruplexes and modify their reactivity, The Journal of Physical Chemistry Letters 11 (4) (2020) 1305–1309, https://doi.org/10.1021/acs.jpclett.9b03667.
[90] T.N. Plank, L.P. Skala, J.T. Davis, Supramolecular hydrogels for environmental remediation: G4-quartet gels that selectively absorb anionic dyes from water, Chem. Commun. 53 (2017) 6235–6238, https://doi.org/10.1039/C7CC03118A.

Прилог 6 – *Self-Assembly of Rylene-Decorated Guanine Ribbons on Graphene Surface for Optoelectronic Applications: A Theoretical Study*

Објављени научни рад (категорија научног часописа M_{21}):

Branislav Milovanović, Mihajlo Etinski, Igor Popov, Self-Assembly of Rylene-Decorated Guanine Ribbons on Graphene Surface for Optoelectronic Applications: A Theoretical Study, *Nanotechnology*, **2021**, 32 (43), pp 435405.

https://doi.org/10.1088/1361-6528/ac162c *IF(2020) 3,874*

Ауторска права код издавача (приступљено дана 15.12.2021.):

[Permissions <permissions@ioppublishing.org>]
Mon, 06-12-2021 14:58

From: [Permissions <permissions@ioppublishing.org>]
To: [Branislav Milovanović <branislavm@ffh.bg.ac.rs>]
Subject: Re: Transfer of permissions for article to use in the doctoral dissertation

Dear Branislav Milovanović,

Thank you for your email. I can confirm I have approved your request through the CCC Marketplace. You should have received an email from them confirming this, which you can provide to your institution as proof of permission.

If you have any questions or need anything further, please feel free to contact us.

Kind regards,

Sophie
Copyright & Permissions Team
Sophie Brittain - Rights & Permissions Assistant
Cameron Wood - Legal & Rights Adviser
Contact Details
E-mail: permissions@ioppublishing.org

For further information about copyright and how to request permission:
https://publishingsupport.iopscience.iop.org/copyright-journals/
See also: https://publishingsupport.iopscience.iop.org/
Please see our Author Rights Policy https://publishingsupport.iopscience.iop.org/author-rights-policies/
Please note: We do not provide signed permission forms as a separate attachment. Please print this email and provide it to your publisher as proof of permission. **Please note**: Any statements made by IOP Publishing to the effect that authors do not need to get permission to use any content where IOP Publishing is not the publisher is not intended to constitute any sort of legal advice. Authors must make their own decisions as to the suitability of the content they are using and whether they require permission for it to be published within their article.

CCC | Marketplace™

Special Requests > Special Request Details

Nanotechnology

GENERAL INFORMATION

Request ID	600062491	**Request Date**	06 Dec 2021	
Request Status	Accepted	**Price**	0,00 EUR	Special Terms

ALL DETAILS

ISSN:	0957-4484
Type of Use:	Republish in a thesis/dissertation
Publisher:	IOP Publishing
Portion:	Chapter/article

LICENSED CONTENT

Publication Title	Self-assembly of rylene-decorated guanine ribbons on graphene surface for optoelectronic applications: a theoretical study	**Country**	United Kingdom of Great Britain and Northern Ireland
Author/Editor	Institute of Physics (Great Britain)	**Rightsholder**	IOP Publishing, Ltd
Date	06/08/2021	**Publication Type**	Journal

REQUEST DETAILS

Page range(s)	complete article	**Distribution**	Worldwide
Total number of pages	10	**Translation**	Original language of publication
Format (select all that apply)	Print, Electronic	**Copies for the disabled?**	No
Who will republish the content?	Author of requested content	**Minor editing privileges?**	No
		Incidental promotional use?	No
Duration of Use	Life of current and all future editions	**Currency**	EUR
Lifetime Unit Quantity	Up to 499		
Rights Requested	Main product		

NEW WORK DETAILS

Title	MSc	**Institution name**	University of Belgrade, Faculty of Physical Chemistry
Instructor name	Branislav Milovanović	**Expected presentation date**	2021-12-20

ADDITIONAL DETAILS

The requesting person / organization to appear on the license	Branislav Milovanović

REUSE CONTENT DETAILS

Title, description or numeric reference of the portion(s)	Self-assembly of rylene-decorated guanine ribbons on graphene surface for optoelectronic applications: a theoretical study	**Title of the article/chapter the portion is from**	Self-assembly of rylene-decorated guanine ribbons on graphene surface for optoelectronic applications: a theoretical study
Editor of portion(s)	Branislav Milovanović, Mihajlo Etinski and Igor Popov	**Author of portion(s)**	Branislav Milovanović, Mihajlo Etinski and Igor Popov
Volume of serial or monograph	Nanotechnology, Volume 32, Number 43	**Publication date of portion**	2021-08-06
Page or page range of portion	Complete Article		

IOP Publishing Nanotechnology
Nanotechnology 32 (2021) 435405 (15pp) https://doi.org/10.1088/1361-6528/ac162c

Self-assembly of rylene-decorated guanine ribbons on graphene surface for optoelectronic applications: a theoretical study

Branislav Milovanović[1], Mihajlo Etinski[1] and Igor Popov[2,3,*]

[1] University of Belgrade, Faculty of Physical Chemistry, Studentski trg 12-16, Belgrade, Serbia
[2] Institute for Multidisciplinary Research, University of Belgrade, Kneza Višeslava 1, Belgrade, Serbia
[3] Institut of Physics, University of Belgrade, Pregrevica 118, Belgrade, Serbia

E-mail: popov@ipb.ac.rs

Received 7 April 2021, revised 3 June 2021
Accepted for publication 20 July 2021
Published 6 August 2021

Abstract

We are witnessing a change of paradigm from the conventional top-down to the bottom-up fabrication of nanodevices and particularly optoelectronic devices. A promising example of the bottom-up approach is self-assembling of molecules into layers with predictable and reproducible structural, electronic and optical properties. Nucleobases possess extraordinary ability to self-assembly into one-, two-, and three-dimensional structures. Optical properties of nucleotides are not suitable for wider application to optoelectronics and photovoltaics due to their large optical band gap, which is in contrast to rylene-based dyes that have been intensively investigated in organic optoelectronics. However, these lack the self-assembly capability of nucleobases. Combinations of covalently decorated guanine molecules with rylene type chromophores present 'the best of the both worlds'. Due to the large size of such compounds and its flexible nature their self-assemblies have not been fully understood yet. Here, we use a theoretical approach to study the structural, energetic and optical properties of rylene-based dye decorated guanine (GPDI), as self-assembled on a graphene sheet. Particularly we utilize the density-functional based tight-binding method to study atomic structure of these systems including the potential energy surface of GPDI and stability and organization of single- and multilayered GPDIs on graphene sheet. Using density-functional theory (DFT) we employ the energy decomposition analysis to gain a deeper insight into the contributions of different moieties to stability of GPDI films. Using time dependent DFT we analyze optical properties of these systems. We find that atomically thin films consisting of only a few molecular layers with large surface areas are more favorable than isolated thick islands. Our study of excited states indicates existence of charge separated states similar to ones found in the well-studied hydrogen bonded organic frameworks. The self-assembly characterized with a large homogeneous coverage and long-living charge-separated states provide the great potential for optoelectronic applications.

Supplementary material for this article is available online

Keywords: DFT, DFTB, guanine, rylene, self-assembly, stability, electronics

(Some figures may appear in colour only in the online journal)

* Author to whom any correspondence should be addressed.

1. Introduction

Complexity and difficulties in fabrication of optoelectronic nanodevices, including photovoltaics, rapidly rise as their minimal structural features decrease. Consequently the conventional top-down solutions are increasingly getting substituted by bottom-up fabrication methods. The self-assembly process provides a highly promising bottom-up approach toward the fabrication of novel functional materials and nanodevices. Nucleobases are the representative example of microscopic building blocks ideally suited for self-assembling into nanostructures. Non-covalent bonding between nucleobases is the key feature that enables nucleobases to build the complex nanostructures including the deoxyribonucleic acid (DNA). In recent years several groups have demonstrated novel nucleotide-based nanostructures beyond the usual helical ones [1–13]. Unfortunately, materials based exclusively on nucleobases are not well suited for optoelectronic and photovoltaic applications due to their photo-activity only to the ultra-violet part of the solar spectrum. To this end a range of organic dyes are considered [14–20], however they usually lack the self-assembly ability of nucleobases. Hydrogen bonded organic frameworks (HOFs) present a prominent 'best of the both worlds' solution [21–25]. The so far experimentally realized nucleobase based HOFs are built up from covalently decorated guanine molecules (G) with rylene type chromophore as a linker. In particular, naphthalene-1,4:5,8-bis(dicarboximide) (NDI) and 2,5,8,11-tetrahexylperylene-3,4:9,10-bis(dicarboximide) (PDI) linkers have been studied [26, 27], where tasks of self-assembly and desired optical properties are assigned to guanine and the dye molecules, respectively. The important advantage of HOFs is a wide choice of molecules to assemble with guanine, which provides a great potential to finely tune materials for desired optical properties. It is demonstrated that G-quadruplexes can serve as effective conduits for photogenerated positive charge in ordered columnar architectures—covalently linked electron rich core (G-quarduplex) and rylene dye based electron acceptors [22–28].This unique hole-trapping ability of guanines within the central quadruplex channel could be exploited for range of applications in optoelectronic devices. Chromophore organization within these systems ensure presence of the long-lived charge-separated (CS) states. Upon photoexcitation to the bright excitonic $\pi\pi^*$ state localized on the rylene dyes, system undergoes charge separation to form CS state ($G^{\bullet+}$-$dye^{\bullet-}$) that later encounter ground state through charge recombination. Such CS states are found for guanine-PDI (GPDI) folded quadruplexes and decays to the ground state within 1.2 ± 0.2 ns [22]. Such long decay is attributed to the electron delocalization over adjacent PDI chromophores. Another, shorter decay time constant is also observed (98 ± 12 ps) and it is associated with PDIs localized excimer-like state decay towards CS state [22]. Fast photoinitiated hole transport within quadruplexes suggest potential utilization for conductive nanodevices. Mechanism of such hole transport is still speculated [28, 29]. Another interesting type of long-lived CS state is observed for guanine coupled to the terrylenediimide (TDI) to form units which build GTDI-quadruplex [24, 25]. High degree of stacking between adjacent TDIs ensures that upon photoexcitation system efficiently populates symmetry-breaking CS (SB-CS) state, i.e. ion pair excited state ($TDI^{\bullet+}$-$TDI^{\bullet-}$) which has undivided attention for the organic photovoltaics application [30]. Similar excited states characteristics are found for G-quadruplex-based organic frameworks [26, 27] and GTDI thin films on the glass substrate [25]. Alternative structures to HOFs with the same guanine-(dye molecule) building blocks and potentially the task sharing capability are quasi-one-dimensional nanoribbons and two-dimensional layered materials based on them. Beside rylene diimide substituted guanine, i.e. NDI and PDI, in literature we find several more compounds of interest for the optoelectronic applications as a guanine/guanosine substituent: oligothiophenes [9, 31–33], oligo(p-phenylene-vinylene) [34], boron-dipyrromethene [35] and butylphyneyl [36]. From the experimental aspect, synthesis of these compounds is complex and time-consuming [22–27]. For instance, synthesis of the GPDI takes place in the solution with total preparation time of ≈116 h (see Synthesis details from the [22]). Particularly in case of GPDI, synthesis is a three-step process: (1) guanine is functionalized at C8 position using ethynyl group (see figure 2(a)); (2) PDI rylene dye is functionalized using 4-iodophenyl (arene linker) at N position of one of the PDI imide groups; (3) GPDI conjugate is prepared in the mixture of organic solvents (dimethylformamide and triethylamine). Likewise, characterization of these compounds requires several complex experimental techniques.

Importantly, having structure of atomically thin films, these materials can be considered for flexible photovoltaic and optoelectronic applications when deposited on a transparent electrode. Graphene has gained the increased interest as transparent electrode. Crystalline semiconductor—graphene heterojunctions, where semiconductor has optical properties tuned for application of interest, have been intensively investigated recently [37–39]. Besides these systems, self-assembled systems of various rylene diimides adsorbed on highly oriented pyrolytic graphite (HOPG) have been reported [40] as well as the covalently decorated guanine/guanosine molecules with oligothiophene derivates [9, 31–34]. However, understanding interfaces of the relatively large flexible molecules and graphene is challenging primarily from the computational aspect, hence details of their structural, energetic, electronic and optical properties remain scarce.

In this paper, we use a theoretical approach, which includes density functional theory (DFT) and density-functional based tight-binding (DFTB) method, to analyze properties of the self-assembled GPDI molecules at the atomic level. This combination of methods provides a very good balance between accuracy and speed necessary to investigate in detail the large systems of interest. We find that GPDI molecules tend to self-assemble in homogeneous atomically thin films, which, as in the case of above mentioned crystalline semiconductor—graphene heterojunction, is important for applications in optical devices. Despite having different structures than HOFs, we show that optical absorption

properties of investigated layered ribbons are very similar to those of HOFs. These optical properties of atomically thin self-assembled layered homogeneous anisotropic graphene-GPDI heterojunctions provide an alternative solid ground for their applications in flexible photovoltaics and optoelectronic devices.

The paper is organized in the following order: after introduction of investigated systems, stability of self-assembled structures will be discussed based on binding energy, energy decomposition analysis (EDA) and electronic density of states (DOS). Optical properties of these systems will be analyzed in detail, and conclusions given at the end.

2. Theoretical methodology

We used DFTB+ program [41] to perform DFTB calculations. DFTB SCC-Hamiltonian is constructed within a framework of the third order density functional tight-binding model (DFTB3) along with D3 correction for disperion interactions [42, 43] in conjuction with 3ob third-order parametrization for organic and biological systems [44]. During DFTB3 optimizations and molecular dynamics runs we also enabled additional corrections for dispersion interactions and hydrogen bonds [45, 46] denoted with H5. Accuracy of DFTB3 method along with other popular semiempirical methods is recently found to have a good accuracy for complex non-covalently glued molecular systems [47–49]. DFTB method has also been tested for a range of organic molecules including nucleobases and its molecular complexes (stacked guanine trimer, guanine-cytosine dimers) [47] and reasonable agreement (structural and energetic) with the reference structures is found. Furthermore, results are not much different from those obtained using more sophisticated DFT functionals such as M06-2X in combination with modest basis sets. Another study conducted comprehensive investigation of the performance of DFTB-D3 method along with various H-bond corrections. [48] In general, non-covalent interactions (binding energies) between π conjugated biomolecules (including nucleobases) are slightly overestimated, while dispersion interactions with graphene-like substrate are slightly underestimated. Another fact is that different H-bonding parametrization can lead to drastic changes from geometry and/or energetic aspects. Transferability of parameters of semiempirical methods among different classes of molecules/interactions is a well-known issue, and therefore evaluation of the parameters on a model system is required. For the benchmark purposes we used G-quartet as a model system. G-quartet is a representative of finely tuned non-covalently glued molecular system. Also, G-quartet is a key motif responsible for the assembly of the HOFs used for the comparison in this work and it exhibit same types of hydrogen bonds which are encountered in studied GPDI ribbons. Various available DFTB general purpose parameter sets are used for the benchmark and the results are reported in the SI. DFTB3-D3H5 in conjunction with 3ob parameter set for bio and organic molecules outperform other tested methods/parameters. In addition, we slightly changed default H5 parameters to even better reproduce results obtained with hybrid functionals (benchmark is also provided in the SI). The DFTB3-D3H5/3ob geometry optimizations were followed by single point (SP) energy calculation at DFTB3-D3/3ob level of theory, i.e. without H5 correction since in this case binding energies are much closer to the DFT results as discussed in the following section. Geometry optimizations are performed using conjugate gradient method and maximal force component threshold of 1×10^{-4} a.u.. All periodic calculations are performed at the Γ-point.

Siesta code [50] was used to perform periodic DFT calculations. These calculations were employed to benchmark binding energies obtained using DFTB methodology. 4770 eV is used for the plane wave cutoff in the real space grid and the Perdew–Burke–Ernzerhof form of the generalized gradient approximation [51], while the core electrons are described by norm-conserving pseudopotentials with partial core corrections [52].

Two-dimensional nature of the material is simulated by setting the lattice vector c (which is perpendicular to the materials plane) to 30 Å , which provides vacuum of around 20 Å between a unit cell and its periodic replica for the largest, multilayared ribbons. Two types of ribbons were investigated. Type I ribbons are simulated using cell vectors of 22.29, 47.30 and 30.00 Å along x, y and z axes, respectively. This resulted in a super-cell containing 660 atoms for single layered type I ribbon in which four GPDI molecules were hydrogen bonded and adsorbed on a graphene surface. Type II ribbons (also four hydrogen bonded GPDIs adsorbed on graphene) are simulated using somewhat smaller cell vectors of 22.29, 43.00 and 30.00 Å along x, y and z axes, respectively, which resulted in a super-cell accommodating 624 atoms in total. We also simulated multilayered ribbons (up to three layers) where each additional stacked ribbon layer contained 264 atoms. For comparison with the ribbons we also investigated previously experimentally realized HOF structures [26]. These are prepared using *in silico* procedure described in the [26]. In HOF structures PDI molecule serves as a covalent linker between two guanines which is denoted with G_2PDI. Hydrogen at N^9 position of guanine is substituted with soluble octyl group as in the case of the experimentally realized HOF [26, 27]. Structure and arrangement of G_2PDI in HOFs require only two G_2PDI per unit cell where both ends of the G_2PDI participate in the hydrogen bonding to form HOF. Cell vectors of such system amount to 43.00, 42.12 and 30.00 Å along x, y and z axes, respectively, which results in a super-cell that contain 960 atoms. Multilayered HOFs (up to three additional layers) are constructed analogously to the multilayered ribbons with additional 280 atoms per layer. Beside structures adsorbed on graphene, we simulate infinite layers of ribbons and HOF by reducing z axis cell vector to 5.97, 6.09 and 6.87 Å for type I, type II ribbon and HOF, respectively. These values correspond to the double value of average interlayer separation since we used two layers and periodic boundary conditions to construct an infinite layer. Parameters characterizing supercells of studied systems are compiled in the table 1.

Table 1. Parameters for constructing super-cells for type I ribbons, type II ribbons and HOFs. Note that *z*-axis is always perpendicular to the molecular frameworks plane. In case of ribbons *x*-axis is positioned in the direction of the H-bonds, while in case of the HOFs *x*-axis is positioned perpendicular to the N–H···O H-bond formed between two G_2PDI in the unit cell. Initial single-layered HOF is prepared following *in silico* procedure described in the [26].

Molecular framework name	Number of layers	Super-cell vectors (*x*, *y*, *z*)	Number GPDI/G_2PDI molecules in the super-cell	Total number of atoms in the super-cell	Atoms per layer
Type I ribbon	1	22.29, 47.30, 30.00	4	660	264
	2	22.29, 47.30, 30.00	8	924	
	3	22.29, 47.30, 30.00	12	1188	
	∞	22.29, 47.30, 5.97	8	528	
Type II ribbon	1	22.29, 43.00, 30.00	4	624	264
	2	22.29, 43.00, 30.00	8	888	
	3	22.29, 43.00, 30.00	12	1152	
	∞	22.29, 43.00, 6.09	8	528	
HOF	1	43.00, 42.12, 30.00	2	960	140
	2	43.00, 42.12, 30.00	4	1240	
	∞	43.00, 42.12, 6.87	4	560	

Total interaction energy between GPDI units adsorbed on graphene is decomposed using EDA [53] implemented in Turbomole program package [54]. In order to make study computationally feasible for EDA purposes we used non-periodic DFT with B-LYP functional [55, 56] and Grimmes' D3 dispersion correction [57] in conjuction with def2-TZVPP basis set [58, 59]. Electronic Coulomb interactions were calculated using multipole accelerated resolution-of-identity.

Electronic absorption spectrum for two layered ribbons and HOF structures is obtained for geometries optimized at DFTB3-D3H5/3ob level of theory. Each system contained 8 GPDI/G_2PDI units without absorbent (graphene) which is mostly transparent within studied excitation window. This amounted to 528 and 736 atoms for the most stable two layered type I/II ribbons and HOF structures, respectively. Excitations were computed using linear response time-dependent density functional theory (LR-TDDFT) and the long-range corrected CAM-B3LYP functional [60] in conjunction with def2-SV(P) basis set [58, 59]. LR-TDDFT calculations were carried out using Gaussian09 software [61]. For each system 64 lowest lying singlet excited states (N_s) were calculated. Vertical electronic transitions are broadened using Gaussian shaped function and electronic absorption spectrum is obtained as:

$$A(E) \sim \sum_{i=1}^{N_s} \frac{f_i}{\sqrt{2\pi}\,\gamma} exp\left(-\frac{(E-E_i)^2}{2\gamma^2}\right), \qquad (1)$$

where f_i and E_i is oscillator strength and energy of the ith electronic excited state, respectively. γ is the broadening parameter set to 0.2 eV in order to better visually resolve spectrum. The density of transition (DOT) is also obtained using equation (1) with f_i values set to 1. Benchmark calculation for the employed method i.e. absorption profile calculation and comparison to the experimental spectrum is available in the SI. Excited states character is analyzed using TheoDORE program package [62–66] which relies on the analysis of the one-electron transition density matrix (1eTDE) and it is useful to resolve types of excitations in the systems of interacting chromophores. Excited states character is determined using two descriptors based on decomposition of the 1eTDE. First descriptor denoted with PR is calculated as arithmetic mean of the participation ratios of hole and electron, i.e. number of fragments on which they are delocalized. Second descriptor denoted with CT is describing charge transfer character of the excited state, with the range of values from zero (locally excited state) to one (completely charge separated state (CS)). PR and CT descriptors are useful for distinction between localized, excimer and charge separation transitions in our case. In addition, we used another descriptor denoted with CT_{nt} which represents amount of charge transferred between the defined fragments. Detailed derivation of used descriptors from the 1eTDM could be found elsewhere [63]. Fragmentation of the system is important for this type of analysis and it is described in the section *The Excited States Densities of Transitions*.

3. Results and discussion

3.1. GPDI organization on graphene

In order to estimate quality of our DFTB structural and energy calculations firstly we optimized GPDI molecule on graphene using orthogonal super-cell that is large enough (34.64 Å × 34.28 Å × 30.00 Å), such that GPDI molecules' replicas could not interact with each other. Afterwards we refined the DFTB structures of GPDI on graphene at PBE/DZP+PP level of theory. We found excellent agreement for the adsorption energy. PBE adsorption energy is 10.147 eV (19.5 meV/atom) while DFTB value is 10.044 eV (19.3 meV/atom). Therefore, the computationally feasible DFTB method still gives us valuable structural and energetic data concerning these large supramolecular assemblies which has been so far treated only with molecular mechanics models on this scale [26].

To examine the orientation of GPDI interaction with graphene we calculated the adsorption energy of GPDI on graphene with respect to the orientation angle and average GPDI-graphene separation (see figure 1).

In total 2400 SP energy calculations were done to explore configurational space by varying the orientation angle in steps of 3° and GPDI-graphene separation in steps of 0.1 Å. The GDPI adsorption interaction with the graphene surface is nearly isoenergetic with respect to the defined orientation angle coordinate. Therefore, there is no preferential angle for GPDI adsorption on graphene. Beside SP calculations, we also performed optimization for different starting GPDI conformations on graphene which introduced multiple minima on the potential energy surface. Adsorption energies for these structures are compiled in the table 2.

Adsorption energies for the optimized structures do not differ much from the SP calculated energies, which indicates that deformation energy of the graphene layer and GPDI molecule due to their mutual interaction is small, amounting to 0.13 meV/atom and 1.14 meV/atom, respectively. The energy released upon GPDI deposition on graphene is sufficient to compensate the deformation penalty. Adsorption energies for optimized structures span in energy range from −18.1 to −19.3 meV/atom. Similar to the case of SP calculations, there is not a preferential orientational angle for adsorption while average separation of GPDI and graphene amounts to 3.08 Å. All attempts to find possible stable side-adsorbed structures (sideways adsorption) failed, since geometry optimization always reorients the GPDI molecule to be parallel to the graphene sheet. Several SP calculations imply that side-adsorption energy amounts to around -4 meV/atom, which is significantly smaller than adsorption energy of parallel conformations.

Various almost isoenergetic GPDI conformations on graphene allows different starting grounds to build up G-ribbons. In the following paragraph we investigate stability and organization of two types of G-ribbons and G_2PDI based HOF structures in mono- and multilayer organizations.

Free-standing guanine-based ribbons have been previously studied in detail [1, 3, 4, 6, 9, 67–71]. Since hydrogen

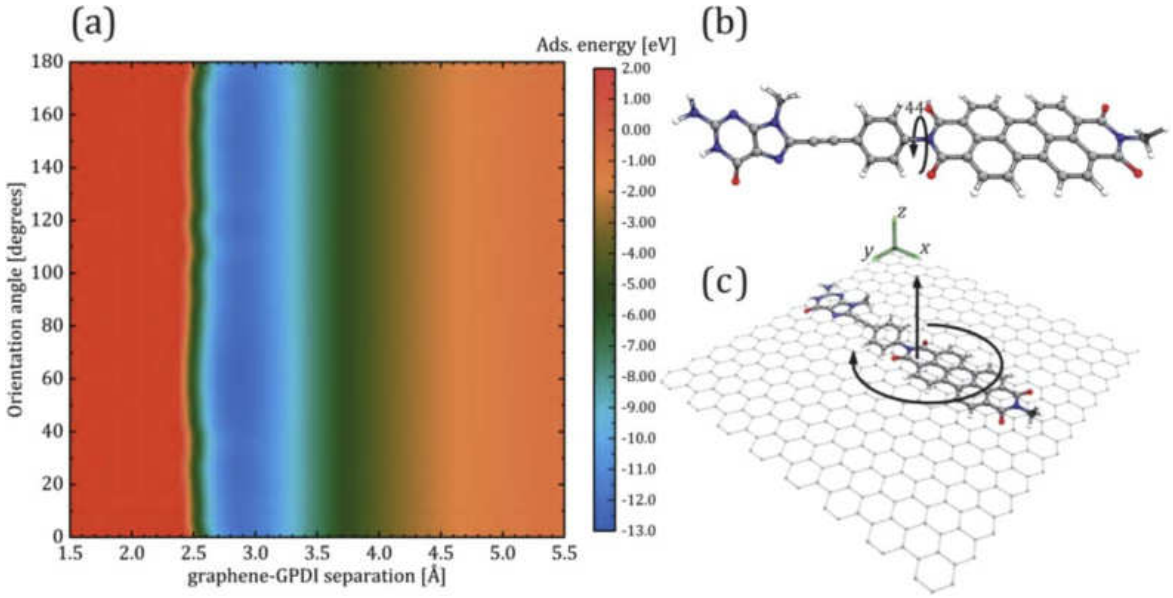

Figure 1. (a) Adsorption energy for single GPDI molecule on the graphene monolayer. (b) GPDI structure optimized at the DFTB3-D3H5/3ob level of theory. Torsion angle between arene and PDI moiety is indicated. (c) Structure of the single GPDI molecule adsorbed on the graphene monolayer. Arrows depicts two coordinates used for molecule positioning on the graphene: orientation angle—angle between longest intramolecular rotational axis and *x*-axis. Graphene—GPDI separation—all atom average separation of GPDI molecule from the graphene at DFTB3-D3H5/3ob level of theory.

Table 2. Adsorption energies for the optimized GPDI structures on the graphene. GPDI molecule positions are characterized with graphene-GPDI separation and orientation angle (see figure 1 for the coordinates definition).

Graphene-GPDI separation [Å]	Orientation angle [degrees]	Adsorption energy [meV/atom]	Graphene—GPDI separation [Å]	Orientation angle [degrees]	Adsorption energy [meV/atom]
3.00	−1.0	−19.3	3.08	100.7	−18.7
3.08	9.0	−18.8	3.08	110.5	−19.1
3.07	20.0	−18.5	3.08	118.3	−19.3
3.09	24.3	−18.6	3.11	123.3	−19.2
3.09	50.6	−18.6	3.06	153.4	−18.9
3.12	60.4	−18.1	3.08	161.8	−18.7
3.09	68.6	−18.7	3.08	169.3	−18.4
3.09	80.2	−19.0	3.05	177.2	−19.1
3.07	89.6	−18.8			

bonds between neighboring guanine molecules are responsible for stability of ribbons, only two ribbon configurations are possible. Following the same spatial reasoning and considering positions of H-bond accepting O6 and N3 and H-bond donating N1 and N2 atoms of guanine moiety (for atom numbering see figure 2), we determine only two possibilities for arranging of GPDI into ribbons on a graphene sheet. The same H-bonding pattern as in type B ribbon of the [12] is employed in GPDI-based ribbon, which we denoted here as type I ribbon. In contrast, H-bonding pattern of type A ribbon of the [12] cannot be realized for GPDI ribbons, since the PDI decoration of guanine at C8 position would encounter steric hindrance between neighboring ribbon units. Same hindrance problem is encountered when considering type III ribbon of the [4]. However, we derived another possible GPDI ribbon geometry from the type I ribbon by rotating one of the GPDI units by 180° around its longest intramolecular axis and than rotating it again by 90° perpendicular to the longest intramolecular axis. We denoted this ribbon as type II ribbon. Both studied ribbon types are presented in the figure 2. To best of our effort we recognized only these two ribbon types.

For both ribbons type, we identified four hydrogen bonds in which guanine moieties participate—two on each non Watson–Crick side of the guanine. For type I ribbon we identified two pairs of two opposite N2–H2⋯N3 and N1–H1⋯O6 H-bonds where N1–H1⋯O6 are slightly shorter (see figure 2). Single type of H-bond is found on each of the non Watson–Crick side of the guanine. For type II ribbon we also identified two types of H-bond, N2–H2⋯O6 and N1–H1⋯N3. In this case both H-bond types are found on both non Watson–Crick sides of guanine also in the opposite arrangement. Type II ribbons have more pronounced geometrical differences in H-bonding pattern between guanines

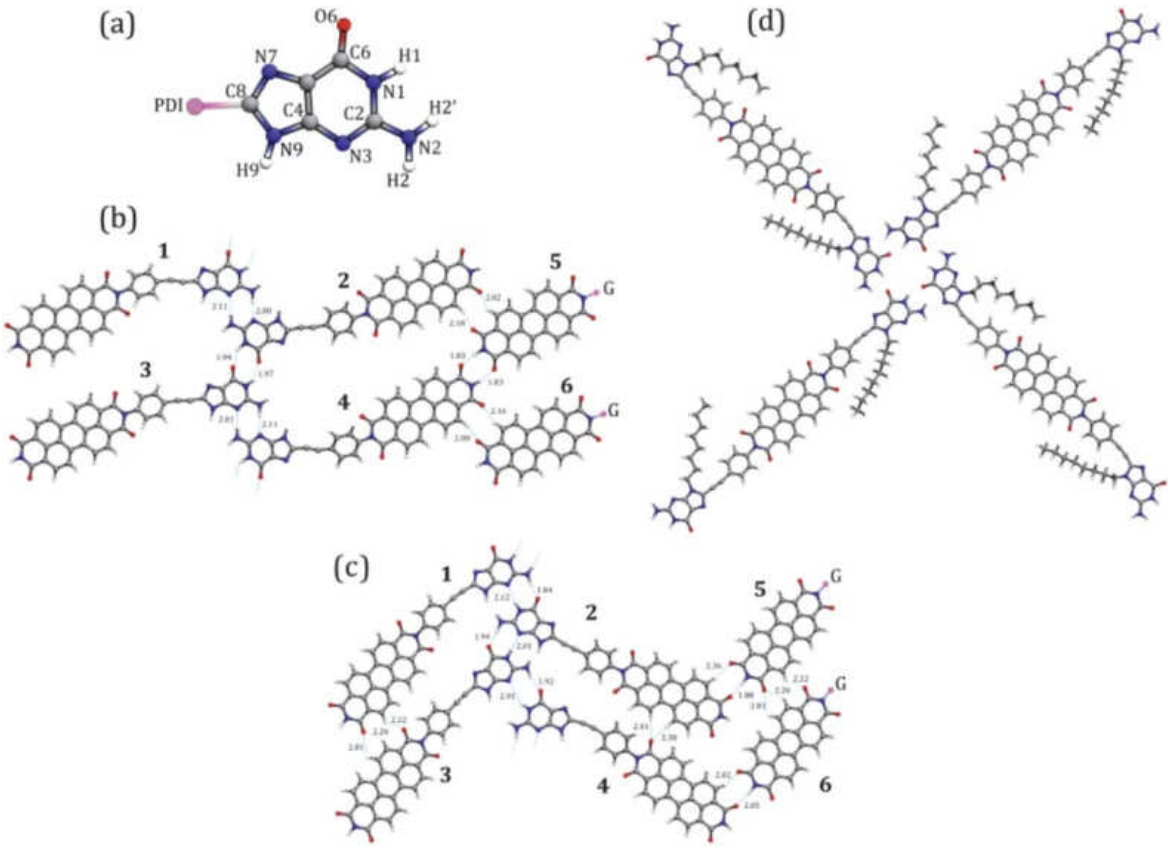

Figure 2. (a) Guanine molecule with its atoms numbering. (b) type I ribbon, (c) type II ribbon and (d) HOF structures. GPDI molecule numbering is indicated with numbers from 1 to 5. PDI moieties on the right-hand side of the ribbons present part of the periodic replicas to illustrate H-bonding between PDI moieties. Blue dotted lines represent H-bonds with their lengths indicated in Å units. Pink atoms show places where rest of the molecule is bound to. Graphene layer underneath structures is excluded due to clarity.

compared to type I ribbons. This is probably due PDI–PDI moieties interactions, i.e. geometrical arrangement of the GPDI units. When analyzing contacts between PDI moieties, i.e. ribbons periodic replicas we find that they establish H-bonds via imide functional groups. Two imide groups are present, front and terminal, i.e. closer and further from the arene moiety linker, respectively. Imide groups oxygen atoms are H-bond acceptor in this case interacting with hydrogens bound to nitrogen and carbon atoms of the PDI. This yields two types of hydrogen bonds: N–H···O and C–H···O. In case of the type I ribbon PDI moieties interact only via terminal imide group forming in total four hydrogen bonds per PDI—two N–H···O and two C–H···O in the opposite directions. Somewhat more complex situation is found for the type II ribbon where front imide group participate in the H-bonding as well. Different geometrical arrangement of the GPDI molecules allow that front imide group oxygens' now interact with neighboring PDI's side C–H groups and form one bifurcated H-bond. As it will be qualitatively described later with EDA analysis, these H-bonds are not strong as ones established between guanines, but their contribution in the total stability of the ribbon cannot be neglected.

To gain a deeper insight into the multilayer GPDI ribbons formation on graphene we analyze the binding energy in figure 3. The binding energy is calculated as difference of the energies of optimized periodical supramolecular assembly and separately optimized geometries of GPDI and graphene under the same periodic conditions. The binding energies without graphene are calculated as a difference of the SP energy of the adsorbed GPDI geometries and separately optimized geometries of GPDI. Ratio of following energies indicates the formation mechanisms of investigated systems: *formation of ribbon in plane parallel to graphene, vertical stacking of molecules, and their interaction with graphene*. GPDI-graphene interaction has a crucial role in the initial steps of ribbon formation. In the formation of type I ribbon the binding energy is lowered by 32 meV/atom when second GPDI is added to initial molecule placed on graphene, whereas the energy is nearly constant when graphene is absent. Addition of second pair of GPDI molecules in the ribbon lowers the energy by about 5 meV/atom. Two pairs of GPDI in the type II arrangement has even larger energy difference of 59 meV/atom when graphene is or is not present. This can be attributed to the local polar nature of the type II ribbon, which will be better understood later in text after the EDA analysis. Introduction of the second layer in the stack significantly stabilizes the system by around 12–18 meV/atom (for type I ribbon, depending on stacking dislocations and mutual layers orientation) and about 23 meV/atom (for type II ribbon, the range of energies is smaller for this ribbon type). We analyzed three types of stacking geometries as illustrated in figures 3(a) and (b): face-to-back (F2B), and two

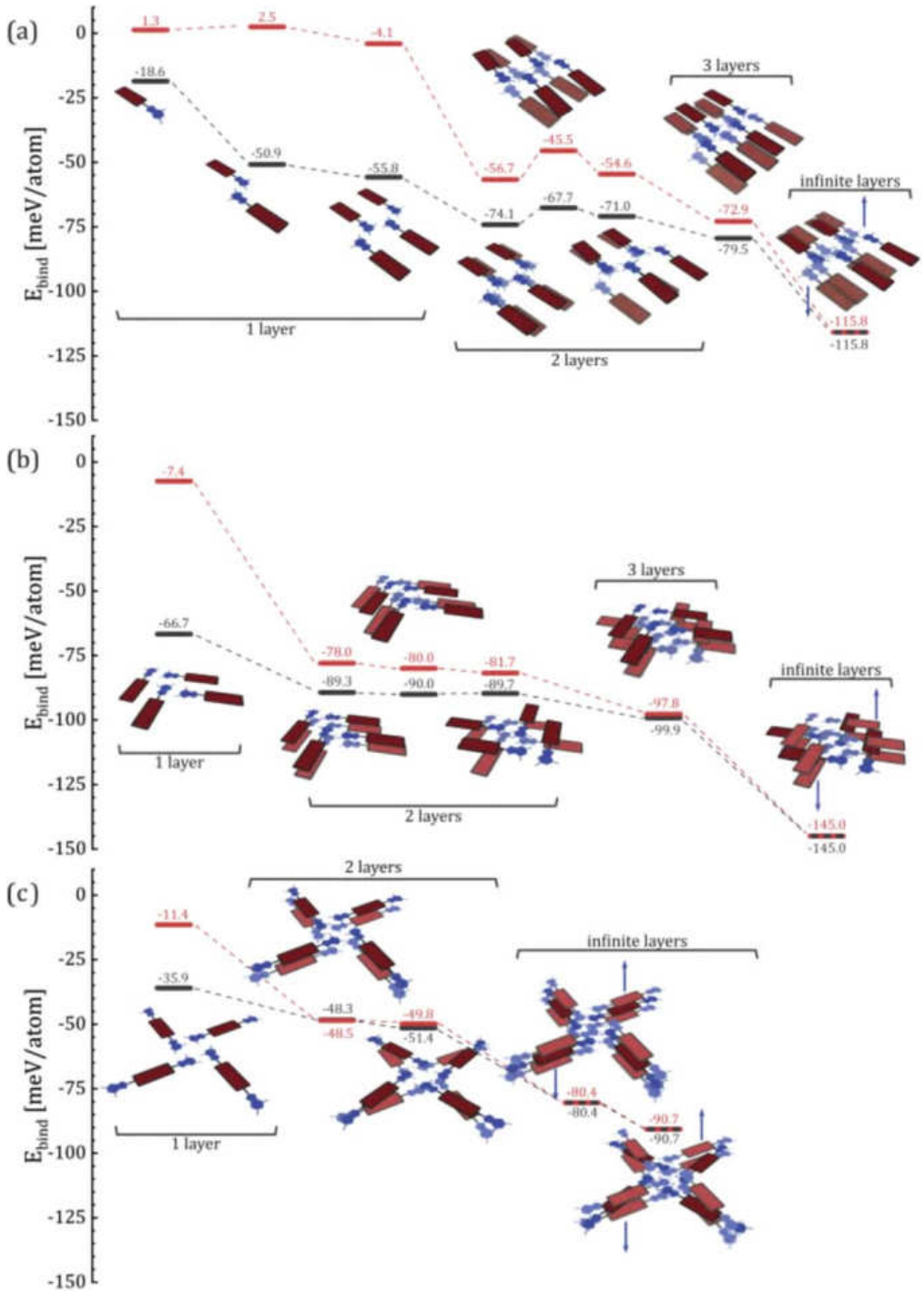

Figure 3. Stability and organization of GPDI and HOF structures on graphene. Binding energy for the system with and without graphene is shown respectively in black and red colors, respectively for type I (panel (a)), type II (panel (b)) ribbons and HOFs (panel (c)). Progressing from left to right are shown structures and binding energies for monolayer, bilayer, trilayer and infinitely thick structures (GPDI/HOF stacks). For each thickness systems the energy and geometries for one, two and more GPDI molecules in ribbon assemblies are presented. Shades of brown rectangles illustrate the PDI moiety in different levels of stacked ribbons. Graphene layer underneath ribbons and HOF structures is omitted for clarity.

face-to-face (F2F) configurations. F2B geometries were derived by adding one ribbon on the top of the another in the same arrangement. One type of the F2F geometries is constructed by rotating upper ribbon layer by 180° with the respect to the central guanine units (i.e. H-bonds directions) whereas subsequent rotation perpendicular to the central guanine units yielded another F2F arrangement. All multilayered ribbon types showed tendency towards interlayer slippage with respect of the directions of guanine-guanine H-bonds. Interlayer slippage between ribbons occures in order to minimize steric hindrance between arene linker moieties (see figure 1(b)). The antiparallel electric dipoles

Table 3. EDA for type I and type II ribbons. See figure 2 for fragments (GPDI molecules) layout. All energies are given in kcal mol^{-1}.

Type I ribbon								
	1–2	**2–3**	**2–4**	**1–3**	**2–5**	**4–6**	**2–6**	**4–5**
ΔE_{tot}	−12.7	−14.7	−1.2	−1.2	−6.3	−5.9	0.0	−14.0
ΔE_{ele}	−15.9	−22.6	−0.5	−0.4	−10.0	−9.6	0.0	−21.7
ΔE_{ex}	−3.7	−5.2	0.1	0.1	−1.8	−1.8	0.0	−5.5
ΔE_{rep}	27.6	34.6	0.0	0.0	19.5	18.8	0.0	37.1
ΔE_{pol}	−10.4	−10.9	−0.2	−0.2	−4.7	−4.6	0.0	−13.0
ΔE_{disp}	−10.3	−10.5	−0.6	−0.6	−9.2	−8.7	0.0	−10.9
Type II ribbon								
	1–2	**2–3**	**2–4**	**1–3**	**2–5**	**4–6**	**2–6**	**4–5**
ΔE_{tot}	−16.7	−18.0	−11.0	−8.8	−9.2	−8.8	−0.5	0.0
ΔE_{ele}	−18.6	−22.2	−7.1	−8.1	−11.0	−12.3	0.5	0.0
ΔE_{ex}	−4.0	−4.8	1.2	−0.2	−1.5	−2.2	0.3	0.0
ΔE_{rep}	31.8	38.0	15.8	19.7	16.9	20.4	0.1	0.0
ΔE_{pol}	−13.7	−14.5	−4.8	−5.1	−5.8	−6.0	−0.4	0.0
ΔE_{disp}	−12.3	−14.4	−16.0	−15.0	−7.9	−8.7	−1.1	0.0

(antiferroelectric-like) in the bilayer stack of the polar type II ribbons is more stable than the parallel orientation by around 4 meV/atom due to the dipole–dipole interaction. Initial stacking from mono to bilayer ribbon (when it is still small containing two pairs of GPDI molecules) has a significantly larger energy change for free-standing ribbons than in the case of the stack growth on graphene. As well, the initial stabilization due to vertical growth is more energy remarkable than the in-plane development of the ribbons. Importantly, these differences rapidly decay already with triplelayer. The effect of graphene-GPDI interaction is crucial at the initial stage of structural growth, while the interaction is becoming irrelevant for thick stacks. Energy difference between infinitely thick stack and a monolayer is 60 meV/atom and 78 meV/atom for type I and type II ribbons, respectively. Importantly, these binding energies have type I/II monolayer ribbons that contain 30/32 GPDI molecules (equivalent 15/32 unit cells) in one layer, which can be estimated from energy decrease of 5 meV/atom with in-plane growth of ribbon by a pair of GPDI molecules (one unit cell). Considering that energy difference in stacking process is relatively large in mono- to bi-layer ribbon of graphene transition (around 18 meV/atom for type I ribbon and 23 meV/atom for type II ribbon) very short ribbons with only 10 GPDI molecules in a monolayer (5 unit cell) are more energy favorable than bilayer ribbons. Therefore, in-plane growth is more likely than stacking and consequently very thin films of GPDI molecules covering large surface areas of graphene are expected, as indicated by the sample energy difference analysis. We also calculated binding energy of reported hydrogen bonded organic frameworks based on GPDI molecules (figure 3(c)) reported in the literature [26, 27]. Due to large systems it was not feasible to calculate energies of their in-plane growth, but only a columnar phase. Similarly to ribbons, the energy difference of free-standing HOFs and HOFs on graphene rapidly decreases by stacking thickness, reaching zero already for a bilayer HOF. Here, we also investigated F2B and F2F arrangements of HOFs. The energy loss in mono- to bi-layer transition of HOF on graphene is only about 13 meV/atom. If we assume that in-plane growth decreases energy close to that value of ribbons (a reasonable assumption since similar types of H-bonds are also responsible for growth of HOFs) then in-plane growth on graphene is also a more preferable than stacking.

It has been experimentally demonstrated that alkylated guanosine derivates can form supramolecular nanoribbons on the solid(HOPG)-solution interface [72]. Role of the solvent and solubilizing alkyl or glycol tails is important in order to effectively furnish these kinds of supramolecular architectures. However, we do not tackle this issue as it would dramatically increase number of atoms in the system and consequently the computational time. Yet, due to the very flexible nature of studied molecules and ribbons and their high mobility when deposited on graphene there can be sufficient space for long alkyl or glycol solubilizing tails with whom GPDI can be functionalized at different positions. Therefore, solubility of GPDI in different organic solvents would be ensured. Assuming a fine balance between solubility and the molecular association on the graphene and according to results from this section (similar binding energies for single-layered ribbons and HOFs with four units, i.e. 55.8 and 35.9 meV/atom, respectively) it is very likely that ribbon-like in-plane organization of GPDI molecules would indeed occur.

3.2. Energy decomposition analysis

In order to gain a deeper insight into guanine-guanine and PDI–PDI moieties interactions, i.e. driving force for GPDI ribbons assemblies, we performed EDA by decomposing total interaction energy (ΔE_{tot}) between GPDI molecules into electrostatic (ΔE_{ele}), exchange (ΔE_{ex}), repulsion (ΔE_{rep}),

polarization (ΔE_{pol}) and dispersion (ΔE_{disp}) energy terms EDA results for type I and type II ribbons are compiled in the table 3. H-bonding patterns for type I and type II ribbons are previously discussed in the text and here we present its energetic aspects.

Most stabilizing interaction for type I ribbon is found between GPDI molecules 2 and 3 (see figure 2 for molecule numbering). Molecules 2 and 3 are glued through guanine moieties with two N1–H1⋯O6 H-bonds in the opposite direction with similar bond lengths of 1.94 and 1.97 Å. Main and only destabilizing term for interaction(s) between these two (any other) molecules is ΔE_{rep} amounting to 34.6 kcal mol^{-1}. This contribution is easily overcomed by all other stabilizing interactions and mainly with ΔE_{ele} (-22.6 kcal mol^{-1}) whereas ΔE_{pol} and ΔE_{disp} terms are of equal importance and amount to -10.9 kcal mol^{-1} and -10.5 kcal mol^{-1}, respectively. The relatively large ΔE_{pol} indicate significant change in the orbital shape and partially covalent character of this H-bond which is expected since O6 of guanine moiety is strong H-bond acceptor. Second strongest interaction for type I ribbon is found between PDI moieties, i.e. molecules 4 and 5. This interaction has almost the same stabilizing effect as H-bonding between molecules 2 and 3. This is expected since same type and number of the H-bonds mediate this interaction, particularly two N-H⋯O with the opposite direction. However, their bond length of 1.83 Å is shorter than those of N1–H1⋯O6 of guanine moieties (1.94 and 1.97 Å) but with less favorable angle between H-bond donor and acceptor–143 and 168°, respectively. Third strongest intermolecular interaction is found between molecules 1 and 2. This interaction is mediated through two N2–H2⋯N3 H-bonds arranged in the opposite direction and its total interaction amounts to -12.7 kcal mol^{-1}. This is somewhat weaker interaction when compared to the total interaction between molecules 2 and 3 or 4 and 5. Weaker affinity of N3 as H-bond acceptor compared to O6 of guanine moiety is responsible for this effect. Non-negligible interactions are also found between molecules 2–5 and 4–6, i.e. neighboring PDI moieties. Total interaction between these molecules amount to -6.3 and -5.9 kcal mol^{-1}, respectively. Similar interplay of the energy terms is found for 2–5 and 4–6 as for the strongest ones except for ΔE_{disp} which now plays even more important role and it amounts to -9.2 and -8.7 kcal mol^{-1}.

More diverse contacts between GPDIs are found for type II ribbon. Strongest interactions are again found between guanine moieties, i.e. molecules 1–2 and 2–3 and ΔE_{tot} for them amount to -16.7 and -18.0 kcal mol^{-1}, respectively. Two H-bonds in the opposite direction are stabilizing guanine moieties—N2–H2⋯N3 and N1–H1⋯O6. Increased stabilization compared to the type I ribbon originate from the favorable locale dipole arrangement of the guanine moieties. Another distinguishable feature for type II ribbons is non-negligible interactions between molecules 1–3 and 2–4 that amounts to -8.8 and -11.0 kcal mol^{-1}. Bifurcated H-bonds are responsible for stabilization between these molecules with pronounced ΔE_{disp} term. PDI–PDI interaction between neighboring molecules (2–5 and 4–6) is also noticeable (-9.2 and -8.8 kcal mol^{-1}) for type II ribbons.

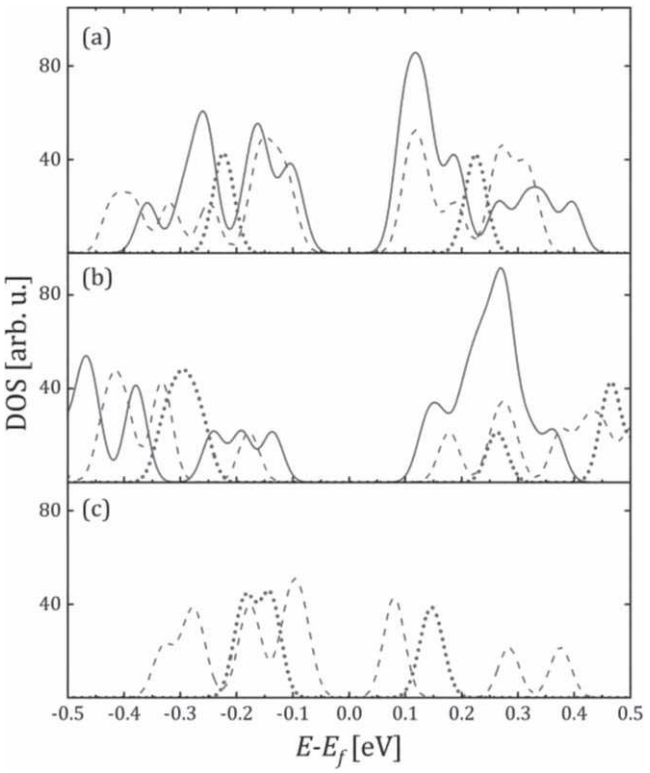

Figure 4. Density of states (DOS) for (a) type I ribbon, (b) type II ribbon and (c) HOF systems. Dotted, dashed and solid lines correspond to the one-, two- and three-layered structures' DOS. Gaussian broadening function is used with broadening parameter set to 0.025 eV.

Overall higher stability (lower binding energy, see figure 3 and accompanying text) of the type II ribbon compared to the type I ribbon is attributed to additional favorable dispersion driven contacts between PDI moieties and dipole enhanced H-bonding within guanine moieties.

Many-body effects are not investigated within this EDA scheme. ΔE_{ele} and ΔE_{ex} terms are pairwise additive, while ΔE_{pol}, ΔE_{rep} and ΔE_{disp} are not and all many-body effects in non-covalenty glued systems like this should originate from the polarization energy [53]. One can also inspect to which extent H-bonding cooperativity is increasing stabilization in these systems since H-bonding cooperativity is a fingerprint property of self-assembled free standing G-quartets and G-ribbons on the surfaces [4] and it is beyond the scope of this paper.

3.3. Electronic DOS

In section 3.1. we showed that in-plane parallel to graphene growth is more likely to occur than the vertical stacking of the molecules. To investigate electronic properties of the proposed structures we calculated DOS for the most stable one-, two- and three-layered ribbon structures as well as for one- and two-layered HOF structures (see figure 3). DOS profiles are calculated with DFTB3-D3/3ob method, i.e. using the same level of theory as for the single-point energy calculations in the section 3.1. DOS diagrams in the vicinity of the

HOMO-LUMO gaps are presented in the figure 4. Complete DOS profiles are reported in the SI.

DOS for all studied structures exhibit characteristic molecular DOS profiles. Type I and type II ribbons' DOS profiles are very similar in the vicinity of the HOMO and LUMO energies. Addition of second layer to these systems leads to broadening of the DOS profile and consequently a reduction of the HOMO-LUMO gap from 0.44 to 0.22 eV and from 0.53 to 0.36 eV for type I and type II ribbons, respectively. On the other hand, adding the third layer does not dramatically influence DOS profiles for the ribbons. Somewhat more pronounced influence of the third layer is observed for type II ribbon due to the antiparallel orientation of the electric dipoles in the three-layered stack. This additional layer slightly reduces the HOMO-LUMO gap for both systems by 0.03 and 0.08 eV for type I and type II ribbons, respectivelly. HOF system's DOS profile initially have smaller HOMO-LUMO separation (0.28 eV) compared to those of ribbons. Addition of a second layer to the HOF structure also reduces the HOMO-LUMO gap by 0.12 eV, i.e. from 0.28 to 0.16 eV. Although, GPDI and G_2PDI molecules that build ribbons and HOF structures, respectively, are not equivalent, their DOS profiles and the HOMO-LUMO separations are found to be similar. This indicates similar electronic properties of these supramolecular architectures.

3.4. The excited states densities of transitions

Faith of rylene dye covalently decorated G-quadruplex long-lived CS states' lifetimes and quantum yields is highly affected via spatial and orbital overlap between stacked dye units, i.e. its structural properties [23, 25, 26]. Solvent polarity plays minor to almost no role in the CS states dynamics due to shielding of aromatic GTDI quadruplex core with aliphatic shell [25] which again can be considered as a structural constraint. Results in the following section are gas phase results. Including implicit solvent model in the calculations would probably lead to the stabilization of the CS states. More polar solvents would lead to the greater stabilization of the CS states than the less polar ones. On the other hand, solvents with a strong H-bond accepting properties could lead to disruption of self-assemblies, like in the case of pyridine and GTDI assemblies. [25] However, we expect this effect to be similar for all of the studied structures and therefore does not affect conclusions withdrawn from the gas phase results.

Structural similarities to those of G-quadruplex based organic frameworks and columnar supramolecular architectures are encountered in multilayered G-ribbons studied here. High-degree of π stacking between PDIs in multilayered G-ribbons could imprint similar CS states properties to those of HOFs and columnar G-quadruplex based donor-acceptor systems. Accurate computational study of the exciton formation, evolution and decay for large molecules' systems such GPDI quadruplexes and ribbons is not yet feasible. Therefore, we are only limited to study excited states' properties in the Frank–Condone region and compare it to their HOFs counterparts.

Types of excitations encountered in the multilayered GPDI ribbons and GPDI based HOFs are presented in the figure 5. In order to distinguish between localized, excimer and CS states we divided system into the fragments in the way that each PDI moiety and each guanine together with arene linker build one fragment. Descriptors obtained within this fragmentation scheme are denoted with CT_1 and PR_1. Thresholds for descriptors are chosen somewhat arbitrary. In that sense excitations with $CT_1 < 0.2$ are considered to be localized, while $CT_1 > 0.8$ are considered as pure CS states. If CT values are between these two threshold values ($0.2 < CT_1 < 0.8$) excimer character is attributed to the given excited state. Furthermore, considering PR_1 descriptor value to be lower or greater than 1.25 we could distinguish between PDI localized and PDI excitonic states, respectively. $PR_1 > 1.25$ means that $1/4$ of the total electron density is delocalized over more than one fragment in the system. Inspection of the natural transition orbitals (NTOs) suggests that only PDIs are involved in the localized transitions within this energy window. Combination of $0.2 < CT_1 < 0.8$ and $PR_1 > 1.25$ characterizes excimer states. States with $0.2 < CT_1 < 0.8$ and $PR_1 < 1.25$ are not encountered in none of these systems. To further distinguish between different types of excimer and CS states different fragmentation of the system is required. CT_4 descriptor is obtained when system is described with two fragments only, one consisting of all PDI moieties and another of all guanine moieties in the system. PDI and G-PDI excimer states are then sorted with $CT_4 < 0.2$ and $0.2 < CT_4 < 0.8$ conditions, respectively. Various types of CS states are also identified and could be divided into two groups, i.e. $G^{\bullet+}$- $PDI^{\bullet-}$ and $PDI^{\bullet+}$-$PDI^{\bullet-}$ CS states which are previously experimentaly identified [22, 30]. Another two fragmentation schemes are required to classify them in more detailed fashion. CT_2 descriptor is acquired when single GPDI/G_2PDI molecule is considered as a separate fragment while CT_3 descriptor is obtained when whole ribbon/HOF layer consisting of four molecules is considered as a fragment. CT_2 would suggest if CS state is monomolecular (occurring withing single GPDI/G_2PDI molecule) while CT_3 would describe inter or intralayer CS. Different combinations of CT_1, CT_2, CT_3 and CT_4 as presented on the figure 5 helps us identify CS $G^{\bullet+}$-$PDI^{\bullet-}$ monomolecular, CS $G^{\bullet+}$-$PDI^{\bullet-}$ intralayer, CS $G^{\bullet+}$-$PDI^{\bullet-}$ interlayer, CS $PDI^{\bullet+}$-$PDI^{\bullet-}$ intralayer and CS $PDI^{\bullet+}$-$PDI^{\bullet-}$ interlayer states. All of the CS states can be considered as almost pure ion-pair excited states since they exhibit high CT_{nt} descriptor value ranging from 0.90 for $G^{\bullet+}$-$PDI^{\bullet-}$ monomolecular CS state to 0.95 for inter- and intralayer CS states in all systems. Localized and CS states involving guanine moieties only are not found within this energy window nor PDI localized states due to high overlap of PDI moieties which favours PDI exciton formation.

Absorption profiles, DOT and its decompositions are given in the figure 6. Absorption spectra (figure 6(a)) of type I ribbon has one pronounced peak located at 2.65 eV originating from transition to the bright PDI excimeric states. Two shoulders to this peak are encountered on the high and low energy part of the spectrum arising from PDI excimeric and

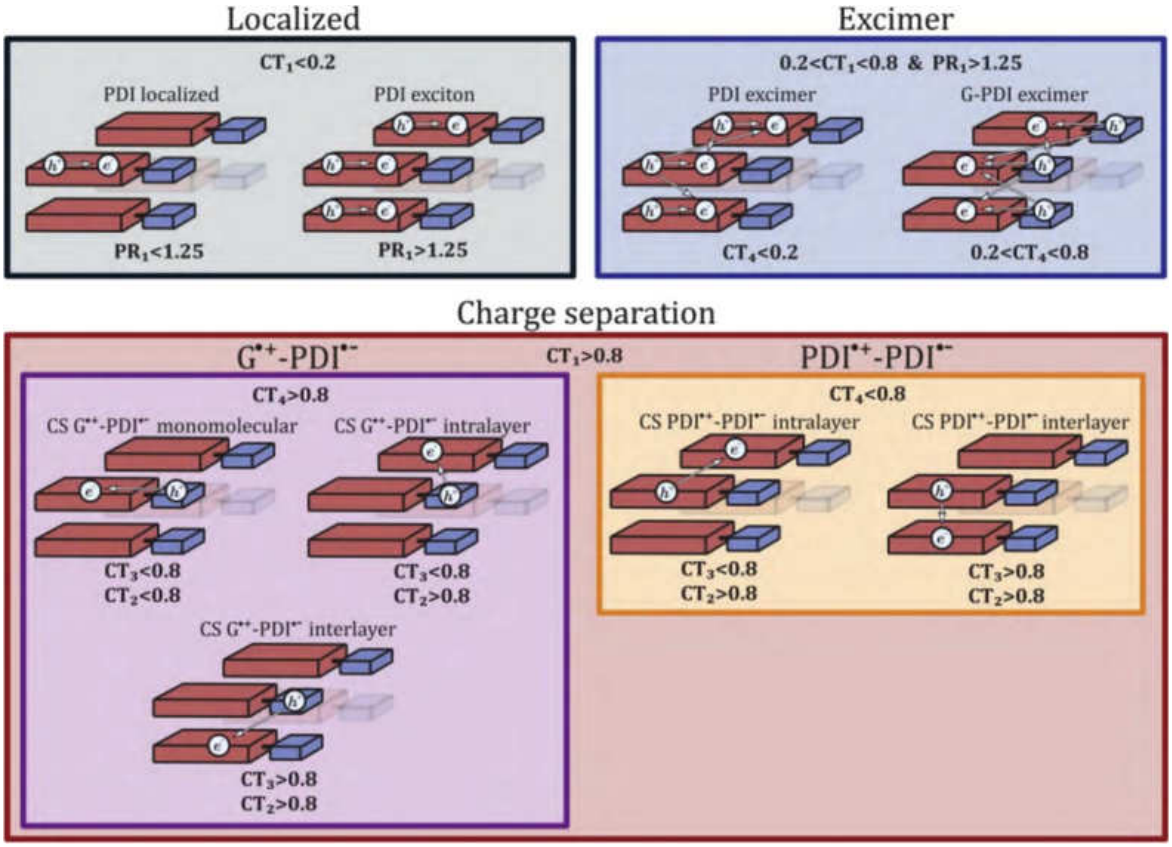

Figure 5. Schematic representation of types of the excited states in multilayered GPDI ribbons. Red and blue rectangular cuboids represent PDI and guanine moieties, respectively. Thresholds for descriptors (PR and CT) are given. h^+ and e^- depicts electron-hole and excited-electron, respectively. Note that same types of excitations are present within HOF absorption profile.

localized PDI excitonic transitions, respectively. Negligible contribution of CS states to the absorption is also observed. Distinctive red tail absorption feature at 2.08 eV for type I is found and attributed to populating four closely lying PDI excimer states. Absorption profile of type II ribbon also has pronounced peak at 2.65 eV. However, in this case localized transitions are not contributing to the absorption spectra but at higher energies (peak at around 2.98 eV) there is non-negligible absorption attributed to the CS $G^{\bullet+}$-$PDI^{\bullet-}$. Two shoulders to the main absorption peak coincide to those of HOF structure making type II ribbon more alike HOFs absorption profile than type I ribbon. Electronic absorption for optimized two layered HOF is found in the almost same energy range (2.15–3.10 eV) as for type I and type II ribbons 2.00–3.15 eV and 2.15–3.15 eV, respectively. However, HOF absorption profile is characterized with two distinct peaks located at 2.42 and 2.82 eV, both originating from the electron promotion to the mixture of PDI and G-PDI excimer states. We also observed that peak located at 2.82 eV has considerable participation of the CS $G^{\bullet+}$-$PDI^{\bullet-}$ which suggest that these CS states could be populated directly upon photon absorption. Same characteristic garnish type II ribbon absorption but in this case different type of CS $G^{\bullet+}$-$PDI^{\bullet-}$ are enrolled. The band gap between the frontier molecular orbitals (HOMO and LUMO) is determined for all three systems (see section 3.3.). It is clear that these energies do not correlate with any of the corresponding absorption maximum energies since the HOMO → LUMO transition is not represented in any of these absorption bands. For example, two most dominant contributions to the absorption band for the type I ribbon located at 2.65 eV are: HOMO-11 → LUMO+4 and HOMO-12 → LUMO+2.

Compared to absorption profiles, DOT profiles appear in the wider energy range, especially for the ribbon arrangements. When analyzing global DOT composition (figure 6(b)) we notice that amount of CS $G^{\bullet+}$-$PDI^{\bullet-}$ states are similar between all the systems and equal for type I ribbon and HOF arrangement (65.6%). Although CS $G^{\bullet+}$-$PDI^{\bullet-}$ states appear in the similar energy range with ribbons' CS contribution blueshifted by around 0.3 eV, their distribution across DOT is not equal. Low energy part of the DOT for type I ribbons lacks of CS $G^{\bullet+}$-$PDI^{\bullet-}$ states but they are supplant by other type CS $PDI^{\bullet+}$-$PDI^{\bullet-}$ states, i.e. 15.6% compared to 4.7% in HOF structure. This is not the case for type II ribbon where CS content is high for for both types of CS excited states, 54.7% and 20.3% for CS $G^{\bullet+}$-$PDI^{\bullet-}$ and CS $PDI^{\bullet+}$-$PDI^{\bullet-}$, respectively. Another interesting feature is greater presence of localized transitions for type I ribbon (7.9%) compared to type II and HOF (1.6%) structures. On the other hand, HOF structure has highest participation of excimeric states, 28.1% compared to 10.9% and 23.4% for ribbons. Most of these excited state characteristics can be explained by different spatial organization of HOF and ribbon structures. Greater $\pi\pi$ overlap between both PDI and guanine moieties in HOF

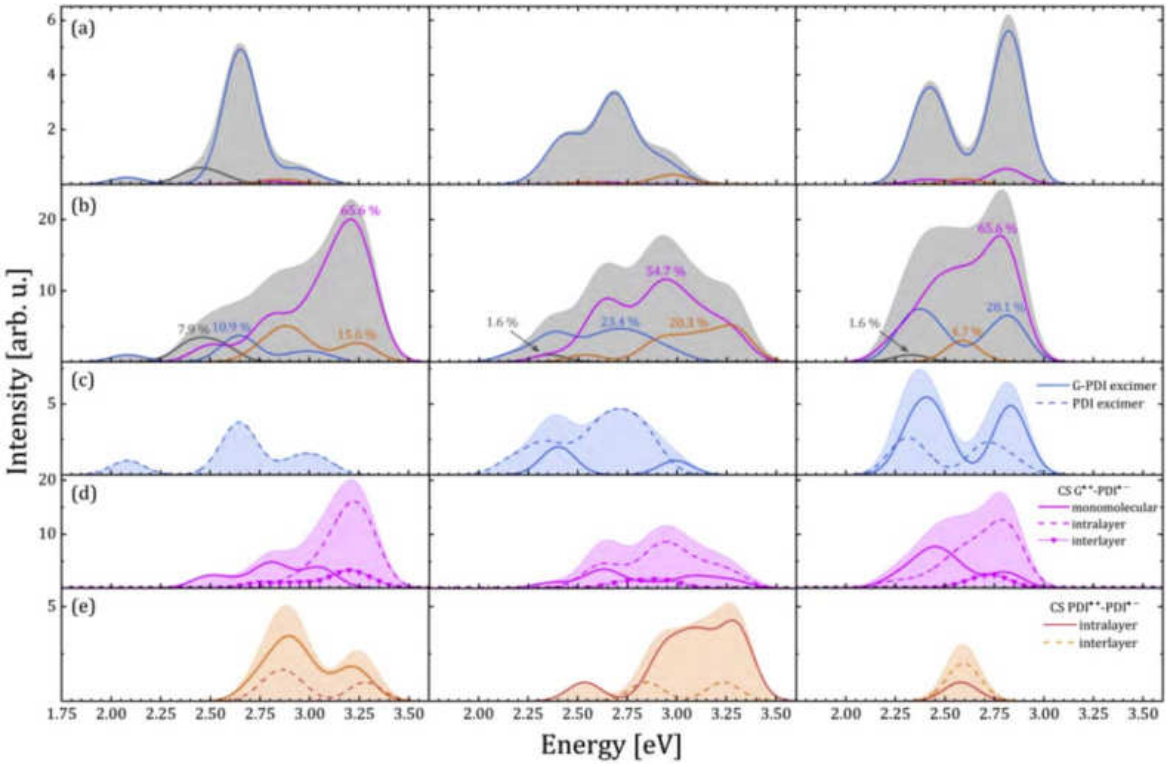

Figure 6. Decomposition of (a) absorption spectrum (shaded area) and (b) density of transitions (DOT) (shaded area) into the localized (black lines), excimeric (blue lines), CS $G^{\bullet+}$-$PDI^{\bullet-}$ (magenta) and CS $PDI^{\bullet+}$-$PDI^{\bullet-}$ (orange) excited states contributions. Percentage of each contribution in DOT is indicated. Type I ribbon absorption profile is presented on the far left, type II ribbon in the middle and HOF absorption profile on the far right panel. Panels (c), (d) and (e) represent more detailed decomposition of excimeric, CS $G^{\bullet+}$-$PDI^{\bullet-}$ and CS $PDI^{\bullet+}$-$PDI^{\bullet-}$ contributions to the DOT, respectively. For excited states types description see figure 5 and corresponding text.

structures compared to ribbons enhances electronic coupling and therefore promotes excimer formation. This can be rationalized via further decomposition of excimeric contribution to the DOT (figure 6(c)) and noticeable absence of G-PDI excimers for type I ribbons. Type II ribbon arrangement is characterized with higher overlap PDIs (comparable to those of HOF) and therefore can accommodate both G-PDI and PDI excimers just like HOF. Due to higher number of identical guanine chromophores within the HOF, G-PDI excimer participation is reasonably higher. Higher degree of chromophore $\pi\pi$ overlap also leaves different imprint to the CS $PDI^{\bullet+}$-$PDI^{\bullet-}$ states (Figure 6(e)), while relative arrangement of CS $G^{\bullet+}$-$PDI^{\bullet-}$ states (figure 6(d)) is relatively similar. Content of intralayer CS $PDI^{\bullet+}$-$PDI^{\bullet-}$ states is significantly higher for the ribbons arrangements due to proximity of adjacent PDI units. Stronger electronic interaction between adjacent PDI moieties is pronounced for type II ribbon where intralayer CS $PDI^{\bullet+}$-$PDI^{\bullet-}$ clearly dominates. This type of excitations would require more energy in the case of HOF arrangement. Relative amount and ordering of CS $G^{\bullet+}$-$PDI^{\bullet-}$ states within DOT profiles is maintained for all three systems. Monomolecular contributions are lowest in energy followed by interlayer and intralayer contributions. It is important to note that characteristics of both types of CS states could be exploited for optoelectronic applications as well as there are not huge differences between type II ribbon and HOF structures absorption and DOT profiles at Frank–Condone region. In fact, in total both types of ribbons exhibit higher amount of total CS withing this energy region compared to HOF, 81.2% and 75% compared to 70.3%, respectively. Furthermore, we believe that these differences would become even less pronounced if we used ensemble average of absorption and DOT profiles and/or model consisting of more GPDI molecules. Overall, surprising similarities of DOT composition are encountered for these systems making ribbons worthwhile for further investigation of exciton dynamics.

4. Conclusions

While HOFs based on GPDI molecules have been studied in detail for application in optoelectronics, layered ribbons made of these molecules supported on graphene have not been studied in such details yet. This is primarily due to complexity of the interfaces of flexible molecules and graphene and relatively large systems that are difficult to study with demanding *ab initio* methods. Our theoretical approach has proved as an excellent choice to overcome this obstacle. We theoretically analyzed favorable growth mechanism and structure of deposits using DFTB method and optical properties by the LR-TDDFT. We found that growth is rather homogeneous and thin few-layers ribbon structures cover large surface area of graphene. Absorption spectra and especially DOT profiles are very similar to those in HOFs in

the investigated energy window. We showed that CS $G^{\bullet+}$-$PDI^{\bullet-}$ states can be directly populated upon photo-excitation in the HOF and type II ribbon structures. Increased presence of CS $PDI^{\bullet+}$-$PDI^{\bullet-}$ states in the ribbons arrangements is encountered and this excited state feature is ascribed to the favorable geometrical organization. Existence of CS states between layers of the stacked structures promises potential application of these atomically thin graphene-GPDI heterostructures in photovoltaics and other optoelectronic devices.

Acknowledgments

The research leading to these results has been co-funded by the European Commission under the H2020 Research Infrastructures contract no. 675 121 (project VI-SEEM). Authors acknowledge the financial support by Ministry of Education, Science and Technological Development of Republic of Serbia through the institutional funding of Faculty of Physical Chemistry, University of Belgrade and Institute for Multidisciplinary Research, University of Belgrade. I.P. acknowledges the financial support of the Ministry for Education, Science and Technological development of the Republic of Serbia, contract with the Institute for Multidisciplinary Research, University of Belgrade 451-03-68/2020-14/200053. I.P. also acknowledges Qatar National Research Fund, cycle eleven, the grant number NPRP11S-1126-170033.

Data availability statement

All data that support the findings of this study are included within the article (and any supplementary files).

ORCID iDs

Branislav Milovanović https://orcid.org/0000-0001-7106-9353
Mihajlo Etinski https://orcid.org/0000-0003-0342-7045
Igor Popov https://orcid.org/0000-0002-2030-3530

References

[1] Li W, Jin J, Liu X and Wang L 2018 *Langmuir* **34** 8092–8
[2] Davis J T and Spada G P 2007 *Chem. Soc. Rev.* **36** 296–313
[3] Bald I, Wang Y G, Dong M, Rosen C B, Ravnsbæk J B, Zhuang G L, Gothelf K V, Wang J G and Besenbacher F 2011 *Small* **7** 939–49
[4] Paragi G and Fonseca Guerra C 2017 *Chem. Eur. J.* **23** 3042–50
[5] Jissy A K and Datta A 2014 *J. Phys. Chem. Lett.* **5** 154–66
[6] Livshits A I and Kantorovich L 2013 *J. Phys. Chem.* C **117** 5684–92
[7] Otero R, Schöck M, Molina L M, Lægsgaard E, Stensgaard I, Hammer B and Besenbacher F 2005 *Angew. Chem. Int. Ed.* **44** 2270–5
[8] Lena S, Masiero S, Pieraccini S and Spada G P 2009 *Chem. Eur. J.* **15** 7792–806
[9] Garah M E, Perone R C, Bonilla A S, Haar S, Campitiello M, Gutierrez R, Cuniberti G, Masiero S, Ciesielski A and Samorì P 2015 *Chem. Commun.* **51** 11677–80
[10] Saikia N, Waters K, Karna S P and Pandey R 2017 *ACS Omega* **2** 3457–66
[11] Rinaldi R, Maruccio G, Biasco A, Arima V, Cingolani R, Giorgi T, Masiero S, Spada G P and Gottarelli G 2002 *Nanotechnology* **13** 398–403
[12] Ciesielski A, El Garah M, Masiero S and Samorì P 2016 *Small* **12** 83–95
[13] Milovanović B, Stanković I M, Petković M and Etinski M 2020 *J. Phys. Chem.* A **124** 8101–11
[14] Jiang W, Li Y and Wang Z 2014 *Acc. Chem. Res.* **47** 3135–47
[15] Ostroverkhova O 2016 *Chem. Rev.* **116** 13279–412
[16] Prakash Neupane G, Ma W, Yildirim T, Tang Y, Zhang L and Lu Y 2019 *Nano Mater. Sci.* **1** 246–59
[17] Murad R, Iraqi A, Aziz A, Abdullah N S and Brza M A 2020 *Polymers* **12** 2073–4360
[18] Schmidt-Mende L, Fechtenkötter A, Müllen K, Moons E, Friend R H and MacKenzie J D 2001 *Science* **293** 1119–22
[19] Zhan X, Facchetti A, Barlow S, Marks T J, Ratner M A, Wasielewski M R and Marder S R 2011 *Adv. Mater.* **23** 268–84
[20] Huang C, Barlow S and Marder S R 2011 *J. Org. Chem.* **76** 2386–407
[21] del Prado A, González-Rodríguez D and Wu Y L 2020 *ChemistryOpen* **9** 409–30
[22] Wu Y L, Brown K E and Wasielewski M R 2013 *J. Am. Chem. Soc.* **135** 13322–5
[23] Wu Y L, Brown K E, Gardner D M, Dyar S M and Wasielewski M R 2015 *J. Am. Chem. Soc.* **137** 3981–90
[24] Powers-Riggs N E, Zuo X, Young R M and Wasielewski M R 2019 *J. Am. Chem. Soc.* **141** 17512–6
[25] Powers-Riggs N E, Zuo X, Young R M and Wasielewski M R 2020 *J. Chem. Phys.* **153** 204302
[26] Wu Y L *et al* 2017 *Nat. Chem.* **9** 466–72
[27] Wu Y L *et al* 2018 *Angew. Chem. Int. Ed.* **57** 3985–9
[28] Thazhathveetil A K, Harris M A, Young R M, Wasielewski M R and Lewis F D 2017 JACS **139** 1730–3
[29] Lech C J, Phan A T, Michel-Beyerle M E and Voityuk A A 2013 *J. Phys. Chem.* B **117** 9851–6
[30] Bartynski A N *et al* 2015 *J. Am. Chem. Soc.* **137** 5397–405
[31] Sabury S, Adams T J, Kocherga M, Kilbey S M and Walter M G 2020 *Polym. Chem.* **11** 5735–49
[32] Pieraccini S, Bonacchi S, Lena S, Masiero S, Montalti M, Zaccheroni N and Spada G P 2010 *Org. Biomol. Chem.* **8** 774–81
[33] Bou Zerdan R, Cohn P, Puodziukynaite E, Baker M B, Voisin M, Sarun C and Castellano R K 2015 *J. Org. Chem.* **80** 1828–40
[34] González-Rodríguez D, Janssen P G A, Martín-Rapún R, Cat I D, Feyter S D, Schenning A P H J and Meijer E W 2010 *J. Am. Chem. Soc.* **132** 4710–9
[35] Li F, Zhang Y, Zhou L, Zhang X and Chen Z 2018 *J. Porphyrins Phthalocyanines* **22** 944–52
[36] Liu X, Kwan I C M, Wang S and Wu G 2006 *Org. Lett.* **8** 3685–8
[37] Britnell L *et al* 2013 *Science* **340** 1311–4
[38] Wong J, Jariwala D, Tagliabue G, Tat K, Davoyan A R, Sherrott M C and Atwater H A 2017 *ACS Nano* **11** 7230–40
[39] Jariwala D, Davoyan A R, Wong J and Atwater H A 2017 *ACS Photon.* **4** 2962–70
[40] Yuan Z, Lee S L, Chen L, Li C, Mali K S, De Feyter S and Müllen K 2013 *Chem. Eur. J.* **19** 11842–6

[41] Hourahine B *et al* 2020 *J. Chem. Phys.* **152** 124101
[42] Grimme S, Antony J, Ehrlich S and Krieg H 2010 *J. Chem. Phys.* **132** 154104
[43] Grimme S, Ehrlich S and Goerigk L 2011 *J. Comput. Chem.* **32** 1456–65
[44] Gaus M, Goez A and Elstner M 2013 *J. Chem. Theory Comput.* **9** 338–54
[45] Řezáč J 2017 *J. Chem. Theory Comput.* **13** 4804–17
[46] Řezáč J and Hobza P 2012 *J. Chem. Theory Comput.* **8** 141–51
[47] Sedlak R, Janowski T, Pitoňák M, Řezáč J, Pulay P and Hobza P 2013 *J. Chem. Theory Comput.* **9** 3364–74
[48] Christensen A S, Kubař T, Cui Q and Elstner M 2016 *Chem. Rev.* **116** 5301–37
[49] Cui Q and Elstner M 2014 *Phys. Chem. Chem. Phys.* **16** 14368–77
[50] Artacho E *et al* 2008 *J. Phys. Condens. Matter* **20** 064208
[51] Perdew J P, Burke K and Ernzerhof M 1996 *Phys. Rev. Lett.* **77** 3865–8
[52] Troullier N and Martins J L 1991 *Phys. Rev.* B **43** 1993–2006
[53] Su P and Li H 2009 *J. Chem. Phys.* **131** 014102
[54] Balasubramani S G *et al* 2020 *J. Chem. Phys.* **152** 184107
[55] Becke A D 1988 *Phys. Rev.* A **38** 3098–100
[56] Lee C, Yang W and Parr R G 1988 *Phys. Rev.* B **37** 785–9
[57] Grimme S, Antony J, Ehrlich S and Krieg H 2010 *J. Chem. Phys.* **132** 154104
[58] Weigend F and Ahlrichs R 2005 *Phys. Chem. Chem. Phys.* **7** 3297–305
[59] Weigend F 2006 *Phys. Chem. Chem. Phys.* **8** 1057–65
[60] Yanai T, Tew D P and Handy N C 2004 *Chem. Phys. Lett.* **393** 51–7
[61] Frisch M J *et al* 2009 *Gaussian Inc 09 Revision D.01* (Wallingford CT: Gaussian Inc)
[62] Plasser F 2020 *J. Chem. Phys.* **152** 084108
[63] Plasser F and Lischka H 2012 *J. Chem. Theory Comput.* **8** 2777–89
[64] Plasser F, Wormit M and Dreuw A 2014 *J. Chem. Phys.* **141** 024106
[65] Mai S, Plasser F, Dorn J, Fumanal M, Daniel C and González L 2018 *Coord. Chem. Rev.* **361** 74–97
[66] Plasser F 2016 *J. Chem. Phys.* **144** 194107
[67] Thornton N J and van Mourik T 2020 *Int. J. Mol. Sci.* **21** 6571
[68] Giorgi T, Grepioni F, Manet I, Mariani P, Masiero S, Mezzina E, Pieraccini S, Saturni L, Spada G P and Gottarelli G 2002 *Chem. Eur. J.* **8** 2143–52
[69] Calzolari A, Di Felice R, Molinari E and Garbesi A 2002 *Physica* E **13** 1236–9
[70] Meng L, Liu K, Mo S, Mao Y and Yi T 2013 *Org. Biomol. Chem.* **11** 1525–32
[71] Kwan I C, Mo X and Wu G 2007 *J. Am. Chem. Soc.* **129** 2398–407
[72] Lena S *et al* 2007 *Chem. Eur. J.* **13** 3757–64

Прилог 7

Изјава о ауторству

Име и презиме аутора: Бранислав Миловановић

Број индекса: 2017/0321

Изјављујем

да је докторска дисертација под насловом

Квантнохемијско проучавање супрамолекулских структура гуанина

- резултат сопственог истраживачког рада;
- да дисертација у целини ни у деловима није била предложена за стицање друге дипломе према студијским програмима других високошколских установа;
- да су резултати коректно наведени и
- да нисам кршио ауторска права и користио интелектуалну својину других лица.

Потпис аутора

У Београду, _____ _____

Прилог 8

Изјава о истоветности штампане и електронске верзије докторског рада

Име и презиме аутора: Бранислав Миловановић

Број индекса: 2017/0321

Студијски програм: докторске академске студије физичке хемије

Наслов рада: Квантнохемијско проучавање супрамолекулских структура гуанина

Ментори: др Михајло Етински, ванредни професор; др Игор Попов, виши научни сарадник

Изјављујем да је штампана верзија мог докторског рада истоветна електронској верзији коју сам предао ради похрањена у **Дигиталном репозиторијуму Универзитета у Београду**.

Дозвољавам да се објаве моји лични подаци везани за добијање академског назива доктора наука, као што су име и презиме, година и место рођења и датум одбране рада.

Ови лични подаци могу се објавити на мрежним страницама дигиталне библиотеке, у електронском каталогу и у публикацијама Универзитета у Београду.

Потпис аутора

У Београду, _____ _____

Прилог 9

Изјава о коришћењу

Овлашћујем Универзитетску библиотеку „Светозар Марковић“ да у Дигитални репозиторијум Универзитета у Београду унесе моју докторску дисертацију под насловом:

Квантнохемијско проучавање супрамолекулских структура гуанина

која је моје ауторско дело.

Дисертацију са свим прилозима предао сам у електронском формату погодном за трајно архивирање.

Моју докторску дисертацију похрањену у Дигиталном репозиторијуму Универзитета у Београду и доступну у отвореном приступу могу да користе сви који поштују одредбе садржане у одабраном типу лиценце Креативне заједнице (Creative Commons) за коју сам се одлучио.

1. Ауторство (CC BY)

2. Ауторство – некомерцијално (CC BY-NC)

3. Ауторство – некомерцијално – без прерада (CC BY-NC-ND)

(4.) Ауторство – некомерцијално – делити под истим условима (CC BY-NC-SA)

5. Ауторство – без прерада (CC BY-ND)

6. Ауторство – делити под истим условима (CC BY-SA)

(Молимо да заокружите само једну од шест понуђених лиценци. Кратак опис лиценције саставни део ове изјаве).

Потпис аутора

У Београду, _____ _____

1. **Ауторство**. Дозвољавате умножавање, дистрибуцију и јавно саопштавање дела, и прераде, ако се наведе име аутора на начин одређен од стране аутора или даваоца лиценце, чак и у комерцијалне сврхе. Ово је најслободнија од свих лиценци.

2. **Ауторство – некомерцијално**. Дозвољавате умножавање, дистрибуцију и јавно саопштавање дела, и прераде, ако се наведе име аутора на начин одређен од стране аутора или даваоца лиценце. Ова лиценца не дозвољава комерцијалну употребу дела.

3. **Ауторство – некомерцијално – без прерада**. Дозвољавате умножавање, дистрибуцију и јавно саопштавање дела, без промена, преобликовања или употребе дела у свом делу, ако се наведе име аутора на начин одређен од стране аутора или даваоца лиценце. Ова лиценца не дозвољава комерцијалну употребу дела. У односу на све остале лиценце, овом лиценцом се ограничава

највећи обим права коришћења дела.

4. **Ауторство – некомерцијално – делити под истим условима**. Дозвољавате умножавање, дистрибуцију и јавно саопштавање дела, и прераде, ако се наведе име аутора на начин одређен од стране аутора или даваоца лиценце и ако се прерада дистрибуира под истом или сличном лиценцом. Ова лиценца не дозвољава комерцијалну употребу дела и прерада.

5. **Ауторство – без прерада**. Дозвољавате умножавање, дистрибуцију и јавно саопштавање дела, без промена, преобликовања или употребе дела у свом делу, ако се наведе име аутора на начин одређен од стране аутора или даваоца лиценце. Ова лиценца дозвољава комерцијалну употребу дела.

6. **Ауторство – делити под истим условима**. Дозвољавате умножавање, дистрибуцију и јавно саопштавање дела, и прераде, ако се наведе име аутора на начин одређен од стране аутора или даваоца лиценце и ако се прерада дистрибуира под истом или сличном лиценцом. Ова лиценца дозвољава комерцијалну употребу дела и прерада. Слична је софтверским лиценцама, односно лиценцама отвореног кода.